Using wind fields from a high resolution atmospheric model for simulating snow dynamics in mountainous terrain

Dissertation der Fakultät für Geowissenschaften

der

Ludwig-Maximilians-Universität zu München

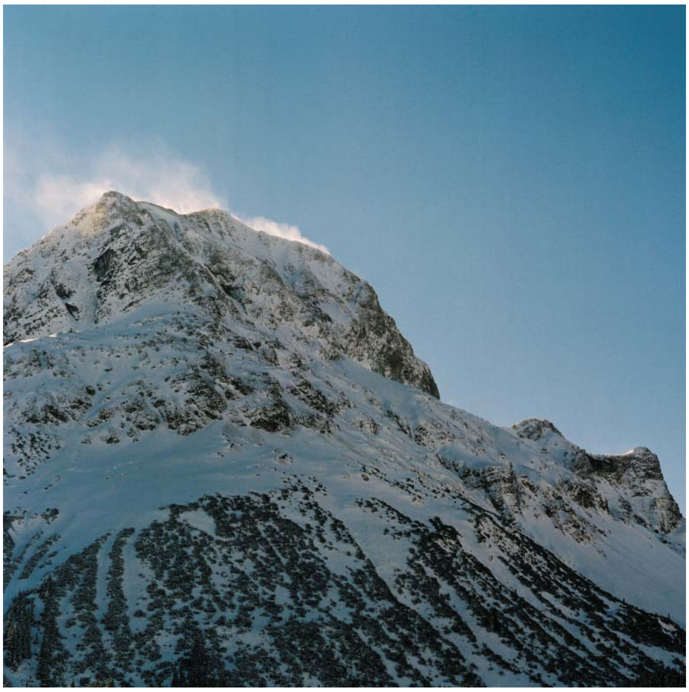

vorgelegt von:

Matthias Bernhardt

aus München

Eingereicht im Juli 2008

Gähds ned übern Berg, gähds außn rum, awa weida geh muaß.

(Bayerische Weisheit)

1. Gutachter: .... Prof. Dr. Wolfram Mauser
2. Gutachter: .... Prof. Dr. Michael Kuhn

Tag der mündlichen Prüfung: 27.10.2008

Zusammenfassung

Der Einfluss der Schneedecke auf die Hydrologie Alpiner Einzugsgebiete ist weithin bekannt und in der Literatur eindrucksvoll beschrieben. Saisonale Schneedecken fungieren als temporäre Speicher für den Niederschlag. Das gebundene Wasser wird den Fließgewässern verzögert als Schmelzwasser zugeführt und bestimmt damit zumindest zeitweise deren Abflusshöhe und –menge. Die Modellierung von mengenmäßigem Inhalt und räumlicher Ausdehnung des Schneespeichers ist hilfreich für die Quantifizierung der vorhandenen Wasserressourcen und für die Bestimmung des Zeitpunkts, zu dem die gespeicherten Wassermengen verfügbar werden. Die Intensität der Schneeschmelze hängt dabei, neben der absoluten räumlichen Lage, auch von der räumlichen Heterogenität der Schneedecke ab. In der vorliegenden Arbeit wurde der Einfluss von wind-induzierten Schneetransportprozessen auf die Heterogenität der Alpinen Schneedecke untersucht. Als Testgebiet wurde der *Nationalpark Berchtesgaden* ausgewählt. Dieses Testgebiet kann aufgrund seiner hohen Reliefenergie als ideal für die durchgeführten Untersuchungen gelten, da Schneetransportprozesse hier besonders effektiv sind. Die Instrumentierung des Parks ist im Hinblick auf die verfügbaren meteorologischen Stationen außerordentlich gut. Darüber hinaus liegen flächendeckende Informationen über die Geländehöhe und die Vegetation in Form eines hoch aufgelösten (10m) Geographischen Informationssystems (*GIS*) vor. Für den Untersuchungszeitraum (Wintersaison 2003/2004 und 2004/2005, jeweils gerechnet von August bis Juli) liegen Daten von 5 meteorologischen Stationen, einer Feldkampagne und zwei *Landsat ETM+* Bildern vor.

Windinduzierter Schneetransport wird in der Literatur häufig als der bestimmende Prozess für die Heterogenität der Schneedecken in gebirgigen Gebieten angesehen. In starkem Kontrast zu der diesem Prozess zugestandenen Bedeutung, steht die Anzahl der Veröffentlichungen, die die numerische Untersuchung der Effektivität desselben zum Inhalt haben. Das liegt vor allem in der Tatsache begründet, dass die Berechnung von qualitativ hochwertigen Windfeldern in gebirgigem Terrain bis heute nahezu unmöglich ist. Diese allerdings sind von zentraler Bedeutung, um quantitative Aussagen über die Richtung der Verlagerung von Schneemengen zu treffen, und um die entsprechenden Erosions- wie Akkumulationsgebiete

zu lokalisieren. Für eine möglichst genaue Charakterisierung der Windfelder im Untersuchungsgebiet wurden in der vorliegenden Arbeit physikalisch basierte Windfelder mit Hilfe des *PSU-NCAR MM5* Atmosphärenmodells berechnet. Diese wurden im Anschluss in dem etablierten Schneemodell *SnowModel* als Antrieb für die Schneetransportroutine (*SnowTran-3D*) verwendet.

Da eine direkte Kopplung von Atmosphärenmodell und Schneemodell unter den heute gegebenen technischen Voraussetzungen zu einer unrealistisch hohen Modell-Laufzeit geführt hätte, wurde eine alternative Methode gewählt: die Windfelder wurden separat berechnet und eine Bibliothek repräsentativer Windfelder für das Untersuchungsgebiet erzeugt. Die zeitliche Synchronisation zwischen Windfeldbibliothek und Schneemodell wurde über das operationelle, mesoskalige Wettervorhersage-Modell des *Deutschen Wetterdienstes* (*DWD*), das *Lokalmodell* hergestellt. Dies wurde aufgrund der Tatsache möglich, dass bestimmte Modellausgaben von *Lokalmodell* und *MM5* im 700 hPa Niveau vergleichbar sind. Um das richtige Windfeld für einen Schneemodellzeitschritt aus der zuvor erzeugten *MM5* Windfeldbibliothek auszuwählen, wurden mittlere Windvektoren der *MM5* Windfelder mit mittleren Vektoren der entsprechenden *Lokalmodell* Windfelder verglichen. So wurde es möglich, zu jedem Modellzeitschritt des *Lokalmodells* (eine Stunde) ein *MM5* Windfeld zu selektieren und im Schneemodel anzuwenden.

Die generierten *MM5* Windfelder haben eine räumliche Auflösung von 200m. Für eine prinzipielle Überprüfung der Funktionalität des Schneemodels in Verbindung mit einer *MM5* Windfeldbibliothek, wurden erste Schneemodelläufe auf der 200m Skala initialisiert. Die zugehörigen Ergebnisse waren plausibel und bestätigten die Anwendbarkeit der Kombination von Schneemodell und *MM5* Windfeldern. Die Schneewasseräquivalentverteilung im Gebiet wurde durch die Applikation der *MM5* Windfelder weniger abhängig von der allgemeinen niederschlagsbedingten Zunahme des Schneewasseräquivalents mit der Höhe. Ein Zusammenhang mit der Exposition des Geländes konnte nun auch aufgezeigt werden. Zudem konnten Transportprozesse über die Bergkämme hinweg simuliert werden. Eine Intensitätszunahme aller Transportterme unter Anwendung der *MM5* Windfelder im Vergleich zu interpolierten Windfeldern konnte ebenfalls festgestellt werden. Die Ergebnisse auf der 200m Skala machten deutlich, dass für eine ausreichende und tiefgreifende Beschreibung und Validierung von Schneetransportprozessen ein feineres Modellgrid erforderlich ist. Als Konsequenz wurden die *MM5* Windfelder auf eine Auflösung von 30m skaliert. Durch die Skalierungsprozedur konnte eine bessere Korrelation zwischen Stationsmessungen und *MM5* Ergebnissen erreicht werden. Die resultierenden 30m Windfelder wurden für hochauflösende 30m Schneemodellläufe genutzt, die auf der Basis von Ergebnissen der durchgeführten Feldkampagnen und Fernerkundungsdaten validiert werden konnten. Auch hier konnte nachgewiesen werden, dass die unter Verwendung der *MM5* Windfeldbibiliothek generierten Resultate von höherer Validität waren, als die Ergebnisse die mit Hilfe von interpolierten Windfeldern erzeugt wurden.

Im Weiteren wurden die Modellergebnisse anhand ausgewählter Resultate diskutiert. Es konnte gezeigt werden, dass die Effektivität von Transportprozessen unter 1800m ü. NN. zu vernachlässigen ist und ab 2200m ü. NN. stark zunimmt. Zudem konnte unter Nutzung der *MM5* Windfelder der Transport von Schnee auf vergletscherte Flächen modelliert werden. Hohe modellierte Sublimationsraten an den Gipfeln wurden diskutiert und ihre Wichtigkeit im Bezug auf die alpine Wasserbilanz aufgezeigt. Im Ganzen konnte nachgewiesen werden, dass die Einbindung von Ergebnisdaten von Atmosphärenmodellen zu einer deutlichen Verbesserung der Beschreibung der Prozesse an der Erdoberfläche führt.

In einem letzten Schritt wurden die Ergebnisse der hochaufgelösten Schneemodellläufe genutzt, um die Schneedeckenheterogenität im Gebiet zu parametrisieren. Ziel war es, eine Möglichkeit aufzuzeigen, die generierte kleinskalige Information auch für regionale Landoberflächenmodelle nutzbar zu machen. Infolgedessen wurde eine einfach zu implementierende Routine für regionale Modelle vorgestellt, die die subskalige Beschreibung der Schneedeckenheterogenität erlaubt. Dies kann in entsprechendem Relief zu einer Verbesserung der Energie- und Feuchteflüsse in regionalen Modellen und damit zu einer akkurateren Beschreibung der Ablationsperiode der Schneedecke und der Abflussgenerierung führen.

Abstract

It is widely known that the snow cover has a major influence on the hydrology of Alpine watersheds. Snow acts as temporal storage for precipitation during the winter season. The stored water is later released as snowmelt and represents an important component of water supply for the downstream population of large mountain-foreland river systems worldwide. Modelling the amount and position of the snow water stored in the headwater catchments helps to quantify the available water resources and to estimate the timing of their release. The presented work investigates wind induced snow transport processes which are considered to be crucial for the snow distribution in Alpine catchments. In contradiction to the importance that is attributed to this process, there are only a few studies available which have quantified the transport intensities on the catchment scale. This can be attributed to the fact that the even today not much is known about the spatial characteristics of wind fields which are the driving force for snow transport processes. The presented thesis tries to overcome this lack of information by using physically based wind fields predicted by an atmospheric model (*PSU_NCAR MM5 model*) for the modelling of the snow cover (simulated by *SnowModel*). All of the used models are described in great detail in the literature, validated in many different regions, and can be seen as applicable with regard to the goal of this work. As snow transport processes are particularly important on a comparatively small scale a numerical inclusion of the responsible processes into regional models is inadequate. Hence, while this study itself mainly uses smaller scale physically based models, a parameterisation scheme is presented at the end of this thesis that is able to incorporate its main findings into larger scale models.

All of the presented work was carried out at the *Berchtesgaden National Park.* The site is highly appropriate because of the extremely rough terrain and the good accessibility. Furthermore, the instrumentation of the area is comparatively good and the data sources (GIS, field campaign data) are excellent. The thesis deals with the winter seasons (August - July) 2003/2004 and 2004/2005. For this period, data of 5 meteorological stations, 1 field campaign and two *Landsat ETM+* images were available.

As mentioned before, physically based wind fields were used as input for the snow transport modelling. An operational coupling between atmospheric model and snow transport model was not pursued because of the high computational costs of the atmospheric model. Thus, a library of representative wind fields was produced in advance and linked to the snow transport model via operational *German weather service Lokalmodell* results. This becomes possible because of the comparability of a *MM5* model layer with one of the *Lokalmodell* model layers. To link the wind field library to the snow model all of the predicted *MM5* wind fields were characterised by information available from the *Lokalmodell*. This enable an easy detection of the *MM5* wind field which is closest to the real climatic wind conditions at any *Lokalmodell* time step (1 hour).

The produced *MM5* wind fields have a spatial resolution of 200 meters. As an initial check if the snow cover simulation of *SnowModel* in association with the wind field library delivers adequate results with respect to the snow distribution, model runs were first carried out at the 200m scale. An analysis of the results showed that the coupled routine delivers acceptable results. It could be seen that with the use of the *MM5* wind fields, the snow cover becomes more anisotropic and that transport processes over crests as well as sublimation processes are predicted to become more intensive. Nevertheless, a higher resolution was needed to quatify the effects and to validate the results.

In a subsequent step the *MM5* wind fields were downscaled to a 30m resolution. The downscaling procedure lead to a better agreement between modelled and measured wind speeds. The resulting 30m wind fields were used for high resolution model runs which were validated on the basis of the field campaign and remotely sensed data. A comparison with model runs using wind fields interpolated from station data showed that the runs performed with the *MM5* wind fields deliver more consistent and comprehensible results.

Subsequently, the validity of the model is discussed on the basis of selected results. High resolution model results indicated that snow transport processes are effective at high elevations but virtually negligible for regions below of 1800m a.s.l.. Furthermore, it could be seen that the correct estimation of snow transport from the surrounding areas to glaciers becomes possible by using the *MM5* wind fields. Very high modelled sublimation rates at the mountains crests are discusses with respect to their importance on the water balance. Furthermore, the influence of preferential snow deposition and snow slides which were not numerically predicted in this work were discusses. Additionally, the applicability of atmospheric model results as input for land-surface models could be confirmed.

In a final step a model scheme is presented that would make the generated information available for regional scale models. This model parameterization scheme which is based on the modelled 30m snow water equivalent distribution within the test area was used for this area. The scheme allows for a quick and simple description of the subscale snow heterogeneity in regional scale models. This can lead to considerable model improvements with respect to the description of the energy and moisture fluxes to and from the surface. An accurate description of these fluxes is essential for an accurate simulation of the melt period and, therefore, for an acceptable calculation of the runoff generation in larger scale models.

Preface

The presented work was realized within the framework of *GLOWA_Danube* a project of the *German Ministry for Education and Research (bmb+f)*. The goal of the work was to investigate how wind induced snow transport processes can influence the Alpine snow cover and how the effects can be implemented in *SVAT* schemes.

The work was carried out at the Department of *Geography* within the workgroup of *Prof. Dr. Wolfram Mauser*. *Prof. Dr. Mauser* gave me the chance to join his group after my Diploma and he also had the fundamental idea for this thesis, which was, to couple a library of MM5 wind fields with a snow transport routine. Additionally, I would like to thank him for his permanent support (in regard to specialist knowledge, the excellent environment, the possibility to travel to workshops and finally to organise the Alpine*Snow*Workshop together with (*Dr. Ulrich Strasser*) and his feeling for the workgroup which has generated the best imaginable work climate at the institute. Furthermore, he gave me the chance to gain first experiences in teaching.

I greatly acknowledge the fruitful collaboration with *Dr. Glen Liston* of the Cooperative Institute for Research in the Atmosphere (*CIRA*) *Colorado State University*. He supported me by providing me with the source code of his models and answered any question in an unbelievable time and detail.

At the institute I would like to thank *Dr. Ulrich Strasser* for his support and interest in this work. The cooperation with him was inspiring and characterized by open discussions inside the institute or at the *Steinheil*.

I would also like to thank *Tobias Hank* and *Thomas Marke* my office roommates. We had a very special work atmosphere, characterized by very useful discussions.

Dr. *Günther Zängl* has supported me with his infinite knowledge about *MM5* and supported me at every time of my work.

I would like to thank Dr. *Stefan Pohl* for his expertise which has helped to improve this work and for the fruitful discussions.

My cordial thanks go to all of my dear colleagues which gave me a lot of support during the last years. They are in alphabetical order: *Dominik Aulehner, Heike Bach, Ludwig Braun, Marco Braun, Andrea Ebner, Rainer Efinger, Heidi Escher–Vetter, Vera Erfurth, Khaled Haider, Christoph Heinzeller, Jochen Henkel, Ingo Keding, Lorenz Köppl, Alexander Löw, Ralf Ludwig (viva FCB), Stefanie Mayer, Christian Michelbach, Markus Muerth, Susan Niebergall, Natascha Oppelt, Monika Prasch, Renate Santl, Roswitha Stolz, Monika Tepfenhart, Michael Vogel, Daniel Waldmann, Ruth Weidinger.*

The *Berchtesgaden National Park Administration* supported me with field campaign data and offered free access to all required data. *Helmut Franz* which has coordinated all of this work should be explicitly mentioned here.

Last but not least I would like to thank my family and my girlfriend *Daniela Funk* who supported me during the last weeks of my work and who has improved the thesis by her work at the institute.

Table of contents

Chapter 1 Introduction

1.1 Aim of the thesis 1
1.2 Introduction and methodology 2
1.2.1 The snow cover an important land surface feature 2
1.2.2 Snow cover modelling 5
1.2.3 Model approach of the presented work 8
1.2.4 Scales used in this work 11
1.3 Test Sites and field measurements 13
1.3.1 Topography 16
1.3.2 Climate 16
1.3.3 Meteorological data 17
1.3.4 Spatial data sets 18
1.3.5 Field campaigns 20

Chapter 2 Model descriptions

2.1 SnowModel 23
2.2 MM5 model 32
2.3 Lokalmodell (LM) 35

Chapter 3 Meteorological fields

3.1 Interpolation of meteorological parameters, capabillities and limitations 37
3.2 Calculation of wind fields in mountainous terrain 40
3.2.1 Theoretical background 43
3.2.2 Comparison of interpolated and modelled wind fields 47
3.3 Creation and synchronisation of a MM5 predicted wind field library 53

Chapter 4 Snow transport modelling

4.1 Results of the meso scale model runs 60
4.1.1 Model results at the point scale 61
4.1.2 Spatial comparison of the model results 63
4.1.3 Spatial validation of the model results 66
4.2 Downscaling of the *MM5* wind fields 72
4.2.1 Spatial correction 73
4.2.2 Statistical revision 74
4.2.3 Inclusion of the elevation difference between *MM5* and 30m *DEM* 75
4.2.4 Integration of subgrid topography 76

4.2.5 Validation of the downscaled MM5 wind fields 76
4.3 Results of the micro scale model runs 76
4.4.1 Results Reiteralm 77
4.4.2 Results Kühroint 80
4.4.3 Spatial comparison of the model results 83
4.4.4 Spatial validation 87

Chapter 5 Discussion of the SnowModel results

5.1 Accurarcy of *SnowModel* at the point scale 91
5.2 Accurarcy of *SnowModel* with respect to remotely sensed data 94
5.3 Scale effects in snow transport modelling 96
5.4 Discussion of enhanced accumulation and sublimation rates when using *MM5* wind fields 99
5.5 High interpolated precipitation rates as a possible reason for the underestimation of the spatial snow heterogeneity 102
5.6 The effects of snow slides and preferential snow distribution 103
5.7 Model formulations 105

Chapter 6 Outlook and Conclusion

6.1 Presentation of a scheme which allows for a better description of the snow cover in regional scale models 107
6.2 Conclusion 114

References 117

Appendix 126

List of figures

Figure 1: Examples for snow heterogeneity in the Arctic region, in undulating terrain and within a mountainous area (Photos by: M. Sturm, D. Marks)................................ 1

Figure 2: a) Snow cover *at Watzmann* Mountain (turquoise) superimposed by a 1km² grid. b) Interrelation between snow covered area and energy fluxes (Qli = incoming longwave radiation, Qle = emitted longwave radiation, Qh = turbulent exchange of sensible heat, Q_e = turbulent exchange of latent heat, Q_{ns} = net solar radiative flux at the surface, $Q_{m =}$ energy flux available for melt) (cp. Liston 1995)............ 4

Figure 3: Schematic of the five nested domains used in *MM5*. The largest one is nesting domain_1, the smallest is domain_5. Domain_3 is marked as red rectangle........ 10

Figure 4: Scales used in this thesis. The work starts at the meso scale for which the MM5 wind fields are representative for (200m). After than the wind fields are downscaled to a 30m resolution (micro scale). The *SnowModel* results at the micro scale are validated on the basis of field campaign and remotely sensed data. The information produced by the micro scale runs is used for a parameterisation scheme for the snow heterogeneity which can be used in regional scale Models. 12

Figure 5: Test site (*Berchtesgaden National Park*) (*Bayerisches Landesvermessungsamt* 1994, modified). The locations of *Reiteralm* 1, 2 and 3, *Schönau*, *Kühroint* and *Jenner* are marked with arrows. The test sites at *Reiteralm* and *Kühroint* are displayed as chequered areas... 14

Figure 6: Profile through the National Park area which displays the rapid changes in altitude in the test area.. 16

Figure 7: Location of the meteorological stations. 18

Figure 8: GIS data used in this work. a) elevation (m a.s.l.), b) vegetation types, c) aspect (°) and d) slope (°)... 19

Figure 9: Sample points at Reiteralm. 15 sample points were installed in the winter season 2004/05 the points are named 1-15. 20

Figure 10: Sample points at Kühroint. 15 sample points were installed in the winter season 2004/05 the points are named A-O... 21

Figure 11: Schematic illustration of the transport model. Qt = mass transport rates of saltation, Qs = mass transport rates of turbulent suspended snow, Qv = sublimation of transported snow particles. P = water equivalent precipitation rate. CV = snow holding capacity. h_* = top of the saltation layer................................ 28

Figure 12: Connection between wind-shear velocity and transport rate (cp. Liston and Strum 1998).. 31

Figure 13: Schematic illustration of the MM5 nesting domains (the largest domain is domain_1, the smallest domain_5) and of the needed input parameters............... 32

Figure 14: a) Spatial distribution of the meteorological stations within the upper Danube catchment, b) Area of the different elevation bands and number of stations at the respective altitudes. 37

Figure 15: Temperature recordings of *Reiteralm II* meteorological station. Comparison of hourly modelled and observed data for the winter season 2003/2004. 39

Figure 16: Incoming solar radiation data from Reiteralm 3 meteorological station. Comparison of hourly modelled and observed data for the winter season 2003/2004.. 40

Figure 17: Relative humidity from Reiteralm 3 meteorological station. Comparison of hourly modeled and observed data for the winter season 2003/2004.............................. 40

Figure 18: Correlation between measured and calculated precipitation rates (winter season 2003/2004) (mm). a) Including hours with precipitation at other stations but no precipitation at the validation station (Reiteralm 1) and b) precipitation at all stations, including Reiteralm 1.. 41

Figure 19: Accuracy of interpolated wind directions in comparison to measurements at *Reiteralm I* (winter season 2003/2004). 42

Figure 20: Comparison of measured and interpolated wind speeds at *Reiteralm 1* (winter season 2003/2004).. 42

Figure 21: Frozen anemometer. This picture shows a very common situation in Alpine regions. The sensor becomes snow covered and becomes therefore unusable. 44

Figure 22: Vertical profile through a *MM5* wind field. a, b and c are fictive meteorological stations. The transects I, II, III are used for declare the wind conditions at the faces of *Watzmann* mountain. The wind speed is slightly enhanced at the windward site (transect I) as the wind direction is constant to North. Transect II and II showing the complex wind conditions at the leeside. The wind speeds are about 6 [m/sec] at transect II, the wind direction is to north. The situation changes at transect III were the wind speed is between 0 and 2 [m/sec] and the wind direction is to south. 45

Figure 23: Generalized flow behaviour over a hill: a) flow separation and b) a rotor (Barry 1992, modified). 46

Figure 24: a) *MM5* wind field (input parameters: wind direction = 140° and 10 [m/sec] at 10m and 25[m/sec] at 100hpa) b) *MM5* wind field calculated with the same input wind speeds but an input wind direction of 270°. 48

Figure 25: Interpolated wind fields. a) The average wind directions at the meteorological stations are 140° and b) 270°.. 49

Figure 26: Spatial characteristics of *MM5* wind direction fields in dependency of the synoptic inflow. The inflow direction is 265 degrees and 270 degrees respectively. 51

Figure 27: Spatial characteristics of an interpolated wind direction field. The wind directions used for the interpolation corresponding to the wind directions produced by *MM5* (fig 26) for the three indicated meteorological stations. 51

Figure 28: Dependency of the calculated *MM5* wind direction field on the input wind speed. The wind speeds used for the model setup were 05 [m/sec] for the 10m model level and 20 [m/sec] for the uppermost model level (cp. fig. 13) 52

Figure 29: Schematic illustration of the synchronization of *MM5* wind field library and *SnowModel* via hourly *DWD* Lokalmodell information. 54

Figure 30: *DWD* historical data for the 700 hPa level (gray dots) vs. averaged *MM5* domain_3 vectors (black dots). The DWD observations were used for defining the initialisation wind speeds and directions needed for the *MM5* runs (cp. fig. 13). 55

Figure 31: The red coloured areas in a) and b) stand for wind speeds >3[m/sec] which would be able to initialise snow transport processes. The *MM5* wind fields were calculated with very moderate input wind speeds (30° / 5[m/sec] at 10m; 16[m/sec] at 100hpa and 143° / 5[m/sec] at 10m; 20[m/sec] at 100hpa)............. 56

Figure 32: Comparison of measured and *MM5* wind a) direction (01.09.03-30.08.04) and b) speed (01.09.03-31.12.03)at Reiteralm I. A comparrison to figures 19 a) and b) clearifies the advantages in contrast to the interpolation routine......................... 57

Figure 33: Wind speed provided by the interpolation procedure of Liston and Sturm (1998) (left) and *MM5* (right). The images represent the situation on January 9, 2004, 7:00. Wind direction is 270 degrees... 58

Figure 34: Wind direction (detail of the Watzmann region), derived after Ryan (1977) (left) and *MM5* (right), respectively. The images represent the situation on January 9, 2004, 7:00. Wind direction is 270 degrees.. 58

Figure 35: a) Percentage of hours with wind speeds higher than 3 [m/sec] (*MM5* fields). b) Percentage of hours with wind speeds higher than 3 [m/sec] (interpolated fields). Difference between the averaged interpolated and *MM5* wind speed for the winter season 2003/2004 (The black line is the 1800 m a.s.l. contour). 59

Figure 36: Comparison of model results and measured values for the meteorological stations a) *Reiteralm II*, b) *III* and c) *Jenner*. 62

Figure 37: Amount of accumulated and eroded SWE within the study area and for the winter season (2003/04) (Please note the different scales of the legends). The accumulation zone at *Blaueis* glacier is marked with a black ellipse. The black line is the 1800m isohypsis. 63

Figure 38: a) SWE [m] – elevation dependency b) SWE - aspect dependency for the total elevation interval c) SWE - aspect dependency for elevations higher than 1800m a.s.l. d) SWE - aspect dependency for elevations higher than 2200m a.s.l. SWE is the average values for the modelled time period. The different volumes under the curves are due to higher sublimation losses within the *MM5* runs. The illustrations belonging to the winter season 2003/04.. 64

Figure 39: Intensities of the different transport terms: saltation, suspension and sublimation in a) c) e) *INTER* and b) d) f) *MM5* (winter season 2003/04). The black line is the 1800m isohypsis.. 66

Figure 40: a) Spectral bands of Landsat ETM+ and spectral characteristics of different snow types. b) spectral Characteristics of different land cover types............................. 68

Figure 41: a) modelled snow cover of April 28, 2004, b) *NDSI* map of the same date, c) modelled snow cover of Mai 30, 2004 d) *NDSI* map of the same date. The black line is the 1800m isohypsis. 70

Figure 42: a) c): *Landsat ETM+* images (April, 28 2004 and May, 30 2004. resampled to a 200m resolution). e) f): Differences between model an classification results at April and May respectively (red indicates: only classified snow cover. Green: only modelled snow cover). 71

Figure 43: a) The smoothed *Reiteralm* area (marked with an arrow) within the *MM5* DEM (200 m resolution) compared to b) the National Park DEM (30 m resolution). ... 72

Figure 44: Performed downscaling steps. The figure shows the a schematic illustration of the downscaling steps conducted in 4.2.1 to 4.2.3. 73

Figure 45: a) Correlation between *MM5* results and station recordings before the downscaling procedure (*Reiteralm I*, daily resolution) b) Correlation between *MM5* results and station recordings after the downscaling procedure. The regression line is forced through the origin.. 76

Figure 46: Comparison of model and measurements. White dots indicating that the model is within 10% of the measurements. Green dots stand for a model overestimation of the snow depth from more than 10%, red dots for a model underestimation from more than 10%.. 78

Figure 47: a) is representative for the upper part of *Reiteralm*. b) For the central region and c) For the lower part. 79

Figure 48: Comparison of model and measurements. White dots indicating that the model is within 10% of the measurements. Green dots stand for a model overestimation of the snow depth from more than 10%, red dots for a model underestimation from more than 10%. 81

Figure 49: Three representative points at Kühroint. Point N) is located at the edge of the forest at the northern part of Kühroint; point F) is located at the clear cut area, and point K) can be found on the meadows in the western part of the area. 82

Figure 50: Mean modeled SWE distribution (of *INTER_30* and *MM5_30*) for a) the total area, b) areas above 1800m a.s.l. and c) areas above 2200m a.s.l. The different volumes under the curves are due to higher sublimation losses within the *MM5* runs. 84

Figure 51: Snow transport rates of a) *INTER_30* and b) *MM5_30.* The black line is the 1800m isohypsis. 84

Figure 52: Intensities of the different transport terms: saltation, suspension and sublimation in a) c) e) *INTER_30* and b) d) f) *MM5_30*. The black line is the 1800m isohypsis.85

Figure 53: Simulated contributions to annual snow sublimation (additive representation) from the ground, canopy intercepted snow and wind-induced, turbulent suspended snow along a cross-section from Hochkalter (2607m a.s.l.) through the Wimbachtal to Watzmann (2713m a.s.l.). (Strasser *et al.* 2008). 86

Figure 54: a) modelled snow cover of April 28, 2004, b) NDSI map of the same date, c) modelled snow cover of Mai 30, 2004 b) NDSI map of Mai the same date, e/f) Differences between model an classification results at April and Mai respectively (red indicates: only classified snow cover. Green: only modelled snow cover. Pink: cloud mask). The black line is the 1800m isohypsis. 88

Figure 55: validation areas of April 28, 2004; Blue: Snow covered regions (Bands: 5,4,3), Red: test areas. 89

Figure 56: validation areas of Mai 30, 2004; Blue: snow covered regions (Bands: 5,4,3), Red: test areas. 90

Figure 57: *DEM* of *Kühroint* test site. 93

Figure 58: a) Comparison of *run_baseline* and *INTER_30* results on April 28, 2004, b) comparison between *run_baseline* and *MM5_30* at the same date. c) Picture of a crest were the snow cover on the windward side (right) is reduced considerably by snow transport processes 94

Figure 59: a) wooded region at *Watzmann* mountain (the snow covered area appears in blue). b) *NDSI* classification in gray, *MM5_30* results in blue. 96

Figure 60: Predicted loss and gain of SWE due to wind induced snow transport at *Blaueis* glacier a) 30m resolution results using MM5 wind fields, b) 200m resolution results using MM5 wind fields. (The results were fitted to the 30m grid for the presentation) 98

Figure 61: Picture of the Watzmann upper east face under full snow coverage.................... 99

Figure 62: Accumulated Snow masses transported by snow slides (winter season 03/04). Strasser at al. (2008) modified. 104

Figure 63: The figure shows a theoretical subscale SWE depth distribution and common model representatios. a) Shows a situation with full snow coverage, b) shows a situation where the model shows no snow coverage.. 108

Figure 64: *Landsat* images of a) April 2002, b) March 2003 and c) April 2004. Channels 3,5,6 (R,G,B) are displayed. The snow cover is indicated by the red colour. It can be seen that the spatial characteristics of the snow distribution is very similar from year to year. 109

Figure 65: results of the CV classification. Predicted on the basis of the ratio between per pixel mean modelled *SWE* and standard deviation of the *SWE* (30m results of *SnowModel* with *SnowTran-3D/MM5*). 110

Figure 66: If the model simulates snow melt the curve shifts against the y-axis and if the curve intersects the axis the area under the curve which is equivalent to the total grid cell is reduced. Any curve stands for the SWE distribution of the respective grid cell.. 111

Figure 67: Subpixel snow coverage in percent on May 30, 2004. a) Results based on a scaled NDSI map, b) Model results based on CV values predicted by the ratio approach with SnowTran-3D and *MM5* wind fields, c) Model results based on CV values generated with the iterative approach.. 111

Figure 68: Average available melt energy per km² grid cell: a) aggregated 30m results (equivalent to MM5_30), (220 W/m²) b) 1km² model runs without the subgrid routine (270 W/m²), c) corrected 1km² results using the subgrid routine (200 W/m²). 112

Figure 69: Upper Danube catchment. Red: Areas for which the parameterization results are potentially applicable. 113

List of tables

Table 1: Geographic position of the National Park 15

Table 2: Meteorological stations which were used, their abbreviations, geographical coordinates, elevation, and associated meteorological fields: global radiation (GR), humidity (H), precipitation (P), snow height (SH), temperature (T), temperature of the snowpack 0cm above ground (TS0), 20cm above ground(TS2), 4cm above ground (TS4) and 60cm above ground (TS6), wind speed (WS), wind direction (WD) 18

Table 3: Hours showing wind speed and direction recordings vs. hours with data lacks compared to recordings of other sensors. 44

Table 4: Column I: Mean value of all 220 wind fields between the average value of the original and the modified *MM5* wind speeds. Column II: Maximal observed difference between original and modified *MM5*. Column III: Minimal observed difference. 75

Table 5: The table shows the standard deviations of the measurements and of the respective model results for the observation dates. 78

Table 6: The table shows the standard deviations of the measurements and of the respective model results for the observation dates. 81

Table 7: Comparison between *SnowModel* results generated with *SnowTran-3D* and with as well as without the usage of *MM5*. The values belonging to the areas highlighted in Figure 55. The areas are snow free in reality, the values within the table showing the improvement of the *SnowModel* results when the transport routine is used. 89

Table 8: Comparison between *SnowModel* results generated with *SnowTran-3D* and with as well as without the usage of *MM5*. The values belonging to the areas highlighted in Figure 56. The areas are snow free in reality, the values within the table showing the improvement of the *SnowModel* results when the transport routine is used. 90

Table 9: Contributions relative to total snowfall and scale-dependent significance of the winter water balance components for *the Berchtesgaden National Park* domain for 2003/2004. The additional amount of snowmelt is caused by rain-on-snow (cp. Stasser et al. 2008). 101

Chapter 1 Introduction

1.1 Aim of the thesis

The presented thesis investigates the Alpine snow cover and its spatial heterogeneity in due consideration of wind induced snow transport processes. An appropriate knowledge of snow transport, its mode of action, and its effectiveness is essential for understanding and predicting the spatial distribution of the snow cover and thereby the correct water balance as well as moisture and energy fluxes in mountainous regions. The thesis presents results of high resolution physically based snow model runs (for the winter seasons 03/04 and 04/05), used for an estimation of the effectiveness of snow transport processes within an Alpine catchment. Furthermore, a parameterisation scheme is presented which allows for consideration of the snow heterogeneity in Alpine regions within regional scale models.

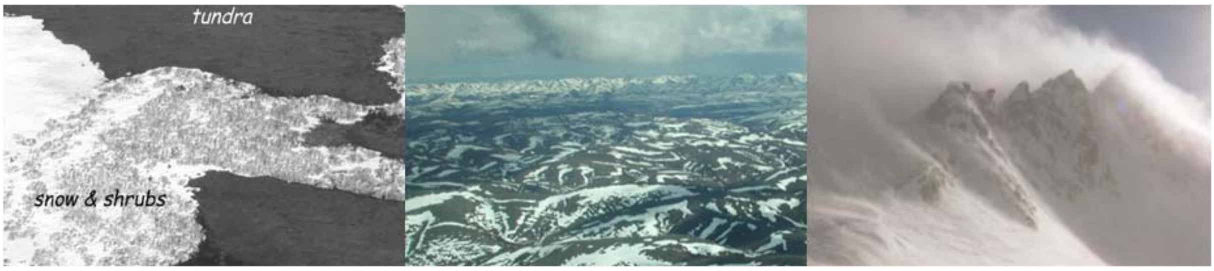

Figure 1: Examples for snow heterogeneity in the Arctic region, in undulating terrain and within a mountainous area (Photos by: M. Sturm, D. Marks)

At the end of the 1970's snow transport processes were not well understood, Gray *et al.* (1979) noted that: "*it is evident that, at the present time, because of the lack of knowledge of the snow transport and deposition processes and the complex nature of the accumulation phenomenon, it is impossible for the hydrologist to define snow cover distribution patterns by a physically-based, mathematical model*." Later on in the 1990's first numerical studies considering the connection between the most important transport terms, saltation and suspension, and wind speed as well as direction were presented by Pomeroy and Gray (1995) and Liston and Sturm (1998). Since this time numerous studies about snow transport and its influence on the water balance were carried out in flat terrain (Pomeroy *et al.* 1993; Déry and Yau 1999) or in slightly undulating terrain (Liston and Sturm 1998) (fig. 1).

In most of these studies it is stated that the mountainous snow cover is especially influenced by snow transport (e.g. Pomeroy *et al.* 1997; Liston 2004) but only a few studies are known which have numerically simulated the efficiency of this process (e.g. Pomeroy *et al.* 1997; Lehning *et al.* 2006; Bernhardt *et al.* 2008). Hence, the real impact of blowing snow processes in hydrological modelling of Alpine regions is still unknown. This lack of information can be traced back to the limited knowledge about the wind conditions in Alpine regions (Balk and Elder 2000; Essery 2001; Liston *et al.* 2006; Bernhardt *et al.* 2007). Liston and Sturm (1998) as well as Winstral and Marks (2002) stated that a reasonable description of wind fields in complex terrain is needed for a satisfying description of the Alpine snow cover. Fulfilling this demand was one of the scopes of this work. Hence, wind fields predicted by the physically based *PSU/NCAR MM5* model (Grell *et al.* 2005) were used as an input for the well established snow model *SnowModel* (Liston and Elder 2006) which uses *SnowTran-3D* (Liston and Sturm 1998, Liston *et al.* 2006) as a snow transport routine. The produced *SnowModel* results are discussed on the basis of results calculated under usage of conventionally interpolated wind fields. A validation of the obtained model results will be achieved with the help of station and field campaign measurements of snow depth and remotely sensed data of the snow distribution. Finally, an approach to parameterise the snow heterogeneity in alpine regions as subscale input for regional models is presented.

The thesis was funded by the *GLOWA_Danube* project of the *German Ministry for Education and Research (bmb+f).*

1.2 Introduction and methodology

1.2.1 The snow cover an important land surface feature

Snow is defined as falling or deposited ice particles formed mainly by sublimation (*UNESCO/IHAS/WMO* 1970). Any snow cover is a product of accumulation and ablation processes. Their occurrence and duration is spatially and temporally variable and depends on the distribution of meteorological parameters, topography, and vegetation. Beside global trends like an increase in both snowfall and duration of the snow cover with altitude and latitude, there are a lot of local phenomena influencing the characteristics of the snow cover (Blöschl 1999; Essery and Pomeroy 2004, Liston and Elder 2006, Bernhardt *et al.* 2007). It has to be recognized that only about 5% of world’s total precipitation falls as snow (Hoinkes

1967). But the values can reach 50% to 100% in Arctic or Alpine regions (Winther and Hall 1999; Strasser *et al.* 2007). In general one has to distinguish between *permanent*, *seasonal,* or *temporal* snow covers. A *permanent* snow cover is retrained for many years, *seasonal* and *temporal* snow covers disappear after a certain period. The difference between a *seasonal* and a *temporal* snow cover is that a *seasonal* snow cover exists for months and a *temporal* snow cover for days. The snow cover type that is the subject of this work is a *seasonal* one. This type can be observed north of 60° and in mountainous regions (Rees 2006). The appearance of snow has remarkable effects on the energy balance of the surface and on the hydrological features of an area. The seasonal snow cover leads to the largest annual and inter-annual variations of the land surface albedo (Armstrong and Brodzik 2002; Rees 2006) with respective consequences on the energy fluxes to and from the surface (fig. 2 b) and therefore on the large and local scale climate. From a hydrological point of view, snow is important because it acts as temporal storage of precipitation during the winter season. The stored water is later released as snowmelt and represents an important component of water supply for the downstream population of large mountain-foreland river systems worldwide. Modelling the amount and heterogeneity of the snow water storage in the headwater catchments helps to quantify the available water resources and estimate the timing of their entrainment.

Snow itself is a complex body which is interacting with the atmosphere and the underlying surface. In response to these interactions the crystal structure of the snow pack transforms. Equilibrium and kinetic metamorphism can be observed. The snow pack additionally acts as a cushion between the underlying surface and the atmosphere. It insulates the soil and the underlying vegetation from low winter air temperatures and leaves them much warmer than they would be otherwise (Liston and Elder 2006). This means that increased snow coverage lowers positive fluxes of sensible heat to the atmosphere. Furthermore, melting snow reduces latent heat fluxes. If the snow coverage drops below of 100%, the proportion of the snow covered area is important for the soil moisture, the runoff generation and the energy and moisture fluxes between surface and atmosphere (Ellis and Lethers 1999; Liston and Elder 2006). The snow free fraction shows a different behaviour in comparison to the snow covered one. First off all, the albedo of the surface decreases instantly if the snow cover is gone and a lot more radiative energy is absorbed in consequence. Furthermore, the surface temperature is able to exceed 0°C now. This and the surplus of absorbed energy lead to a rapid increase of the sensible heat fluxes. The available melt energy on the other hand decreases with the snow covered fraction. When considering fig 2 b) it becomes obvious that all of the mentioned fluxes are linearly coupled. Patchy snow covers are common in high alpine regions where wind induced and gravitational snow transport, preferential deposition of precipitation, as well as hillside-inclinations of more than 50°, which prohibit the adherence of snow on the surface, lead to an extremely uneven snow distribution. The resulting snow coverage is mostly below 100% even during the high winter season. Figure 2 a) shows a *Landsat ETM+* image (bands 5, 3, 2; 28.04.04) of the *Watzmann* mountain which illustrates this effect. The turquoise colour represents the snow covered regions. The mesh size of the *Gauss/Krüger* coordinate system is one kilometre (green coloured cells) which matches the medium resolution of many Soil Vegetation Atmosphere Transfer (*SVAT*) models. As one can imagine, all of these cells are partly snow free and would fall in the range of 10% to 90% snow coverage. Understanding the reasons for this heterogeneity and making information about the spatial heterogeneity of the snow cover available for regional scale models (like presented in Mauser and Bach 2008) is the aim of this thesis.

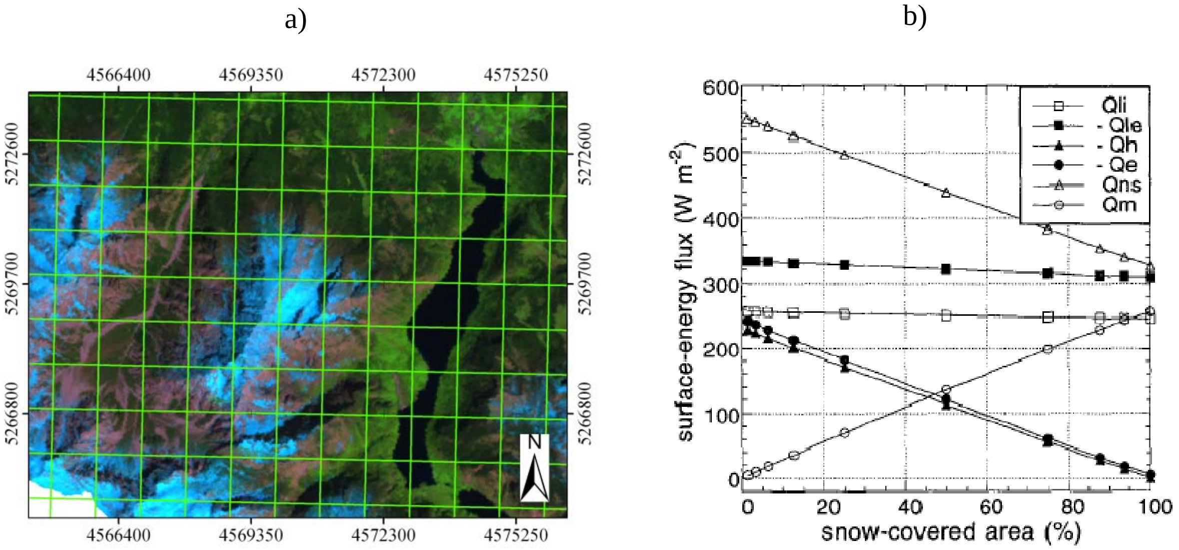

a)

b)

Figure 2: a) Snow cover *at Watzmann* Mountain (turquoise) superimposed by a 1km² grid. b) Interrelation between snow covered area and energy fluxes (Qli = incoming longwave radiation, Qle = emitted longwave radiation, Qh = turbulent exchange of sensible heat, Q_e = turbulent exchange of latent heat, Q_{ns} = net solar radiative flux at the surface, Q_{m} = energy flux available for melt) (cp. Liston 1995)

1.2.2 Snow cover modelling

Over the last decades, a lot of snow models calculating the vertical and the spatial development of the snow cover were presented (Pomeroy *et al.* 1993; Liston and Sturm 1998; Dery and Yau 1999; Essery *et al.* 1999; Winstral and Marks, 2002; Lehning *et al.*, 2006). According to Marsh (1999) and Liston (2004) and Liston and Elder (2006) most of these models tend to a more physically based description of the relevant processes. When omitting empirical or temperature index models the remaining physically based models can be divided into three different groups. The following classification gives a broad but sufficient overview over the most important models and their range of operation. It has to be mentioned that the classification is not strict; the models which are listed under *1-dimensional* models could also be used in a distributed mode. Nevertheless, this is unusual and often impossible because of a lack of input data and because of the computational resources that would be needed. The presented classification is based on the spatial dimensions on which the models are working on.

- *1-dimensional* models are often used for the assessment of avalanche or flood risk. The aim is a precise calculation of the vertical stratification of the snow pack and of the metamorphism of snow and its connection to mechanical properties such as thermal conductivity and viscosity (Spreitzhofer *et al.* 1993). For an adequate description of the mentioned factors, complex and physically based formulations are needed. A numerical solution of these models is only possible if comprehensive input data is available. As this is commonly not the case, these models are limited to well instrumented sites. Very prominent representatives are: *CROCUS* (Brun *et al.* 1989; Brun *et al.* 1992), *SNOWPACK* (Bartelt and Lehning 2002; Lehning *et al.* 2002) and *SNTHERM* (Jordan 1991). The numerical model *CROCUS* has been developed by Météo-France to predict the evolution of the snow pack and its stability with respect to avalanches. *SNOWPACK* was developed by the *Eidgenössisches Institut für Schnee- und Lawinenforschung* (*SLF*) for supporting avalanche warning in *Switzerland* and runs operationally at approximately 100 sites. *SNTHERM* has a different scope and was developed as a routine for runoff forecasting models and is widely used both in the United States and in other countries.

- *2-dimensional* models are usually used as subroutines in atmospheric models and *Soil Vegetation Atmosphere Transfer schemes* (*SVAT*). Stand alone models are seldom but known (e.g. *AMUNDSEN* of Strasser *et al.* 2007). *2-dimensional* models conventionally dispose over one single layer and do not explicitly predict snow crystal metamorphism. Lateral transport processes by wind or gravity are ignored and the subscale snow distribution is commonly approached by a modification of the snow albedo (Liston 2004).
- *3-dimensional* models consist of at least two components, one which calculates the vertical snow cover evolution while the other simulates the snow transport processes. The complexity of the individual components determines whether a model can be used for simulating a complete snow cover period or just some individual transport events. Hence, they have to be divide between I) event based and II) seasonal models:
  - Event based models are usually very complex and used for basic research: Uematsu *et al.* (1991) and Sundsbø (1997) modelled snow transport rates around snow fences; Gauer (2001) modelled snow drift around a single crest. Lehning *et al.* (2002) coupled *SNOWPACK* with a snow drift routine (Doorschot 2002) and with the *Advanced Regional Prediction System* (*ARPS*) (Xue, *et al.* 2000) and applied it to *Gaudergrat* ridge (*Switzerland*).
  - Seasonal transport models in contrast are generally of intermediate complexity. They commonly use a first order approximation of the transport physics and a single layer snow evolution model. The first known seasonal and physically based transport model is the *Prairie Blowing Snow Model* (*PBSM*) (Pomeroy *et al.* 1997) which has strongly influenced the latter development in this area. *SnowTran-3D* which is used in this work is one of the most prominent successors of *PBSM*. Other models like *SYTRON3* (Durand *et al.* 2005) and *ALPINE-3D* (Lehning *et al.* 2006) can be found in literature but are currently not very well documented.

The *Snow Models Intercomparison Project* (*SnowMIP*) (Etchevers *et al.* 2002) has shown that present-day *1-dimensional* snow models are able to reproduce the snow cover evolution very well in close vicinity of a meteorological station. Results become less confident for spatially distributed *2- or 3-dimensional models* especially in areas with complex or mountainous terrain or in forested areas (e.g. Liston 2006). This is due to errors and uncertainties of the meteorological fields that drive the models and due to simplifications of the model formulations with respect to snow-canopy interactions, windblown snow, gravitational snow transport, and preferential snow deposition (e.g. Lehning *et al.* 2006). The extent of which an integration or omission of the indicated processes can improve or deteriorate the accuracy of a snow model depends on the observed scale and area:

- In flat and forested environments snow-canopy interactions like snow sublimation from canopy stands or snow released from branches are the controlling parameters with respect to snow heterogeneity. The involved processes are effective at scales of one to hundreds of meters (Liston 2004; Strasser *et al.* 2007). First results of *SnowMIP2* have shown that a misinterpretation of snow-canopy interactions can lead to almost unusable model results (Rutter and Essery 2006) in these areas/scales.
- In *tundra*, *prairies*, *Arctic* and *Alpine* environments wind induced transport processes, which can be observed at scales of tens to hundreds of meters, are described as decisive (Sturm *et al.* 1995; Essery *et al.* 1999; Essery, 2001; Bernhardt *et al.* 2008a). The high frequency of blowing snow conditions (wind speeds higher than 3m/sec (Liston and Sturm 1998) and the lack of snow cover stabilizing vegetation (Pomeroy *et al* 1997; Pohl *et al.* 2007) is mentioned as the reason for the assumed large impact of blowing snow processes in these regions. But, to the knowledge of the author there is no study available which is describing the quantity of the transported snow masses and the areas which are mainly influenced for an *Alpine* region and on the catchment scale.
- Finally, on scales larger than 1 kilometre, snow cover heterogeneity is mainly influenced by the orographic precipitation gradient (Barros *et al.* 1994; Liston 2004).

1.2.3 Model approach of the presented work

The presented work uses a *seasonal 3-dimensional* model and is focused on wind induced snow transport in *Alpine* regions. For an accurate modelling of snow transport events knowledge about the different transport terms, the snow conditions at a given time step, and the driving force, namely the current wind field, are prerequisites. While the first two requirements can be numerically solved in a satisfying way (Marsh 1999), the calculation of realistic wind fields especially in alpine regions is still an open research topic (Liston and Sturm1998; Winstral and Marks 2002; Raderschall *et al.* 2002; Walter and McCool 2004; Liston *et al*. 2007).

An literature review has shown that wind fields are commonly predicted in two different ways: I) simple interpolations between stations that may or may not include statistical approaches that incorporate information about elevation and relief (Essery 2001; Winstral and Marks 2002) and II) calculations using physically based models (Lehning *et al.* 2002; Bernhardt *et al.* 2008a). It is well known that I) is not feasible in areas with complex terrain (Liston and Sturm 1998; Winstral and Marks 2002; Bernhardt *et al.* 2008a). This is mainly due to the spatial characteristics of wind fields. They are extremely heterogeneous and unsteady because of a nonlinear relation between wind speed and height, as well as synoptic flow and topography dependent wind direction fields. The whole system is furthermore complicated by the turbulent movement of air masses. On the other hand, the hydraulic computation of wind fields with a *meso* scale or *regional* atmospheric model is time-consuming and thus does not allow for the modelling of snow-transport processes over large areas at the spatial scales required to adequately represent the underlying physics (that operate at spatial scales of 200 meters or less). Furthermore, most of the available atmospheric models were not able to estimate high resolution wind fields for complex terrain until today due to unresolved numerical problems.

For the presented work a modified version of the *PSU/NCAR MM5* model (Grell *et al.* 1995; Zängl 2002; Zängl 2003) was used. The model was set up with 5 interactively nested domains (fig. 3). The largest covers most of *Europe* the smallest an *Alpine* area with an extent of 400km². Due to a new formulation of the vertical diffusion term (Zängl 2003) a target resolution of 200 meters could be realized. Since an operational use of *MM5* would reduce the performance of a coupled *SnowModel*/*MM5* algorithm significantly (the calculation of one 200meter wind field needs three days on a high performance computer) a new approach was developed and applied. A static library of separately calculated *MM5* wind fields was used instead of operational model results. The library is connected with the snow model by means of the *German Weather Service Lokalmodell* (*LM*) (*Chapter 3*). This becomes possible as *LM* produce hourly wind fields for an area comparable to one of the *MM5* nesting domains (red rectangle in fig. 3) at the 700hpa level. Using the average wind vector of the *LM* wind field of this area as selection criteria and comparing it to the equivalent information of the available fields in the *MM5* wind field library makes a selection of the most identical field in the library possible. The respective field is used in the *SnowModel* for the current model time step. Hence, the static precompiled *MM5* wind field library is synchronized with the snow transport model over hourly information delivered by *LM*. The presented approach has the advantage that it combines modelling efficiency with a physically based description of the processes affecting local winds and the associated snow redistribution processes. A further advantage is that all of the used models are validated and have been shown to perform well.

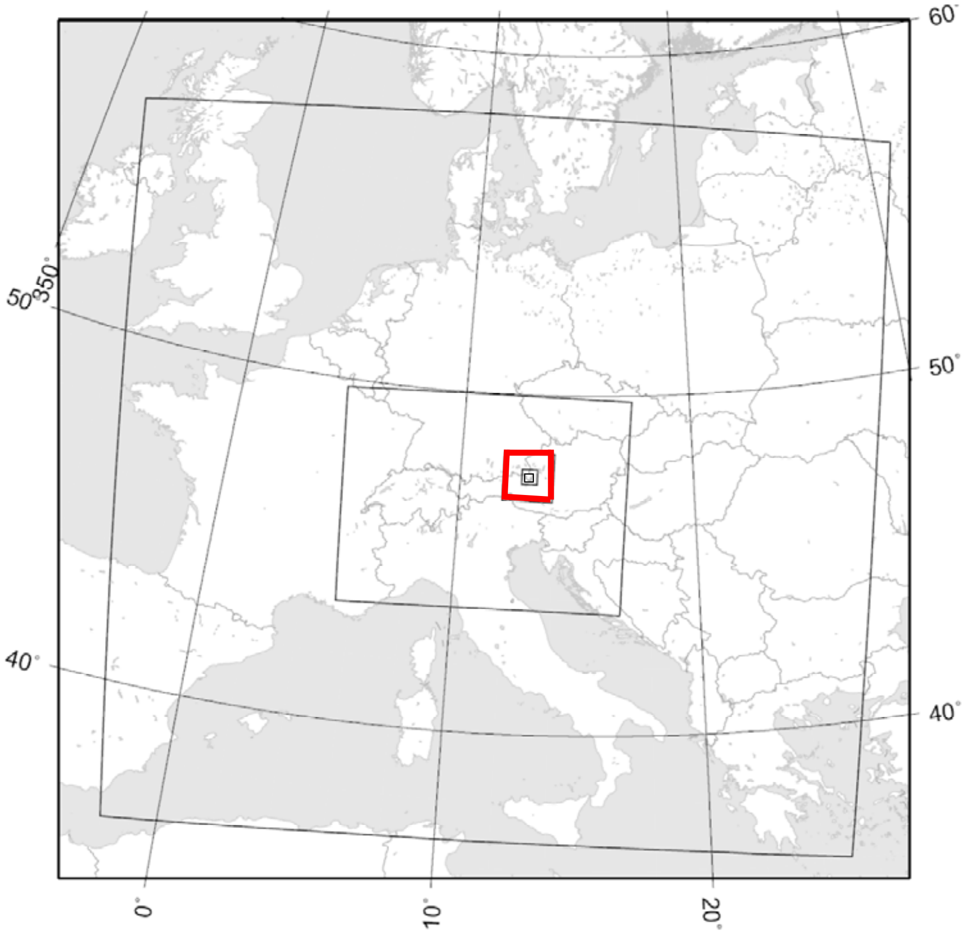

Figure 3: Schematic of the five nested domains used in *MM5*. The largest one is nesting domain_1, the smallest is domain_5. Domain_3 is marked as red rectangle.

It is well known to the author that there are atmospheric or aerodynamic models available which are working at finer scales than the mentioned *MM5* model. Detailed studies of the *Eidgenössisches Institut für Schnee- und Lawinenforschung (SLF)* have shown the capabilities of *ARPS* (Xue *et al.* 2000; Xue *et al.* 2001) and *CFX-4* (AEA, 2001) for event based modelling at a scale of 25 meters. The application of these models is very useful for a better theoretical understanding of wind induced snow transport processes including sublimation of turbulent suspended snow particles. Nevertheless, an operational coupling between these models and snow models is currently impossible because of model limitations and/or unrealistic computational demands.

At the outlook (*chapter 6*), the results of the high resolution model runs serve as the basis for the parameterization of a subscale routine which is able to predict the snow covered fraction of grid cells of *regional* models.

The presented work deals with processes and models which are occurring and working at significantly different scales. Furthermore, it uses data from a coarse scale model (*MM5*) for predicting processes which are occurring at scales of 200m or less (Liston et al. 2006). So, a definition and explanation of the used scales is given in the following section.

1.2.4 Scales used in this work

Operations at three different scales were performed in connection with the presented work, so the used scales and their connection will be declared here. Blöschl (1999) defines three different scales for snow hydrology: 1) the *process* scale 2) the *measurement* scale and 3) the *model* scale. The *process* scale is characterized over the specific characteristic length of a natural process (like the correlation length of the spatial *SWE* variability), the *measurement* scale over the size of e.g. a snow density sample, and the *model* scale over the grid cell size of a distributed model (Blöschl 1999). The *measurement* and the *model* scale are further characterized with three additional terms: *spacing*, *extent* and *support* (Blöschl and Sivaplan 1995). The term *spacing* refers to the distance between samples, the *extent* defines the overall coverage of the data and *support* refers to the integration volume of a sample. Following these terms the *measurement* scale is defined by the distance between the snow poles (*spacing*), the extent of the measurements (*extent*), and the area for which the measurement is representative for (*support*). The *model* scale is defined by the model resolution (*spacing*), the total area which is respected (*extent*) and the scale for which the model formulations are representative for (*support*).

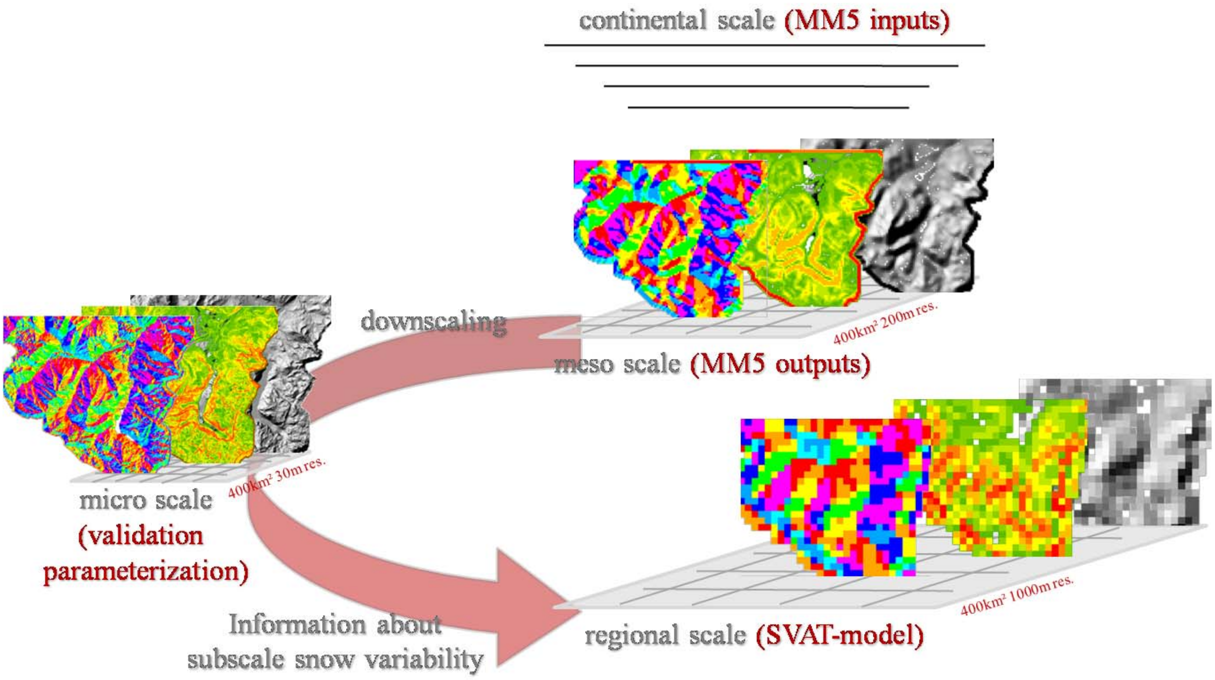
continental scale (MM5 inputs)
downscaling
meso scale (MM5 outputs)
400km^2 200m res.
micro scale
(validation
parameterization)
400km^2 30m res.
Information about
subscale snow variability
regional scale (SVAT-model)
400km^2 1000m res.

Figure 4: Scales used in this thesis. The work starts at the meso scale for which the MM5 wind fields are representative for (200m). After than the wind fields are downscaled to a 30m resolution (micro scale). The *SnowModel* results at the micro scale are validated on the basis of field campaign and remotely sensed data. The information produced by the micro scale runs is used for a parameterisation scheme for the snow heterogeneity which can be used in regional scale Models.

In accordance to Blöschl (1999) the *measurement* and the *model* scale should not differ too much from each other. Hence, the application and validation of the model was progressed at different scales. These scales are defined as the *micro*, *meso* and *regional* scale in the following (fig. 4).

At the *micro* scale the snow model was performed with a spatial resolution of 30 meters and within a total area of 400km². The total area remains the same at the *meso* and *regional* scale but the grid size increases to 200 meters and 1000 meters respectively. As illustrated in Figure 4 the study starts at the *meso* scale (200m resolution) which corresponds to the reachable *extent* and *support* of the meteorological model and to the upper limit of the physical descriptions within the snow transport model (and consequently to the upper limit of the *support* of this model). The overlap between *extent* and *support* of these models allows for a common usage. Hence, the general performance of the coupled wind field/snow model algorithm was tested at this scale and first plausibility checks were made (*Chapter 4*). Subsequently, the *MM5* results were downscaled to a 30 meter resolution (*micro* scale) which exactly fits the *support* and *extent* of the *Landsat ETM+* data and which is close to the *extent* of the snow courses (*Chapter* 4). In a last step, the information which was obtained at the *micro* scale was parameterised to make it available for *regional* scale (1km) land surface models (*Chapter 6*)

1.3 Test Sites and field measurements

The *Berchtesgaden National Park* is located in southeast *Germany* in *Bavaria*, at the southern corner of the administrative district *Berchtesgadener Land* (fig. 5). The park was founded in 1978 and comprises an area of 210 km^2. For the most part, the border of the National Park is represented by the national boundary to *Austria*. Only in the north, the National Park adjoins the settlement areas of the communities *Berchtesgaden*, *Schönau* at the *Königssee* as well as *Ramsau*, all of them at the border of the *National Park*. The valley areas are characterized by extensive forests with larch, spruce and mountain pine stands, subordinated to the *National Park Authority* since 1987. The high alpine area of the National Park includes the massifs *Watzmann* (2713m a.s.l.) and *Hochkalter* (2606m a.s.l.) as well as parts of the massifs *Hoher Goell*, *Hagengebirge*, *Steinernes Meer* and *Reiteralm*, separated from each other by the deep valleys stretching mostly from south to north. Lakes cover an area of approximately 6 km^2. The hydrological drainage of the area is represented by the rivers *Bischofswieser Ache*, *Ramsauer Ache* and *Königseer Ache*. All of these creeks flow into the *Salzach* (*Danube* river system).

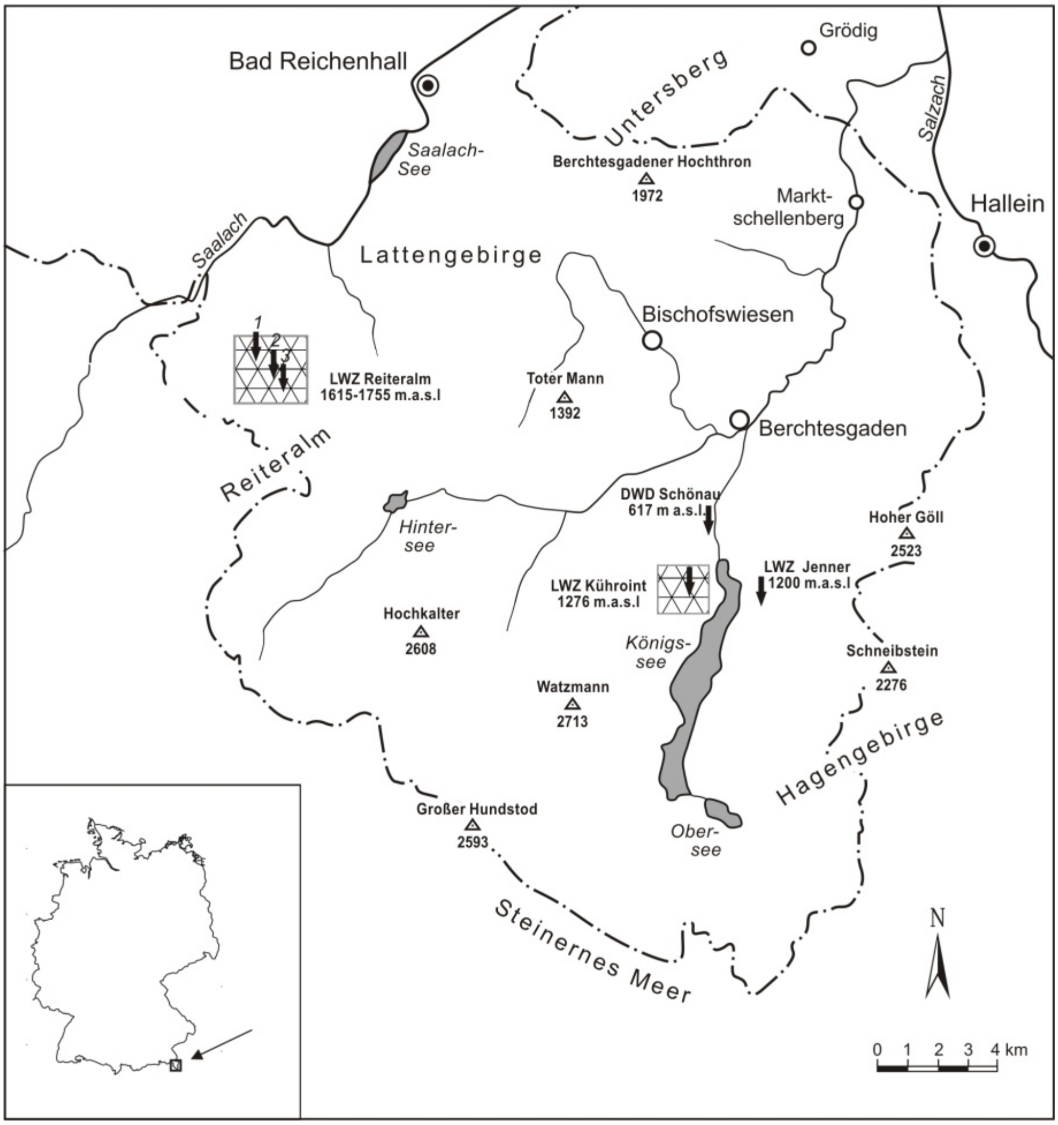
Bad Reichenhall
Grödig
Untersberg
Salzach
Saalach-See
Berchtesgadener Hochthron
1972
Markt-schellenberg
Hallein
Saalach
Lattengebirge
Bischofswiesen
1
2
3
LWZ Reiteralm
1615-1755 m.a.s.l
Toter Mann
1392
Berchtesgaden
Reiteralm
DWD Schönau
617 m a.s.l.
Hinter-see
Hoher Göll
2523
LWZ Kühroint
1276 m.a.s.l
LWZ Jenner
1200 m.a.s.l
Hochkalter
2608
Königs-see
Schneibstein
2276
Watzmann
2713
Hagengebirge
Großer Hundstod
2593
Ober-see
Steinernes Meer
N
0 1 2 3 4 km

Figure 5: Test site (*Berchtesgaden National Park*) (*Bayerisches Landesvermessungsamt* 1994, modified). The locations of *Reiteralm* 1, 2 and 3, *Schönau*, *Kühroint* and *Jenner* are marked with arrows. The test sites at *Reiteralm* and *Kühroint* are displayed as chequered areas.

As an effect of local topography, some small glaciers still exist at altitudes where their specific mass balance would always be negative if only the climatologically processes were taken into account. The *Blaueisgletscher*, the most northern glacier of the Alps, is shaded by the surrounding steep rock walls and fed by wind induced snow transport and avalanches. The *Watzmanngletscher* also receives additional accumulation by wind-blown snow originating from the west slopes of *Watzmann*. Finally, the *Eiskapelle* at 920m a.s.l., a perennial snowfield at the base of the *Watzmann* east face, is fed by both wind-blown snow from the

Watzmann crest and frequent avalanches from the east face which effectively is a snow funnel depositing masses of snow at a location far from where it has fallen, or been eroded. Nevertheless, the glaciers in the *Berchtesgaden Alps* have retreated dramatically during the past decades and it can be assumed that they will completely disappear in the near future (Winkler 2005). Only the *Eiskapelle* has shown little reaction on the changing climate.

Because of the extremely steep topography it is very challenging to model snow processes and snow transport processes here.

Table 1: Geographic position of the National Park

	Geographical		Gauss Krüger (Zone 4)	
Corner	Longitude [°]	Latitude [°]	Easting [m]	Northing [m]
Upper Right	13° 06’ 22’’	47° 43’ 05’’	4583001.00	5287682.00
Lower Left	12° 45’ 17’’	47° 27’ 23’’	4556920.69	5258267.75

The test site was selected for the following reasons:

- The topographic characteristics which guarantee high wind speeds and therefore high snow transport intensities. The area can be seen as representative for high alpine regions.
- The instrumentation of the site. Meteorological Networks of the *Avalanche Warning Service* (*LWD*) and of the German Weather Service / Berchtesgaden National Park (*DWD / NPB*) were available.
- The availability of a high resolution *GIS* database including sophisticated land use information which allows for high resolution distributed modelling.
- The chance to carry out field campaigns with the help of skilled *National Park* Rangers, which had long term experiences in conducting snow courses.
- The general assistance of the partners: the *Avalanche Warning Service* (*LWD*) and the administration of the *Berchtesgaden National Park* (*NPB*), who have provided any data free of charge.

1.3.1 Topography

The *Berchtesgaden* Alps can be seen as a solitary part of the northern limestone Alps. They are located between the rivers *Saalach* and *Salzach* and are characterized by the plateau type of the different massifs and by the petrographical attributes of the rocks. The *Dachstein* limestone is determined within the sediment sequence of this area (*Institut für Landeskunde,* 1970). The area shows steep terrain which traces back to massive crust movements during the Eocene, 45 million years ago. The relief was additionally intensified by the glaciations of the last ice ages.

The minimum elevation of the area is 514 m a.s.l located at the outlet of the *Berchtesgadener Ache* in the north-eastern part of the area whereas the maximum elevation is the crest of *Watzmann* (2713m a.s.l.) Figures 6 give an idea about the relief energy of the area.

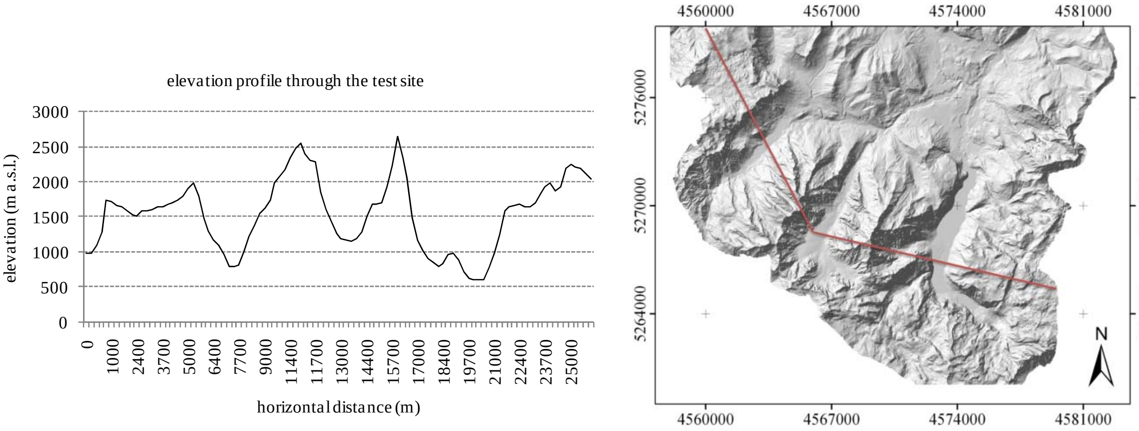
elevation profile through the test site
3000
2500
2000
1500
1000
500
0
elevation (m a.s.l.)
0
1000
2400
3700
5000
6400
7700
9000
11400
11700
13000
14400
15700
17000
18400
19700
21000
22400
23700
25000
horizontal distance (m)
4560000
4567000
4574000
4581000
5276000
5270000
5264000
N

Figure 6: Profile through the National Park area which displays the rapid changes in altitude in the test area.

1.3.2 Climate

The climate of the *National Park* area is subject to significant spatial variability and strongly influenced by a relief gradient of more than 2000 m. Small scale local differences are caused by, for example, the general position in the mountainous landscape, the position in relation to the prevailing winds (windward or leeward), and the solar incidence angles.

The observed mean temperature is 8.1 °C at 470m a.s.l. while for the maximum elevation of 2713 m a.s.l a mean of -2.5 °C was calculated (Enders, 1979). The observed average gradient in temperature with elevation is 0.47 °C per 100 meters (Enders 1979). According to a study of Frei and Schär (1998) the area is located within a wet anomaly extending along the northern side of the Alps. This region shows the highest frequency of days with precipitation (precipitation ≥ 1 mm). The annual precipitation shows measured values of 1655 mm at 500m a.s.l. and estimated values of 2711 mm for an elevation of 2500m a.s.l. The calculated mean for the total area is 1992 mm (Enders 1979). The model runs presented in this work were progresses from August to Juli for covering the total snow cover period. The observed winter seasons are on average if one compares the precipitation and temperatures measured at *Schönau* with the long term average of 1960-1990 (precipitation = 1519mm and temperature = 7.2 °C). The precipitation sum of 2003/2004 was 1532mm and 1473mm in 2004/2005 and the average temperature was 7.1 °C for 2003/2004 and 7.8 °C for 2004/2005.

1.3.3 Meteorological data

Data of four different meteorological stations was available for the presented work. The network of meteorological stations is owned by two different institutions: the stations at *Jenner*, *Kühroint* and *Reiteralm* are operated by the *Bavarian avalanche warning service* (*LWZ*) whereas the *Schönau* station belongs to the network of the *DWD*. Figure 7 shows the location of the different stations.

By connecting these automatic stations via wireless *Global System for Mobile Communications* (*GSM*) transmission with a central database a unique data pool is available which allows the continuous operation of distributed models with a high temporal resolution. Table 3 gives an overview of the parameters which are recorded at each station. All data are aggregated to hourly means (i.e., average for temperature, humidity, wind speed, radiation, and air pressure; sum for precipitation; maximum for maximum wind speed) and checked for plausibility. Missing values due to periods in which a sensor was out of operation are characterized as such. Continuous records of the meteorological parameters start in 1998.

Table 2 Meteorological stations which were used, their abbreviations, geographical coordinates, elevation, and associated meteorological fields: global radiation (GR), humidity (H), precipitation (P), snow height (SH), temperature (T), temperature of the snowpack 0cm above ground (TS0), 20cm above ground(TS2), 4cm above ground (TS4) and 60cm above ground (TS6), wind speed (WS), wind direction (WD)

Station	**Elev (a.s.l.)**	**Long**	**Lat**	**Resolution**	**Parameters**
Kühroint	1407	12,57	47,34	10 min	T,H,GR,WS, WD, P
Reiter Alm I	1755 m	12,80	47,65	10 min	WS, WD
Reiter Alm II	1670 m	12,80	47,64	10 min	H, SH, T, TS0, TS2, TS4,TS6
Reiter Alm III	1615 m	12,81	47,64	10 min	GR, H, P, SH, T
Jenner	1200 m	13,01	47,58	10 min	H, SH, T, TS0, TS2, TS4
Schönau	617 m	12,98	47,60	10 min	T, H, GR, WS, WD, P

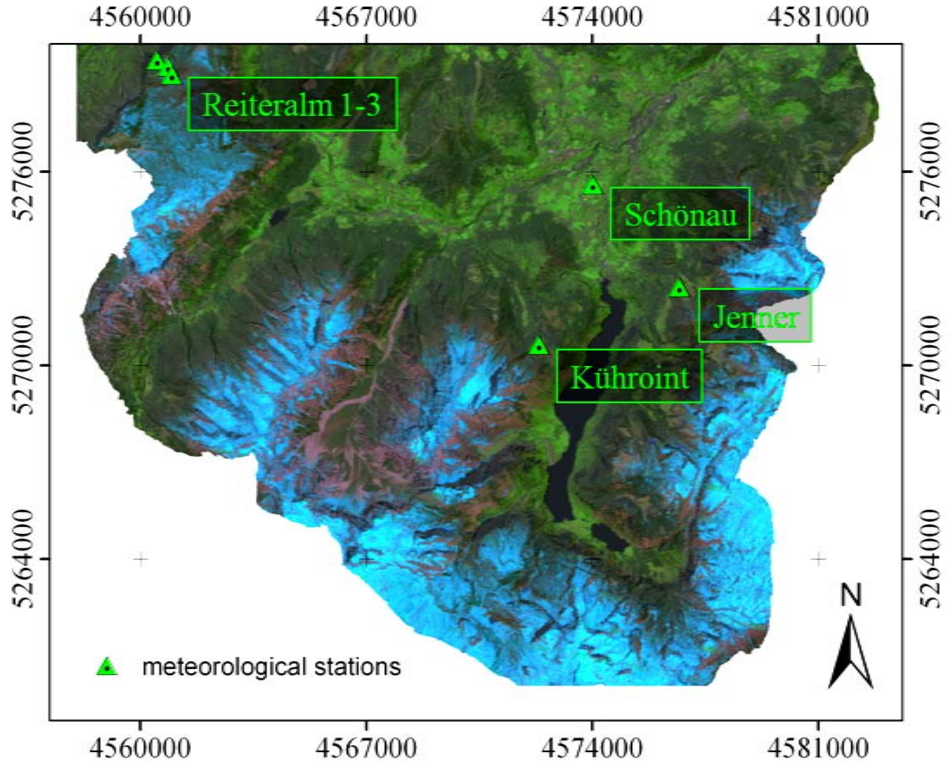
4560000
4567000
4574000
4581000
5276000
5270000
5264000
Reiteralm 1-3
Schönau
Jenner
Kühroint
N
meteorological stations

Figure 7: Location of the meteorological stations.

1.3.4 Spatial data sets

In addition to the meteorological data, a *GIS* providing information on vegetation and topography was used. The administration of the *Berchtesgaden National Park* has developed a wide set of GIS data over the past years. The cartographic reference system of all data is

Gauss Krüger (*Zone 4*/*WGS 84* ellipsoid). The original data has a resolution of 10m x 10m but was resampled to 30m x 30m and 200m x 200m respectively using the mean value for the elevation data and the majority in the case of vegetation data. These resolutions correspond to the available remotely sensed data *(Landsat ETM+/*30m) and to the topographic information and grid increment used by the *MM5* model (200m) (fig. 8). The elevation data set originates from an analysis of 20m contour line maps (personal communication H. Franz 2007). The individual vegetation types were classified over a hierarchical scheme presented by the *Bundesamt für Naturschutz* (1995), using colour infrared aerial photos of 1997. As the resulting 101 classes are too detailed for this work they were aggregated to a final of 23 classes. This number of classes was chosen because it is slightly below the maximum number of classes the snow transport model (chapter 2.1.2) can process and allows for a meaningful aggregation of the original classes.

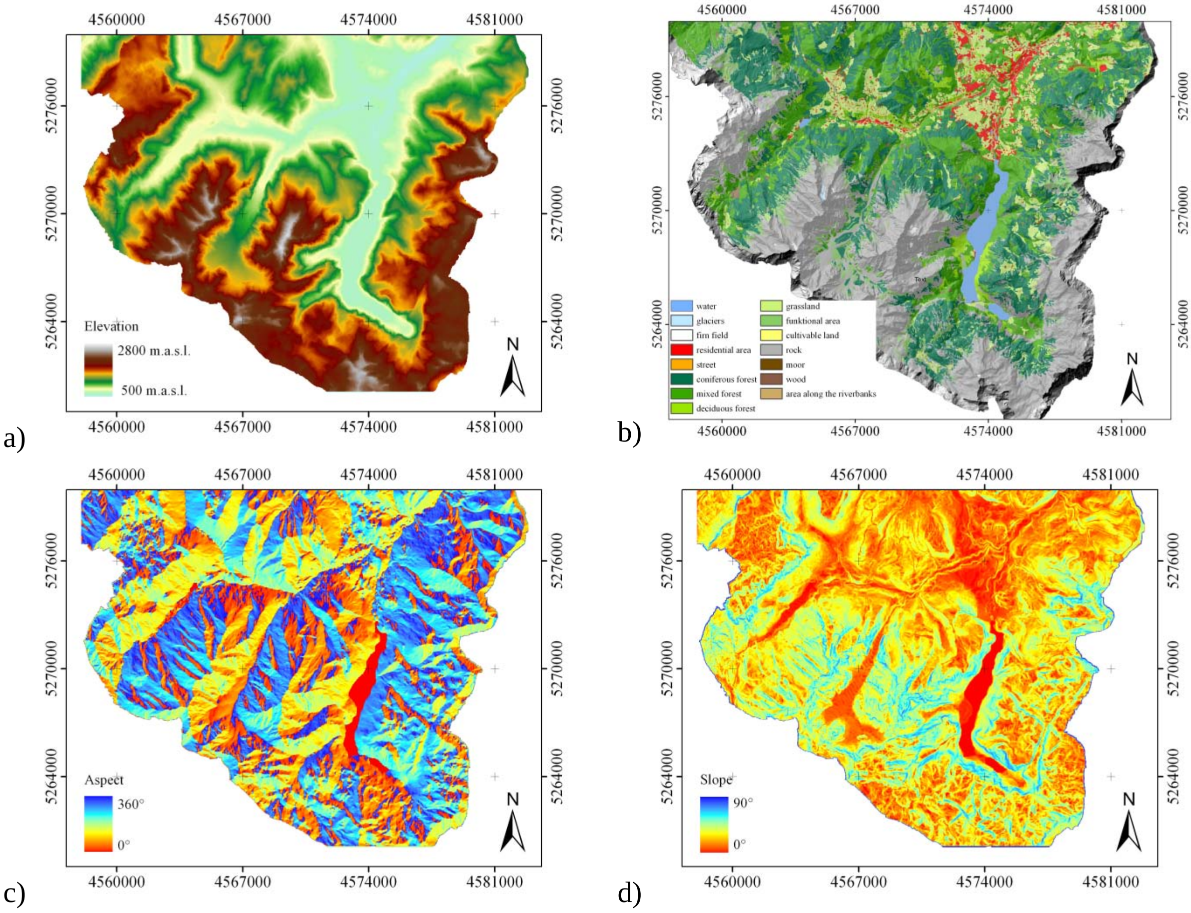
4560000
4567000
4574000
4581000
5276000
5270000
5264000
Elevation
2800 m.a.s.l.
500 m.a.s.l.
N
a)
water
glaciers
firn field
residential area
street
coniferous forest
mixed forest
deciduous forest
grassland
funktional area
cultivable land
rock
moor
wood
area along the riverbanks
b)
Aspect
360°
0°
c)
Slope
90°
0°
d)

Figure 8: GIS data used in this work. a) elevation (m a.s.l.), b) vegetation types, c) aspect (°) and d) slope (°)

1.3.5 Field campaigns

To evaluate the *micro* scale simulations, field measurements of snow depth were carried out. The choice of test sites was determined mainly by the accessibility of the region during the winter season. Hence, areas at *Kühroint* and *Reiteralm* were chosen (fig. 9 and fig. 10). Both can be reached easily, the first over a logging route and the second over a cable railway.

The *Reiteralm* (fig. 5, fig.9) plateau as a whole is made of *Dachstein* limestone and *Ramsau* dolomite and is characterized by an extensive flatland perched between 1500m a.s.l. and 2000m a.s.l. and sharp drops around the edges. The average elevation of the part in which the test-site is located in is 1700m a.s.l. the minimum and maximum elevations are 1610m a.s.l. and 1753m a.s.l. respectively. Mountain pine is the dominant vegetation type, followed by meadows and spruce.

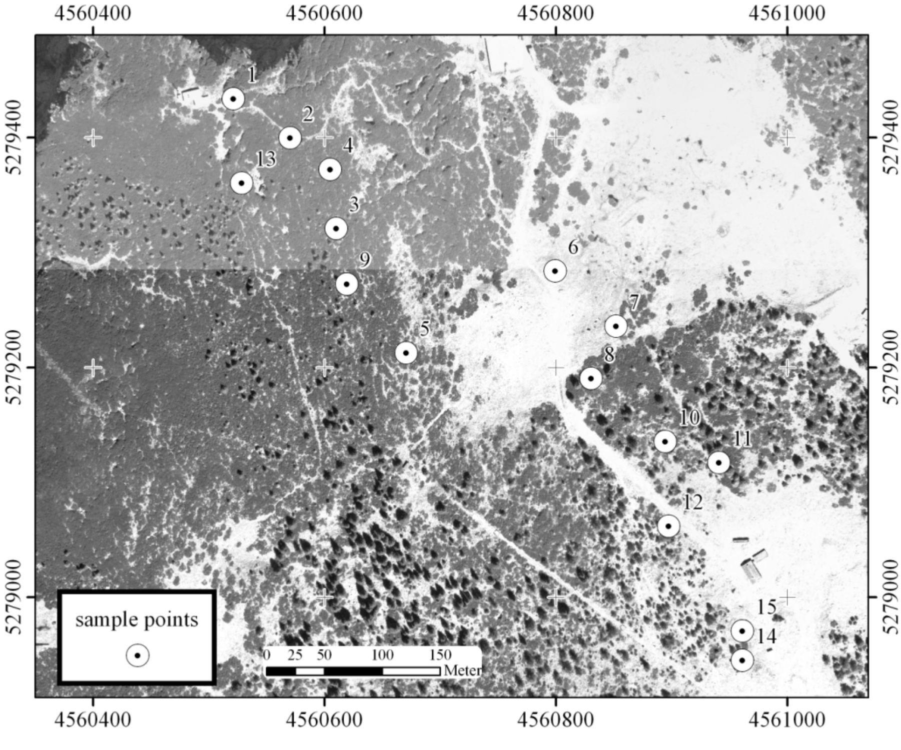

Figure 9: Sample points at Reiteralm. 15 sample points were installed in the winter season 2004/05 the points are named 1-15.

The mountain pasture *Kühroint* is located at approximately 1420m a.s.l. in the north-eastern part of the *Watzmann* massif (fig. 5). Three different land use types can be found at this site:

grassland, clear cut, and coniferous forest (fig. 10). The absolute difference in elevation is small (70 meters in total). The clear cut and the coniferous forest show undulating terrain with small hills of about five meters in height and an extent of 30 to 40 meters. The grassland in contrast is more planar and rises in a westerly direction. In 2004, the existing meteorological station at *Kühroint* was replaced with a new, fully automated, station of the *Avalanche Warning Service of Bavaria* (*LWD*) (the instrumentation can be found in tab. 2). Additionally, a snow pillow was installed but the data was not available for the winter season of 2004/05 due to a technical problem.

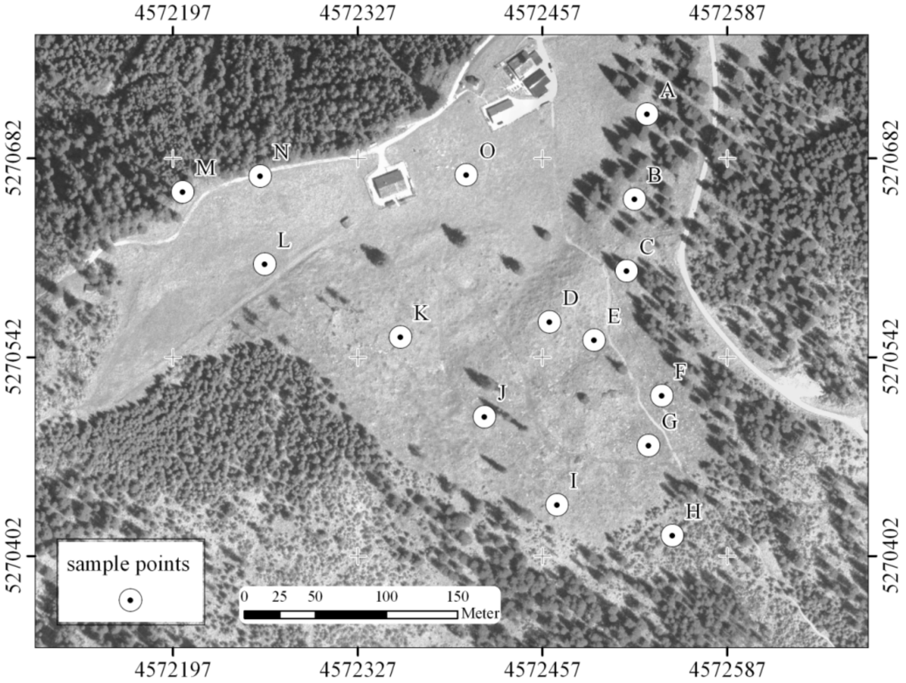

Figure 10: Sample points at Kühroint. 15 sample points were installed in the winter season 2004/05 the points are named A-O.

More remote sites at higher elevations would be desirably but were not feasible because of the expected risks.

A major problem of snow depth measurements is that every measurement influences the snow pack and its further development. To minimize this effect staff gauges were installed which can be read with the help of binoculars. The snow depth indicated by the staff gauges was routinely checked with snow pole measurements. These additional controls were needed because of the possible drift of the staff gauges due to e.g. snow pressure.

Measurements on 11 dates at 30 staff gauges were taken between February and April 2005 (the exact dates of the measurements are given in Tables 7 and 8). The choice of the location of the sample points bases on an analysis of the *GIS* and of the vegetation map. The objective of this process was to find representative points which allow for a characterization of the total study area. It was our plan to carry out a continuous series of weekly measurements but in some cases the intended interval could not be maintained due to difficult meteorological conditions and high avalanche risk

Chapter 2 Model descriptions

The output from four different models was used for the presented work. For the estimation of the snow cover evolution, and of the meteorological fields, *SnowModel* (Liston *et al.* 2006) was utilized. Wind fields were predicted by a modified version of the *PSU/NCAR MM5* model (Grell *et al.* 1995). To connect *SnowModel* and the *MM5* wind fields during runtime, analysis results of *DWD Lokalmodell (LM)* (Adrian and Frühwald 2002) were used. As all of the named models are well documented in literature, only a short overview about the most important model formulations and modifications will be given in the next sections.

2.1 SnowModel

The ***SnowModel*** (Liston and Elder 2006) consists of six independent parts:

The quasi-physically-based meteorological distribution model ***MicroMet*** (Liston and Elder 2006) is used for the spatial interpolation of measurements of: air temperature, incoming longwave radiation, incoming solar radiation, precipitation, relative humidity, surface pressure, wind direction, and wind speed.

In a first step a Barnes objective scheme is applied (Eq. 1, Barnes 1964, 1973; Koch *et al.* 1983) to interpolate data from irregularly spaced stations to a regular grid (Liston and Elder 2006).

$$w = exp\left[\frac{r^2}{f(dn)}\right] \qquad \text{(Eq. 1)}$$

Barnes interpolation scheme (Koch, et al. 1983): w = interpolation weights, r = distance between observation and observed grid point, *f*(dn) = filter parameter which defines how smooth the interpolated field will be.

Afterwards different known relationships between meteorological parameters and terrain are used to modify the datasets (Liston and Elder 2006).

In the case of air temperature, lapse rates between the existing meteorological stations are used for the spatial distribution of the point measurements (Eq. 2 and 3).

$$T_0 = T_{stn} - \Gamma(z_0 - z_{stn}) \qquad \text{(Eq. 2)}$$

$$T = T_0 - \Gamma(z - z_0) \qquad \text{(Eq. 3)}$$

Calculation of the gridded air temperature: T [°C]. T_0 = air temperature at reference level, T_{stn} = observed temperature at station elevation, z = topographic elevation of the topographic dataset, z_0 = sea level, z_{stn} = station elevation, Γ = lapse rate [$C°m^{-1}$], T [°C] = gridded air temperature at the elevation of the topographic dataset.

As the relative humidity (Eq. 4) is a non-linear function of elevation the relative linear dew point temperature is used for elevation adjustments. In order to do that, the station measurements are first converted into dew point temperatures (Eq. 6), and subsequently adjusted to a common reference level using the dew point temperature lapse rate (Eq. 7) (Kunkel 1989) which can be predicted through station measurements. The reference level data are then distributed using the Barnes objective scheme and converted back into relative humidity in a final step (Liston and Elder 2006).

$$RH = 100\frac{e}{e_s} \qquad \text{(Eq. 4)}$$

Calculation of the relative humidity: RH = relative humidity, e = actual vapour pressure [Pa] e_s = saturation vapour pressure (Eq. 5)

$$e_s = a\ exp\left(\frac{bT}{c+T}\right) \qquad \text{(Eq. 5)}$$

Calculation of the saturation vapour pressure: e_s[Pa] = saturation vapour pressure at temperature T [°C], for water (a = 611.21[Pa], b = 17.502, c= 240.97[°C]), for ice (= 611.15[Pa], b = 22.452, c= 272.55[°C]) (Buck 1981)

$$T_d = \frac{c\ ln(e/a)}{b - \ln(e/a)} \qquad \text{(Eq. 6)}$$

Calculation of the dew point Temperature: T_d = dew point temperature.

$$\Gamma_d = \lambda\frac{c}{b} \qquad \text{(Eq. 7)}$$

Calculation of the dew point temperature lapse rate (Kunkel 1989)

Equation 8 was used to interpolate the measured precipitation rates to the model grid. The topographic reference level was calculated with the help of station elevations. This was done since the precipitation adjustment factor (Thornton *et al.* 1997) is a nonlinear function that uses elevation difference not total elevation.

$$P = P_0 \left[\frac{1+ \chi(z-z_0)}{1-\chi(z-z_0)}\right] \quad \text{(Eq. 8)}$$

P is precipitation [mm h-1], P0 = interpolated station precipitation, z = topographic elevation of the topographic dataset, z_0 = station elevation surface, χ = monthly varying factor [km^{-1}] (Thornton et al. 1997)

The incoming solar radiation is predicted with a set of equations, considering the influence of the cloud cover, direct and diffuse solar radiation, as well as slope and aspect of the respective pixel. The cloud fraction is predicted over the relative humidity at the 700-mb level (Eq. 9, Walcek 1994).

$$\sigma_c = 0.832 \exp\left(\frac{RH_{700}-100}{41.6}\right) \quad \text{(Eq. 9)}$$

Calculation of the cloud fraction. σ_c = cloud fraction [$0 \leq \sigma_c \geq 1$], RH_{700} relative humidity at 700hpa level which is predicted over the presented temperature lapse rates.

The solar radiation which is striking earth’s surface is predicted via Equations 10. The direct and diffuse proportion of the net sky transmissivity is predicted over equations 11 and 12 (Burridge and Gadd 1974).

$$Q_{si} = S * (\psi_{dir}\text{cos}i + \psi_{dir}\text{cos}Z) \quad \text{(Eq. 10)}$$

$$\psi_{dir} = (0.6 - 0.2cosZ)(1.0 - \sigma_c) \quad \text{(Eq. 11)}$$

$$\psi_{dif} = (0.3 - 0.1cosZ)\sigma_c \quad \text{(Eq. 12)}$$

Calculation of the solar radiation in dependence of the sloping and zenith angle. Q_{si} = solar radiation which is reaching earth’s surface [W m^{-2}], i = angle between a sloping surface and solar radiation, S* = 1370 W m^{-2} (Kyle et al., 1985), Ψ_{dir} = direct net sky transmissivity, Ψ_{dif} = diffuse net sky transmissivity.

Following Liston and Sturm (1998) wind speed and direction were spatially distributed using empirical wind topography relationships (Ryan 1977; Liston and Sturm 1998). To avoid the 0/360° direction line problem when interpolating the station measurements, wind speed *W* (m/s) and direction θ were converted into zonal and meridional components u (m/s) and *v* (m/s) (Liston and Sturm, 1998; Liston and Elder 2006).

$$u = -Wsin(\theta) \quad \text{(Eq. 13)}$$

$$v = -Wcos(\theta) \quad \text{(Eq. 14)}$$

Calculation of the zonal and meridional components of wind speed and direction: u = zonal component, v = meridional component, W = wind speed, θ = wind direction.

After spatial interpolation the resulting values are converted back to speed and direction:

$$W = \sqrt{u^2 + v^2} \qquad \text{(Eq. 15)}$$

Conversion of meridional and zonal components to W = wind speed [m/sec]

$$\theta = \frac{3\pi}{2} - \tan{}^\wedge - 1\left(\frac{v}{u}\right) \qquad \text{(Eq. 16)}$$

Conversion of meridional and zonal components to θ = wind direction [°]

Finally, wind speed and direction are modified with respect to topography using approaches by Liston and Sturm (1998) and Ryan (1977). For the modification of the wind speed a scaled slope (Ω_s) and a scaled curvature (Ω_c), in combination with two weighing factors (λ_s and λ_c) were used (Liston and Elder (2006) give a precise description of these parameters):

$$W_W = 1 + \lambda_s\Omega_s + \lambda_c\Omega_c \qquad \text{(Eq. 17)}$$

Modification of the wind speed with respect to the topography: W_W = Modification value, λ_s and λ_c = empiric weight factors, Ω_s = scaled slope, Ω_c = scaled curvature.

Based on this the terrain modified wind speed (W_t), is calculated from:

$$W_t = W_W * W \qquad \text{(Eq. 18)}$$

Calculation of the terrain modified wind speed W_t [m/sec] (Liston and Sturm 1998). W = wind speed, W_W = Modification value

The wind direction is modified by the diversion factor θ_d (Ryan, 1977) which is added to the wind direction (ζ is the slope aspect):

$$\theta_d = -0.5\Omega_s \sin[2(\xi - \theta)] \qquad \text{(Eq. 19)}$$

Calculation of the diversion factor θ_d[°] (Ryan 1977): θ = wind direction, Ωs = scaled slope, ζ is the slope aspect.

The terrain modified wind direction (θ_t), is calculated from:

$$\theta_t = \theta + \theta_d \qquad \text{(Eq. 20)}$$

Calculation of the terrain modified wind direction θ_t [°] (Ryan 1977). θ = wind direction, diversion factor $\theta_{d.}$

Finally, the wind fields are modified with a vegetation weighting factor considering the leaf area index (LAI) and the vegetation height (ρ).

$$W_{ca} = e^{((0.9*LAI)(1.0-(0.6*\rho)/\rho))} \qquad \text{(Eq. 21)}$$

Calculation of the wind speed in canopy stands W_{ca} [m/sec]. LAI = leaf area index, ρ = vegetation height.

The snow model wind interpolation routine was identified as a limiting part of the model that should be improved or replaced (Liston and Sturm 1998). Hence, a *MM5* wind field library was created in the course of this work and was used instead of the described interpolation routine (cp. eq. 13-20).

Enbal is described in detail in Liston (1995) and Liston *et al.* (1999). It predicts the surface temperature of the snow pack as well as the energy and moisture fluxes to and from the snow pack (eq. 22). The driving meteorological fields are provided by *MicroMet.*

$$(1-\propto)Q_{si} + Q_{li} + Q_{le} + Q_h + Q_e + Q_c = Q_m \tag{Eq. 22}$$

Basis equation of EnBal: Q_{si} = solar radiation, Q_{li} incoming longwave radiation, Q_{le} emitted longwave radiation, Q_h = turbulent exchange of sensible heat, Q_e = turbulent exchange of latent heat, Q_c = conductive energy transport, $Q_{m\,=}$ energy flux available for melt, α = surface albedo.

The formulations used within the model allow for an application in complex mountainous terrain (Liston 1995). In a first step the melt energy Q_m is defined to be zero and Eq. 22 is solved in an iterative way. A resulting surface temperature greater than 0° in the presence of snow indicates that energy for melt is available. In this case the surface temperature is fixed to 0°C and Eq. 22 is solved for Q_m.

SnowPack (Liston and Hall 1995): is a simple, single layer snowpack evolution model. This model should not confused with *SNOWPACK* of Bartelt and Lehning (2002) which is the operational snow model of Switzerland's avalanche warning service.

Within *SnowPack* the precipitation is assumed to fall as snow if the wet-bulb temperature (eq. 23) is lower than 1°C (Liston and Hall 1995).

$$T_{wb} = T_a + \left(e_a - e_s(T_{wb})\right)\left(\frac{0.622}{Pa}\frac{L_s}{C_p}\right) \tag{Eq. 23}$$

Approach for the calculation of the wet bulb temperature T_{wb} (Rogers 1979): e_a = vapour pressure of the air, e_s = vapour pressure of the surface, T_a = air temperature, L_s = specific heat of air, L_s = latent heat of sublimation, Pa = atmospheric pressure.

The fallen precipitation is then added to the snow pack, and its new density is predicted with an equation of Anderson (1976):

$$\rho_{ns} = 50 + 1.7(T_{wb} - 258.16)^{1.5} \tag{Eq. 24}$$

Calculation of the snow density ρ_{ns}(Anderson 1976): T_{wb} = wet bulb temperature.

As snow is, in general, a mixture of ice crystals, liquid water, and air, the snow density can also be modified by the liquid water content and the weight of the overlying snow. If melt occurs the liquid water will stay within the snow pack until a threshold density is reached. If this is the case any additional water will leave the snow pack (Liston and Hall 1995). All energy related calculations at the surface of the snow cover including ground sublimation are processed in *EnBal*.

SnowTran3D (Liston and Sturm 1998) is a three-dimensional model, able to simulate the transport terms: saltation, suspension, and sublimation (fig. 11). *SnowTran3D* has proven its applicability in a wide variety of landscapes (Green *et al.* 1999; Liston *et al.* 2000; Prasad *et al.* 2001; Hiemstra *et al.* 2002, Hasholt *et al.* 2003; Bruland *et al.* 2004) including the European Alps (Bernhardt *et al.* 2008a). The model algorithms which are important for a better understanding of subsequent steps are presented in the next section. A more detailed documentation of the model can be found in Liston and Sturm (1998) and Liston *et al.* (2006).

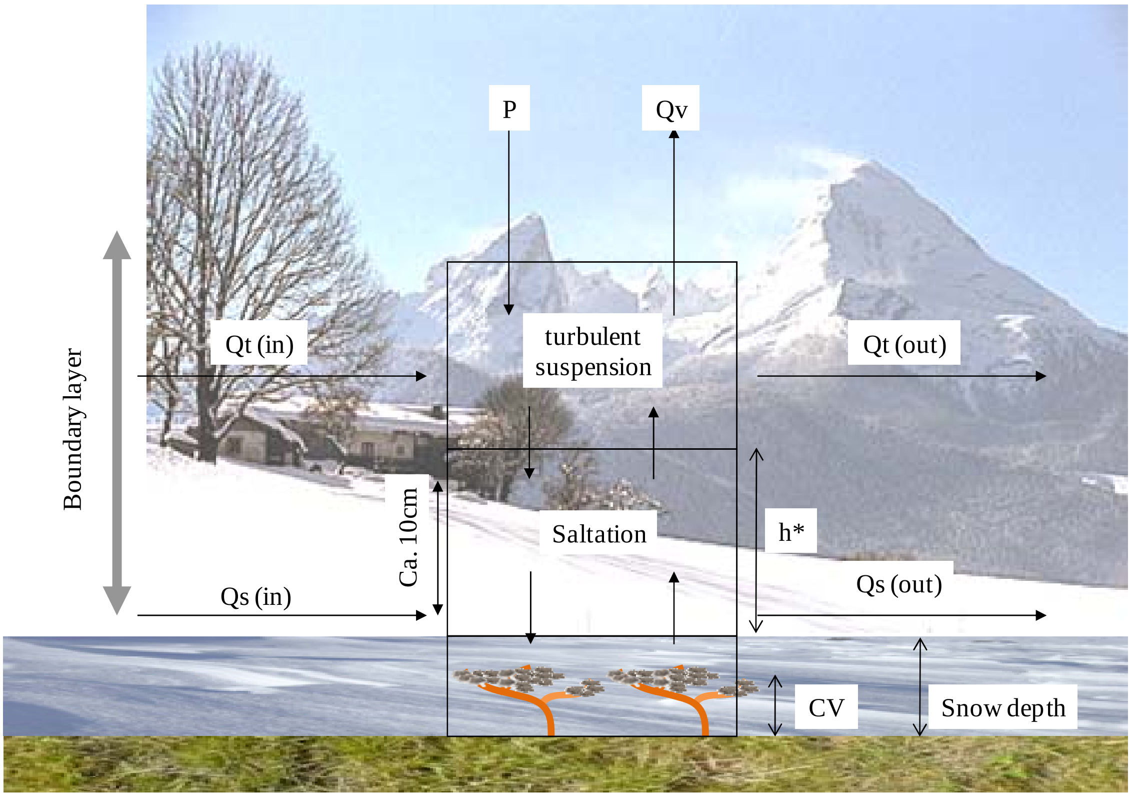

Figure 11: Schematic illustration of the transport model. Qt = mass transport rates of saltation, Qv = mass transport rates of turbulent suspended snow, Qs = sublimation of transported snow particles. P = water equivalent precipitation rate. CV = snow holding capacity. h_* = top of the saltation layer.

Equation 25 shows the mass balance equation on which *SnowTran-3D* is based on.

$$\frac{\mathrm{d}\zeta}{\mathrm{d}t} = \frac{1}{\rho_s}\left[\rho_w P - \left(\frac{\mathrm{d}Q_s}{\mathrm{d}x} + \frac{\mathrm{d}Q_t}{\mathrm{d}x} + \frac{\mathrm{d}Q_s}{\mathrm{d}y} + \frac{\mathrm{d}Q_t}{\mathrm{d}y}\right) + Q_v\right] \qquad \text{(Eq. 25)}$$

Mass balance equation of *SnowTran-3D*. ζ = snow depth (m), ρ_s = snow density (kg m^{-3}), ρ_w = water density (kg m^{-3}), P = precipitation rate (m s^{-1}), Q_s = saltation rate (kg m^{-1} s^{-1}), Q_t = amount of turbulent suspended snow (kg m^{-1} s^{-1}), Q_v = sublimation of transported snow particles (kg m^{-1} s^{-1}), t = time (s), x = horizontal coordinates in west east direction (m), y = horizontal coordinates in north south direction (m).

SnowTran-3D is able to predict the most effective transport terms saltation and turbulent suspension while creeping is neglected. The description of the saltation process follows Pomeroy and Gray (1990).

$$Q_{s\_max} = \frac{0.68}{u_*}\left(\frac{\rho_a}{g}\right) u_{*t}\left(u_*^2 - u_{*t}^2\right) \qquad \text{(Eq. 26)}$$

Estimation of the equilibrium saltation rate: Q_{s_max} = saltation transport rate (kg m^{-1} s^{-1}), ρ_a = air density (kg m^{-1}), u_* = friction velocity, g = gravity (m^{-1} s^{-2}), t = time(s) u_{*t} = 0.25 (m s^{-1}).

The amount of snow which is transported at a given time step largely depends on the shear stress which the wind exerts on the surface. Bagnold (1941) has defined two threshold values, the impact and the fluid threshold velocity, with the fluid threshold velocity exceeding the impact threshold velocity. Pomeroy (1988) found that the difference between the two threshold velocities is negligible. Based on his work, the threshold friction velocity u_* (Eq. 27) is commonly used instead of the terms defined by Bagnold.

$$u_* = u_r \frac{\kappa}{ln(z_r/z_0)} \qquad \text{(Eq. 27)}$$

Threshold friction velocity u_* (m s^{-1}) (Pomeroy, 1988): u_r = wind speed at reference height (m s^{-1}), z_r = reference height (m), z_o = roughness length, κ = Kármán’s constant.

The threshold velocity which is needed for initializing the saltation can be modified by the roughness length of the surface (z_0) (eq. 29). The roughness length mainly depends on the snow depth fraction (eq. 28) and on the vegetation types of an area.

$$F_s = \frac{\zeta}{C_v} \qquad \text{(Eq. 28)}$$

Estimation of the depth fraction of vegetation covered by snow F_s: ζ = snow depth (m), C_v = vegetation specific snow holding capacity (m).

The snow holding capacities are between 0m (rock) and 15m (coniferous forest) (Liston and Sturm 1998).

$$z_0 = F_s\, z_{0\_snow} + (1 - F_s) z_{0\_veg} \tag{Eq. 29}$$

Calculation surface roughness length z_0. F_s = depth fraction of vegetation covered by snow, z_{0_snow} = roughness length of snow (0.001), $z_{0\_vegetation\_}$ = roughness length of a vegetation covered surface (this value is approximated by: 0.25 * snow holding capacity)

If the wind speed is strong enough snow particles can be picked up by turbulent eddies and will enter into suspension. During snowdrift suspension the particle paths are fluctuating around a certain average height which is dependent on the immersed weight of the particles and on the balance between turbulent energy and gravity (Bintanja, 2000). The maximum thickness of the suspension layer is an object of discussion, the values in literature ranging from a few meters (Kobayashi, 1972; Takeuchi, 1980) to a several hundred meters (Budd et al., 1966).

Saltation has to be present to initialise turbulent suspension (eq. 30) (Liston and Sturm 1998). The saltation layer provides the lower boundary conditions and determines whether and to which degree turbulent suspension occurs. The equation which defines the concentration of snow within the turbulent-suspension layer follows Kind (1992).

$$\phi_t(x^*, z) = \phi_r \left[\left(\frac{\phi^*}{\phi_r} \frac{u_*}{s} + 1 \right) \left(\frac{z}{z_{tr}} \right)^{-s/ku^*} - \frac{\phi^*}{\phi_r} \frac{u_*}{s} \right] \tag{Eq. 30}$$

Concentration of blowing snow within the suspension layer (Kind 1992): $ø_t$ = turbulent suspension layer (kg m^{-1} s^{-1}), $ø_r$ = mass concentration at reference level (kg m^{-1} s^{-1}), z = height coordinate (m), x^* = horizontal coordinate (m), $ø^*$= is a concentration scaling parameter, u_* = wind shear velocity (m s^{-1}), s = particle settling velocity (m s^{-1}), z_{tr} = height of the reference level, k = Kármán’s constant.

The concentration reference level z_{tr} (m) corresponds to the top of the saltation layer h_* (m) which ensures continuity between these two model layers. The horizontal particle velocity within the saltation layer (u_*) that is needed to solve Eq. 31 is assumed to be constant with height and follows Pomeroy and Gray (1990) (fig. 12).

$$h_* = 1.6 \frac{u_*^2}{2g} \tag{Eq. 31}$$

Particle velocity within the saltation layer (Pomeroy and Gray 1990): h_* = top of the saltation layer (m), u_* = wind shear velocity (m s^{-1}), g = gravity (m s^{-2}).

The saltation layer mass flux is defined as independent of height, which is a known oversimplification (McKenna-Neuman and Nickling, 1994) but has to be used in this form until more valid formulations are available (Liston and Sturm 1998).

Lehning et al. (2002) criticised the presented algorithms of turbulent saltation/suspension for unsteady terrain because of Equation 26 which neglects advective and non-steady effects. This is a valid argument at the point scale but the effect at the catchment scale should be negligible (personal communication Liston and Pomeroy 2006) which makes the Equation applicable for this study.

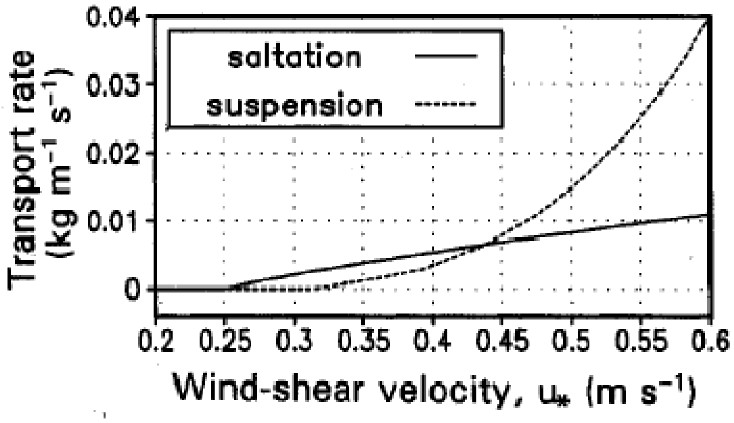

Figure 12: Connection between wind-shear velocity and transport rate (cp. Liston and Strum 1998)

The moisture fluxes due to sublimation between a snow pack and atmosphere are comparatively small, but considerable fluxes can be observed if snow particles are in transport (Hood et al. 1999, Strasser et al. 2007). The exact explanation of the equations used in *SnowTran-3D* can be found in Schmidt (1972), Pomeroy et al. (1993), Pomeroy and Gray (1995) and Liston and Sturm (1998). The principle formulation of the sublimation rates are given in Eq. 32 for one homogenous transport layer and Eq. 33 for saltation in combination with turbulent suspension.

$$Q_v(x^*) = \int_0^{z_t} \Psi\,(x^*, z)\phi(x^*, z)\mathrm{d}z \qquad \text{(Eq. 32)}$$

Sublimation rates if only one transport layer exists: Q_v = sublimated amount of transported snow per unit area of snow cover (kg m^{-1} s^{-1}), Ψ = sublimation loss rate coefficient (s^{-1}), ø = vertical mass distribution (kg m^{-3}). The integration limits are from the surface through the upper boundary of the transport layer, x^*= horizontal coordinate (m), vertical coordinate, z_t =

$$Q_v(x^*) = \Psi_s\phi_s \mathrm{h}_* + \int_{h_*}^{z_t} \Psi_\mathrm{t}\,(x^*,z)\phi_t(x^*,z)\mathrm{d}z \qquad \text{(Eq. 33)}$$

Sublimation rates of the saltation and sublimation layer: Q_v = sublimated amount of transported snow per unit area of snow cover (kg m^{-1} s^{-1}), the nomenclature is like in Eq. 32. The subscripts s and t refer to the saltation and turbulent suspension layer.

The calculation of the sublimation rates additionally depends on the humidity gradients between the snow particles and the atmosphere, conductive and advective moisture fluxes, snow particle size, and the intercepted solar radiation per snow particle (Liston and Sturm 1998).The respective Equations can be found in the Appendix I.

2.2 MM5 model

The numerical simulations used to compile the *MM5* wind field library were conducted with an adapted version of the *Penn State University-National Center for Atmospheric Research MM5 model, version 3.3* (Grell *et al.*, 1995).

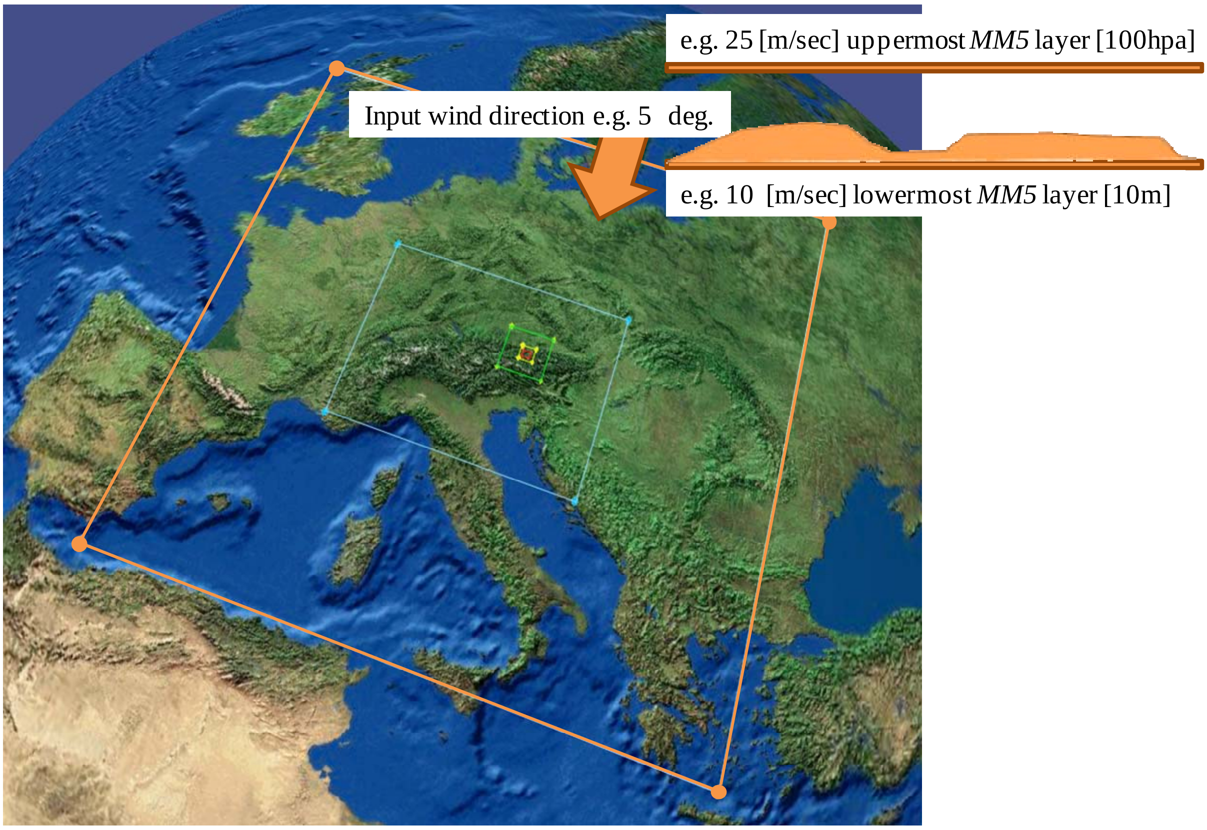
e.g. 25 [m/sec] uppermost *MM5* layer [100hpa]
Input wind direction e.g. 5 deg.
e.g. 10 [m/sec] lowermost *MM5* layer [10m]

Figure 13: Schematic illustration of the MM5 nesting domains (the largest domain is domain_1, the smallest domain_5) and of the needed input parameters.

The model solves the nonhydrostatic equations of motion in a terrain-following sigma coordinate system. Five interactively nested model domains were used, having a horizontal mesh size of 16.2 km, 5.4 km, 1.8 km, 600 m, and 200 m, respectively. The corresponding numbers of grid points were 148×142, 166×127, 88×88, 82×82, and 121×97, respectively. The area covered by the model domains is displayed in fig. 13. In the vertical, 39 full-sigma levels were used, corresponding to 38 half-sigma levels where all variables except the vertical wind are computed. The lowermost half-sigma level is located about 10 m above the ground, and the vertical distance between the model layers increases with height from about 20 m near the ground to about 700 m near the upper boundary which is located at 100 hPa. The needed model topography was created from *US Geological Survey* (*USGS*) terrain data with a horizontal resolution of 5' for domain_1 and 30" for model domains_2-_3. For the two inner model domains (4 and 5), high resolution topography data with a grid spacing of 600 m and 200 m was derived from 50 m *DEM* data (Ludwig *et al.*, 2003). Information on surface roughness was based on land use classes derived from *USGS* data with a resolution of 30".

For the initialisation of the model information about the wind direction and wind speed for the lowermost (10m) and the uppermost model layer (100hpa) was needed (fig. 13). Specifically, the boundary conditions are defined by a wind direction, the (theoretical) geostrophic wind speed at sea level, and by the wind speed set for the lowermost (10m) and uppermost model level (100hpa) of domain_1. The ration between the wind speed used for the lowermost and the uppermost model layer was 1 (ground level) to 1.5 (100hpa level) which corresponds to the common difference in wind speed between these two layers (personal communication G. Zängl 2004). These three parameters constitute the backbone for setting up the computation of the wind field library. The target area corresponds to the *MM5* nesting domain_5.

The diurnal cycle related to radiation is not taken into account, because solar radiation delivers only a comparatively small amount of energy during the winter season. Hence, thermally induced local wind systems usually don't induce significant snow transport processes. Consequently, the specified large scale fields are kept constant throughout the simulations, which are conducted for 24 hours so that the resulting fields represent steady state conditions. To keep the computational expense at a reasonable level, the first 15 hours of simulation are conducted with the three outer domains only. The fourth and fifth domain are started at t = 15 h and at t = 21 h respectively, so that the innermost domain is active for three hours only. Sensitivity tests with various wind directions revealed that this is sufficient to reach quasi steady state in the 200 m domain. This can be explained by the fact that the vertical group velocity of orographic gravity waves is inversely proportional to their horizontal scale, so that small scale waves rapidly reach a steady state.

The described large-scale wind field is assumed to be in geostrophic balance with the pressure field except for the frictional boundary layer. The Coriolis parameter is assumed to be constant at 10^{-4} 1/s throughout the model domain. The large scale wind field is allowed to have vertical shear, as is usually the case for real flows, but is forced to be unidirectional in order to limit the degrees of freedom.

The large scale temperature profile starts with a sea level temperature of 278.5 K, followed by a vertical temperature gradient of -6.5 K/km up to the tropopause. Above that, an isothermal stratosphere is assumed. Though the low level static stability is frequently higher in winter, this temperature profile is reasonable for our purposes because strong wind conditions (which are critical to this study) force vertical mixing and thus tend to reduce the low level static stability. Unless mentioned otherwise, the large scale relative humidity starts with 75 % at sea level, increases with height to reach a maximum of 90 % between 750 hPa and 650 hPa, and then decreases with height down to a value of 20 % at tropopause level. The motivation for this setting is to allow for the formation of clouds and orographic precipitation under northerly flow conditions which may affect flow dynamics due to the reduction of the effective static stability. However, sensitivity experiments with lower humidity (no more than 60 % throughout the troposphere) indicated that the local wind pattern in the target area is relatively insensitive to moisture conditions.

To properly account for the frictional processes relevant for setting up the local wind field in the target area, a sophisticated boundary layer parameterization with 1.5 order closure based on a prognostic equation for *turbulent kinetic energy* (*TKE*) was used (Shafran *et al.*, 2000). Moreover, a cloud microphysics scheme of medium complexity was used to simulate cloud formation and precipitation processes (Reisner *et al.*, 1998). To adapt *MM5* to the extremely steep topography of our target area, several modifications of the model numerics were applied (Zängl 2002). Numerical diffusion of temperature and moisture is computed with the truly horizontal scheme implemented by Zängl (2002), which has proved to greatly reduce numerical errors over steep topography. To improve the numerical accuracy of horizontal advection over steep topography, the generalized vertical coordinate described by Zängl (2003) was used. Unlike standard terrain-following coordinates, this coordinate definition allows for a very rapid decay of the topographic structures with height in the coordinate surfaces. In addition, the numerical damping of sound waves has been increased in the implicit sound wave solver of *MM5* in order to improve the numerical stability over very steep slopes (slope angle > 50°). Despite this, the 200 m *DEM* used had to be smoothed at some locations to prevent numerical instability.

2.3 Lokalmodell (LM)

The second atmospheric model which was used is the *Lokalmodell* (*LM*) of the *German Weather Service* (*DWD*), serving as a link between the actual atmospheric situation and the *MM5* wind fields.

Launched in December 1999, *LM* and *Globales Modell Europa* (*GME*) represent the operational model chain of the *DWD*. *GME* is the operational global forecast model that provides the lateral boundary conditions for *LM*. *LM* itself is a nonhydrostatic model and can be used for forecasting as well as for analysis issues (Doms and Schättler 1999). LM is applicable for different areas and scales; the *DWD* uses it for an area of 2000x2000 km. The coordinate system uses rotated spherical coordinates in the horizontal and a height based terrain-following coordinate in the vertical (zeta) (Gal-Chen and Somerville 1975; Doms *et al.* 2002). The zeta coordinates divides the model atmosphere into 35 levels ranging from the earth's surface to 20 hPa. The used mesh width of *LM* is 7 km, the second edition of *LM* has an improved resolution of 2.8 km becomes operational in 2007 but was not used here.

For this study operational *LM* analysis data were used; the data were derived from modelling and continuous assimilation of observation data by a nudging system: Modelled data is shifted towards the observed data while maintaining dynamic and physical consistency. As a consequence, the analysis data reflects the actual atmospheric situation much better than the forecasting results (Wergen 2002). Operational analysis data are provided at an hourly resolution.

Chapter 3: Meteorological fields

3.1 Interpolation of meteorological parameters, capabilities and limitations.

For a proper modelling of the snow cover, valid meteorological fields are needed as driving force. The following chapter will discuss I) the quality and number of the available measurements II) the possibility to generate adequate wind fields with the help of the interpolation scheme described in *chapter 2* and III) the spatial characteristics of *MM5* generated wind fields.

The horizontal and vertical distribution of the meteorological stations within the upper Danube catchment is used as baseline for the following discussion. The area was chosen because it reflects the general distribution of meteorological stations. A discussion on the basis of the test site *Berchtesgaden National Park* would be misleading because the site is exceptionally well equipped and is therefore not representative. Figure 14 a) shows that the horizontal distribution of the stations is nearly uniform but the vertical distribution shows a clear trend towards a lesser number of stations at higher altitudes. In the upper Danube catchment 313 of 360 available stations are located between 0m a.s.l. and 1000m a.s.l., 37 between 1000m a.s.l. and 2000m a.s.l. and only 10 stations are located above 2000m a.s.l. (fig. 14 b)). The thinning of the network from 1000 meters on is due to the steep alpine topography, extreme weather conditions, problematic data transfer from the stations to the receptor, limited power supply, and difficult maintenance of the stations.

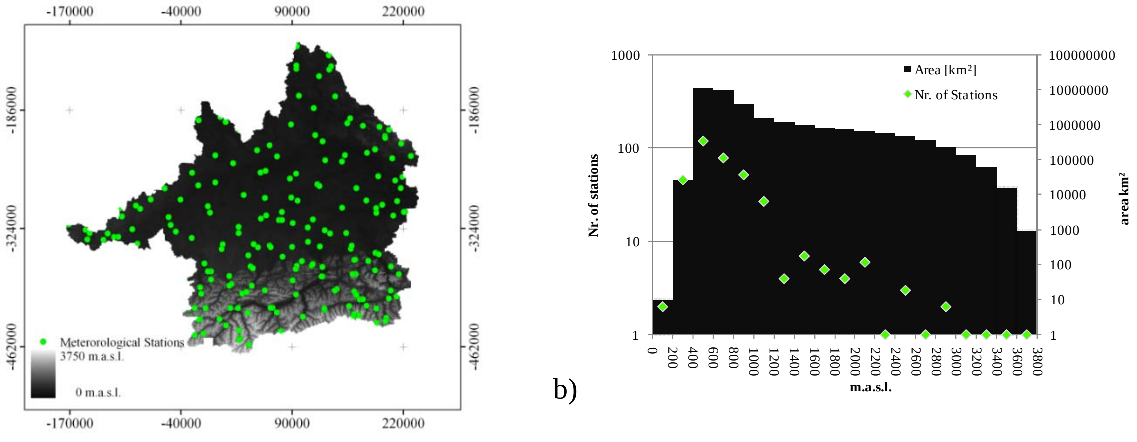

a)

b)

Figure 14: a) Spatial distribution of the meteorological stations within the upper Danube catchment, b) Area of the different elevation bands and number of stations at the respective altitudes.

The thinning of the station network with altitude stands in direct contrast to the demands formulated by Barry (1992). He stated that the network of meteorological stations in mountainous regions should be 10 to 20 times denser than in flatlands to observe just the correct trend of the different meteorological parameters. The higher number is needed because the heterogeneous mountain terrain causes such a broad band of local weather conditions that the measurement at any particular station can only be seen as representative for a limited area (Barry 1992). That means that the *spacing* of the stations becomes especially wide if the *support* of the data becomes small. Furthermore, the measurements conducted in Alpine regions are less reliable than such in the flatlands which is due to frequent heavy weather conditions (Barry 1992). Apart from the measurements, the interpolation of meteorological parameters is a challenge in regions with remarkable elevation differences. The computation of continuous meteorological fields on the basis of point measurements is especially difficult if a meteorological variable is not directly coupled to a certain topographic parameter or if the topography is very complex. Furthermore, the limited number of meteorological stations from 1000 meter on (fig. 14 b)) leads to the need of an extrapolation of the meteorological measurements for regions which are located above the highest available station in the surrounding. This procedure has no physically based background and does not respect the real processes of the higher regions (e.g. inversion layers). The application of a gradient of e.g. precipitation which was predicted under usage of lower elevation stations can lead to an appreciable overestimation of the precipitation in high mountain regions. This is due to the fact that a decreasing or steady precipitation amount at higher elevations cannot be computed with common interpolation techniques. Nevertheless, the procedure of applying the respective gradient determined from lower elevation stations to regions above the elevation of the highest meteorological station was chosen for this study as there is no plausible reason that would legitimate the fixing of the gradients to a definite value or the modification of the gradient

The parameters required by the model used here are, temperature, relative humidity, precipitation, incoming solar radiation, wind speed and wind direction. The following discussion will consider just these parameters for the winter season 2003/04. For the validation of the interpolated values the stations at Reiteralm (fig. 5) were excluded from the interpolation scheme and used as the basis for comparison between model results and measured values as shown in Figures 15-20. The interpolation is based on data delivered by the meteorological stations, *Schönau, Jenner* and *Kühroint*. Interpolation results which show a good correspondence to the test station *Reiteralm* are only discussed shortly.

Air temperature is typically simple to interpolate because it shows a relatively stable correlation with height. Figure 15 shows that the temperature at *Reiteralm* station II can be reproduced in a satisfying way by the interpolation routine (eq. 2 and 3). However, the temperature calculations can be complicated for higher regions if inversion layers are present. Furthermore, the interpolation can become erroneous if the upper regions are snow covered while the areas with the meteorological stations are snow free.

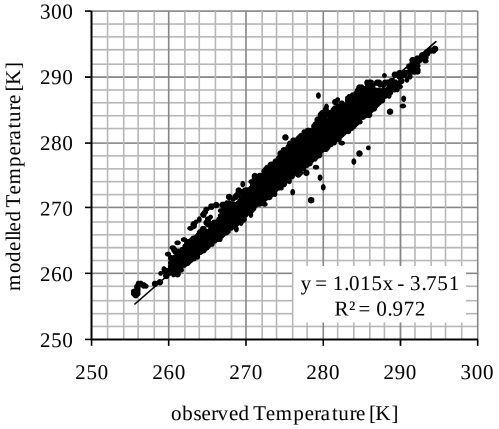

Figure 15: Temperature recordings of *Reiteralm II* meteorological station. Comparison of hourly modelled and observed data for the winter season 2003/2004.

Figure 16 shows that the calculation of the incoming solar radiation leads to a reasonably good correlation between measurements and model results ($R^2 = 0.71$). However, it becomes obvious that model results tend to be higher than observed values. This effect is due to an underestimation of the cloud cover (Eq. 9). More sophisticated radiation models like the one used in e.g. *AMUNDSEN* (Strasser *et al.* 2007) are able to describe the radiation balance at a given point more accurately because they respect shading effects and reflected longwave radiation from the surrounding terrain and applies. Nevertheless, it could be seen that the error of the interpolation scheme is especially high in summer and more accurate in winter which allows for an application of the presented formulations.

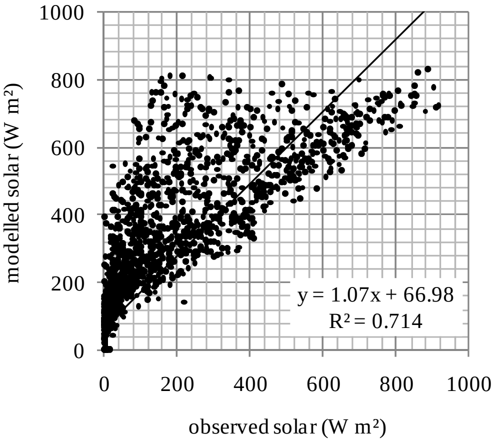

Figure 16: Incoming solar radiation data from Reiteralm 3 meteorological station. Comparison of hourly modelled and observed data for the winter season 2003/2004.

The interpolated humidity values show a strong correlation ($R^2 = 0.97$) between the modelled and measured values (fig. 17).

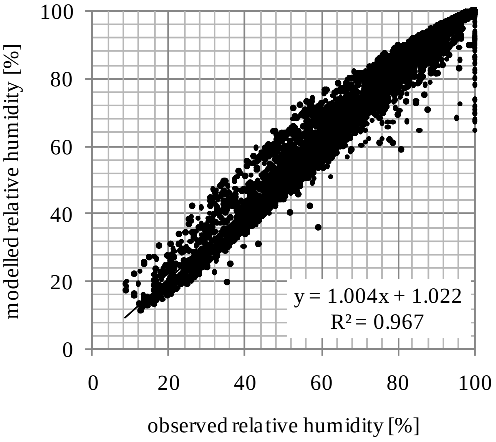

Figure 17: Relative humidity from Reiteralm 3 meteorological station. Comparison of hourly modeled and observed data for the winter season 2003/2004.

Other meteorological parameters like precipitation rates and phase as well as wind fields are more problematic to predict. This is due to the fact that these fields are not continuous in reality and that the local characteristics of these fields are caused by mechanisms which are not dependant on the location of their appearance.

The error of precipitation measurements can reach up to 100% if the precipitation gauge is snowed in or during high wind speeds which are affecting the catch of the gauges.

Furthermore, the correct distinction between snow and rain is difficult because the phase of the precipitation is commonly not recorded and the air temperature as well as the wet bulb temperature can only be an indicator for the phase of the precipitation. Nevertheless, a comparison of modelled with measured snow depths at the meteorological stations indicates that these errors are small for the observed period. Figures 18 a) and b) show that the calculation of the precipitation rates works well if precipitation occurs at station *Reiteralm* and at the stations used for the interpolation (fig. 18b)). The precipitation calculation, however, is much less accurate if that is not the case (fig. 18a)) which causes a decrease in the overall correlation between station measurement and interpolation results (fig. 18 a) and b)).

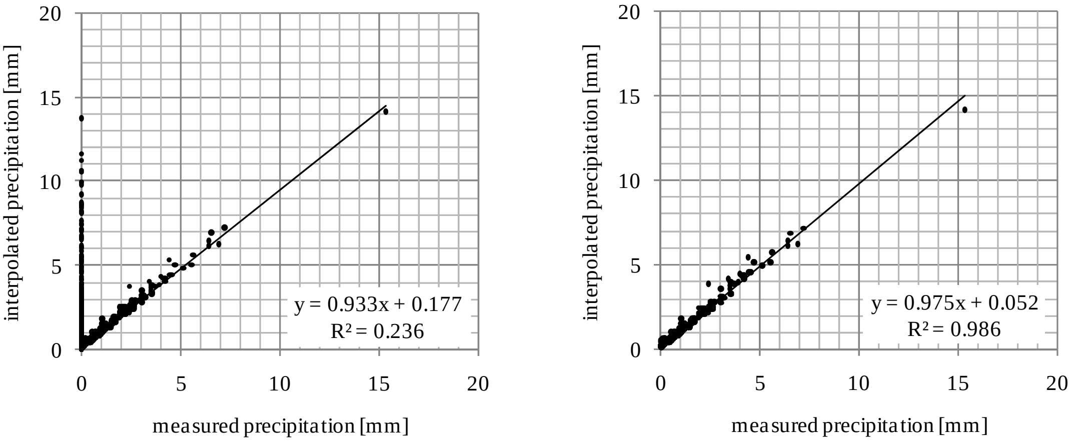

a) b)

Figure 18: Correlation between measured and calculated precipitation rates (winter season 2003/2004) (mm). a) Including hours with precipitation at other stations but no precipitation at the validation station (Reiteralm 1) and b) precipitation at all stations, including Reiteralm 1.

The interpolation results of wind speed and direction are less substantive. It can be seen that the wind directions at *Reiteralm 1* cannot be reproduced by the interpolation scheme (eq. 13-21). The probability to compute a correct wind direction is approximately equal to the probability to predict any other wind direction (fig. 19).

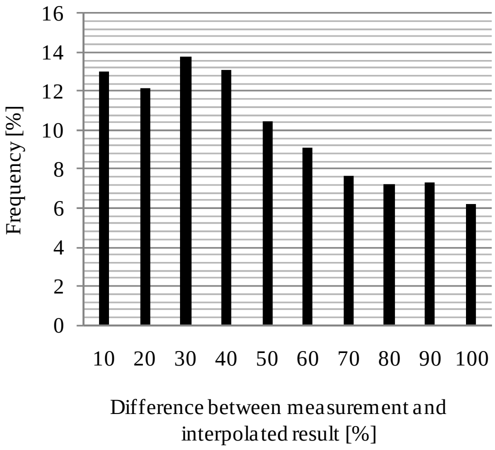

Figure 19: Accuracy of interpolated wind directions in comparison to measurements at *Reiteralm I* (winter season 2003/2004).

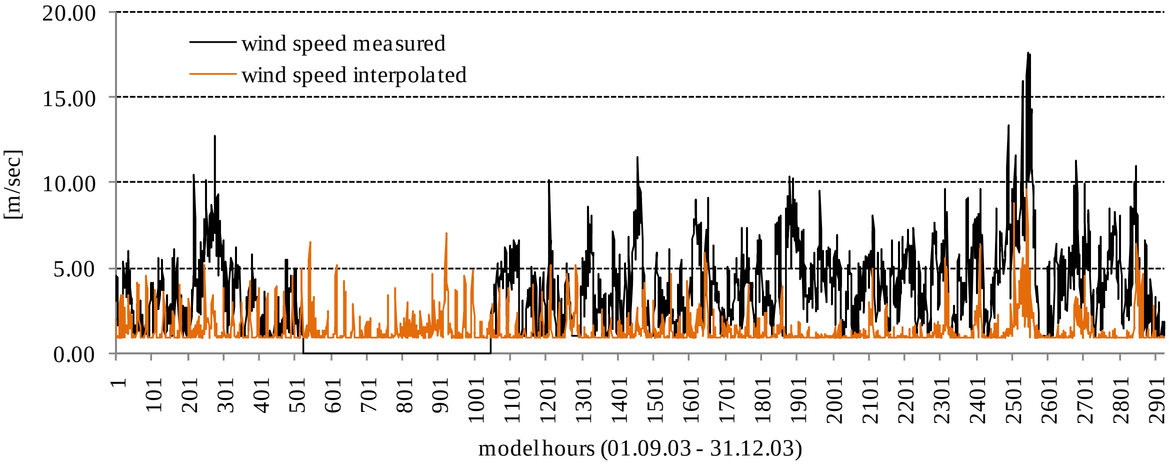

Figure 20: Comparison of measured and interpolated wind speeds at *Reiteralm 1* (winter season 2003/2004).

The interpolated wind speeds (fig. 20) are commonly to low in comparison to the wind speeds measured at *Reiteralm 1*. Most of the situations with high wind speeds were not reproduced by the interpolation routine (fig. 20). This is because beside of the *Reiteralm 1* station, there is no other meteorological station at a higher elevation which results in an even elevation wind speed gradient.

To recapitulate the former section, most of the needed meteorological input parameters can be computed with the help of the interpolation routines presented in *Chapter 2* as most of these routines deliver results which are representative for the excluded station. Wind speed and direction have to be seen as an exception. The results does not show any connection to the test station in the case of wind direction and can only reflect the trend but not the level of the wind speed measurements. As the spatial characteristics of the used wind fields are from special importance for this work, possible reasons for the improvable results shown in figures 19 and 20 and general difficulties which can accrue when measuring and interpolating wind speed and direction are discussed in more detail in the next section.

3.2 Calculation of wind fields in mountainous terrain

The calculation of appropriate wind fields is a prerequisite for a more in-depth understanding of the patterns of erosion and accumulation areas in Alpine regions. This is due to the fact that any snow transport model directly “reacts” to the amount of energy supplied by the current wind field. The available energy determines if snow transport conditions exist or not. Furthermore, the wind direction given by the wind field is essential for the location of the modelled accumulation and erosion zones. In general, it could be stated that the difficulty of wind measurements and wind field calculations rise with the complexity of the terrain. The variables influencing the quality of the resulting wind fields are dependent on the method used:

- I) Influencing variables (When using interpolation scheme):
  - a. The quality of wind speed and direction measurements.
  - b. The ability of the interpolation scheme to factor in the underlying topography.
- II) Influencing variables (When using an atmospheric model):
  - a. A sufficient spatial resolution to adequately capture the local wind situations.
  - b. A numerical complexity which corresponds to the complexity of the terrain.

3.2.1 Theoretical background

Starting with I) a). With respect to the measurements it has to be considered that the local wind field is affected by the anemometer and the complete meteorological station itself as well as by barriers in the environment (e.g. Wieser *et al.* 2001). These local modifications of the wind field have a direct influence on the measurements and limiting their representativeness for the surrounding. This can be one reason for the limited accuracy of the results shown in fig. 19 and 20. Furthermore, anemometers are vulnerable to freezing (fig. 21; tab. 3 model hours 500-1000) since they consist of many mobile parts. Table 3 compares the operational hours of the wind sensor with hours without measurements at the meteorological station *Reiteralm*. A comparison to other measured values shows that the anemometer has much more missing data than the other sensors which can make a modelling of snow transport processes completely impossible.

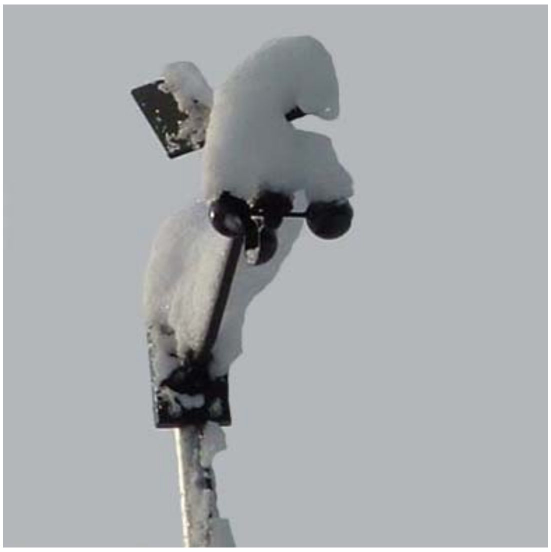

Figure 21: Frozen anemometer. This picture shows a very common situation in Alpine regions. The sensor becomes snow covered and becomes therefore unusable.

Table 3: Hours showing wind speed and direction recordings vs. hours with data lacks compared to recordings of other sensors.

Season	Operating hours	Hours without measurement (anemometer)	Hours without measurement (temperature)	Hours without measurement (humidity)
01/02	8760	1775	0	0
02/03	8760	38	66	40
03/04	7880	2920	0	0

The argument mentioned under I) b) belongs to the ability of the interpolation routine to factor in the underlying topography. Literature analyses has shown that the interpolation routine used by Liston and Sturm (1998) (eq. 14 to 21) works well for gently rolling terrain (Liston and Elder, 2006). The results presented in 3.1 on the other hand indicating that the scheme is unable to reproduce the wind conditions for a meteorological station located within an *Alpine* environment (fig. 19 and 20). This can be declared by some theoretical considerations. For the interpolation of the wind field measurements it is important to know that wind speed and direction are not directly correlated to a single topographic feature. If this were the case a few measurements would be enough to predict a wind speed/direction field. But, according to Barry (1992) wind speed is more closely coupled to the topography of a mountainous region than to their altitude. That means that all topographic parameters (aspect, slope, elevation) influence the wind field depending on the synoptic inflow. The assumption that wind speed increases with altitude might be correct if one is considering long term averages but not for a single event. Figure 22 shows a profile through a *MM5* simulated wind field which displays the facts mentioned before. The upwind velocity is pretty much the same (approx. 4 m/s) over the whole south face of *Watzmann* (transect I), with only a small peak that can be observed at the crest. The situation changes at the north face were lower velocities (approx. 2 m/s) and a change from downwind (transect II) to upwind (transect III) conditions can be observed. This small example gives an idea about the complexity of air flows at one mountain and for one specific situation.

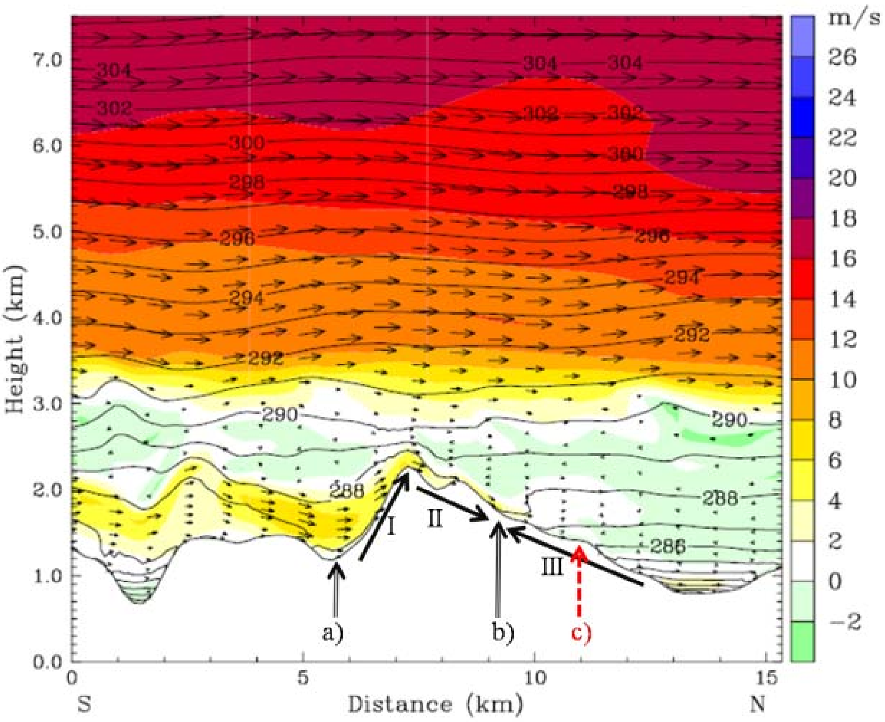

Figure 22: Vertical profile through a *MM5* wind field. a, b and c are fictive meteorological stations. The transects I, II, III are used for declare the wind conditions at the faces of *Watzmann* mountain. The wind speed is slightly enhanced at the windward site (transect I) as the wind direction is constant to North. Transect II and II showing the complex wind conditions at the leeside. The wind speeds are about 6 [m/sec] at transect II, the wind direction is to north. The situation changes at transect III were the wind speed is between 0 and 2 [m/sec] and the wind direction is to south.

Furthermore, if one would assume that two meteorological stations would be available at this mountain (fig. 22) point a) and b)), which is commonly not the case; one can imagine that it would be impossible to predict the wind speed and direction on point c) with the data from these two stations. This is because the wind speed and direction measured by these stations cannot include any information about a change from downwind to upwind conditions at the lower depths. A statistical inclusion of topographic parameters into any interpolation routine would not solve the problem because the phenomenon can be due to flow separation or a rotor (fig. 23 a) and b)) and would be caused by a large scale interaction of topography and airflow in this case. Such phenomena have nothing to do with the local topography and can be therefore not displayed with a 2D interpolation scheme which bases on point measurements at the 10m level and which only figures in the local topography wind speed/direction interactions.

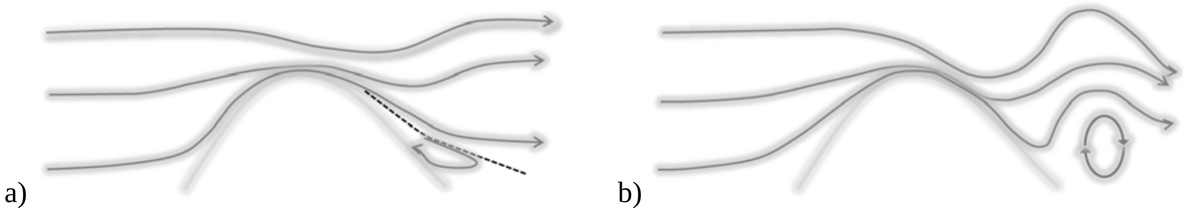

Figure 23: Generalized flow behaviour over a hill: a) flow separation and b) a rotor (Barry 1992, modified).

Another problem which complicates the interpolation of wind direction measurements can also be explained on the basis of Figure 22. If one would shift meteorological station b) to point c), the wind direction would be the exact opposite of station a). The interpolation of these values would lead to questionable results because the average between e.g. 180° and 360° is not defined. Although, the described situation would never occur in flat or slightly undulated terrain, it is common in mountainous terrain.

The next questions formulated at the begin of this section were if *MM5* has a sufficient resolution for describing the prevailing wind systems in the test region and if the numerical complexity of *MM5* is adequate with respect to the topography of the test site. These answers can be answered shortly. *MM5* has a target resolution of 200m in the current setup. This resolution is the absolute maximum with respect to the model formulations of *MM5* in combination with the very rough topography of the test-site. The ability of *MM5* to deliver acceptable results for a site like the *National Park* and the explanation that the model formulations of *MM5* are sufficient for areas with steep topography is widely described in Zängl (2002) and (2003), as well as in Bernhardt et al. (2008a).

3.2.2 Comparison of interpolated and modelled wind fields

The *MM5* wind fields shown in figures 24 a) and b) were produced using input wind directions of 140 and 270 degrees respectively (cp. fig. 13). The used input wind speed corresponds to the average in the test region (Bernhardt et al. 2008a) and was set to 10 [m/sec] at the lowest model level (10m) and to 25 [m/sec] at the uppermost model level (100hpa) (cp. fig. 13). An analysis of the resulting fields reveals that the two situations have significantly different spatial characteristics. Most of the differences can be traced back to windward and leeward effects, which are particularly evident at the massifs of *Watzmann* and *Hochkalter* as well as at the *Reiteralm* plateau (fig. 24 a) and b), cp. fig. 5). In the case of an overflow of air masses over the crests, the relief-induced convergence of the air stream leads to a local increase in wind speed at the windward side (Barry, 1992) (fig. 24b). The interpolation routine by Liston and Sturm (1998) is not able to reproduce this effect because of the implemented linear increase of wind speed with height (fig. 25 a) and b)). Furthermore, the local variations in wind speed are much more distinctive in the *MM5* field which makes it possible to easily identify of crest regions, windward and leeward sides and troughs at the north-western parts of the massifs. The interpolation routine, in contrast, produces a more homogenous field which is mainly dependent on the vegetation pattern (fig. 25 a) and b)). The interpolation routine generates a slight increase of wind speed with height which does not reflect the conditions observed in reality (Reiter, 1962; Barry, 1992). This is due to two factors: First, a lack of meteorological observations at higher elevations which would be necessary to generate a steeper wind speed gradient and secondly, the interpolation scheme is based on a *Gaussian* function (Barnes, 1964) and, therefore, predicts a continuous wind field which does not allow for an abrupt change of the magnitude of an parameter (eq. 17). With the help of the weight factor (eq. 17), wind speeds can be modified between 0.5 to 1.5 times the original value, which is by far not enough to reproduce the *MM5* results.

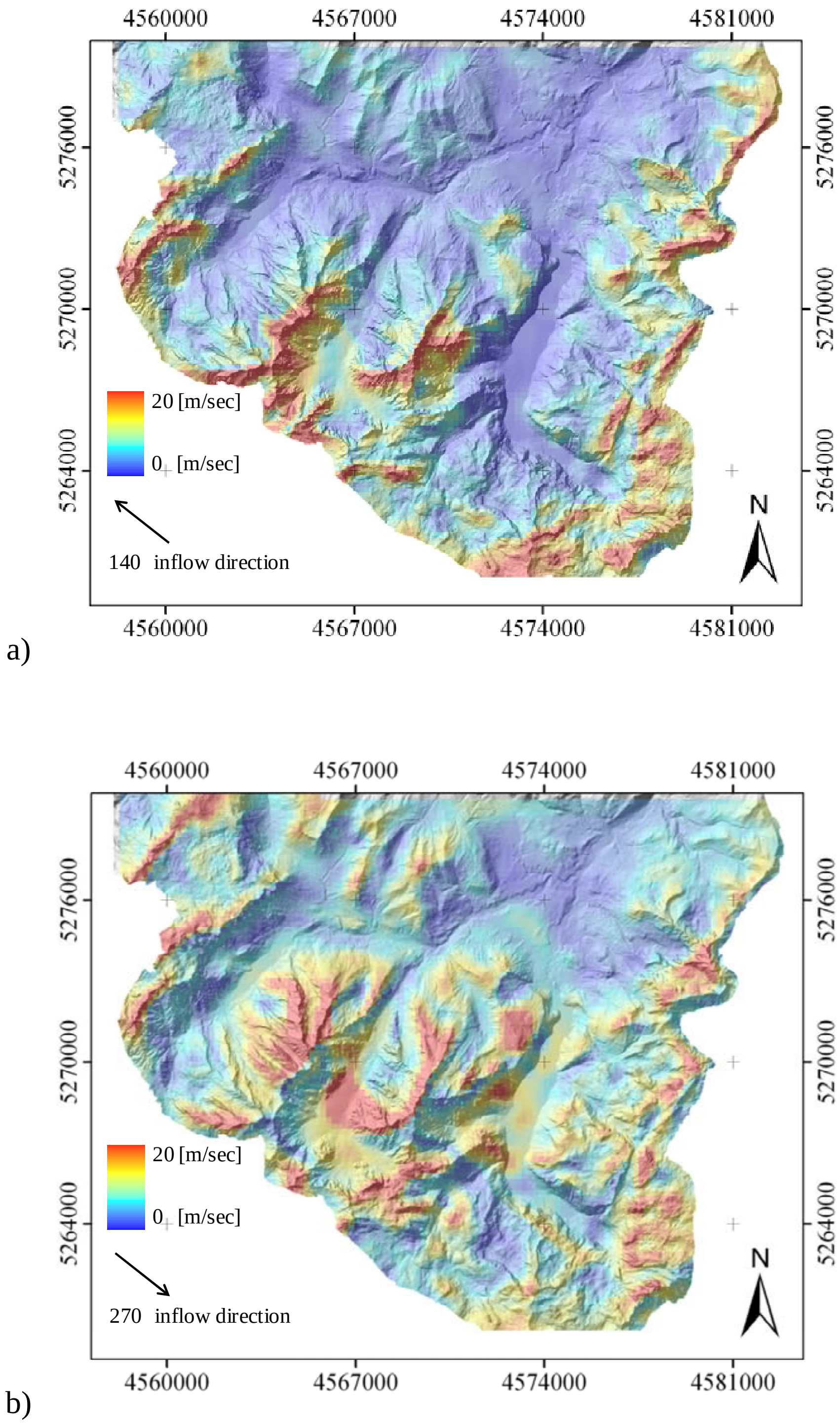
4560000
4567000
4574000
4581000
5276000
5270000
5264000
20 [m/sec]
0 [m/sec]
140 inflow direction
N
a)
4560000
4567000
4574000
4581000
5276000
5270000
5264000
20 [m/sec]
0 [m/sec]
270 inflow direction
N
b)

Figure 24: a) *MM5* wind field (input parameters: wind direction = 140° and 10 [m/sec] at 10m and 25[m/sec] at 100hpa) b) *MM5* wind field calculated with the same input wind speeds but an input wind direction of 270°.

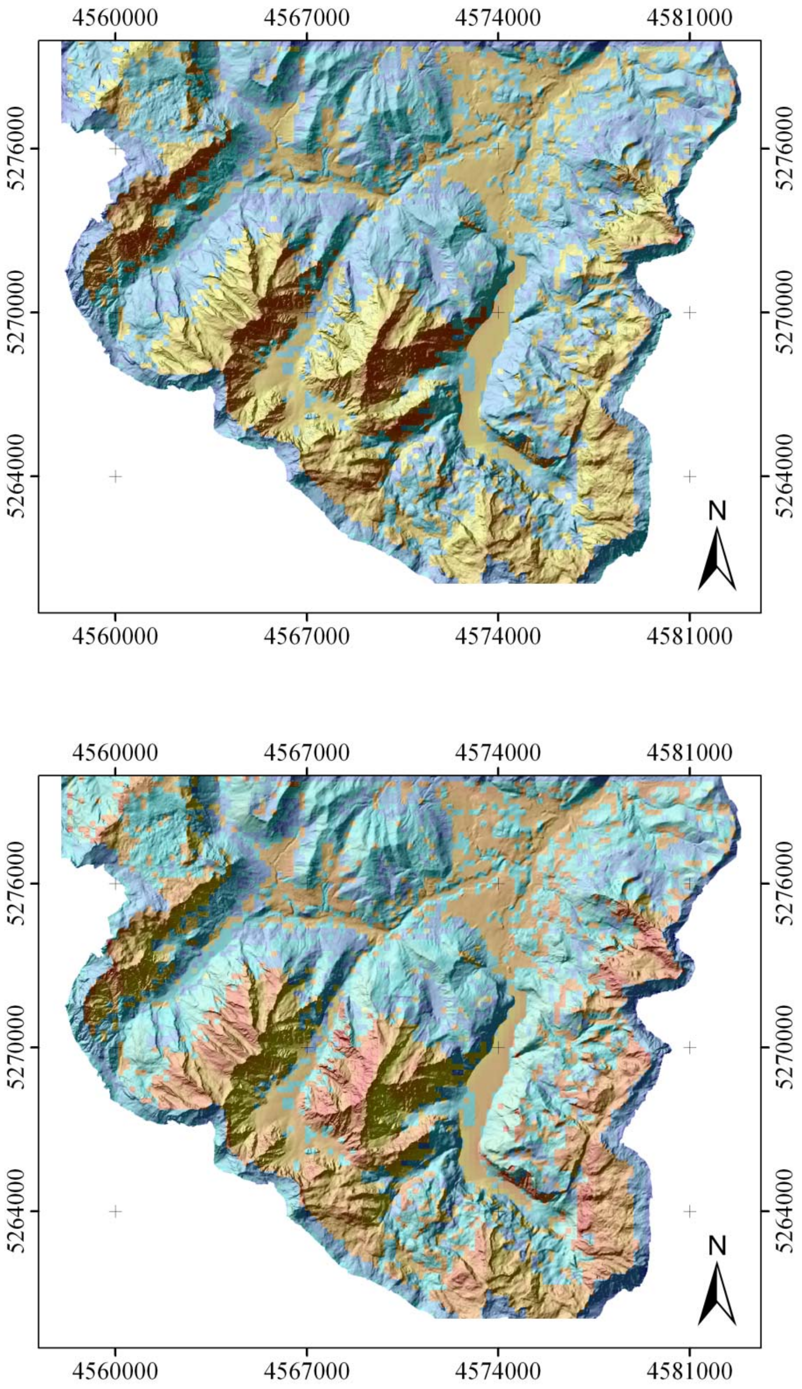
4560000
4567000
4574000
4581000
5276000
5270000
5264000
N
4560000
4567000
4574000
4581000
5276000
5270000
5264000
N

Figure 25: Interpolated wind fields. a) The average wind directions at the meteorological stations are 140° and b) 270°.

An analysis of *MM5* and interpolated wind direction fields reveals similar findings. Bendix (2004) stated, that wind direction is a highly variable factor in space and heavily dependent on the surrounding topography which modifies the synoptic flow direction. Based on this assumption the *MM5* input wind direction was changed to analyze the effects on the local wind direction field. Subsequently, the wind directions predicted by *MM5* for the meteorological stations *Schönau*, *Jenner,* and *Kühroint* were interpolated via *Micromet* and compared to the *MM5* results.

Figure 26 shows *MM5* wind direction fields, representative for input wind directions of 265° and 270° (the input wind speed was 10 [m/sec] (at 10m) and 25 [m/sec] at the uppermost model level (100hpa) for both model runs). Notwithstanding that the input wind direction differs by only 5 degrees, the resulting per pixel difference can reach up to 180° (fig. 26). It is obvious that both *MM5* wind direction fields show approximately the same value for pixels which are representative for a meteorological station (marked as coloured dots in figures 26 and 27) but the wind direction characteristics between the stations differ significantly (fig. 26). The range of occurring wind directions lies between 1 and 360 degrees which is not the case when using the interpolation scheme (286 to 317 degrees) (eq. 14-21; fig. 27). An interpolation of the *MM5* predicted wind directions for the positions of *Schönau, Jenner* and *Kühroint* (results displayed in fig. 26) delivers uniform results (fig. 27), which are somewhere between the three *MM5* calculated station values. Furthermore, the field does not show a noticeable sensibility to the underlying topography. The uniformity of the interpolation results can again be attributed to the applied Barnes scheme (Barnes, 1964) and the underlying *Gaussian* function which forbids abrupt changes within the calculated wind direction field.

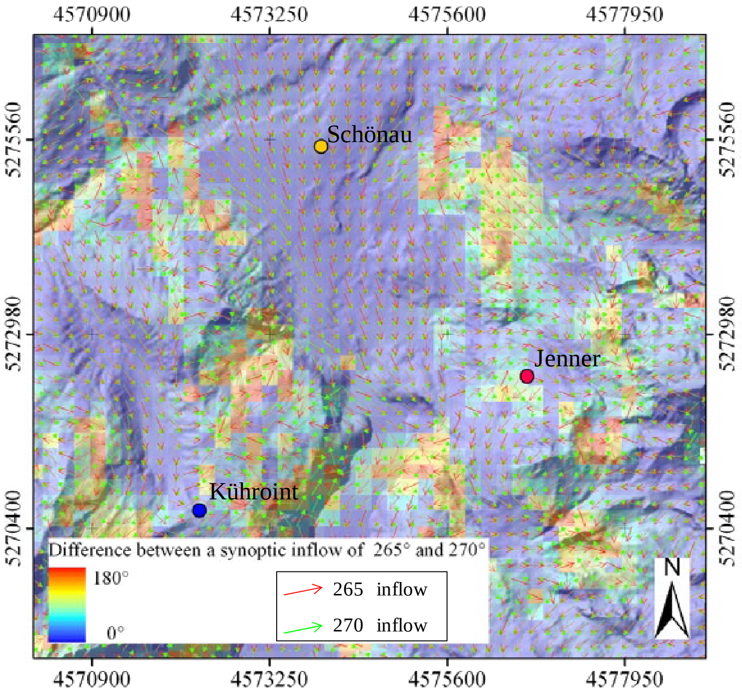
4570900
4573250
4575600
4577950
5275560
5272980
5270400
Schönau
Jenner
Kühroint
Difference between a synoptic inflow of 265° and 270°
180°
0°
265 inflow
270 inflow
N

Figure 26: Spatial characteristics of *MM5* wind direction fields in dependency of the synoptic inflow. The inflow direction is 265 degrees and 270 degrees respectively.

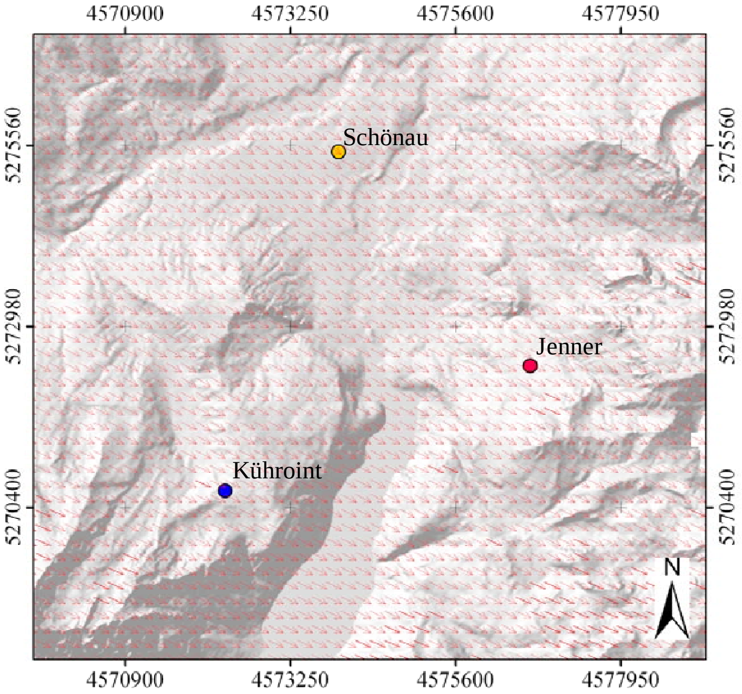
4570900
4573250
4575600
4577950
5275560
5272980
5270400
Schönau
Jenner
Kühroint
N

Figure 27: Spatial characteristics of an interpolated wind direction field. The wind directions used for the interpolation corresponding to the wind directions produced by *MM5* (fig 26) for the three indicated meteorological stations.

A similar finding can be made when analysing the change in local wind directions dependent on *MM5* input wind speeds (fig. 28). The input wind speeds were changed from very moderate wind conditions (5[m/sec] at 10m to 13[m/sec] at 100hpa) to high wind conditions (20 [m/sec] at 10m a.s.l to 50 [m/sec] at 100hpa), while keeping the input wind direction constant (180°). The effect is a per pixel change in wind direction reaching up to 180 degrees mainly caused by a shift of local eddies. The presented interpolation routine would not reflect changes of wind speed in the wind direction results because both parameters are treated separately. This seems to be inadequate when respecting the *MM5* results.

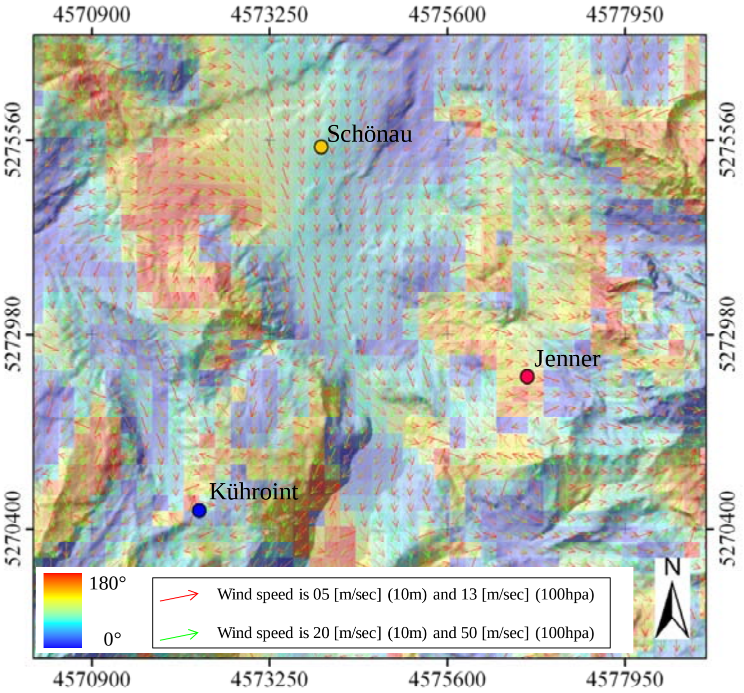
4570900
4573250
4575600
4577950
5275560
5272980
5270400
Schönau
Jenner
Kühroint
180°
0°
Wind speed is 05 [m/sec] (10m) and 13 [m/sec] (100hpa)
Wind speed is 20 [m/sec] (10m) and 50 [m/sec] (100hpa)
N

Figure 28: Dependency of the calculated *MM5* wind direction field on the input wind speed. The wind speeds used for the model setup were 05 [m/sec] for the 10m model level and 20 [m/sec] for the uppermost model level (cp. fig. 13)

The examples show that the interpolation routine delivers almost uniform and therefore questionable results in *Alpine* terrain. It has to be assumed that the estimation of a detailed and meaningful wind field is only possible if wind speed and wind direction are treated in combination for the simulation of distributed wind fields. This is done within *MM5* where the complete aerodynamic flow around mountain massifs is calculated and wind speed as well as wind directions are results of the local flow conditions. The analysis shows that *MM5* delivers highly variable and plausible wind fields, which, however, are useless if they are not taken within a temporal context. The next section will show how the *MM5* library was compiled, synchronized with *SnowModel,* and how the *MM5* wind fields performed compare to the measurements at the meteorological station *Reiteralm*.

3.2 Creation and synchronisation of a MM5 predicted wind field library

The concept of a pre-produced wind field library instead of conducting operational *MM5* simulations at every model time step, allows the combination of a snow model with an atmospheric model at a high level of computational performance. The data used and the corresponding scales can be seen in fig. 29. The wind field library is based on two assumptions: First, a specific wind field is considered representative for a defined synoptic situation, and second, all situations leading to significant snow transport can be described by a finite set of wind fields. The creation of the library comprises two steps: 1) the modelling of the wind fields itself, and 2) the provision of an access key which defines the most appropriate *MM5* wind field of domain_5 (fig. 13 and fig. 29) for the current *SnowModel* time step. For the creation of the wind field library and the access key two of five *MM5* nesting domains were used (domains_3 and _5 in fig. 13). These domains are mutually dependent and give information about meteorological parameters at different scales and pressure levels. While domain_5 provides the high resolution wind fields, domain_3 can be used to provide the link to the *LM* analysis data (fig. 13 and fig. 29).

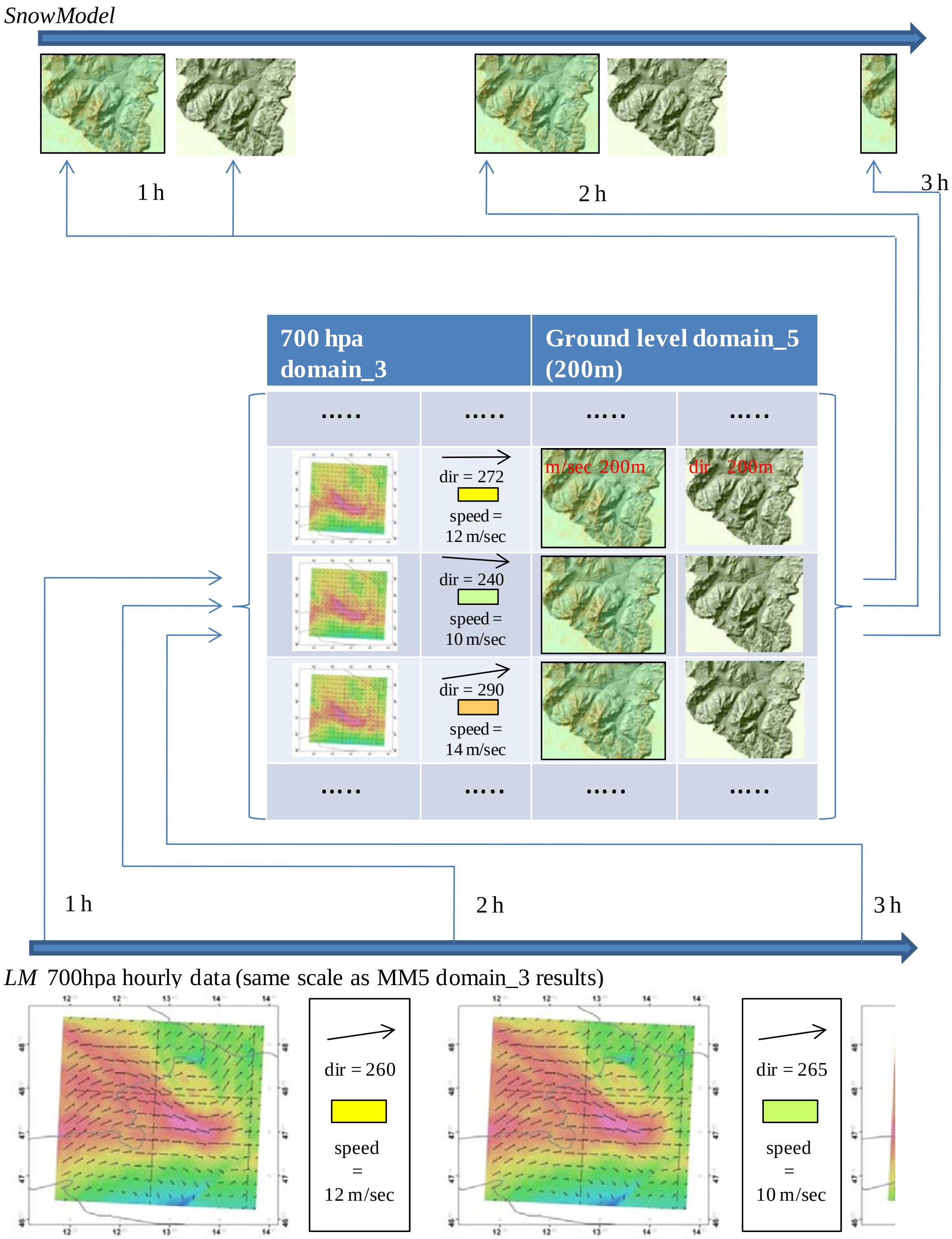
SnowModel
1 h
2 h
3 h
700 hpa domain_3
Ground level domain_5 (200m)
.....
m/sec 200m
dir 200m
dir = 272
speed = 12 m/sec
dir = 240
speed = 10 m/sec
dir = 290
speed = 14 m/sec
1 h
2 h
3 h
LM 700hpa hourly data (same scale as MM5 domain_3 results)
dir = 260
speed = 12 m/sec
dir = 265
speed = 10 m/sec

Figure 29: Schematic illustration of the synchronization of *MM5* wind field library and *SnowModel* via hourly *DWD* Lokalmodell information.

To determine the set of *MM5* wind fields needed to cover the climatologically range of the test region; achieved *DWD* analysis data for the time period of 1991 to 2001 for an area approximately equivalent to *MM5* nesting domain_3 were used (fig. 3 and fig. 30). However, an iterative approach with respect to the settings of the *MM5* boundary conditions was needed because the resulting domain_3 fields had an average wind vector that differs from the large-scale boundary conditions set for domain_1. This means that the input wind speed and direction used for the set up is not identical to the average domain_3 vector. The difference between setup and domain_3 values is due to the nonlinear interaction of the atmospheric flow with the Alpine massif. Hence, a first series of wind fields (from 0 to 360 degrees, with a step width of five degrees) was modelled under the assumption of a constant wind speed at the model boundary (10 m/s at sea level and 25 m/s at tropopause level). Based on the deviations of the averaged domain three vectors from the set up values, it becomes obvious how the boundary conditions have to be modified in order to get the required domain_3 results. As the computation of one wind field needs about three days on a high performance computer the absolute number of fields had to be limited. It was determined that an adequate coverage of the total *DWD* data could be achieved with 220 computed wind fields.

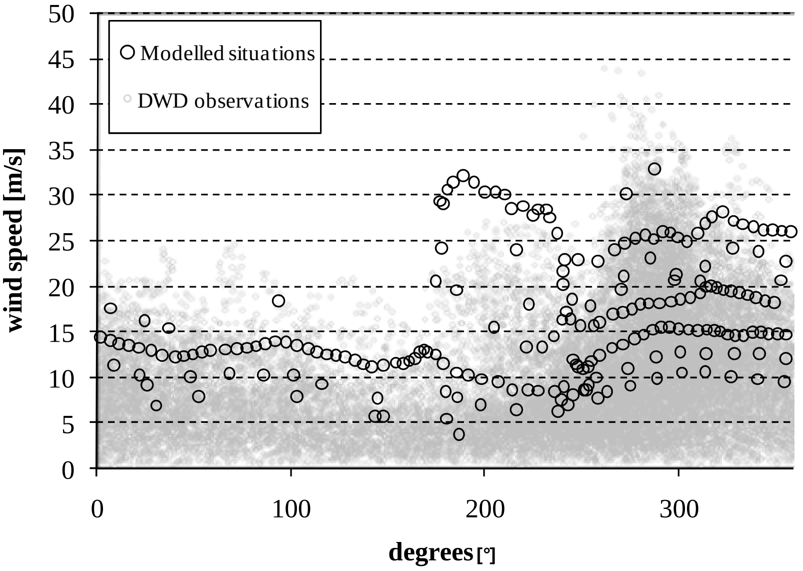

Figure 30: *DWD* historical data for the 700 hPa level (gray dots) vs. averaged *MM5* domain_3 vectors (black dots). The DWD observations were used for defining the initialisation wind speeds and directions needed for the *MM5* runs (cp. fig. 13).

It has to be taken into account that due to friction the shown 700hpa wind speeds are significantly smaller at the earth surface. Since snow transport events which are of relevance only starts when the surface wind speed exceeds a threshold value of about 3-5m/s (Barry 1992; Liston and Sturm, 1998), wind conditions below of 3 [m/sec] were disregarded. Consequently, there was only few wind fields modelled for situations with wind speeds less than 10 [m/s] at 700 hPa at domain_3 (fig. 30) because they generally produce velocities less than the threshold at the surface of the National Park area (fig. 31).

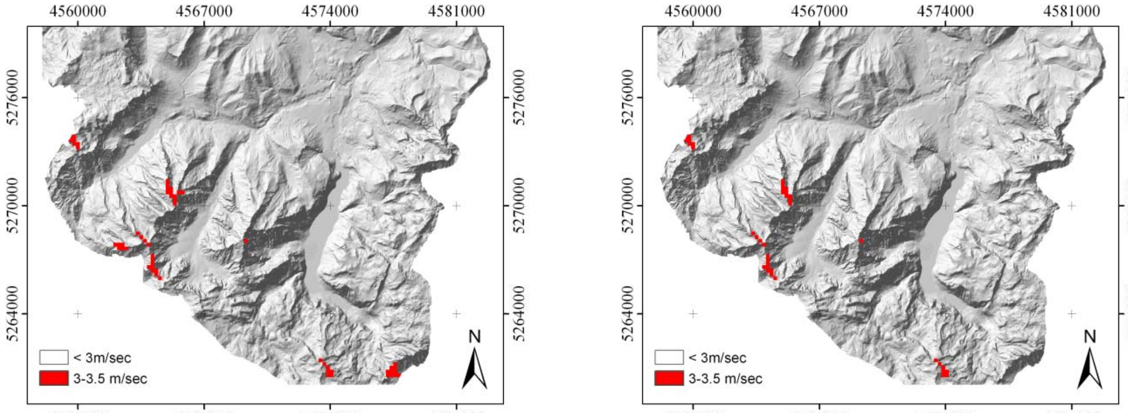

a) b)

Figure 31: The red coloured areas in a) and b) stand for wind speeds >3[m/sec] which would be able to initialise snow transport processes. The *MM5* wind fields were calculated with very moderate input wind speeds (30° / 5[m/sec] at 10m; 16[m/sec] at 100hpa and 143° / 5[m/sec] at 10m; 20[m/sec] at 100hpa).

To extract the corresponding wind field from the library, *LM* and *MM5* domain_3 700 hPa results were used as selection criterion. The 700 hPa level was chosen because it is the lowest standard pressure level of *MM5* at which the large scale flow deflection of the *Alps* becomes negligible. Furthermore, *LM* results of the 700hpa layer are easily accessible. *MM5* nesting domain_3 contains 87x87 mesh points while the corresponding *LM* dataset has 22x22 points. For each of the mesh points the two-dimensional vector $\vec{u}$ represents wind speed and direction. The average of these vectors was used as the measure for the library access key. Hence, the *LM* results were averaged for every model hour and compared to averaged *MM5* domain_3 results which were attached to the corresponding *MM5* domain_5 files. This allows for an extraction of the one *MM5* wind field that has the minimum difference between the averaged *LM* vector and the attached *MM5* domain_3 vector from the library (fig. 29).

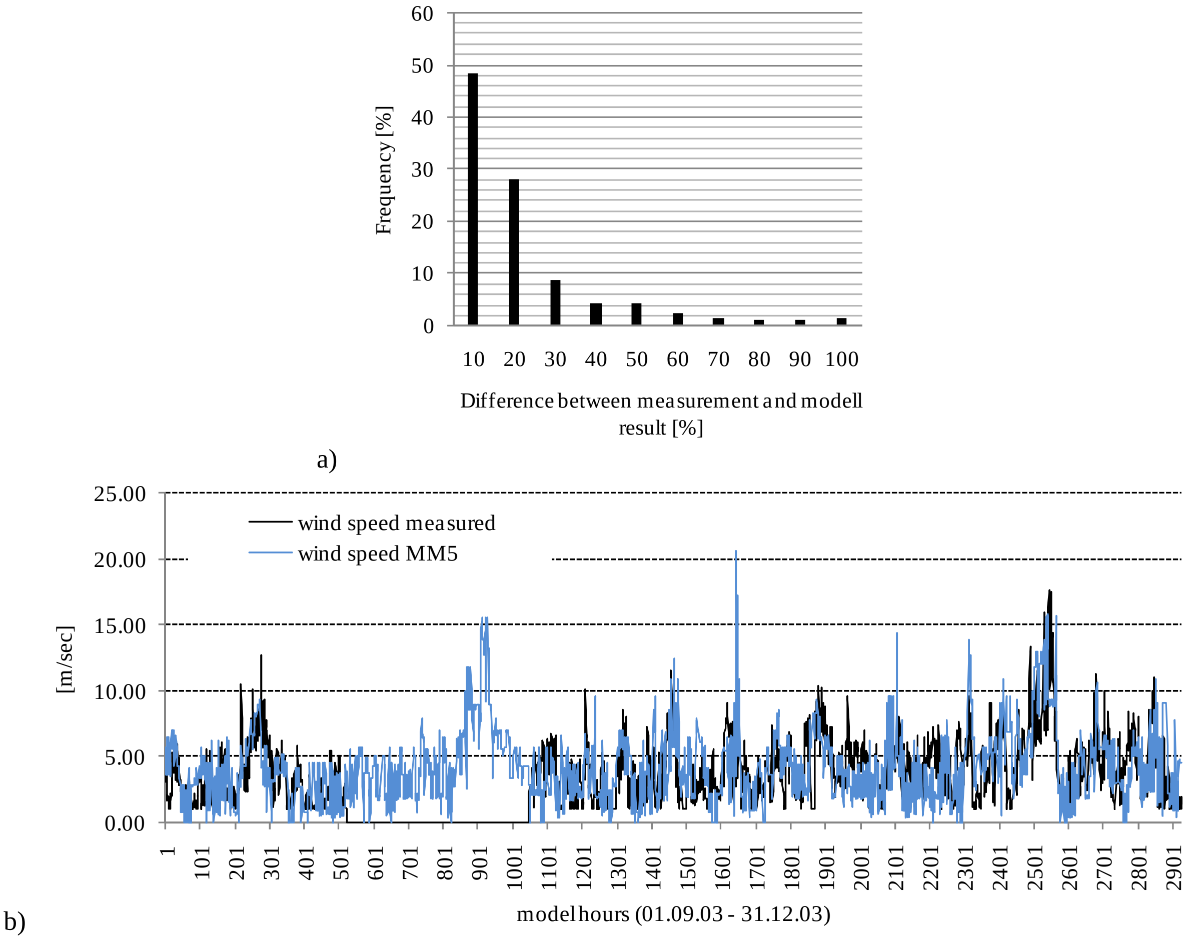

Figure 32: Comparison of measured and *MM5* wind a) direction (01.09.03-30.08.04) and b) speed (01.09.03-31.12.03)at Reiteralm I. A comparrison to figures 19 a) and b) clearifies the advantages in contrast to the interpolation routine.

The upcoming results are extremely encouraging. The convergence of modelled *MM5* wind direction with the measurements of *Reiteralm* is much better than that of the interpolation results. The accuracy of the model is within 10% in about 50% of all cases (the observed period is September 2003 to August 2004) and within 20% in about 75% of the cases (fig. 32a). As there was nearly no connection between interpolation results and measurements (fig.19 and 20) this has to be seen as fundamental improvement. When analysing *MM5* and measured wind speed (fig. 32 b)) it becomes obvious that *MM5* delivers reasonable results here. *MM5* wind speeds are on the same level as the measurements and the course of the measurements is reproduced very well.

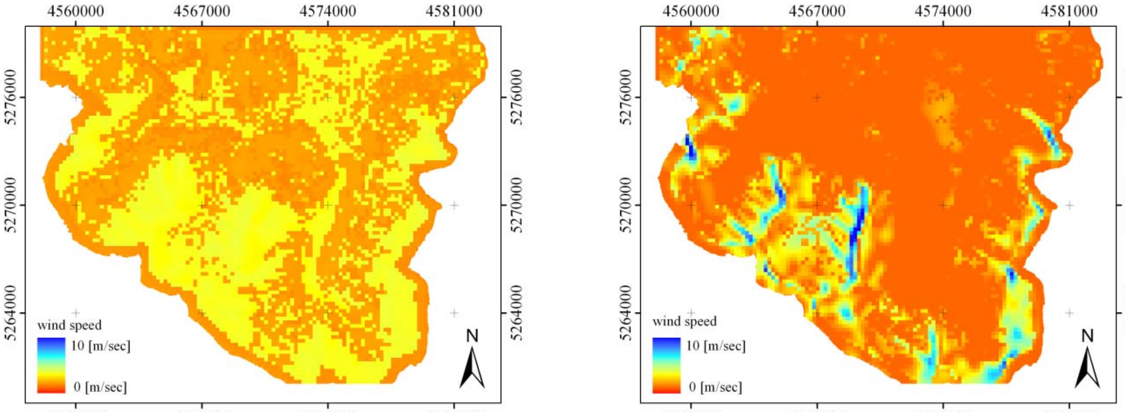
4560000
4567000
4574000
4581000
5276000
5270000
5264000
wind speed
10 [m/sec]
0 [m/sec]
N

a) b)

Figure 33: Wind speed provided by the interpolation procedure of Liston and Sturm (1998) (left) and *MM5* (right). The images represent the situation on January 9, 2004, 7:00. Wind direction is 270 degrees.

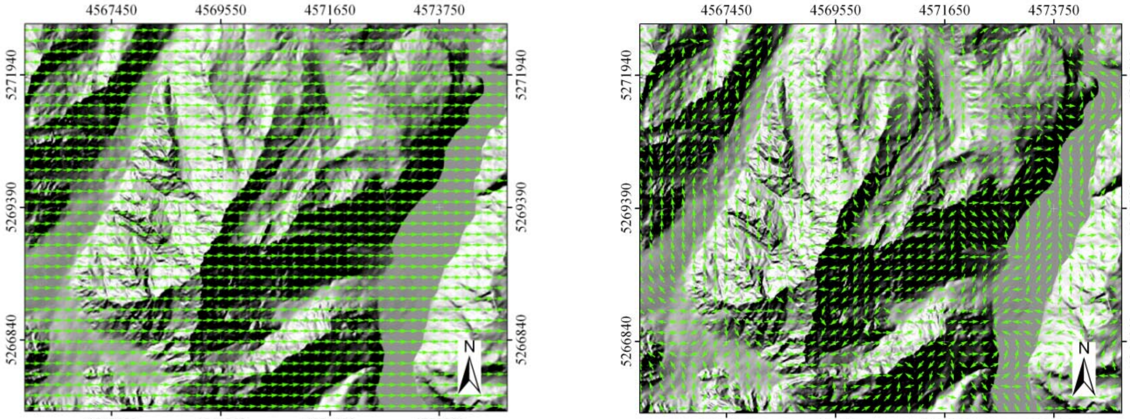
4567450
4569550
4571650
4573750
5271940
5269390
5266840
N

a) b)

Figure 34: Wind direction (detail of the Watzmann region), derived after Ryan (1977) (left) and *MM5* (right), respectively. The images represent the situation on January 9, 2004, 7:00. Wind direction is 270 degrees.

Figures 33 and 34 show a comparison between interpolated and *MM5* wind fields for a specific model step (January 9, 2004, 7:00, a cut-out of the Watzmann region cp. fig. 5 is shown). The reasons for the differences of the spatial characteristics of interpolated (fig. 33a) and 34a)) and of *MM5* wind fields (fig. 33b) and 34b)) was mentioned before. An additional example underlines the validity of the *MM5* wind fields in *Alpine* terrain. During the period of Mai 1994 through December 1999 an anemometer was installed at the *Watzmannhaus* at 1918m a.s.l (fig. 35a the location of the anemometer is marked with an arrow). The available measurements indicate that about 600 hours per year (or 6.8% of all hours) are showing wind speeds of more the 10 [m/sec]. When analysing the *MM5* data 634 hours (or 7.2% of all hours) with wind speeds of more than 10 [m/sec] were predicted for this location (fig. 35 a)), whereas 0 hours with wind speeds above 10 [m/sec] could be found in the interpolated data (fig. 35 b)).

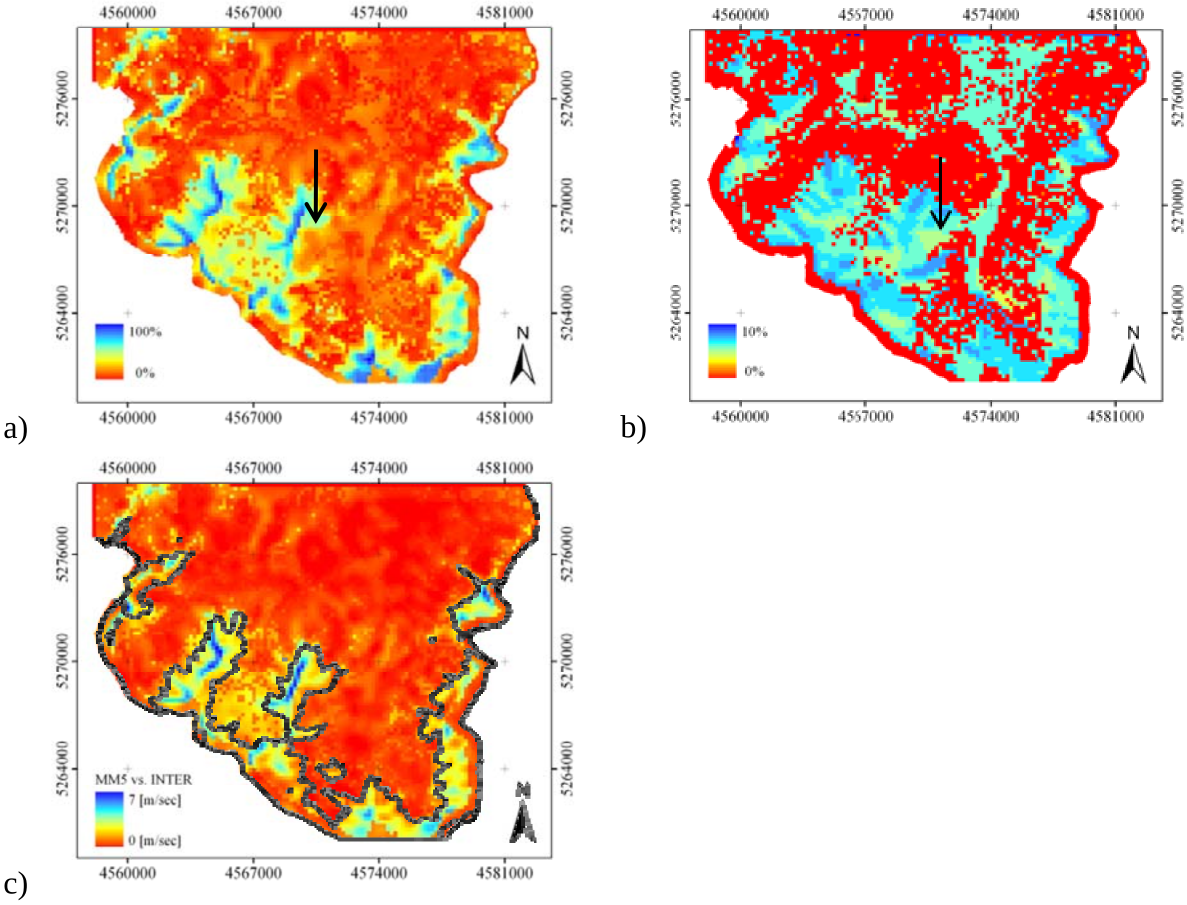
a)
4560000
4567000
4574000
4581000
5276000
5270000
5264000
100%
0%
N
b)
4560000
4557000
4574000
4581000
5276000
5270000
5264000
10%
0%
N
c)
4560000
4567000
4574000
4581000
5276000
5270000
5264000
MM5 vs. INTER
7 [m/sec]
0 [m/sec]
N

Figure 35: a) Percentage of hours with wind speeds higher than 3 [m/sec] (*MM5* fields). b) Percentage of hours with wind speeds higher than 3 [m/sec] (interpolated fields). Difference between the averaged interpolated and *MM5* wind speed for the winter season 2003/2004 (The black line is the 1800 m a.s.l. contour).

Finally, it can be assumed that *MM5* delivers more applicable data (fig. 32 to 35) for the test site. As the accuracy of *MM5* should be almost similar for all modelled cells, figure 32 a) and b) can be seen as representative for the whole area.

Chapter 4 *Snow transport modelling*

For the simulation of snow transport, accumulation, and ablation processes the *SnowModel* (Liston and Elder, 2006) including *SnowTran-3D* (Liston and Sturm, 1998) was used. *SnowTran-3D* as described in section 2.1 is a three dimensional, physically based model which simulates the wind forcing field (which was replaced by the *MM5* simulations lateron), the wind shear stress at the surface, the transport of snow by saltation and turbulent suspension, the sublimation of saltation and suspended snow, and the accumulation and erosion of snow. Therefore, the initial entrainment and the intensity of snow transport processes are dependent on the current wind conditions and on the modelled surface conditions.

First, *SnowTran-3D* runs were performed using interpolated station data (of *Snowmodel/Micromet*), and afterwards the interpolation scheme was substituted by the application of the *MM5* wind field library. This procedure was applied at the *meso* (200m) and *micro* (30m) scale. The topographic information for the *meso* scale runs was provided by the same *DEM* as used for the *MM5* wind field generation: This implies that the smoothing of the *DEM* which was conducted to ensure numeric stability of *MM5* is also reflected in the results of the snow model. For the succeeding *micro* scale runs downscaled *MM5* wind fields and topographic information provided by the *DEM* of the National park authority were used.

4.1 Results of the meso scale model runs

The results of the *SnowModel* runs were studied in three different steps. First, model grid elements which coincide with meteorological stations were analysed and the snow cover development of these grid cells was compared with the measurements. Secondly, the spatial characteristics of the modelled snow cover were analysed for *SnowModel* runs with (these runs will be indicated by *MM5* from now on) and without the *MM5* wind field library (these runs will be indicated by *INTER* from now on) and thirdly the results were compared with remotely sensed data.

4.1.1 Model results at the point scale

For checking the general model performance, modelled snow depth results were compared with ultrasonic snow depth measurements from meteorological stations *Reiteralm II*, *III,* and *Jenner*. Obviously a direct comparison of modelled and measured data is problematic due to different scales of the compared quantities: The ultrasonic measurements are representative for the observed point only, whereas a simulated grid cell represents the average of an area of 40,000 m² (200x200 m). Snow water equivalent measurements or data from field campaigns were not available for the observed winter season.

In general, the model reproduces the snow depth of the observed season quite well for both the *MM5* and the *INTER* inputs (fig. 36a) b) c)). The overall accuracy seems to depend only little on the method used, which can be explained by the fact that the average wind speed derived from interpolated station data and the *MM5* wind field library are relatively similar for altitudes below 1800m a.s.l. (fig. 35c). Unfortunately, there are no meteorological stations available above 1800m a.s.l. where such differences are much greater (fig. 35c)). However, the results computed for *Reiteralm II* and *Jenner* are slightly more accurate when using the *MM5* library instead of the *INTER* input data, although *Reiteralm II* is located in the vicinity of a wind sensor. Further analysis also revealed, that the timing of observed transport events correlates very closely with those predicted by *INTER* and *MM5* at *Reiteralm II*. This indicates that the *MM5* library reflects the situation at the stations very well.

a) *MM5* method vs. measured: $r^2 = 0.85$ INTER method vs. measured: $r^2 = 0.73$

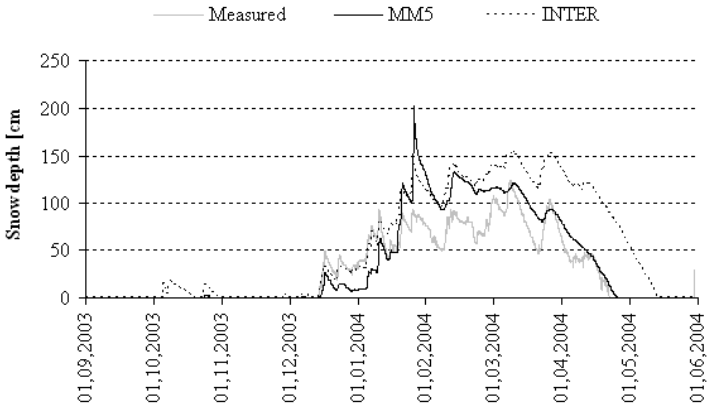

b) *MM5* method vs. measured: $r^2 = 0.88$ INTER method vs. measured: $r^2 = 0.88$

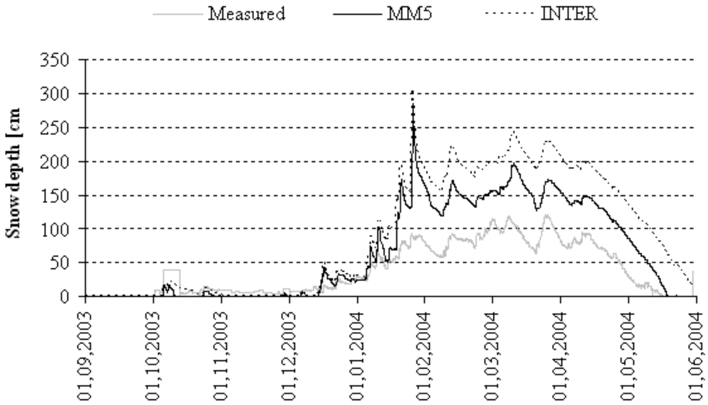

c) *MM5* method vs. measured: $r^2 = 0.73$ INTER method vs. measured: $r^2 = 0.64$

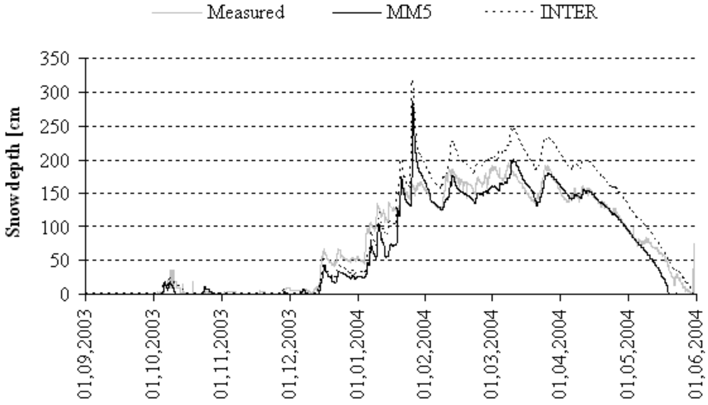

Figure 36: Comparison of model results and measured values for the meteorological stations a) *Reiteralm II*, b) *III* and c) *Jenner*.

Nevertheless, the model runs produce transport rates at the observed points which are too small compared to observations of the *Bavarian Avalanche Warning Service* (*LWZ*) for the

Reiteralm stations. This is likely caused by the smoothed topography in the used *DEM* and its relatively coarse resolution of 200 m. A similar result was reported by Liston et al. (2006) who found that snow transport events are underestimated when using a grid spacing larger than 100 m. Additionally, snow depth is overestimated in most cases, which can be explained by a precipitation event on January 24-25 registered at *Reiteralm III*: This event produced a significant increase of snow depth within all model results though a corresponding increase in measured data cannot be detected. Whether this results from an error in the station data or an inaccuracy in the conversion of snow-water-equivalent (*SWE*) to snow depth cannot be decided here because of the lack of additional meteorological data.

4.1.2 Spatial comparison of the model results

As mentioned in section 3.1.3, the increase in wind speed with elevation and the differentiation between windward and leeward areas is more distinctive when using *MM5* wind fields. This leads to regional differences within the *SWE* and snow transport rates when comparing *INTER* and *MM5* results (fig. 37 a) and b)). In a first step the *SWE* distribution in relation to altitude and aspect was analysed. The *INTER* scheme which induces less snow transport events with less intensity (fig. 37 a) and b)), produces a *SWE* distribution that is almost exclusively driven by the altitudinal increase of precipitation (fig. 38a)).

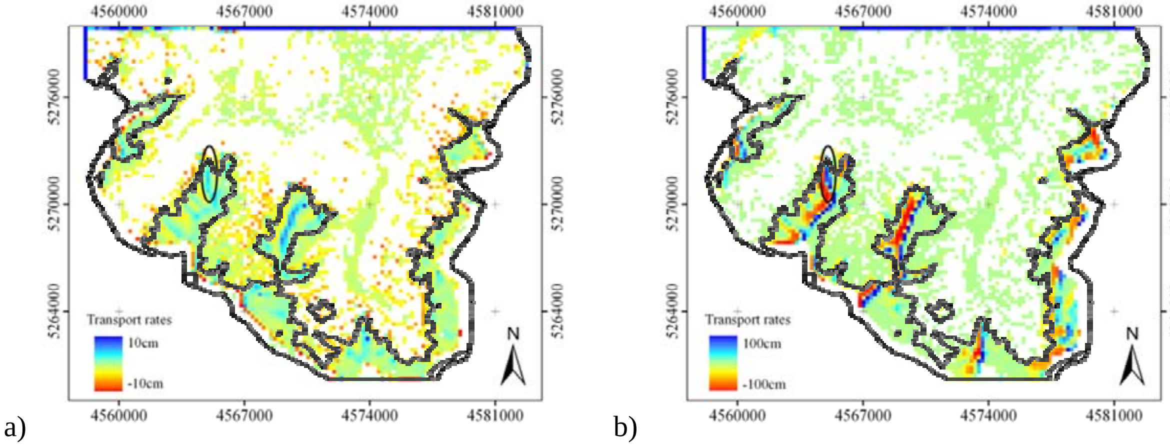

Figure 37: Amount of accumulated and eroded SWE within the study area and for the winter season (2003/04) (Please note the different scales of the legends). The accumulation zone at *Blaueis* glacier is marked with a black ellipse. The black line is the 1800m isohypsis.

Almost 96 % of the variance within the *SWE* distribution can be explained by elevation (fig. 38a)). The scattering around the mean *SWE* at a given elevation zone is small (fig. 38 a)). A noticeable dependency of *SWE* on aspect could not be found when using *INTER*. This can be explained by the fact that the homogeneous wind fields predicted by the interpolation routine lead to almost similar transport rates for all aspects. The transport terms saltation, suspension, and sublimation show a slight increase with altitude, but no significant dependency on the aspect (fig. 38 a), c), e)).

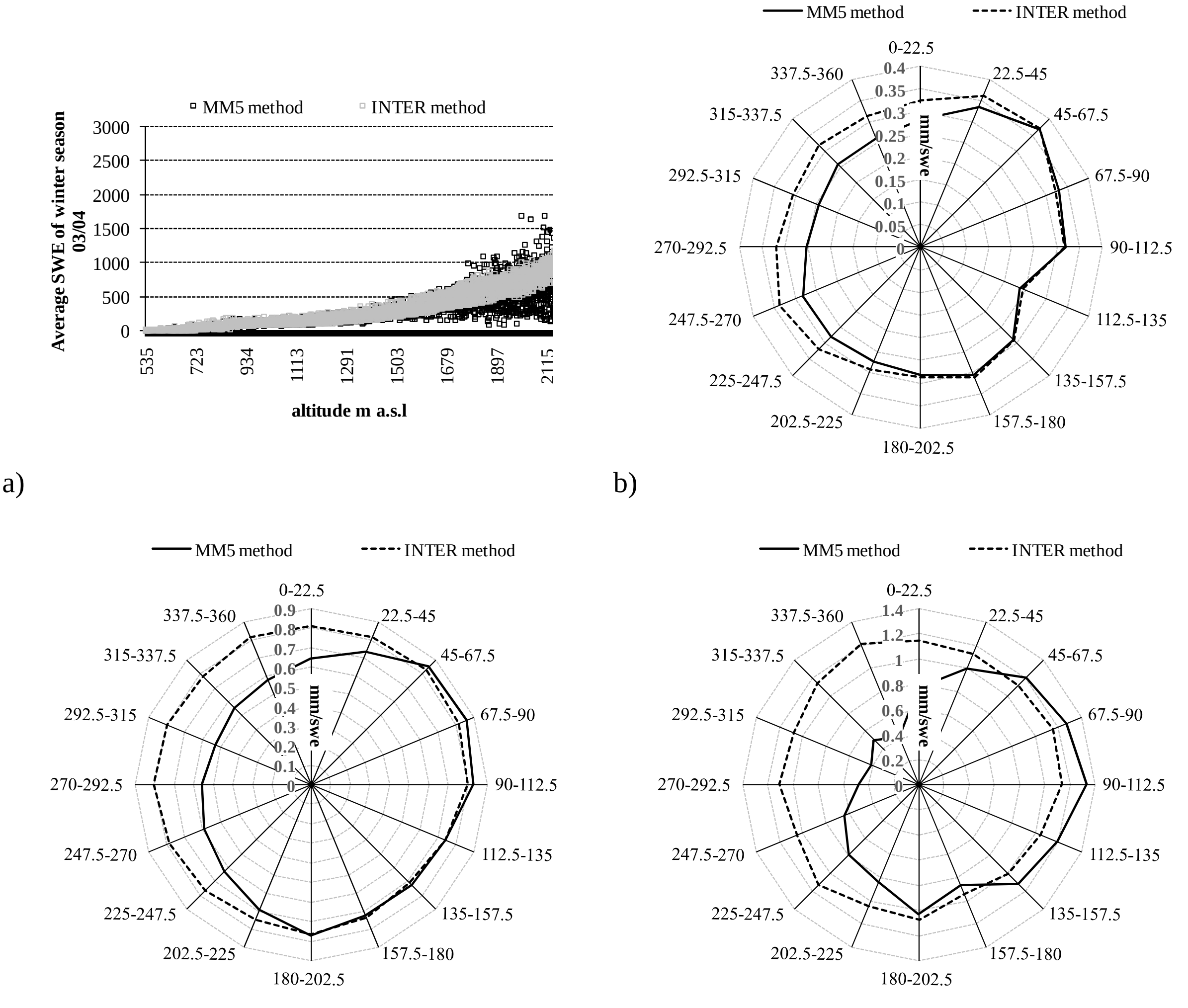

a)

b)

e)

d)

Figure 38: a) SWE [m] – elevation dependency b) SWE - aspect dependency for the total elevation interval c) SWE - aspect dependency for elevations higher than 1800m a.s.l. d) SWE - aspect dependency for elevations higher than 2200m a.s.l. SWE is the average values for the modelled time period. The different volumes under the curves are due to higher sublimation losses within the *MM5* runs. The illustrations belonging to the winter season 2003/04

Using the *MM5* method, only 84 % of the modelled variance within the *SWE* distribution can be related to altitudinal effects. The remaining variance is due to aspect (fig. 38 b), c), d)): Below 1800m a.s.l. the correlation of *SWE* and aspect explains only 2 % of the variances, whereas aspect accounts for 17 % of the variance above 1800m a.s.l., and 21 % above 2200m a.s.l (fig. 38 b), c), d)). This dependency is caused by anisotropic transport effects which are represented in the *Snowtran-3D* model when using the *MM5* wind fields of the library. The application of this method leads to a considerable differentiation of the windward sides with predominantly erosion areas and of the leeward sides where snow preferentially accumulates (fig 39 b), d), e)). These accumulations are especially intense at the eastern slopes of *Watzmann* and *Hochkalter* (cp. fig. 5). Again, it was seen that the transport and sublimation rates are negligible for elevations below 1800m a.s.l. (fig. 39 a)-e)) which explains the minor differences between the model results for the lower altitudes and in particular for the areas around the meteorological stations. Above 1800m a.s.l. the rates of the different transport terms increase greatly when using *MM5* whereas the increase was minor under usage of *INTER* (fig. 39). Furthermore, measurements of De Quervain and Meister (1987) have shown that transport fluxes are enhanced at mountain crests and slopes perpendicular to the main wind direction (230 degrees for the observed winter season). This result was reproduced when using the *MM5* model wind fields (fig. 37b). An additional effect related to the higher transport rates generated by the *MM5* method are increased sublimation rates at elevations above 1800m a.s.l. (39 e) and f)). The modelled sublimation loss rate is considerable larger when using the *MM5* method and for elevations above 1800m a.s.l. (fig. 39 f)). Sublimation losses can be neglected for elevations below 1800m a.s.l., but can reach 860 mm *SWE* or 27 % of the total precipitation for altitudes between 2400m a.s.l. to 2500m a.s.l. (fig. 39f)). The results when using the *INTER* method are one magnitude smaller and show maximum values of 50mm (fig. 39 e)).

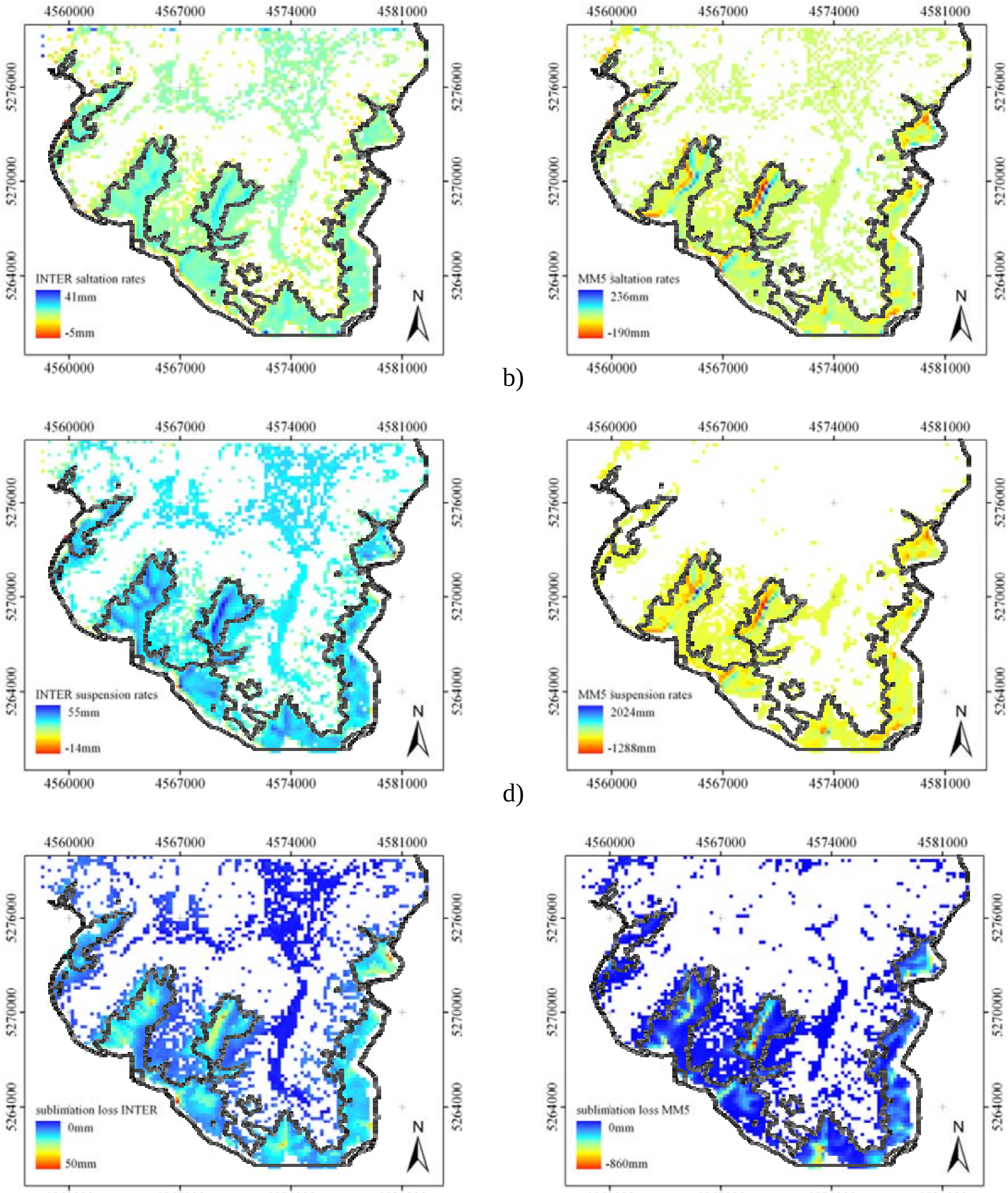
4560000
4567000
4574000
4581000
5276000
5270000
5264000
INTER saltation rates
41mm
-5mm
MM5 saltation rates
236mm
-190mm
INTER suspension rates
55mm
-14mm
MM5 suspension rates
2024mm
-1288mm
sublimation loss INTER
0mm
50mm
sublimation loss MM5
0mm
-860mm
N

a) b) c) d) e) f)

Figure 39: Intensities of the different transport terms: saltation, suspension and sublimation in a) c) e) *INTER* and b) d) f) *MM5* (winter season 2003/04). The black line is the 1800m isohypsis.

4.1.3 Spatial validation of the local scale results

For the spatial validation of the model results, remotely sensed data was used. Hence, a short overview about remote sensing of snow and the techniques used in this work will be given.

Optical and microwave remote sensing techniques are powerful tools for acquiring information about the spatial distribution and the physical properties of the snow cover. As in-situ data collection in the *National Park* area is both sparse and non-uniform, depends heavily on human observers and the accessibility of the region and data verification is almost impossible, remotely sensed data is needed to get a comprehensive picture of the snow distribution. The mapping of snow by optical systems can still be seen as the most common application in snow remote sensing. But there are also other applications. Knap *et al.* (1999) used *Landsat TM* data for the estimation of the albedo of the *Arolla* glacier (*Switzerland*) whereas the *Multiangle Imaging SpectroRadiometer* (*MISR*) is used for the same variable by Stroeve and Nolin (2002). In another work, Klein and Stroeve (2002) predicted the surface grain diameter of a snowpack with albedo information. Painter *et al.* (2003) utilized hyperspectral data for an improved subpixel description of the snow heterogeneity. A comprehensive overview about the work with microwave sensors for the estimation of the *SWE* can be found in Durand and Margulis (2005).

For the presented work optical data was used exclusively, due to the problems of microwave sensors in regions with steep topography and due to the limited spatial resolution of the respective sensors. *Landsat TM* and *ETM+* have shown their applicability for high resolution snow mapping in a lot of studies (e.g. Hall *et al.* 1995). The resolution of 30m and the arrangement of the spectral bands (fig.40 a)) make Landsat images applicable for this task. Two Landsat *ETM+* images, April 28, 2004 and May 30, 2004, were available and analysed to estimate the snow cover extent for the *National Park* area. The data was geometrically, terrain and radiometrically corrected for this behaviour. Comparison of the available *GIS* data and the spatially corrected *Landsat* images has revealed that the displacement of the 30m pixels is below of one pixel.

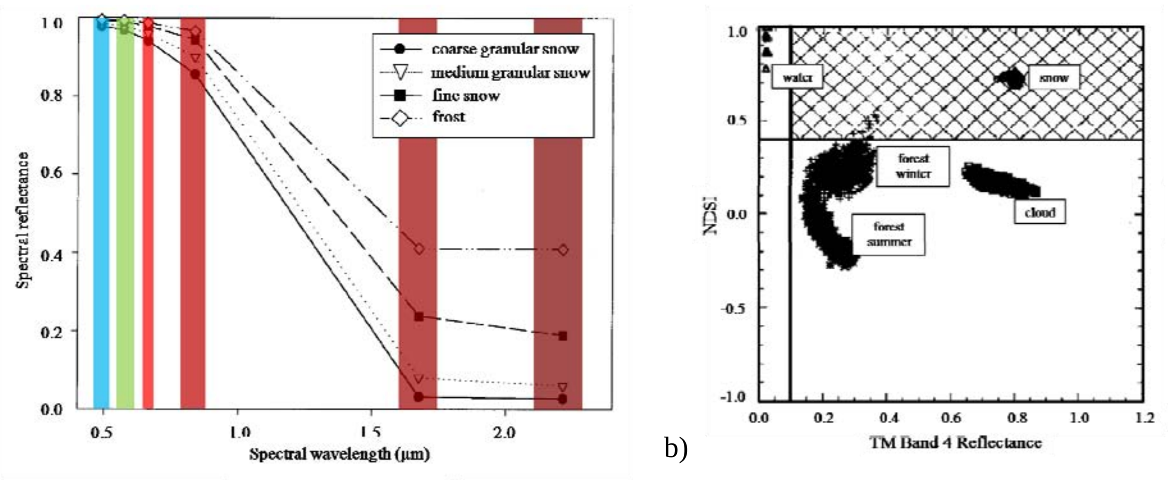

a)

b)

Figure 40: a) Spectral bands of Landsat ETM+ and spectral characteristics of different snow types. b) spectral Characteristics of different land cover types

For the estimation of the snow covered area the normalized difference snow index (*NDSI*) was used (Eq. 34). The *NDSI* trace back to band rationing techniques (Kyle *et al.* 1978; Dozier 1984) and is related to the *NDVI* (Tucker 1976).

$$NDSI = (ETM{+}2 - ETM{+}5) \,/\, (ETM{+}\,2 + ETM{+}\,5) \qquad \text{(Eq. 34)}$$

The *NDSI* profits from the fact that snow reflects visible radiation much more intensively than it reflects radiation in middle infrared. According to Hall *et al.* (2001) the index achieves an accuracy of about 99% in non-forested areas and about 85% in forested areas under full snow coverage. If water bodies are present within the investigation area the inclusion of an additional threshold becomes necessary. Open water shows a more or less identical *NDSI* value as snow does, which can lead to a misinterpretation of the respective areas. When considering figure 40 b) it becomes obvious that water and snow can be differentiated by means of the reflectance between 0.76µm and 0.90µm. Hence, an additional inquiry was introduced if the *NDSI* exceeds 0.35. It is also checked, if the reflectance in *TM* channel 4 exceeds 0.4, if both are warranted the pixel is classified as snow. The threshold of 0.35 was chosen on the basis of literature (Hall *et al.* 1995) and because of visual comparisons. At lower thresholds many non-snow-pixels were identified as snow, greater values lead to an underestimation of the snow cover especially in wooded areas. Hall *et al.* (1995) found that an additional classification error of about 3% has to be expected if the *NDSI* is applied to images without a radiometric correction. They predicted a greater snow cover when reflectance was used instead of Digital Number (*DNs*). Thus, the used Landsat images were processed with the help of *PULREF-H* (Bach 1995).

According to Hall *et al.* (1995) the detection of snow with the help of the *NDSI* is straightforward and accurate in open and fully snow covered areas. The situation changes if the snow coverage drops below of 100%, or if the snow is covered by e.g. trees. Snow in mixed pixels is widely detected by the *NDSI* at the 30m scale of the Landsat images and is therefore not a significant source of errors. The existence of dense woods on the other hand can make the detection of snow nearly impossible, which has to be regarded as a bigger limitation of optical systems than an error during analysis. It is a common approach to classify wooded areas as snow covered if they are completely surrounded by snow (e.g. for the *NOAA* snow product Hall et al. (1995)). Nevertheless, this procedure is only useful if one can assume identical melt rates for the woods and for the surrounding areas. This is often not the case due to the fact, that a forest canopy can lead to both less *SWE* and shorter duration, or more *SWE* and longer duration of the snow cover beneath the trees, depending on many factors such as canopy density, gap size and distribution, geographic location, and meteorological conditions (Pomeroy et al. 2002). This makes any conclusion drawn from the surrounding conditions to snow conditions within canopy stands difficult.

Data processing has shown that the *NDSI* is nearly independent of the resampling sequence. This fact causes that the *NDSI* value to stay approximately the same, weather the Landsat image is resampled first to a 200m resolution and the *NDSI* is predicted afterwards or if the procedure is reversed. For the estimation of a cloud mask for the April scene the *NDSI* was used again. Clouds and snow are both highly reflective in Landsat *ETM+* Band 2, but the reflectance differs at band 5 were the cloud reflectance is higher than the snow reflectance. An iterative adaption of the threshold value has lead to a satisfying cloud mask (pink areas in fig. 41a/b). As the *MM5* and *INTER* results does not differ with respect to the snow line they are not separately discussed. The *MM5* results can be seen as representative for both which is due to the fact that the snow line is located below of 1800m a.s.l. (black line in fig. 41) and therewith below of the region were wind induced snow transport processes significantly influence the snow distribution (cp. fig. 39).

Model and classification results are shown in fig. 41 a) to d). The analysis shows that the model is overestimating the snow coverage on both dates and for all of the four massifs in the region. The modelled snow line lies approximately 200-400 meters (1-2 pixels) in distance lower than the observed one. It has to be stated that an exact analysis of the model error is difficult due to the fact that the snow line is located in wooded regions on both observation dates. Furthermore a quantitative validation is impossible on the basis of optical remote sensing data.

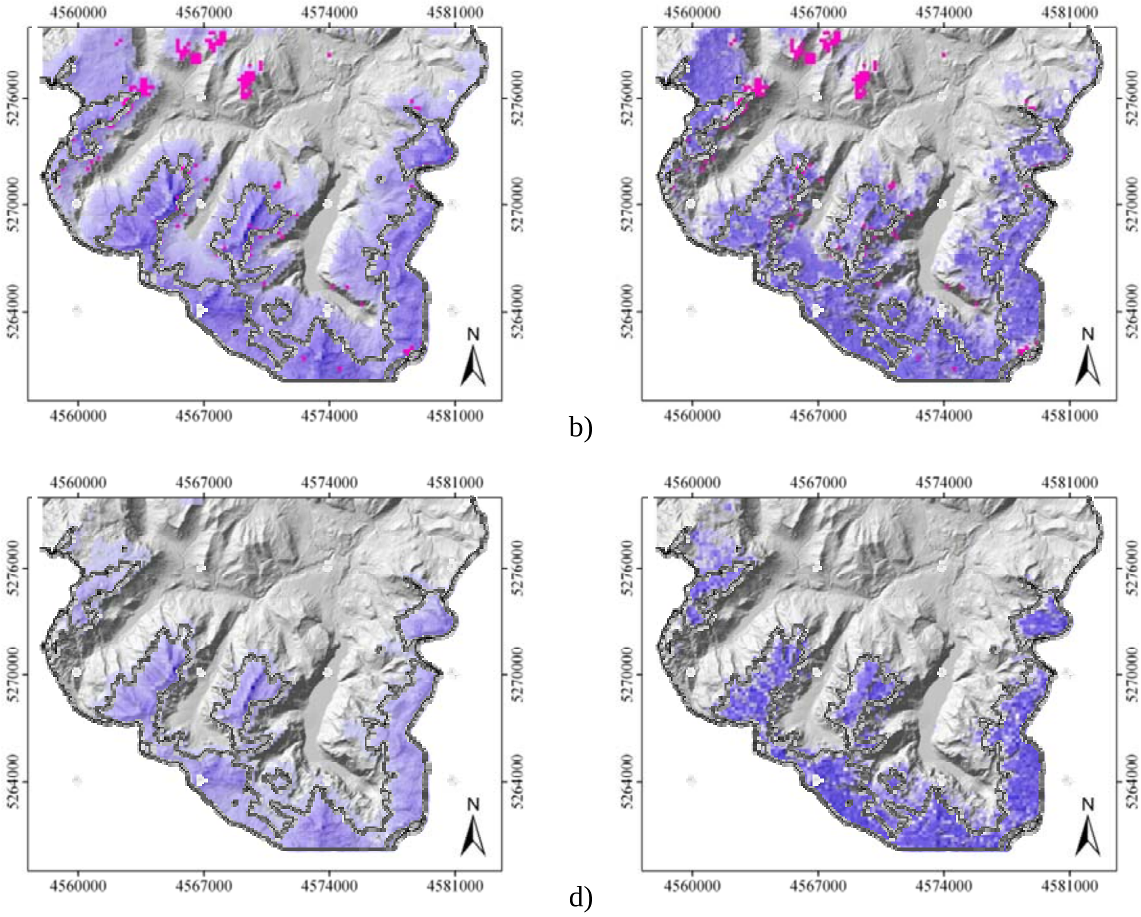

a) b) c) d)

Figure 41: a) modelled snow cover of April 28, 2004, b) *NDSI* map of the same date, c) modelled snow cover of Mai 30, 2004 d) *NDSI* map of the same date. The black line is the 1800m isohypsis.

86% of the pixels show an agreement between modelled and classification results on April 28. 3% of the pixels are classified as snow free but are snow covered in the model results whereas 11% of the pixels are defined as snow covered by the model but are snow free in the classification. The results of May 30 are very similar; the agreement is 88%, 2% of the pixels show a classified snow cover but no modelled one, and 10% show a modelled snow cover but no classified one. The Landsat images are shown in fig. 42 a) and c), the differences between classification and model results in fig. 42 b) and d).

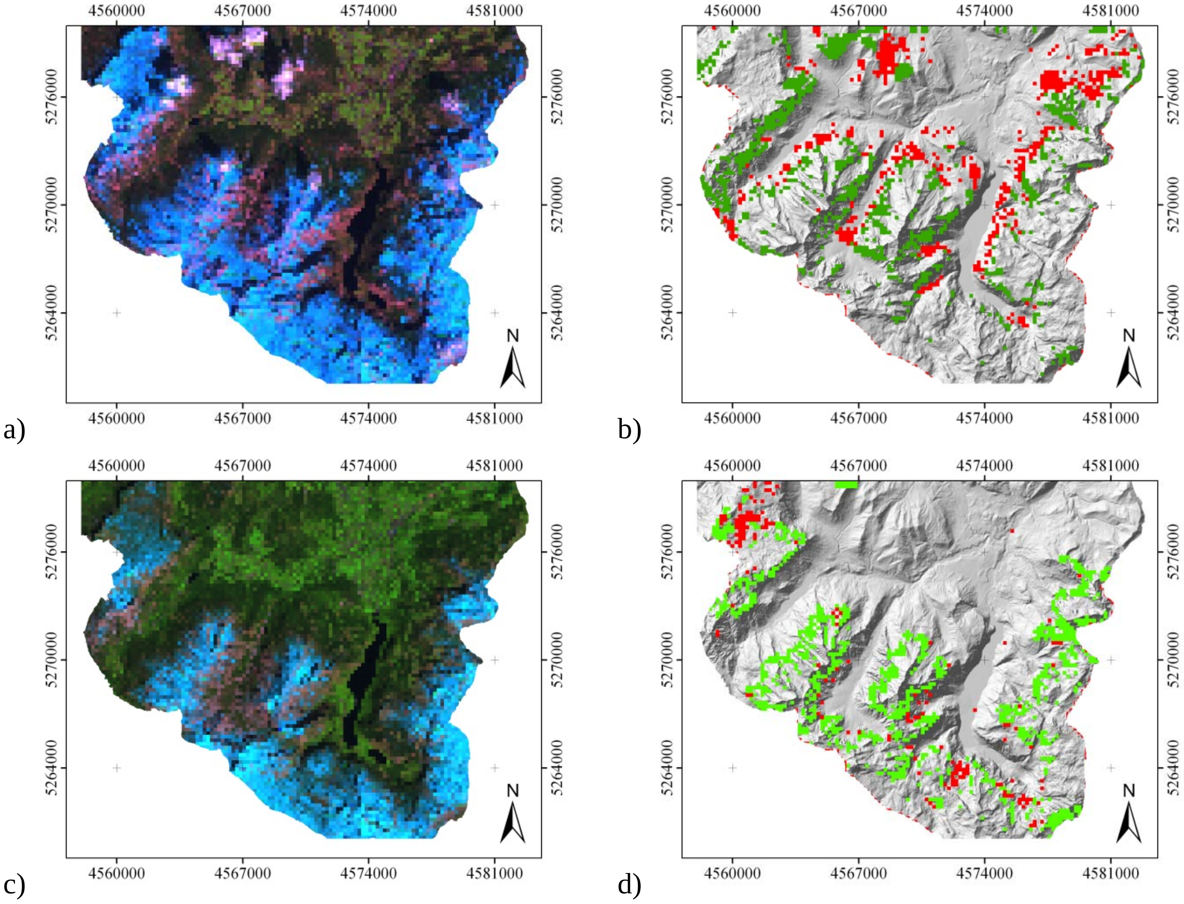
4560000
4567000
4574000
4581000
5276000
5270000
5264000
N

a) b) c) d)

Figure 42: a) c): *Landsat ETM+* images (April, 28 2004 and May, 30 2004. resampled to a 200m resolution). e) f): Differences between model an classification results at April and May respectively (red indicates: only classified snow cover. Green: only modelled snow cover).

4.2 Downscaling of the MM5 wind fields

It can be seen that the model delivers plausible results at the 200m scale. Nevertheless, a definition of the precise locations of accumulation and erosion is impossible at the *meso* scale (Liston et al. 2006).

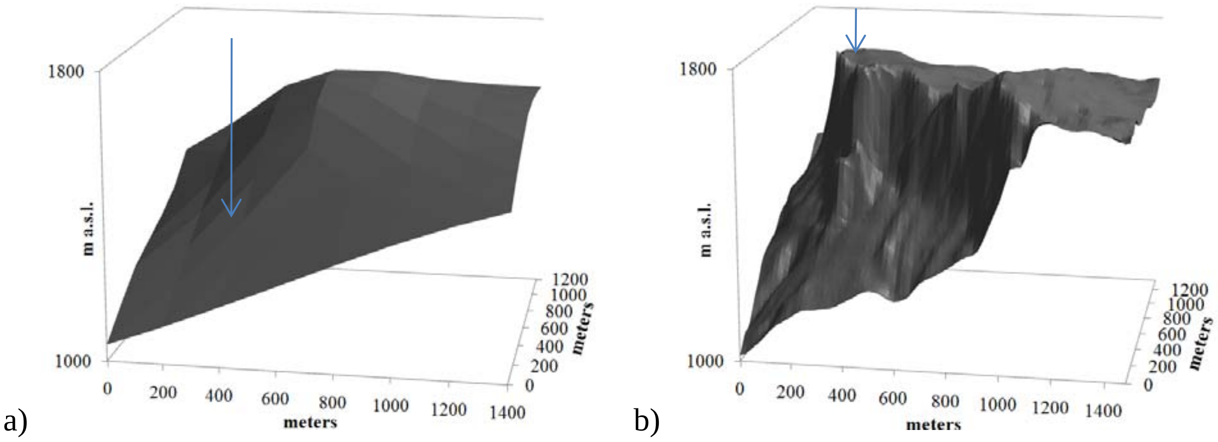

Figure 43: a) The smoothed *Reiteralm* area (marked with an arrow) within the *MM5* DEM (200 m resolution) compared to b) the National Park DEM (30 m resolution).

To determine these locations, model runs with a higher spatial resolution are needed. Furthermore, a finer resolution than 200m is needed to analyze the model performance by comparing the model results to the close meshed field campaign data and to remotely sensed data. The selected target resolution of 30m meets the requirement that the *support*, *spacing*, and *extent* of model results, remotely sensed data and field measurements are unitary. The adaption of *SnowModel* to a 30m resolution was unproblematic because all components are scale independent and permit model runs up to a resolution of 5 meters (Liston *et al.* 2006). However, to realise the 30m model runs, the *MM5* wind fields had to be downscaled to this resolution. A downscaling and correction of the *MM5* wind fields is required because of the smoothing of the *DEM* which processed in prior of the *MM5* model runs. Figures 43 show the area around Reiteralm (marked with an arrow) within the 200m and the 30m *DEM*. The effect is apparent; *Reiteralm* is located at the mountains slope in the 200m *DEM* and not at the crest like in reality. Hence, the original *MM5* data is not representative for the “real” location of *Reiteralm* and has to be overworked therefore. The different downscaling steps are displayed in figure 44.

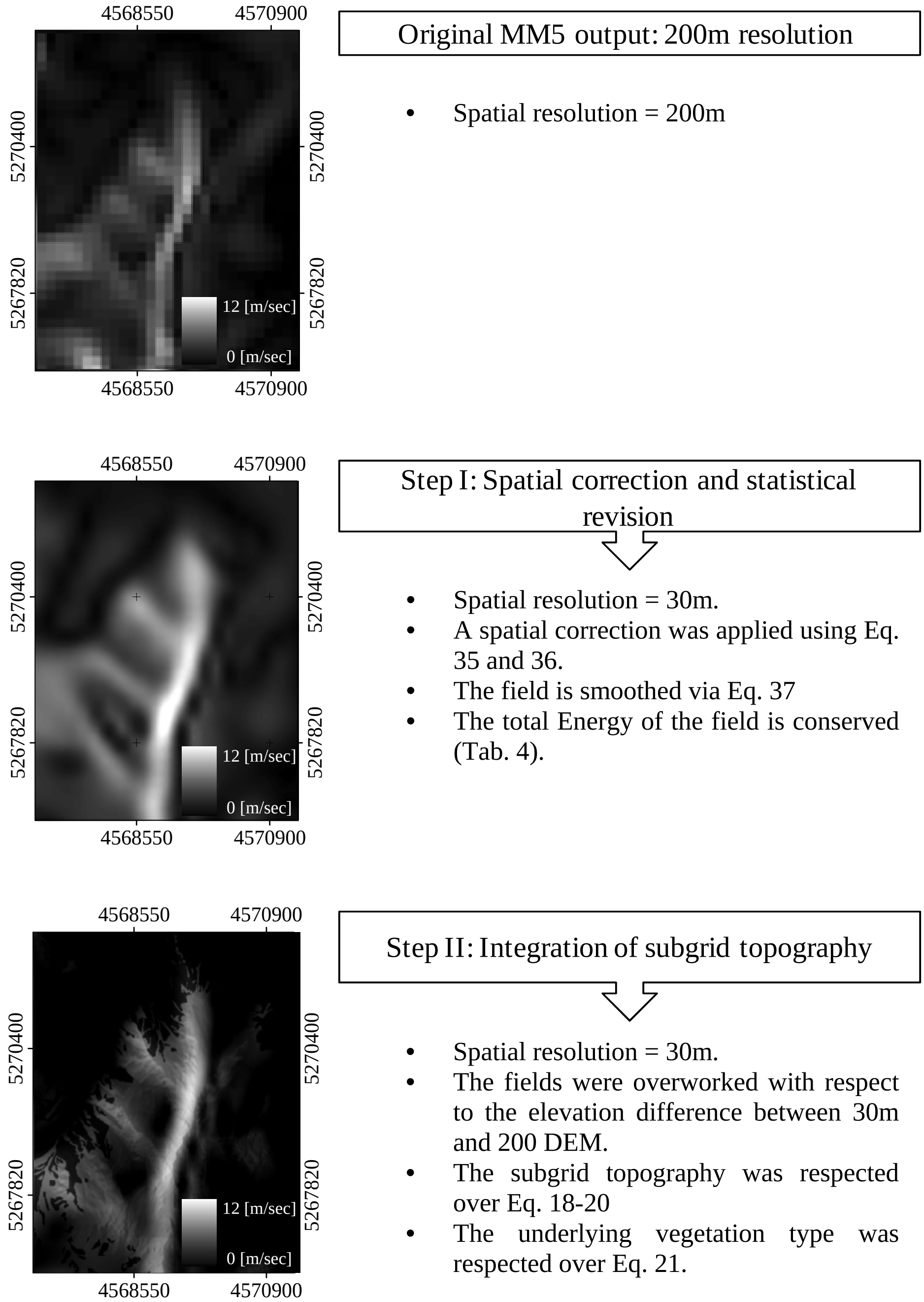

Original MM5 output: 200m resolution

- Spatial resolution = 200m

Step I: Spatial correction and statistical revision

- Spatial resolution = 30m.
- A spatial correction was applied using Eq. 35 and 36.
- The field is smoothed via Eq. 37
- The total Energy of the field is conserved (Tab. 4).

Step II: Integration of subgrid topography

- Spatial resolution = 30m.
- The fields were overworked with respect to the elevation difference between 30m and 200 DEM.
- The subgrid topography was respected over Eq. 18-20
- The underlying vegetation type was respected over Eq. 21.

Figure 44: Performed downscaling steps. The figure shows the a schematic illustration of the downscaling steps conducted in 4.2.1 to 4.2.3.

4.2.1 Spatial correction

A prerequisite for the model runs at the 30 m scale was a geometric correction of the *MM5* wind fields. This is necessary for two reasons I) the modifications at the 200 m *DEM* to guarantee numerical stability of the *MM5* model (Bernhardt et al. 2008a and b) and II) resolution dependent shifts of the apexes and minima between 30 m and 200 m *DEM*. The deviations resulting from the higher resolution are especially obvious at very exposed areas like *Reiteralm* (fig. 43) *Watzmann*, or *Hochkalter* (cp. fig. 5) and can be observed when comparing the 30m *DEM* with the 200 m *DEM* as well as the predicted wind fields. In the case of *Reiteralm* the crest of *Wartsteinkopf* (fig. 43 a)) still appears, but not in the position that it is in in reality (fig. 43 a)). Therefore, a validation of predicted data with the help of station measurements is complicated without a correction. Compared to the 30m *DEM* the crests of *Watzmann* and *Hochkalter* (cp. fig. 5) are shifted eastwards within the 200m *DEM*. This offset can be also detected when analyzing the wind fields itself. The topographically caused convergence of the airstream and the resulting acceleration of the air masses at the mountains crests are shifted into the eastward faces of the respective massifs under usage of the 30m *DEM*.

For the correction a well known approach used by a number of remote sensing applications was used. The correction was achieved with two 2 dimensional second order polynomials:

$$Z' = a1 * Z^2 + a2 * S^2 + a3 * Z + a4 * S + a5 * Z * S + a6 \qquad \text{(Eq. 35)}$$

$$S' = b1 * Z^2 + b2 * S^2 + b3 * Z + b4 * S + b5 * Z * S + b6 \qquad \text{(Eq. 36)}$$

Equation 35 stands for the new row coordinate and equation 36 for the new column coordinate. Pass points were used for the determination of the coefficients a1-a6 and b1-b6. Under usage of more than six control points the system of equations becomes over-determined and could be solved with the smallest quadratic deviance between the coefficients a1-a6 and b1-b6. As all of the *MM5* wind fields are based on the same *DEM* the whole library could be adapted to the 30 m *DEM* using the same set of control points.

4.2.2 Statistical revision

The statistical revision was done in order to prevent of artefacts of the original 200 m pixels in the downscaled 30 m data and in the snow model results, respectively. A *Radial Basis Function* (*RBF*) (eq. 37) was used to smooth the wind fields and to eliminate the coarse grid structure while conserving the total amount of energy of each wind field (tab 4, fig. 44)).

RBF is a local statistical technique, calculating predicted values from measured points within a defined neighbourhood that is smaller than the total area. As this approach maintains the total energy, the modeled 200 m pixel values are conserved. For verification, comparisons of mean wind speeds were made before and after applying this statistical approach between the original 200 m pixels and the 30 m pixels corresponding to the area of the original 200 m grid cell. The differences were close to zero (tab. 4).

Table 4: Column I: Mean value of all 220 wind fields between the average value of the original and the modified *MM5* wind speeds. Column II: Maximal observed difference between original and modified *MM5*. Column III: Minimal observed difference.

Mean deviation	Maximal deviation	Minimal deviation
0.003 [m/s]	0.02 [m/s]	0.00 [m/s]

The completely regularized spline function that was used is:

$$\phi(r) = -\sum_{n=1}^{\infty} \frac{(-1)^n (\sigma * r)^{2n}}{n!n} = \ln(\sigma * r/2)^2 + E_1(\sigma * r/2)^2 + C_E \qquad \text{(Eq. 37)}$$

ϕ *(r)* = Radial basis function, r = the Euclidean distance ($r = ||s_i - s_0||$ is the distance between the estimation location s_0 and each data location s_i), σ = the smoothing parameter, *ln* = natural logarithm, E_l = exponential integral function, C_E = Euler constant.

4.2.3 Inclusion of the height difference between MM5 and 30 m DEM

The coarser resolution of the modified *MM5 DEM* leads to smoothed elevation minima and maxima. This has a direct effect on the generated wind fields, which also show over- or underestimated wind speeds. To address this effect, the difference between the two *DEM* was calculated for the thirty meter resolution. Subsequently, the elevation gradient of wind speed was calculated for each modelled wind field. It became obvious that there are two distinguishable elevation gradients within the datasets. There is one gradient for the interval from 500 to 1800m a.s.l. and another for 1800 to 2700m a.s.l.. This separation was necessary because the gradient above 1800m a.s.l. was considerably steeper than the gradient for the lower elevation interval. As a result, this analysis provides a value for the increase of wind speed per meter elevation for the two intervals. In a subsequent step, these gradients were combined with the elevation difference of the two *DEMs*. As a result, higher wind speeds were generated at locations with positive divergences, and reduced values were computed at locations where *MM5 DEM* elevation values are higher than the ones of the 30 m *DEM*. Therefore, the resulting correction file contains a positive or negative correction value for all 30 m pixels. These values were added to the statistically corrected *MM5* wind field.

4.2.4 Integration of subgrid topography

Due to the relatively coarse resolution of 200 meters most of the small scale sinks and hills of the 30 m *DEM* were not considered during the *MM5* modelling procedure which means that they had no influence on the generated wind fields. That makes a subsequent consideration of this subscale information necessary. The algorithms of Ryan (1977) and Liston and Sturm (1998) described in 2.1.2 were used for this purpose.

Figure 44 shows a detailed view of the *Watzmann* region, fig. 44 (Original MM5 output) shows an unprocessed wind field as fig. 44 (step 1) show a wind field after application of the statistical revision and fig. 44 (step II) shows the final result of the downscaling process. It is obvious that the downscaled version shows much more details. Furthermore, it can be seen that the influence of the vegetation leads to very small wind speeds in forested regions (identifiable as black edges).

4.4.5 Validation of the downscaled MM5 wind fields.

The correlation between measured and modelled daily wind speeds was greatly improved by the downscaling procedure. The original modelled data correlated with an r^2 of 0.23 to the measurements while the downscaled set produced an r^2 of 0.62 for the season 2003/2004 (fig. 45 a) and b)). The regression line is forced through the origin in both cases. It can be argued that the measured wind speeds could only be reproduced adequately by using the downscaling routine. The hourly data show a lower convergence between measurements and model results the r^2 is 0.21 here. The limited accuracy of the hourly data is mainly due to the fact that the measurements have a higher variability than the modelled data (fig. 32)) which is due to local phenomena (like cooling or heating of some areas etc.). These temporary effects cannot and should not reproduced by the *MM5* model when using the presented scheme, since the *MM5* model was run with the intention that the wind fields reach steady state conditions under a certain synoptic inflow. This was done because of the assumption that high wind speeds which are generating remarkable snow transport events are due to the synoptic inflow and not to local and micrometeorological influences. These were ignored due to their abundance and because of the fact that they are not the driving force for snow transport processes. To sum it up, the determination of the current wind field depends on the synoptic situation which changes less frequently than the local conditions and the results are therefore in line with expectations. Overall, the application of the downscaling routine leads to a considerable improvement of the model results which are now reflecting the local conditions much better than before.

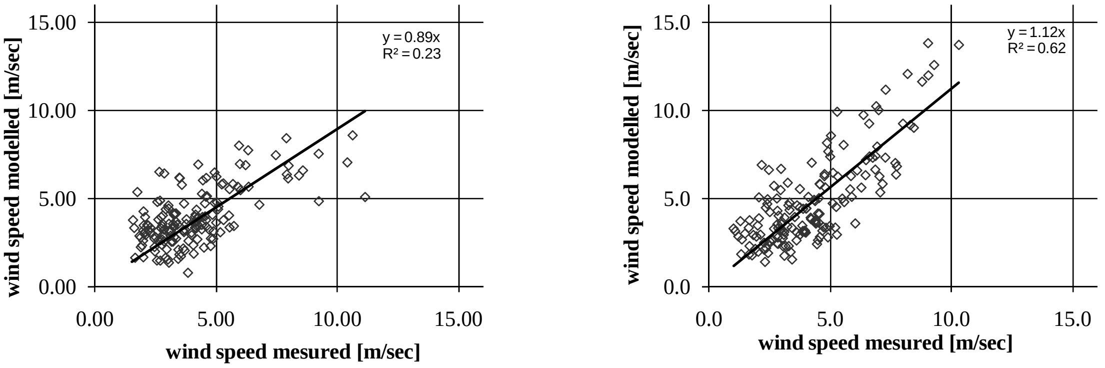

Figure 45: a) Correlation between *MM5* results and station recordings before the downscaling procedure (*Reiteralm I*, daily resolution) b) Correlation between *MM5* results and station recordings after the downscaling procedure. The regression line is forced through the origin.

4.3 Results of the micro scale model runs

The model runs presented within the next section cover the winter seasons of 2003/04 and 2004/2005. Unfortunately, there was no winter season where field campaign data, remotely sensed data, and *Lokalmodell* data for the library key, were available simultaneously. Hence, the 30m model runs of 2003/04 were validated on the basis of remotely sensed data, while the runs of 2004/05 were compared to the field measurements. The required input parameters were provided by the same meteorological stations as described before (tab. 2). In accordance to section 4.1 where model runs with *MM5* wind fields were named *MM5* and *INTER* if the interpolation routine was used, the different 30m runs will be also indicated by two different abbreviations. The runs will be called: *INTER_30* (*SnowModel*/*SnowTran-3D/interpolated wind fields*) and *MM5_30* (*SnowModel*/*SnowTran-3D/MM5wind fields*) in the following sections.

The well instrumented sites *Reiteralm* and *Kühroint* were selected for this behaviour (cp. fig. 5, fig. 46 and fig. 47)**.** *Reiteralm* has an area of about 2 km². Two of the three available automatic stations were installed for observe snow transport processes from the higher situated area (meteorological station *II*), to the lower area around station *III* (fig. 5).). This site was used to test the ability of the coupled *MM5_30* model algorithm to reproduce the recorded transport events. At *Kühroint*, which is more sheltered from the wind, the correct reproduction of minimal or no transport conditions by *MM5_30* was tested.

4.3.1 Results at Reiteralm

The results at *Reiteralm* showed a satisfying convergence between modelled and measured snow depth. However, the modelled snow depth was generally overestimated at the upper part of *Reiteralm* and underestimated at the lower parts (fig. 46). Figure 46 shows the location of the measuring points. The green colour indicates that the modelled snow depth was in average 10% higher than the measured one, whereas the red colour indicates that the modelled snow depth was in average 10% below of the measurements. The white colour denotes measuring points were the model results were within these thresholds.

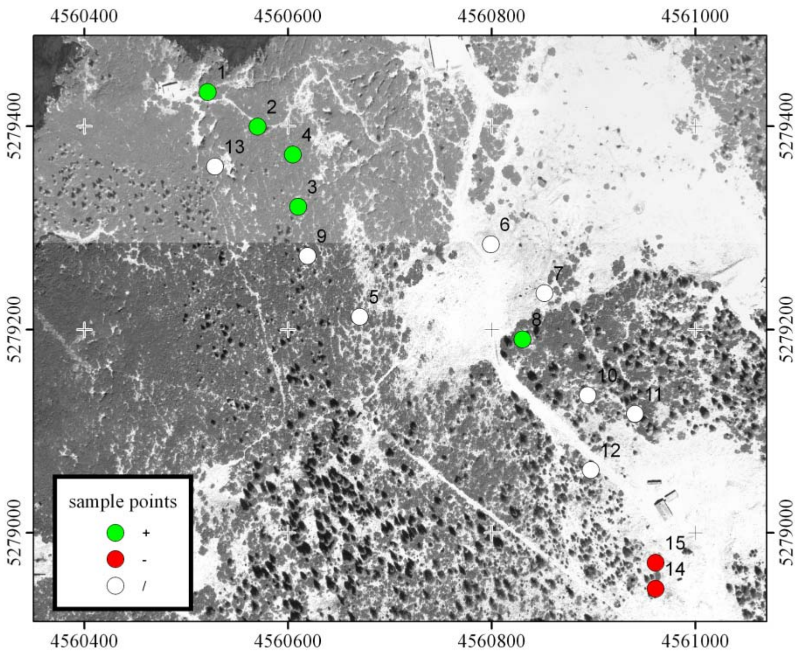

Figure 46: Comparison of model and measurements. White dots indicating that the model is within 10% of the measurements. Green dots stand for a model overestimation of the snow depth from more than 10%, red dots for a model underestimation from more than 10%.

A comparison of model and field campaign results also reveals that differences between the measurements at the sample points could be reproduced by the model to some degree, but the modelled variability is generally too small (tab. 5).

Table 5: The table shows the standard deviations of the measurements and of the respective model results for the observation dates.

	08.02.04	15.02.04	23.02.04	02.03.04	10.03.04	14.03.04	23.03.04	30.03.04	05.04.04
Measured	43mm	41mm	35mm	39mm	54mm	53mm	38mm	37mm	39mm
Modelled	19mm	19mm	21mm	20mm	24mm	23mm	17mm	14mm	12mm

Table 5 show the standard deviations of all measurements per date and the same information for the respective model results. It can be seen that the standard deviations between the measurements are a magnitude higher than that of the *SnowModel* results. Furthermore, the variation of the measured snow depth between the dates is higher, than that of the modelled values. The differences within the model results are approximately similar for the first seven dates and only slightly smaller for the last two dates.

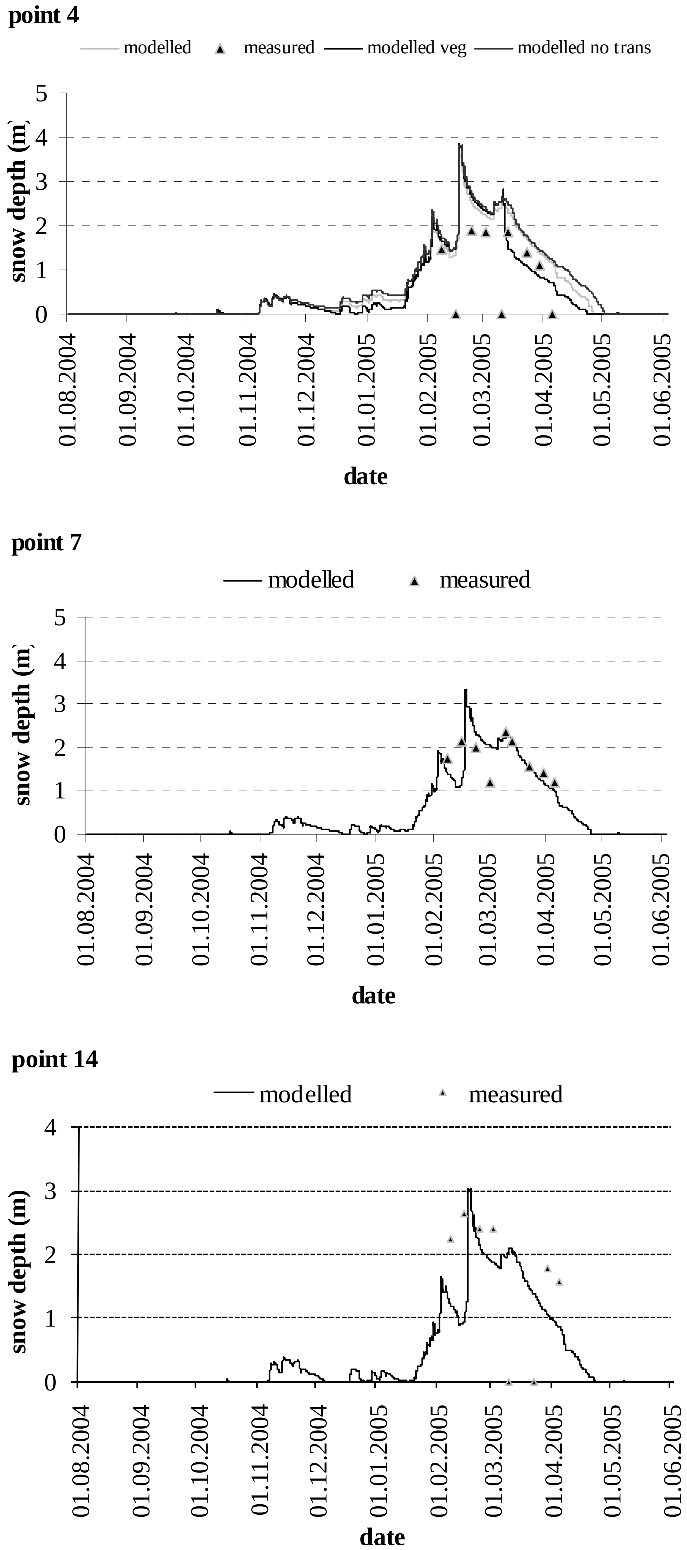

Figure 47: a) is representative for the upper part of *Reiteralm*. b) For the central region and c) For the lower part.

Experiences of the *Avalanche Warning Service of Bavaria* which has observed this site for over 10 years indicate that considerable amounts of snow are blown from the upper (characterised by sample points 1-8, fig. 46) to the lower part of the site (sample points 14 and 15, fig. 46). This experience is confirmed by the snow depth measurements of the automatic meteorological stations *Reiteralm II* and *III* but could not be reproduced to some degree by the snow transport model. Hence, the transport processes were underestimated during the first model run and using the existing vegetation snow holding capacities. For the first model run at *Reiteralm* the parameterisation of the vegetation classes was adopted from Liston and Sturm (1998). After that, the vegetation type *mountain pine* was introduced and adapted with respect to field measurements and to model results. Additionally, a vegetation type *sporadic trees* was created for areas with sparse canopy stands. For doing so the snow holding capacities of the vegetation type, deciduous forest were reduced.

By adding the new vegetation types and *MM5* wind fields the model results could be improved at the upper part of the *Reiteralm* (fig. 47 a)), but there are only minor changes at the lower part. A difference in the model results caused by the use of modelled *MM5* versus the interpolated wind fields could only be found at the upper stations. The other stations are close to the forest or within the forest which causes the differences to be negligible.

4.3.2 Results Kühroint

The overall accuracy of the *SnowModel* results is very well for *Kühroint*. The convergence of modelled and measured results is good. The model is within 10% error at seven of 15 sample points. It underestimates the snow depth by more than 10% in average for six points and overestimates the snow depth by more than 10% in average for two points. The distribution of the sample points is visualized in fig. 48. It can be seen that the snow depth is especially underestimated by the model for the sample points in the north eastern part, whereas the results at the centre and at the western parts fitting very well to the measurements.

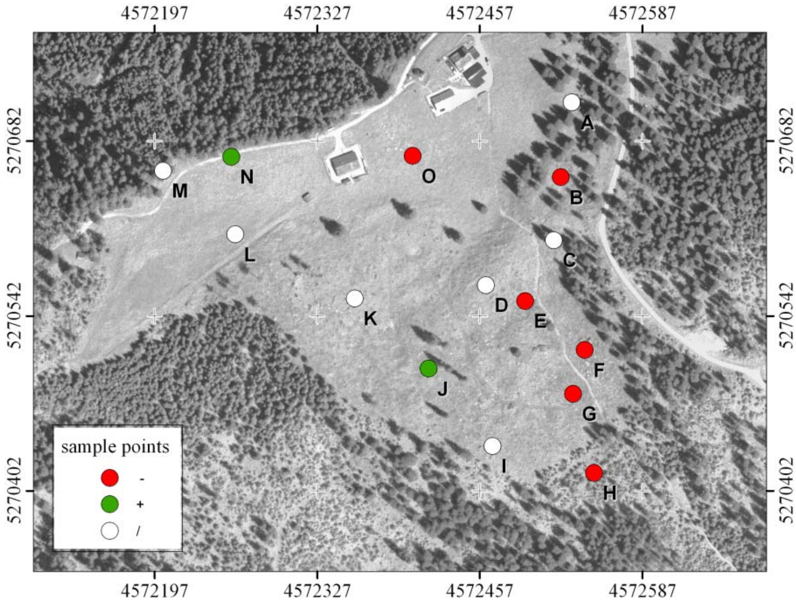

Figure 48: Comparison of model and measurements. White dots indicating that the model is within 10% of the measurements. Green dots stand for a model overestimation of the snow depth from more than 10%, red dots for a model underestimation from more than 10%.

The results shown in table 6 corresponding to them found at the test site *Reiteralm*. The standard deviations of the measurements are again higher than these of the model results. The predicted values lie between 31mm and 43mm (tab. 6). The range of the values is smaller than that detected for the measurements at *Reiteralm* (12mm). The predicted standard deviations for the *SnowModel* results are especially small at the first five dates (around 4mm) and reach up to 17mm for the succeeding dates.

Table 6: The table shows the standard deviations of the measurements and of the respective model results for the observation dates.

	08.02.04	15.02.04	22.02.04	02.03.04	08.03.04
Measured	37mm	36mm	31mm	32mm	40mm
Modelled	4mm	5mm	4mm	4mm	4mm

	15.03.04	22.03.04	29.03.04	12.04.04	19.04.04
Measured	37mm	33mm	36mm	43mm	36mm
Modelled	17mm	15mm	13mm	16mm	14mm

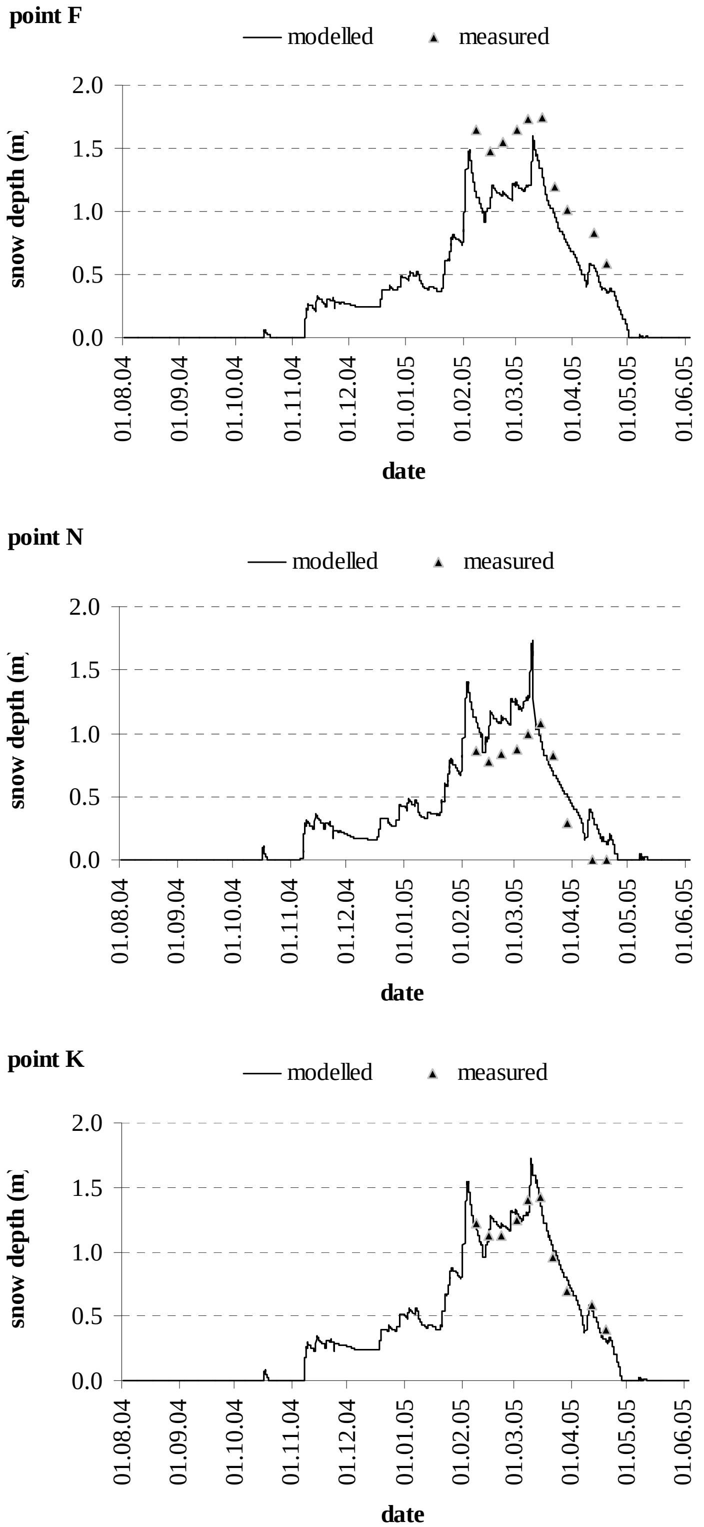

Figure 49: Three representative points at Kühroint. Point N) is located at the edge of the forest at the northern part of Kühroint; point F) is located at the clear cut area, and point K) can be found on the meadows in the western part of the area.

Figure 49 shows three sample points at *Kühroint*. Point N) is located at the edge of the forest at the northern part of *Kühroint*; point F) is located at the clear cut area, and point K) can be found on the meadows in the western part of the area. The three points represent the range of model results of snow depth versus observational data: maximum overestimation N), best fit K) and maximum underestimation F). It is important to note that there are almost no differences in amount and timing of snow transport between the *MM5* wind fields and interpolated wind fields, for the observed winter season. This proves the applicability of the *MM5* wind fields, because the wind speed and direction measured by the meteorological station *Kühroint* can be seen as representative for the whole clearance. As a result, the *MM5* wind fields can be regarded as representative for *Kühroint*.

4.3.3 Spatial comparison of the model results

The spatial comparison of the 30m results will be performed on the basis of section 4.1.2. The analysis will show to which extent the model raster resolution influences the general pattern of the snow distribution. Figure 50 a) (model results at 30m resolution) seems to be very similar to figure 38 a) (model results at 200m resolution) at first sight. However, other than in the 200m model resolution runs, the statistical correlation of elevation and *SWE* is approximately the same for *INTER_30* ($r^2=0.94$) and *MM5_30* results ($r^2=0.93$). This effect can also be seen in Figures 50 b) to d). Both Figures show that there is no significant interrelation between *SWE* distribution and aspect.

The transport intensities in opposite show a similar distribution to the 200m runs with the application of the *MM5* wind fields leading to a considerable increase of the transport rates (fig. 51 and fig. 52 a)-f)). But the spatial extent of the areas affected by intensive transport processes is smaller in the *micro* scale results and does therefore not significantly influence the absolute *SWE* distribution of the area. A comparison of fig. 38 and 50 illustrates this fact. Furthermore, in comparison to the 200m *MM5* results the *MM5_30* transport pattern is more heterogeneous and does not show the clear transport tendency from west to east (fig. 51 b) fig. 52 b) and d)). For example, transport processes with a south to north component can now be observed at the small crests at the west side of *Hochkalter* or *Watzmann* which are stretching from west to east.

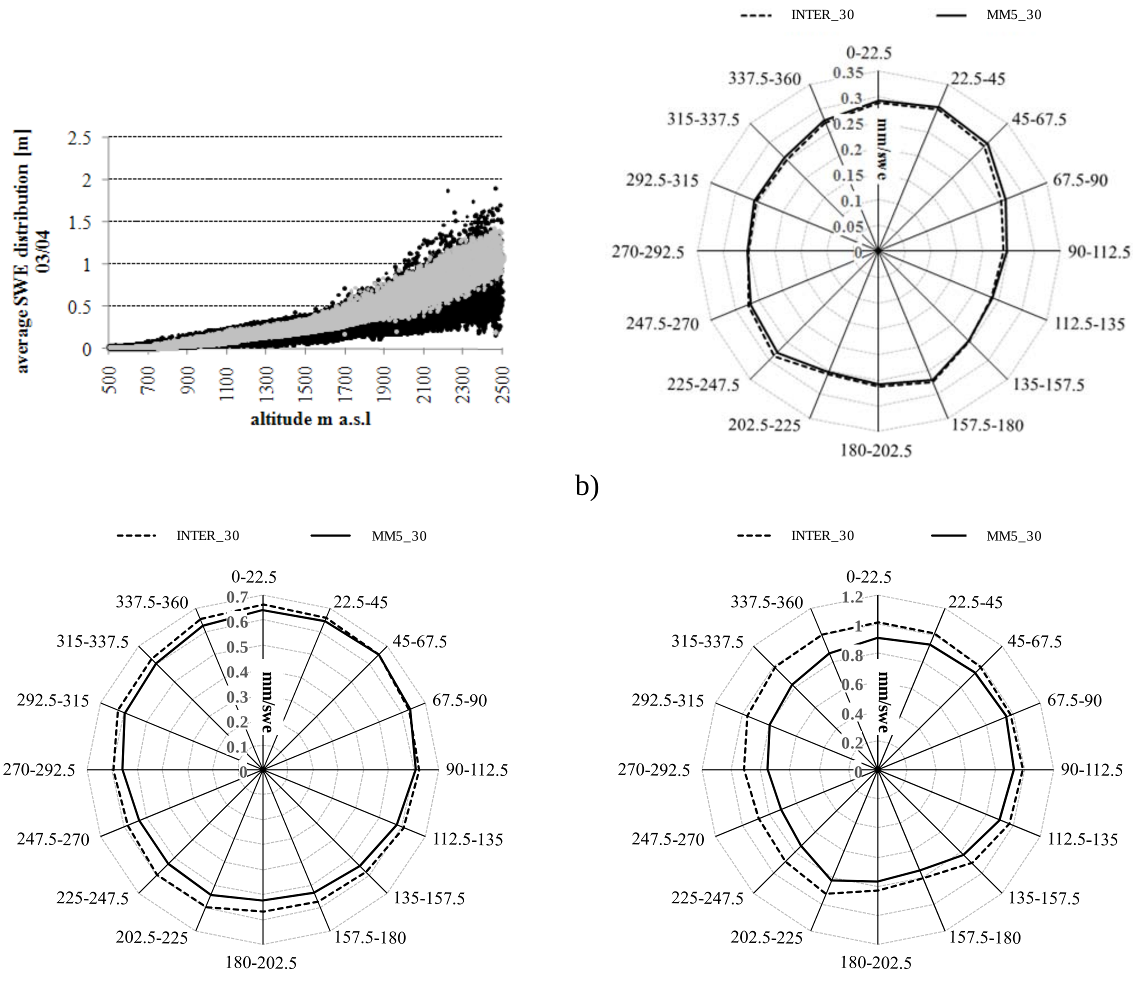

a) b) c) d)

Figure 50: Mean modeled SWE distribution (of *INTER_30* and *MM5_30*) for a) the total area, b) areas above 1800m a.s.l. and c) areas above 2200m a.s.l. The different volumes under the curves are due to higher sublimation losses within the *MM5* runs.

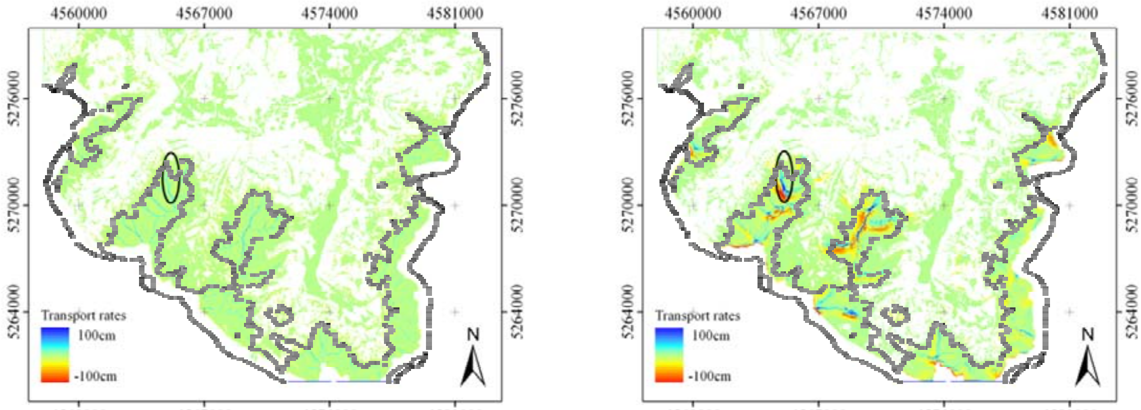
4560000
4567000
4574000
4581000
5276000
5270000
5264000
Transport rates
100cm
-100cm
N

a) b)

Figure 51: Snow transport rates of a) *INTER_30* and b) *MM5_30*. The black line is the 1800m isohypsis.

The inclusion of these transport rates in *MM5_30* improves the model accuracy (cp. section 4.4.5) in a considerable way.

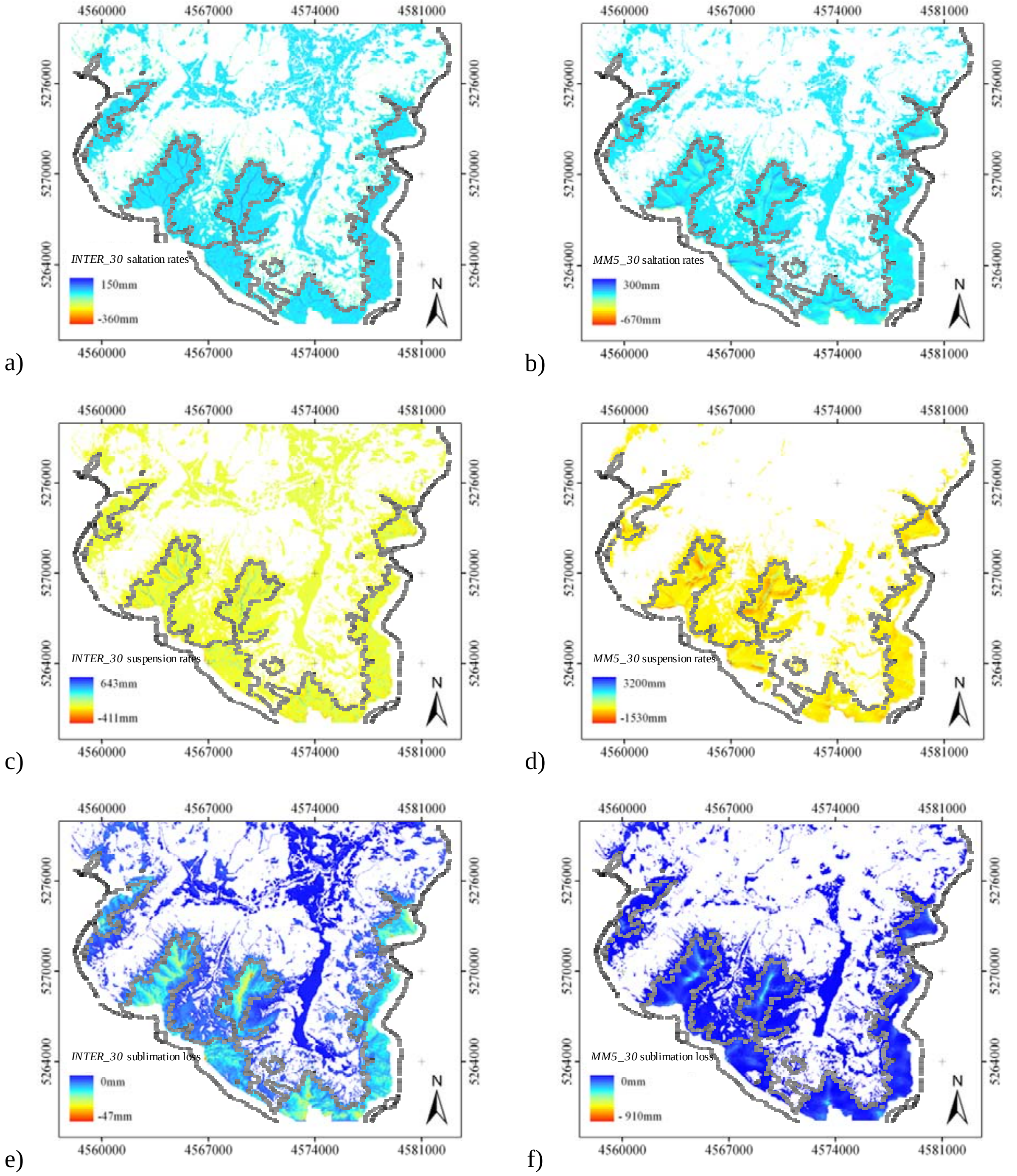
4560000
4567000
4574000
4581000
5276000
5270000
5264000
INTER_30 saltation rates
150mm
-360mm
N
a)
MM5_30 saltation rates
300mm
-670mm
N
b)
INTER_30 suspension rates
643mm
-411mm
N
c)
MM5_30 suspension rates
3200mm
-1530mm
N
d)
INTER_30 sublimation loss
0mm
-47mm
N
e)
MM5_30 sublimation loss
0mm
- 910mm
N
f)

Figure 52: Intensities of the different transport terms: saltation, suspension and sublimation in a) c) e) *INTER_30* and b) d) f) *MM5_30*. The black line is the 1800m isohypsis.

The effect of sublimation processes within the *MM5_30* results can be observed in fig. 50 b) to d) where the total amount of *SWE* declines with height compared to *INTER_30* which produces transport and sublimation rates that are considerably lower (fig. 52 e) and f)). The maximum modelled sublimation rates are overall slightly higher than those of the 200m *MM5* runs (920mm to 860mm) but the total amount of sublimation for the whole area is significantly smaller (0.5mm to 12mm per 30m grid cell in average). This is due to the fact that areas with high sublimation rates are limited to the crest regions which have a smaller spatial extent in the high resolution *DEM*. Figure 53 by Strasser *et al.* (2008) shows a profile between *Hochkalter* and *Watzmann* (cp. fig. 5) with the respective sublimation losses. The yellow curve corresponds to *MM5_30* results. It becomes obvious that the influence of sublimation from turbulent suspended snow is comparably small in the valley regions but reaches considerable amounts in the crest regions. This can be explained by the pronounced turbulence resulting from the wind simulations at such exposed locations (fig. 35c).

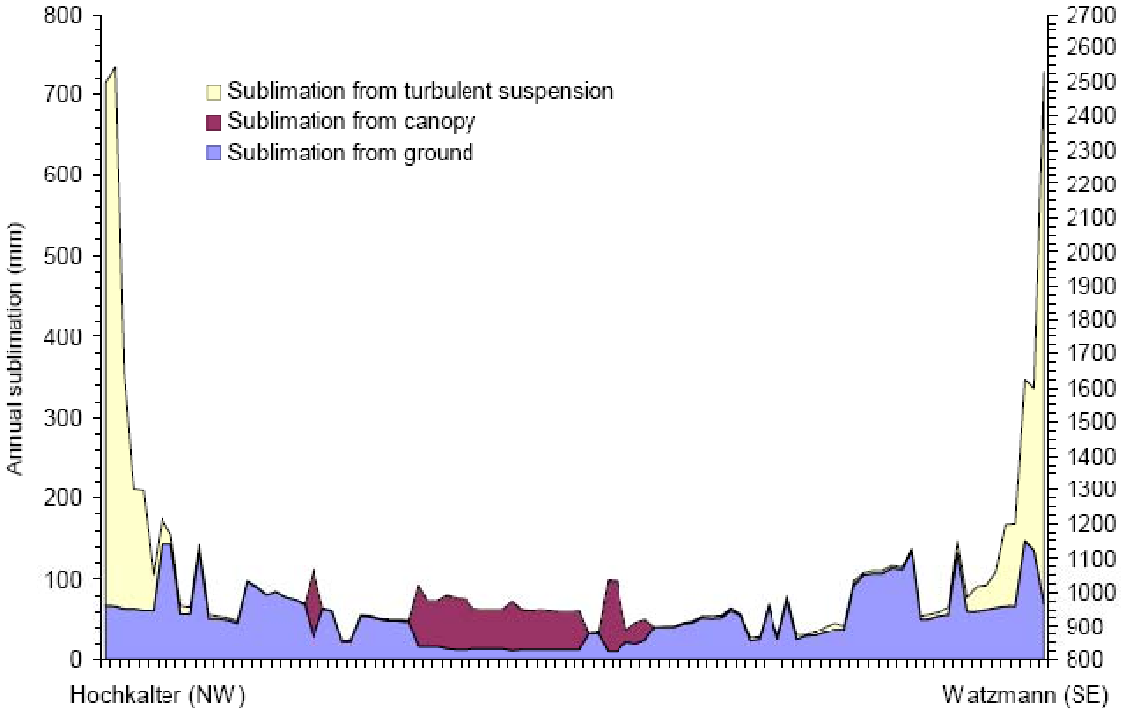

Figure 53: Simulated contributions to annual snow sublimation (additive representation) from the ground, canopy intercepted snow and wind-induced, turbulent suspended snow along a cross-section from Hochkalter (2607m a.s.l.) through the Wimbachtal to Watzmann (2713m a.s.l.). (Strasser *et al.* 2008).

4.3.4 Spatial validation

The 30m results correspond to the *extent* and *support* of the *Landsat ETM+* data. Hence, a direct comparison of the data becomes possible. In a first step, the spatial extent of the mapped and modelled snow cover was compared for both available dates. As it is impossible to quantify the *SWE* distribution via the available optical remotely sensed data a different way to validate the model results was chosen. Areas which are snow free within the *Landsat* images but are predicted to be snow covered by the model were detected in a first step. After than *INTER_30* and *MM5_30 SWE* depths were compared with a *SnowModel* stand alone model run (without transport routine) which is called *run_baseline* from now on. When using the *run_baseline* results as basis one can determine to which extent the results could be improved by including the blowing snow model algorithm in *INTER_30* and *MM5_30*.

The results of *INTER_30* and *MM5_30* are virtually identical with respect to the snow line and can be discussed on the basis of the *MM5_30* results. A comparison of classified versus modelled snow cover from *MM5_30* has shown that the model once again produced a snow cover that was too homogenous (fig. 54 a) to d)). This can be attributed to an inability of the model to reproduce the extent of the real transport rates or to the fact that the model is not able to predict all processes leading to the real distribution. Which of these two reasons is more likely to be responsible for the underestimation of the snow cover distribution will be discussed later on. As a first step, the extent of the predicted snow cover from *MM5_30* was compared to the remotely sensed data. 86 percent of the model grids are in agreement with the produced snow map for April 28, 2004 and 88 percent for May 30, 2004. 5 percent of the pixels are classified as snow but do not show a snow cover within the modelled data on April 28, 2004 (4 percent at Mai 30) while 9 percent (for both dates) of the modelled grid cells are predicted to be snow covered but are snow free within the classification (fig. 54 e)-f)).

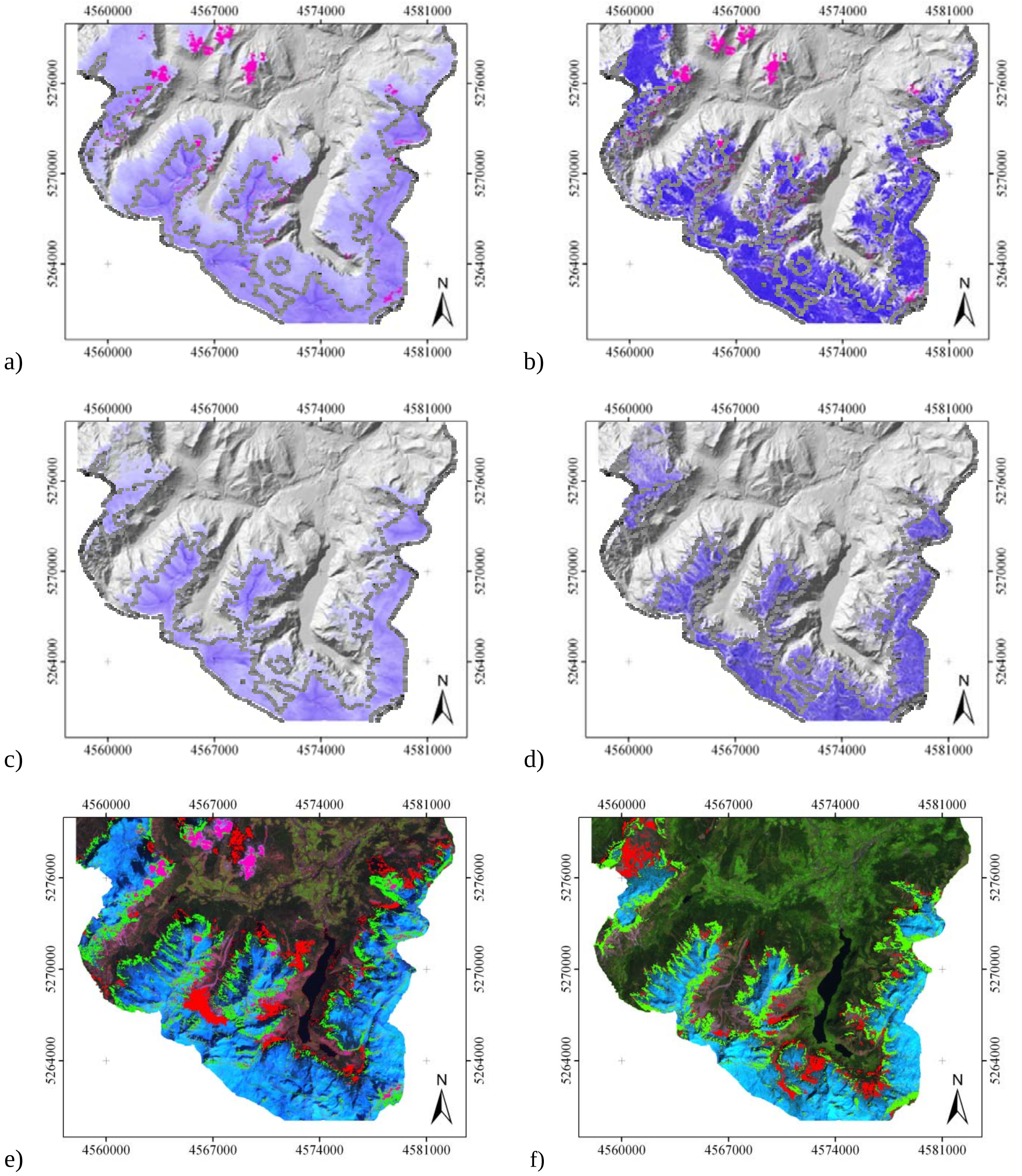

Figure 54: a) modelled snow cover of April 28, 2004, b) NDSI map of the same date, c) modelled snow cover of Mai 30, 2004 b) NDSI map of Mai the same date, e/f) Differences between model an classification results at April and Mai respectively (red indicates: only classified snow cover. Green: only modelled snow cover. Pink: cloud mask). The black line is the 1800m isohypsis.

In a subsequent step, nine validation areas were selected within the *Landsat* April image and six for the May image (fig. 55 and fig. 56, Table 7 and 8). The criteria for the selection was that the respective areas are snow free in the satellite images while they are snow covered in the model results. The values shown in Table 7 and 8 are averages for the whole test areas Results show that *run_baseline* is overestimating the *SWE* depth significantly on April 28, 2004 and slightly on May 30, 2004 (tab. 7 and 8). It is also obvious that *INTER_30* does not lead to a significant improvement of the results. Moreover, it could be seen that the accuracy of the results can even decline in *INTER_30* (tab. 7: area 7 and 9; tab. 8: area 2). *MM5_30* on the other hand shows improvements for all results and at all dates. On April 28 the results were improved by approximately 23% while results on May 30 were improved 60% in average when using the *MM5* wind fields *(MM5_30*).

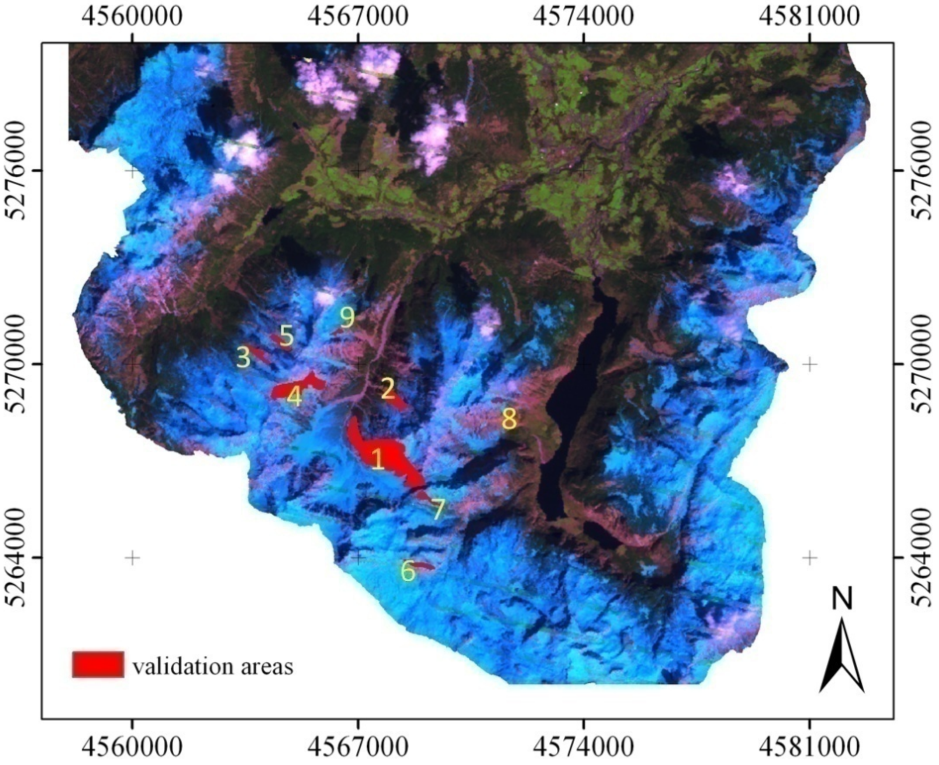

Figure 55: validation areas of April 28, 2004; Blue: Snow covered regions (Bands: 5,4,3), Red: test areas.

Table 7: Comparison between *SnowModel* results generated with *SnowTran-3D* and with as well as without the usage of *MM5*. The values belonging to the areas highlighted in Figure 55. The areas are snow free in reality, the values within the table showing the improvement of the *SnowModel* results when the transport routine is used.

Improvement when using:	Area 1	Area 2	Area 3	Area 4	Area 5	Area 6	Area 7	Area 8	Area 9
*INTER*_30 %	5%	3%	3%	0%	2%	2%	-100%	0%	-2%
*MM5*_30 %	28%	26%	9%	16%	30%	26%	12%	22%	26%
*INTER*_30 SWE	-3mm	-2mm	-1mm	0	-2mm	-2mm	+132mm	0mm	+2mm
*MM5*_30 SWE	-18mm	-20mm	-3mm	-18mm	-26mm	-23mm	-16mm	-22mm	-21mm

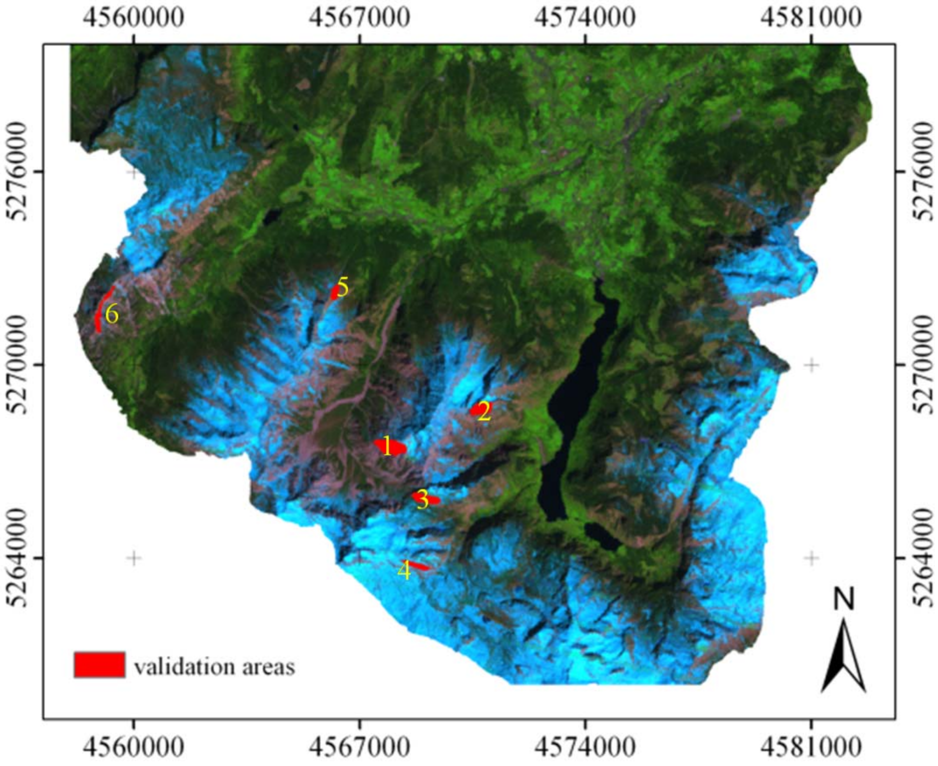
4560000
4567000
4574000
4581000
5276000
5270000
5264000
1
2
3
4
5
6
N
validation areas

Figure 56: validation areas of Mai 30, 2004; Blue: snow covered regions (Bands: 5,4,3), Red: test areas.

Table 8: Comparison between *SnowModel* results generated with *SnowTran-3D* and with as well as without the usage of *MM5*. The values belonging to the areas highlighted in Figure 56. The areas are snow free in reality, the values within the table showing the improvement of the *SnowModel* results when the transport routine is used.

Improvement when using:	Area 1	Area 2	Area 3	Area 4	Area 5	Area 6
*INTER*_30 %	0%	-2	1%	0%	1%	12%
*MM5*_30 %	80%	46%	63%	55%	35%	86%
*INTER*_30 SWE	0mm	+2mm	-1mm	0mm	-1mm	-2mm
*MM5*_30 SWE	-78mm	-43mm	-39mm	-84mm	-30mm	-31mm

Chapter 5: Discussion of the SnowModel results

Validating wind fields and snow transport processes in mountainous areas is a highly difficult and mostly impossible task (Klemes 1988). The limited accessibility of high alpine and crest regions, which are most interesting for model validation, leads to a remarkable lack of validation data which can only be overcome if one has “a team of Olympic skiing heroes available for the field campaign” (Klemes 1988). Remotely sensed information can balance this deficit to some degree but generally also shows deficiencies in areas with steep topography or forested regions (Klemes 1988, Hall *et al.* 1995). Because of these difficulties, a detailed validation of the spatial *SWE* distribution is virtually impossible. Hence, the performance of the model was checked where validation data was available and only the qualitative plausibility of the results is discussed for locations where no validation data was available.

5.1 Accuracy of SnowModel at the point scale

To evaluate the advantages of using physically based *MM5* wind fields in snow transport modelling, *SnowModel* results generated with and without transport routine using interpolated wind fields were used as baseline. Subsequently these baseline results were compared to coupled *SnowModel/MM5* results and to observed snow data. Furthermore, the scaling effect when using resolutions of 30m and 200m resolution is discussed. In a first step, the results of the sections 4.1.1 and 4.3.1 are summed up.

A first validation was performed by using comparisons between measured and modelled snow depths. Results at the *micro* and *meso* scale have shown a good correlation to field measurements and remotely sensed data. The correlations between measurements and model results are at a satisfying level (fig. 47 a)-c)) for all available snow measuring points (*MM5/INTER* r^2=0.85/0.73 [*Reiteralm II*], r^2 = 0.88/0.88 [*Reiteralm III*] and r^2 0.73/0.64 [*Jenner*]]). The overall accuracy of the results corresponds to the results presented in other studies (cp. Liston *et al.* 2007). When considering the operational snow depth measurements of the meteorological stations and the field campaign data, the performance of the coupled

MM5 and MM5_30 model was identical or better than *INTER or INTER_30* results using interpolated fields (fig. 47 a) to c)). The validation has shown that *MM5_30* is able to reproduce the measured snow depth at *Reiteralm* and *Kühroint* in a satisfying way but the modelled variability between the different measuring points was still too small (cp. section 4.3.1 and 4.3.2, tab. 5 and 6). Transport processes from the higher to the lower part of *Reiteralm* could not be displayed. Further analysis revealed that this is due to the forest which subdivides *Reiteralm* into two parts. The model treats this forest as a physical barrier which blocks snow transport. The introduction of the vegetation class *sporadic trees* resulted in no improvement. This can be attributed to the general model setup. So, a simple reduction of the snow holding capacity (fig. 11) makes more snow available for transport but cannot solve the existing lack within the model formulations. The model predicts a boundary layer wind speed which is modified by eq. 21. The wind speed is reduced in accordance to the *LAI* of the vegetation type of the respective model grid. The used *LAI* has been derived from a combination of forest inventory data, a colour infrared photo interpretation, as well as by application of these relations by Hammel and Kennel (2001) and is therefore a fixed value. A usage of the given *LAI* values at *Reiteralm* leads to calculated wind speeds which are by far too low for initialising snow transport events from the higher to the lower area of this site. For accounting for the real process, namely snow transport over the forest land cover, two different wind velocity layers would be required within *SnowModel* but only one is available. The needed input wind fields would be available as the second model layer of *MM5* can deliver the needed information.

The results at *Kühroint* have demonstrated that *SnowTran-3D/MM5* can reproduce no-transport conditions at a wind sheltered site, but the variability observed between the different measuring points was again underestimated by the model (cp. section 4.3.2, fig. tab. 5 and 6). In correspondence to the results at *Reiteralm*, the overall variance of the modelled data is too small with respect to the snow depth differences between the sample points. This might be due to the *DEM* used in this study which describes *Kühroint*, which is undulated in reality, as an almost completely flat area.

The *DEM* at *Kühroint* was checked because of model runs which produced an unexpectedly homogenous snow distribution. The analysis revealed some inaccuracies within the data, which were unfortunately only detected after the progression of the field campaign. It became evident that the small knolls in the area are not displayed in the *DEM* even in its original 10m resolution. The inner area of *Kühroint* is portrayed as absolutely flat within the *DEM* which does not correspond to the reality.

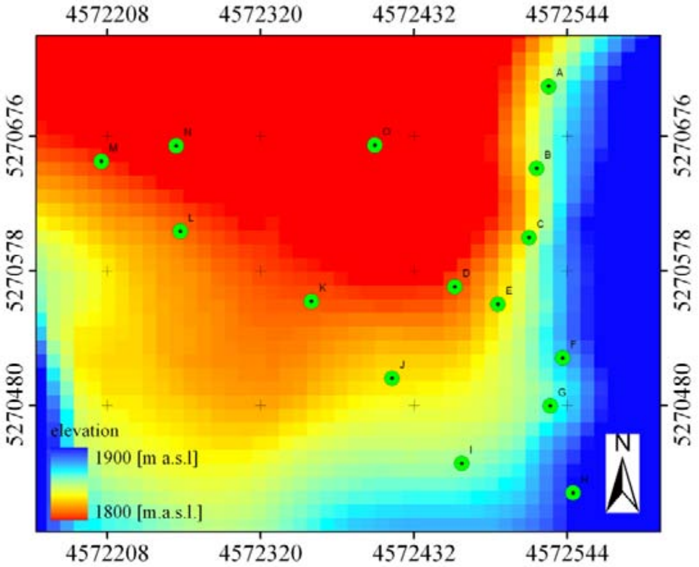

Figure 57: *DEM* of *Kührowint* test site. The area which is undulated in reality but flat in the DEM involves points D), K), L), M), N), O).

Considering this, the model results are meaningful because as the *DEM* is used for distributing meteorological variables the model estimates an even distribution of the different meteorological variables for *Kühroint*. As this is the case the calculated snow cover is also homogenous and does not show significant differences in snow depth or *SWE*. However, the example shows that the generation of topographical input parameters can be problematic in Alpine regions and can therefore represent a source for deviations between model and measurements. A faithful investigation, if these errors are widespread within the data or if they are only observable at a few locations was impossible because of a lack of reference data. These will be available in the coming years since a 1m resolution DEM is in preparation for the *National Park* and will be available for future investigations (personal communication H. Franz 2007).

5.2 Accuracy of SnowModel with respect to remotely sensed data

In regard to the spatial distribution of the snow cover, the inclusion of the *MM5* wind fields leads to an overall more heterogeneous *SWE* distribution. The *SWE* becomes less dependent on elevation (fig. 38 a) and 50a)) and an efficient transport of snow from the windward to the leeward sides of mountains was predicted (fig. 39 and 52). This is in agreement with expectations and with the work of other authors (e.g. Barry 1992). The overall transport efficiency was considerably higher for all transport terms when using *MM5* wind fields (fig. 38 and 50) especially for elevations higher than 1800m a.s.l. where the *MM5* wind speeds were significantly higher (fig. 35c).

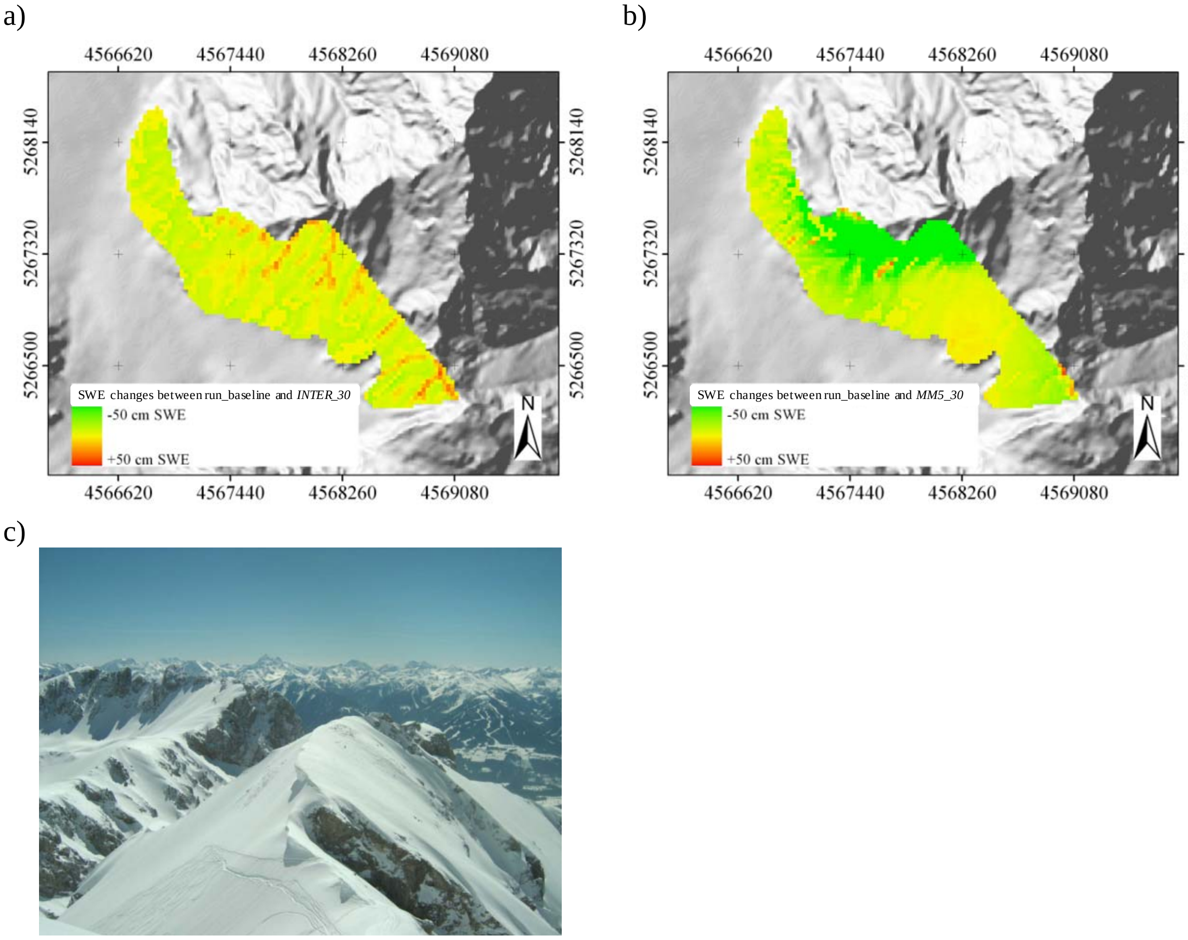
a)
b)
4566620
4567440
4568260
4569080
5268140
5267320
5266500
SWE changes between run_baseline and INTER_30
-50 cm SWE
+50 cm SWE
SWE changes between run_baseline and MM5_30
N
c)

Figure 58: a) Comparison of *run_baseline* and *INTER_30* results on April 28, 2004, b) comparison between *run_baseline* and *MM5_30* at the same date. c) Picture of a crest were the snow cover on the windward side (right) is reduced considerably by snow transport processes

The generated, more heterogenic snow cover also shows a better agreement with the remotely sensed data, with respect to the spatial heterogeneity of the snow cover (tab. 7 and 8). This was proven for areas which are snow free in the satellite pictures but snow covered in the model results. Analysis of these test areas shows that the reduction of the *SWE* depth of *INTER_30* in comparison to *run_baseline* shows no clear trend or pattern over the areas (cp. fig 58 a); tab. 7) and 8). Moreover, it could be seen that the snow is mainly redistributed within the areas but not transported out of the areas when using *INTER_30*. This is caused by the comparatively low interpolated wind speeds and unrealistic wind direction fields used in *INTER_30*. Hence, the snow is sometimes transported back and forth and not into a specific direction. In contrast, the results of *MM5_30* show a trend within the spatial pattern; the *SWE* depth is particularly reduced at higher elevations and in the direction of the next crest (fig. 58b). This conforms to observations one can make in nature (fig, 58 c)) where it can be seen that the *SWE* depth are especially reduced on the windward side of the crest regions (fig. 55 c)).

The integration of the *MM5* wind fields can improve the results at the point scale and in comparison to the satellite images, as *SnowTran-3D* in combination with interpolated wind fields can also reduce the accuracy of the results (tab. 7 and 8). This indicates that the *MM5* wind fields are more trustable at least in Alpine settings than the interpolated *MicroMet* fields which are generally used in the application of *SnowModel*. The more accurate wind direction fields provided by *MM5* furthermore prevent the calculation of accumulation zones that do not correspond to zones that can be observed in nature (tab. 7 and 8).

According to Hall *et al.* (1995) it can be stated that wooded areas are limiting the usability of remotely sensed data as validation tool in snow sciences. Trees obscure the underlying snow cover and make a reliable detection of the snow cover/line impossible. This effect is especially pronounced in the study area because the snow line is located in wooded areas on all satellite image acquisition dates.

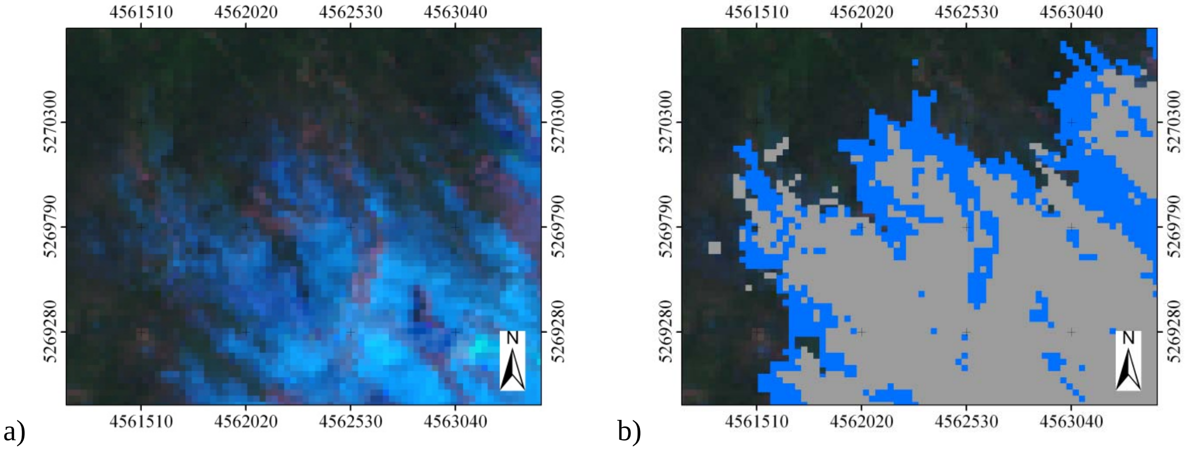

Figure 59: a) wooded region at *Watzmann* mountain (the snow covered area appears in blue). b) *NDSI* classification in gray, *MM5_30* results in blue.

A visual comparison of model and classification results indicates that an assessment if the model or the classification results are more accurate is difficult or simply impossible in the respective regions. Figure 59 can serve as an example for this dilemma. The model has predicted a snow cover which is of a larger expanse than the classified one (this reflects the situation for the whole area). A visual analysis of the satellite scene has shown that the snow line seems to be somewhere between the model and classification results (fig. 59 a) and b)). An adaption of the *NDSI* threshold for including these local phenomena only leads to a partial improvement of the results but decreases the accuracy of the total classification. It is therefore difficult to assess the accuracy of the model results with respect to the snow line with the help of the available satellite data. Nevertheless, the modelled snow line is always close to the classification in case which indicates that the extent of the modelled snow cover has the correct dimension.

5.3 Scale effects in snow transport modelling

The influence of wind induced snow transport on the spatial distribution of the *SWE* is more significant with respect to the total area at the *meso* scale. Figures 38 b) to d) indicate that the *SWE* distribution within the *test site* becomes heavily dependent on wind induced snow transport processes from 2200m a.s.l. on. This effect was not reproduced in the *micro* scale results. Rather, they suggest that wind induced snow transport can have a remarkable effect on the snow distribution in limited areas but do not modify the general *SWE* distribution in the test site. This finding is in line with other studies that have stated that general transport intensities can be simulated adequately at coarser scales but the location of individual accumulation and erosion zones can be misinterpreted in a significant way (e.g. Liston *et al.* 2006). The *Blaueis* glacier serves as an example. It was found that the amount of transported *SWE* considerably depends on the selected model scale and wind simulation method. Wind induced transport of *SWE* form surrounding areas to Alpine glaciers is mentioned as important for their existence (Kuhn 1993, 1995). Especially small *kar* glaciers like the *Blaueis* glacier (fig. 5 and fig. 60)) and many other glaciers e.g. in the *Karwendel* region are dependent on additional *SWE* delivered by avalanches or wind induced snow transport (Kuhn 1995). Plattner *et al.* (2006) have applied a statistical analysis of the *SWE* distribution at *Vernagtferner* (*Tirol/Austria*) and have found that the *SWE* distribution is very likely dependent on the wind conditions and on wind induced snow transport. However, a quantitative estimation of the transported amounts was not possible. The work presented here shows that a numerical calculation of the transported *SWE* amounts is possible via the presented scheme. Principally, it can be stated that the use of *SnowTran-3D* does not lead to any transport rates from and to the glacier if interpolated wind fields are used. This finding is independent of the used scale. When *MM5* wind fields are used on the other hand, significant transport processes can be observed. The *MM5_30* 30m runs produce a maximum *SWE* gain per pixel of 2140mm *SWE*. The average contribution of windblown snow over the total glacier area is 220mm *SWE*. The additional amount of SWE corresponds to 12% of the total precipitation (1850mm) and to 23% of the snow fall (950mm) within the observed period (03/04) (fig. 60a). The 200m runs in contrast produce considerably different results. The maximum per pixel gain is greatly reduced (740mm *SWE*) and the total average contribution is only 4mm *SWE* (fig. 60b). This can be explained by the fact that because of a scale dependent shift like presented at *Reiteralm* before (fig. 43 a) and b)) the accumulation zone of the glacier is located in the crest region of *Hochkalter* within in the 200m *DEM*. Hence, erosion prevails and the *SWE* is reduced and not enhanced like it is in the 30m runs. Figure 60 a) and b) show the wind induced gain and loss of *SWE* for the *Blaueis* glacier (30m and 200m again). The figures further illustrate that the accurate estimation of the location of the accumulation and erosion zones becomes problematic at coarser scales.

The results show that the quantitative calculation of wind induced transport of snow from neighbouring areas to adjacent glacier areas becomes possible via the presented scheme at the *micro* scale. A validation of the transported snow amounts at *Blaueis* glacier or at other well instrumented glaciers like the *Vernagtferner* is the subject of future work. The obtained knowledge about gain rates is crucial for a better understanding for accurate mass balance calculations of the respective glaciers.

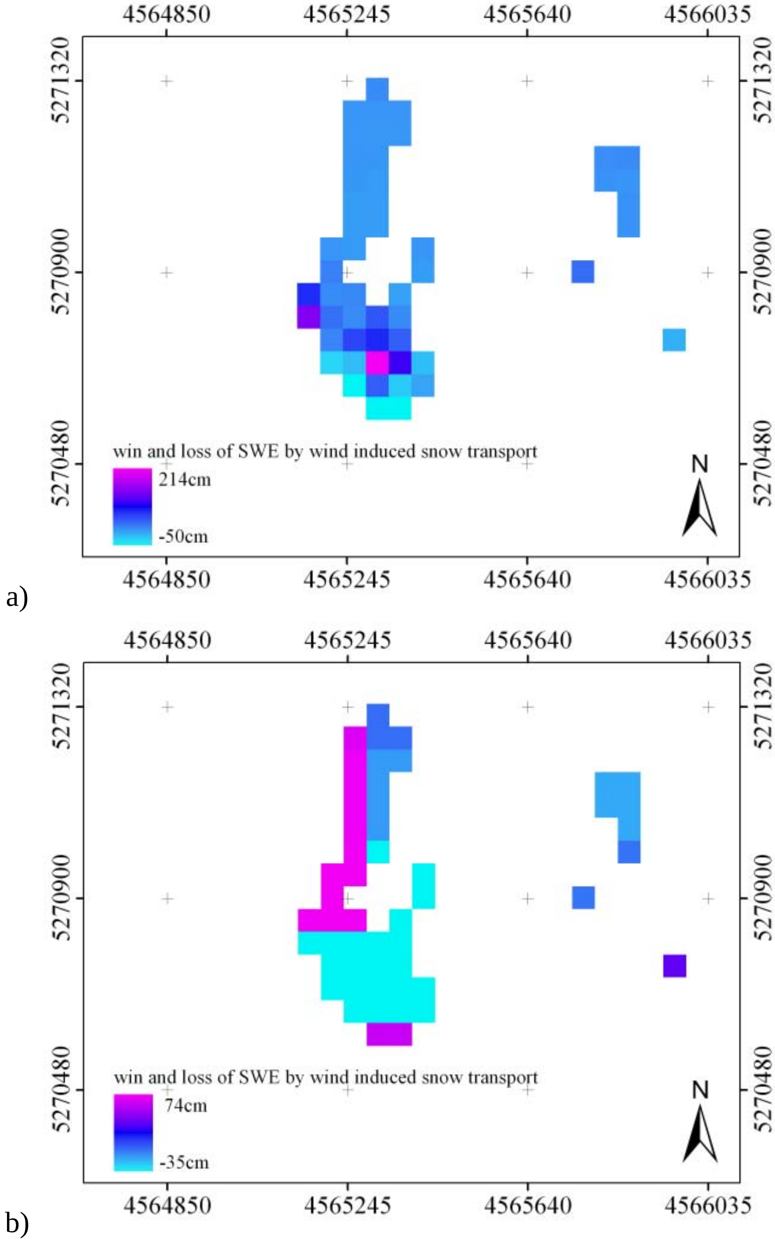
4564850
4565245
4565640
4566035
5271320
5270900
5270480
win and loss of SWE by wind induced snow transport
214cm
-50cm
N
a)
74cm
-35cm
b)

Figure 60: Predicted loss and gain of SWE due to wind induced snow transport at *Blaueis* glacier a) 30m resolution results using MM5 wind fields, b) 200m resolution results using MM5 wind fields. (The results were fitted to the 30m grid for the presentation)

Very high modelled accumulation rates on the leeward sides of the mountains and remarkable sublimation rates on the mountain crests which could not be directly validated should be and are discussed in the next paragraphs.

5.4 Discussion of enhanced accumulation and sublimation rates when using MM5 wind fields

The inclusion of *MM5* wind fields leads to remarkable simulated snow depths, on the leeward side of the crests. At *Watzmann* crest region (predicted precipitation: 3100mm) a maximum *SWE* depth of about 6000mm (*MM5_30* 30m results) and 4500mm (*MM5 method* 200m results) were calculated for the leeward side. These values were not obtained with *INTER_30* or with *INTER* method (the maximum was about 3000mm here for both runs (30m and 200m)). A direct validation of the modelled *SWE* depths is impossible but fig. 61 gives an idea about the conditions at this site and shows that 6000mm *SWE* could probably exist.

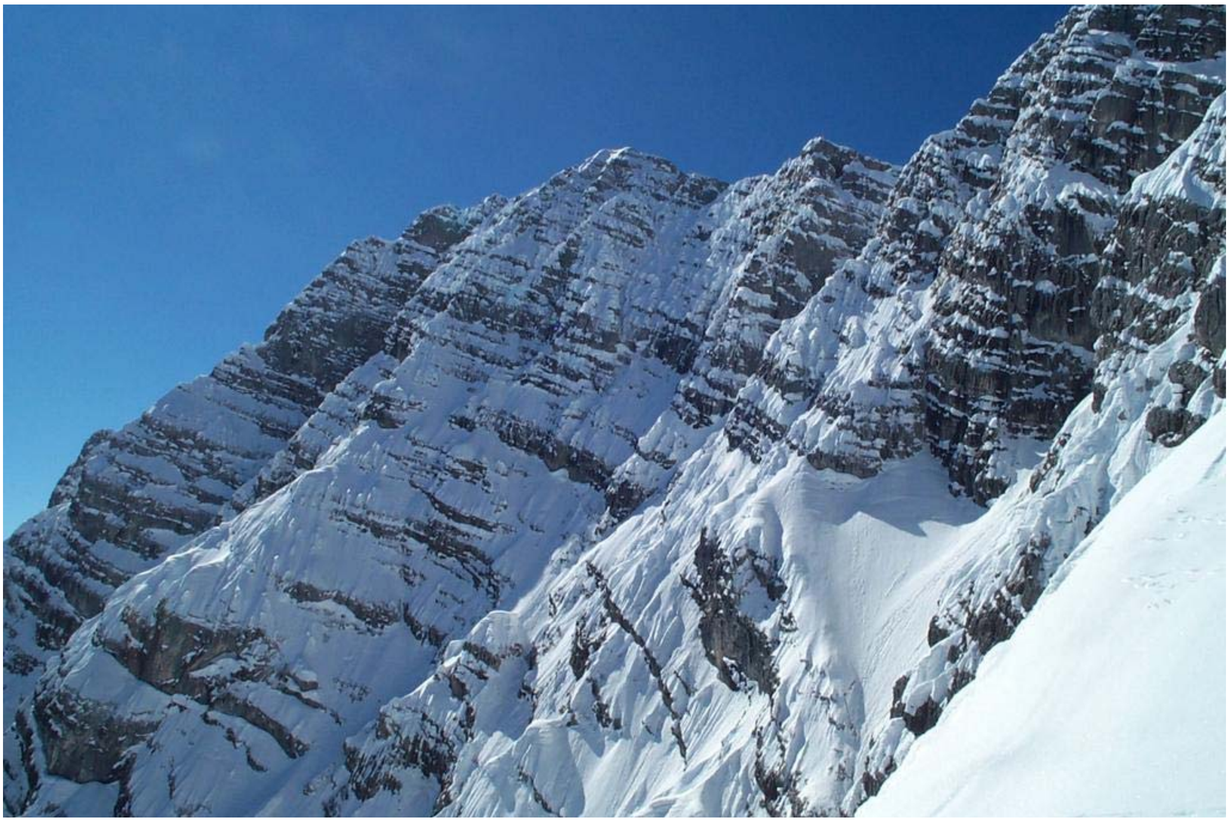

Figure 61: Picture of the Watzmann upper east face under full snow coverage.

The predicted sublimation rates of up to 910mm (*MM5_30*) or 860mm (*MM5*, 200m) (fig. 39 e) and f) and 52 e) and f)) when using the *MM5* wind fields are very high and, therefore, need to be discussed.

Total sublimation can be differentiated in three major sources: Sublimation from the ground snow cover (Weber, 2005), loss from previously intercepted snow from within the canopy (Essery *et al.,* 2003), and sublimation of airborne snow particles during blowing snow conditions (Schmidt, 1972; Liston and Sturm, 1998; Pomeroy and Essery, 1999). Strasser *et al.* (2007) have quantified the effect of all three sublimation processes on the water balance in the *Berchtesgaden National Park* region (fig. 53 and tab. 9). While the first two of them are mostly driven by the amount of available radiation, the sublimation of airborne snow particles is mainly steered by the transport efficiency at a given place. The formulation of the sublimation process within *SnowTran-3D* follows that of Schmidt (1972), Pomeroy *et al.* (1993) and Pomeroy and Gray (1995) were the sublimation rate depends on the amount of snow within the saltation and suspension layer (eq. 32 and 33). The sublimation loss rate coefficient, describing the rate of particle mass loss as a function of height within the drifting snow profile, is a function of temperature-dependent humidity gradients between the snow particle and the atmosphere, conductive as well as advective energy and moisture transfer mechanisms, particle size and solar radiation intercepted by the particle. It is assumed that I) the mean particle size decays exponentially with height, II) the relative humidity follows a logarithmic vertical profile, III) the air temperature in the snow-transport layer is well mixed and constant with height, IV) the variables defined within the saltation layer are constant with height and those in the turbulent suspension layer vary with height, and V) the solar radiation absorbed by snow particles is a function of the solar elevation angle and fractional cloud cover (eq. 9). In *SnowTran-3D*, high sublimation rates (fig. 39 f) and 52 f)) are projected during blowing-snow events due to the high snow particle surface-area to mass ratios and the high ventilation rates achieved when the particles are in the wind stream (Schmidt 1972), and assuming the existence of a pool of dry air overlying the surface layer with efficient mixing between the two (the model belongs to the "*Schmidt-type*" family of sublimation models, Liston and Sturm 2004). Using Schmidt-type sublimation models, 15 – 50 % of the snow cover were found to be returned to the atmosphere by sublimation in the Arctic (e.g., Liston and Sturm 1998, Essery and Pomeroy 1999, Pomeroy and Essery 1999), and 15 – 41 % in the

Canadian prairies (Pomeroy and Gray 1995). In contrast, other studies suggest that during blowing-snow events, the air above the surface rapidly saturates with moisture, limiting the amount of snow that can sublimate (e.g. Déry and Yau 2001, King *et al*. 2001). As thoroughly discussed in Liston and Sturm (2004), there is not necessarily a contradiction between the two types of sublimation: both regimes may exist depending on the interaction of the surface layer with the overlying air mass. Above inclined snow surfaces, efficient mixing is particularly forced by the frequent catabatic flows and related entrainment of air masses into the shallow surface layer (Smeets *et al.* 1998). Hence, for the application here, a mixing of the surface layer with an overlying mass of dry air was assumed which leads to an efficient removal of moisture from the turbulent suspension layer during blowing-snow events. This leads to enhanced sublimation rates from up to 95% of the annual snowy precipitation for several crest regions. The overall losses which are due to sublimation of turbulent suspended snow are small in contrast and are only about 4.1% of the total snowfall for the whole test site (tab. 9).

Table 9: Contributions relative to total snowfall and scale-dependent significance of the winter water balance components for *the Berchtesgaden National Park* domain for 2003/2004. The additional amount of snowmelt is caused by rain-on-snow (cp. Stasser et al. 2008).

Water balance component:	Seasonal amount [mm]	Relative contribution [%]	Local significance	Regional significance
Snowfall	+651.1	100%	high	high
Ground resublimation	+15.8	+2.4%	moderate	small
Ground sublimation	-44.9	-6.9%	moderate	small
Canopy sublimation	-84.9	-13.0%	moderate	moderate
Sublimation from turbulent suspension	-26.5	-4.1%	high	small
Snowmelt	-693.1	-106.5%	high	high

The scheme presented here has produced results which are pretty close to data measured by Hood *et al.* (1999, *Nivot ridge Colorado*). Their measurements are the only known and published sublimation measurements in Alpine regions. When comparing the meteorological information and *SWE* accumulation rates given by Hood *et al.* (1999) with the *Berchtesgaden* site, it becomes obvious that their measurements correspond closely to predicted values for the elevation zone around 2100m a.s.l. Here a mean sublimation rate of 250mm (*MM5_30* and *MM5*) was predicted for the *National Park* area, as Hood *et al.* (1999) measured 195mm for their site at *Nivot ridge* (*Colorado*). The results obtained with interpolated wind fields (maximum = 47mm *INTER_30* and 50mm *INTER*; fig. 39e) and 52 e)) were outside the range of this data. In which way the measurements of Hood *et al.* (1999) are representative for the *Watzmann* region cannot be concluded but the comparison shows that the results obtained in this study are within the range of data published by other authors. It is also an open question whether the very high sublimation rates in the crest regions are valid (e.g. fig. 53). This will be an open research topic until sublimation measurements from the respective regions become available. Nevertheless, the questionable areas are limited to the apexes of the mountains and should not have a significant importance for/or influence to the water balance of the overall catchment (tab. 9; Strasser et al. 2008).

5.5 High interpolated precipitation rates as a possible reason for the underestimation of the spatial snow heterogeneity

The spatial homogeneity of the modelled snow cover in comparison to the classification results was mentioned in connection with the remotely sensed data. The difference to the real more heterogenic snow cover can be due to an underestimation of the amounts of snow transported by wind or because of the negation of snow slides etc. Another possible explanation are to high amounts of interpolated snow fall. The interpolation results have demonstrated that the spatial interpolation of the precipitation measurements works well for the available stations (fig. 18) but produces questionably high amounts of precipitation for higher elevation levels within the *test-site*. An exact evaluation of the model error is impossible because of a lack of meteorological stations at the respective elevation belts. Nevertheless, a comparison to the values presented by Enders (1979) for the *National Park* area, who predicted an amount of 2711mm precipitation for an elevation of 2500m a.s.l. (the value is based on a comparison to the station *Plattachferner* at 2660m a.s.l., which could be seen as representative for this elevation belt of the *National Park* (Enders 1979)), indicates that the 3100mm (September 2003 to August 2004) predicted by *MicroMet* are comparatively high. The high values can also not be explained by extreme weather conditions since a comparison to the time period of 1960 to 1990 (average precipitation at *Berchtesgaden* = 1519mm) reveals that the precipitation amounts of September 2003 to August 2004 (1532mm) were close to the long term average for this region. Nevertheless, the overestimated precipitation rates do not justify a substitution of the respective routine as the available station values are well reproduced and a conclusive calculation of the severity of the error in higher altitudes is impossible.

However, based on Enders (1979) an overestimation of about 15% for the elevation belts above 2000 meters can be assumed. Because of low temperatures in these regions most of the additional precipitation falls as snow and is therefore added to the snow pack. As a result, the analysis, in section 4.3.4 has shown too much modelled *SWE* for all test areas. An effect of the overestimated *SWE* depth is that areas which are snow free in the satellite images, while showing lower snow depth when using the snow transport routine with *MM5* compared to the other model schemes, are still predicted to be snow covered within the model results. Hence, the surplus of about 15% precipitation masks the improvements which were achieved through the use of the *MM5* wind fields with respect to the spatial distribution of the snow cover.

5.6 The effects of snow slides and preferential snow distribution

It became obvious, that wind induced snow transport is not the only factor which produces the remarkable spatial heterogeneity of the Alpine snow cover. There are other processes which are occurring before, during, and after the snow accumulation process that potentially can have a major impact on the snow distribution. Particularly important seem to be: preferential snow distribution and snow slides. The influence of preferential snow distribution is so far not well understood but it is assumed that it can have considerable effects especially at regions with steep topography (Lehning *et al*. 2002). Reduced snow accumulations on steep slopes are commonly mentioned as the main effect of preferential snow distribution but where the snow is accumulated instead is still a subject of speculations. On the other hand, recently there has been remarkable progress in the calculation of snow slides and there are inspiring publications which are illustrating the importance of this process (Gruber 2007; Strasser *et al.* 2007). Strasser *et al.* (2007) predicted *SWE* depositions due to snow slides of up to 10000mm per winter season for some areas in the *National Park* (fig. 62). This value seems to be very high but members of the *Commission of Glaciology* of the *Bavarian academy of science and humanities* have found that snow depositions by snow slides at the *Icechapel* (*Watzmann* east face) reach these amounts (personal communication M. Weber 2008). Furthermore, Kuhn

(1995) stated that an additional amount of 8000mm *SWE* is needed for reaching equilibrium conditions of the mass balance for some small avalanche fed glaciers.

With respect to wind induced snow transport, gravitational snow transport has the effect that remarkable amounts of snow are shifted into regions where the wind induced processes are of subordinate importance because of low wind speeds (fig.35 c)). This and the fact that areas with slope angels of more than 50° are commonly snow free (because of gravitational processes), should lower the amount of wind induced snow transport in a natural setting because of a lack of transportable snow. As these effects are neglected in the current model formulations it can be argued that the real wind induced transport rates should be lower than the modelled ones. This would also have an effect on the very high sublimation rates (fig. 39 f) and 52 f)) predicted in the crest areas.

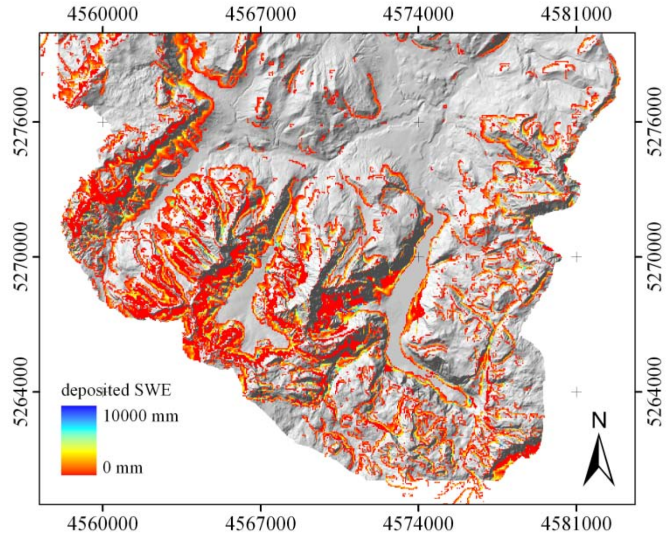

Figure 62: Accumulated Snow masses transported by snow slides (winter season 03/04). Strasser at al. (2008) modified.

A quantification of the efficiency of gravitational snow transport processes in combination with wind induced transport rates is complicated by the fact that there are no coupled model algorithms available which account for wind induced snow transport and snow slides. This would be a prerequisite for predicting correct transport rates for both modes of snow transport because wind induced transport could make snow of adjacent catchments available for snow slides, while snow slides, on the other hand, can prevent snow from being included in wind transport processes by shifting the snow masses to lower elevation bands where wind induced transport processes are far less effective. Furthermore, the estimation of the effect of snow slides is difficult because some available model routines, used by e.g. Strasser *et al.* (2007), are triggered at a given hour once per day and not as a result of snow pack conditions at a given time step. Therefore, it could only be assumed that the enhanced snow coverage in the valley areas (cp. Chapter 5.3) below snow free areas on steep slopes of more than 50 degrees are caused by this process.

5.7 Model formulations

This section will discuss in which way the used model schemes can deteriorate the model results and what improvements could be made in the model with respect to the accuracy of the available input data. It was mentioned before that the presented formulation of the saltation layer flux (eq. 26), was a subject of discussion in recent years (e.g. Lehning *et al.* 2006). The work presented here adds important points to this ongoing discussion. While very sophisticated model algorithms are useful and generally lead to more accurate results if suitable input data is available, they are useless if the input data is of less accuracy. The presented study shows that interpolated wind fields, routinely used in *SnowModel* applications, can decline the accuracy of the results by 100%. This error is significantly higher than the errors which could potentially be produced because of the oversimplification of the saltation process (personal communication Liston (2006) and Pomeroy (2006)). The results of the presented study suggest another possible model improvement which could greatly enhance the performance of the model. It could be observed that the inclusion of a second suspension layer would be very favourable to allow the transport of suspended snow over trees and to make the explicit calculation of snow transport rates in areas of flow separation possible. In the current model setup, the model accumulates the transported snow particles instantly if the wind speed drops below a certain threshold. Hence, significant snow accumulations can be observed at the wood sites or immediately beyond mountain crests. The inclusion of a second suspension layer driven by e.g. the second model layer of *MM5* which is still available would lead to a better description of the transport processes at the respective locations and could probably lead to a better description of the accumulation and erosion zones. The need for this model extension could be clearly seen at *Reiteralm* test site (cp. section 4.3.1).

Hence, it can be stated that the snow distribution that is obtainable with the current *SnowModel* version shows some deficits which were discussed in the former sections but was significantly improved over the inclusion of *MM5* wind fields. The inclusion of additional processes could definitely improve the model results in the future but currently the presented results have to be seen as state of the art as they are from comparable accuracy as results published by other authors but for less complex terrain (cp. Liston et al. 2007) and are therefore applicable for future studies.

Chapter 6 *Outlook and conclusion*

6.1 Presentation of a scheme which allows for a better description of the snow cover in regional scale models

The following section will present a method which allows the wider usage of the presented results in hydrologic modelling. As discussed in the previous chapters, the Alpine snow cover has a remarkable heterogeneity which is dependent on numerous factors. It was shown that in snow cover modelling, the explicit calculation of the transport processes and the required meteorological fields is time consuming and only functional at certain scales. It was also shown that the amounts of transported snow are dependent on the selected scale. Furthermore, the physically based description of snow transport processes is only valid up to a grid cell size of 200m (Liston 2006). As this is much lower than the resolution of *regional SVAT* or most hydrological models, an alternative method of describing the sub-grid snow distribution and with this accurate energy and moisture fluxes on the basis of this work is presented. Figure 63 illustrates the representation of the snow cover in a common snow model module where the snow or *SWE* depth is considered to be constant over the entire grid cell. This simple assumption results in:

- An instant snow covered or snow free effect for any grid cell during accumulation or ablation.
- Energy and moisture fluxes which are representative for the snow covered or the snow free part of the grid cell only.
- A general misinterpretation of the melt period (Liston 2004).

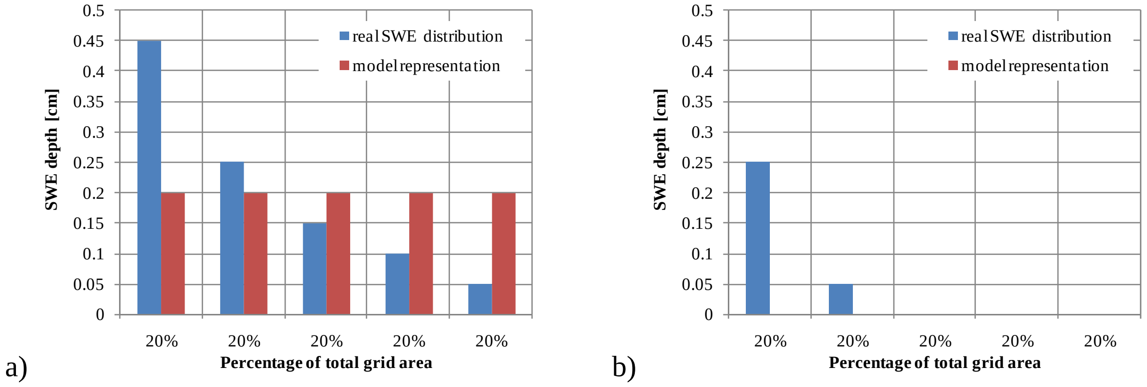

Figure 63: The figure shows a theoretical subscale SWE depth distribution and common model representatios. a) Shows a situation with full snow coverage, b) shows a situation where the model shows no snow coverage.

A possible solution for the mentioned problems is presented here. A scheme of Liston (*SSNOWD*, 2004) is used to describe the subscale snow heterogeneity in regional scale models (the equations used here can be found in the Appendix II). The model is based on two basic assumptions that are supported by many studies over the last decades (Donald *et al*. 1995; Marks *et al.* 1999; Faria *et al.* 2000; Liston 2004). First, the spatial distribution of the snow cover is persistent and can be seen as approximately similar over the years (fig. 64). Secondly, the snow water equivalent within a given area is lognormal distributed (fig. 65 a)).

The accuracy of *Subgrid Snow Distribution* (*SSNOWD*) (2004) depends on the available information about the spatial heterogeneity of the snow cover. A good description of the spatial distribution of the *SWE* is crucial to parameterize the model. The parameterisation of *SSNWOD* requires the definition of a log-normal distribution (fig. 65 a)) which is characteristic for the snow distribution in a regional model grid cell. The general form of the curve is characterised by a coefficient of variation (*CV*) within *SSNOWD* (fig. 65a)).

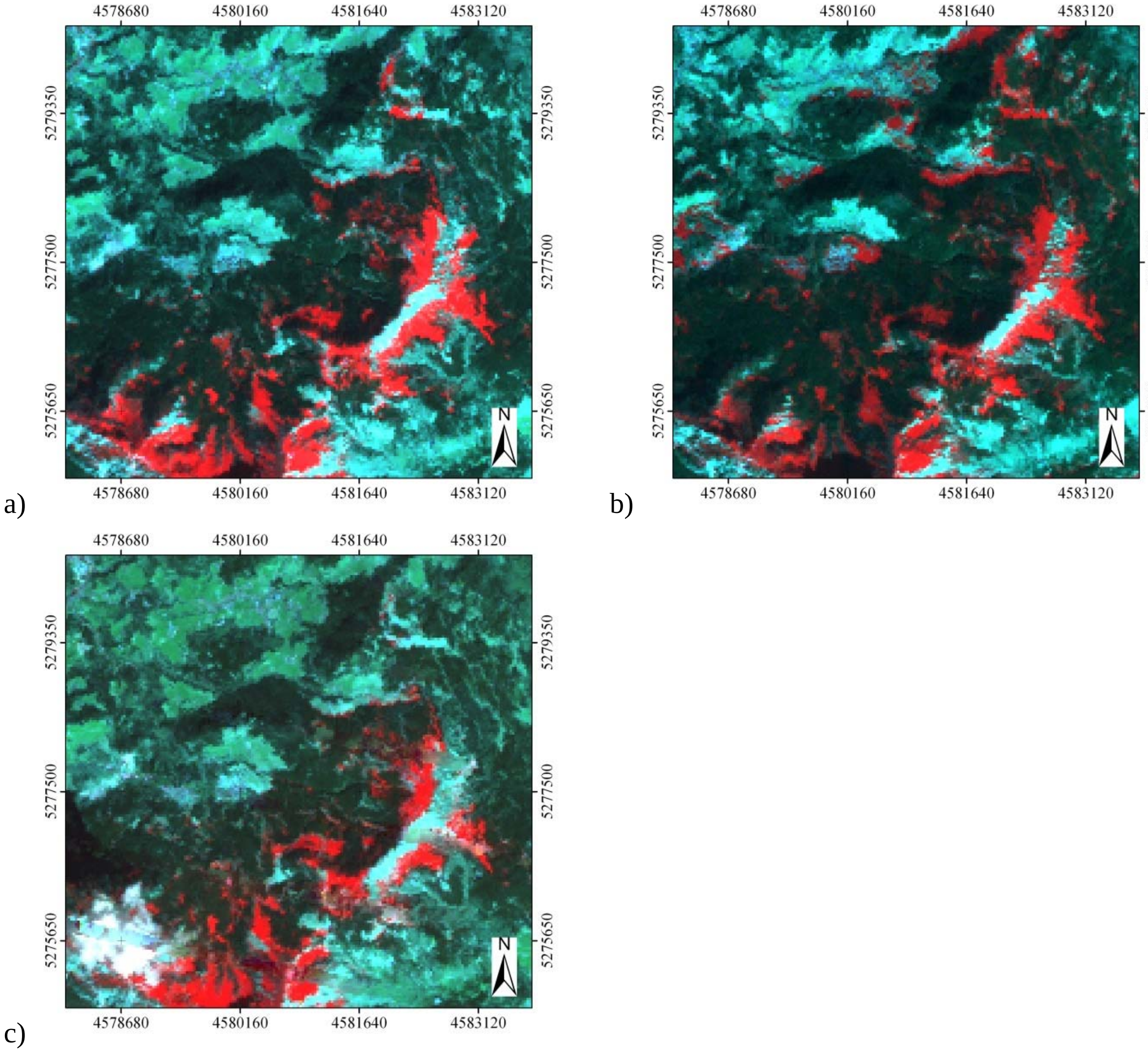

Figure 64: *Landsat* images of a) April 2002, b) March 2003 and c) April 2004. Channels 3,5,6 (R,G,B) are displayed. The snow cover is indicated by the red colour. It can be seen that the spatial characteristics of the snow distribution is very similar from year to year.

The coefficient can have values between 0 and 1. *CV* values can be determined directly through extensive snow surveys as was done by Pomeroy *et al.* (1998) and subsequently used to validate blowing snow model results (Essery *et al.* 1999) or to create an initial snow cover at the start of snowmelt simulations (Pohl and Marsh 2006). The necessary detailed snow surveys, however, are extremely time consuming and virtually impossible to carry out in the difficult topography of *Alpine* regions. Alternative methods of obtaining *CV* values are needed therefore. Liston (2004) used a decision tree to derive *CV* values for the *Regional Atmospheric modelling system* (*ClimRAMS*, grid size 80 km) which bases on the analysis of temperature, topography, and wind conditions. Since this classification scheme was designed for worldwide use, the predefined classes are relatively broad. An application of this scheme to the test site *Berchtesgaden* would lead to rather undifferentiated results with only a few different *CV* values. The presented work presents an alternative approach which bases on the *SnowModel MM5_30* results presented before. As Liston (2004) defines the *CV* value as the ratio between the mean *SWE* depth and the standard deviation of the *SWE* depth of a given area, it is easy to predict one value for a regional scale model box (which is assumed to be 1km² here) on the basis of the *micro* scale results (fig. 63 d). Hence, 1111 *micro* scale (30m*30m) *SWE* depths had to be analysed for the calculation of one *CV* value per km² box. The results are illustrated in fig. 65 b).

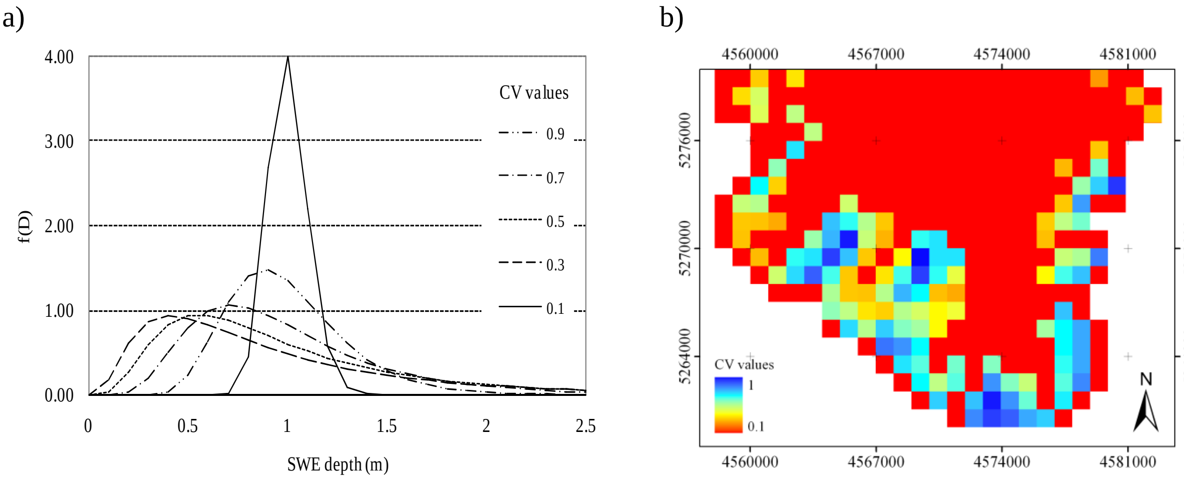

Figure 65: a) dependency of the log-normal distribution which is representative for the subscale per Pixel SWE distribution in dependency of the *CV* value b) results of the CV classification. Predicted on the basis of the ratio between per pixel mean modelled *SWE* and standard deviation of the *SWE* (30m *MM5_30 results*).

The scheme of Liston (2004) bases on the assumption that if the snow depth drops below a given threshold one has to assume that some parts within a defined area (whether this is a model grid cell or a natural area like a field, a slope or a basin), become snow free while others stay snow covered. If the model simulates snow melt the curve shifts against the y-axis (fig. 66) and if the curve intersects the axis the area under the curve which is equivalent to the total grid cell is reduced. The remaining area, determines which fraction of the snow model grid cell remains covered.

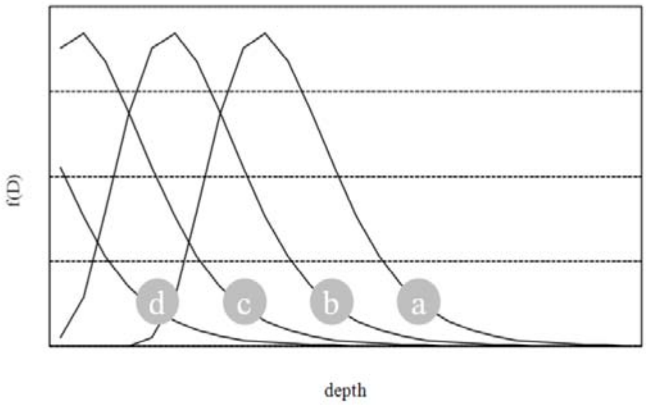

Figure 66: If the model simulates snow melt the curve shifts against the y-axis and if the curve intersects the axis the area under the curve which is equivalent to the total grid cell is reduced. Any curve stands for the *SWE* distribution of the respective grid cell.

As a first estimation whether the integration of information's about the subscale snow heterogeneity can improve the calculations of a regional scale model, *SSNOWD* (the equations are presented in the Appendix II) was integrated into *SnowModel*. The model was set up with a one kilometre resolution and driven with the input parameters used for the *INTER*_30 model runs. For the validation of the results the *NDSI* snow cover map of May 30, 2004 was used to determine the real snow covered fraction of the target 1km² grid cells (fig. 67 a)). The resulting dataset was subsequently used for a comparison with the model simulation using subscale information (fig. 67 a) and b)).

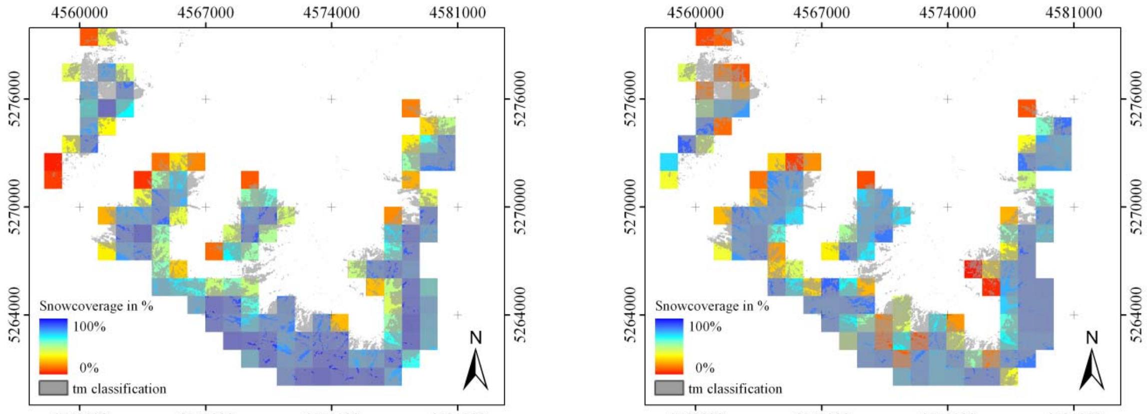

a) b)

Figure 67: Subpixel snow coverage in percent on May 30, 2004. a) Results based on a scaled NDSI map, b) Model results based on CV values predicted by the ratio approach with SnowTran-3D and *MM5* wind fields, c) Model results based on CV values generated with the iterative approach.

Overall, the Figures show that the modelled spatial pattern of the subscale heterogeneity is acceptable as it is fairly similar to the pattern of the *NDSI* classification. However, the absolute values can differ greatly. In a next step, the melt energy on May 30, 2004 13:00 was predicted. To do so, *MM5_30* results were aggregated to 1 km² grid cells and compared to *SnowModel/SSNOWD* results using a 1km² resolution. It could be seen that the average melt energy for the snow covered area is higher in the *SnowModel/SSNOWD* 1km² results (without the subgrid snow cover parameterization) (270 W/m²) than within the aggregated *MM5_30* results (220 W/m²). As the melt energy is linearly coupled with the snow covered fraction (fig. 2b)), the inclusion of a subgrid scale snow cover representation as shown in Figure 68 should lead to a reduction of the predicted melt energy. As expected, the modelled melt energy using the subgrid snow cover routine is much lower and lies slightly below the aggregated results (200 W/m²).

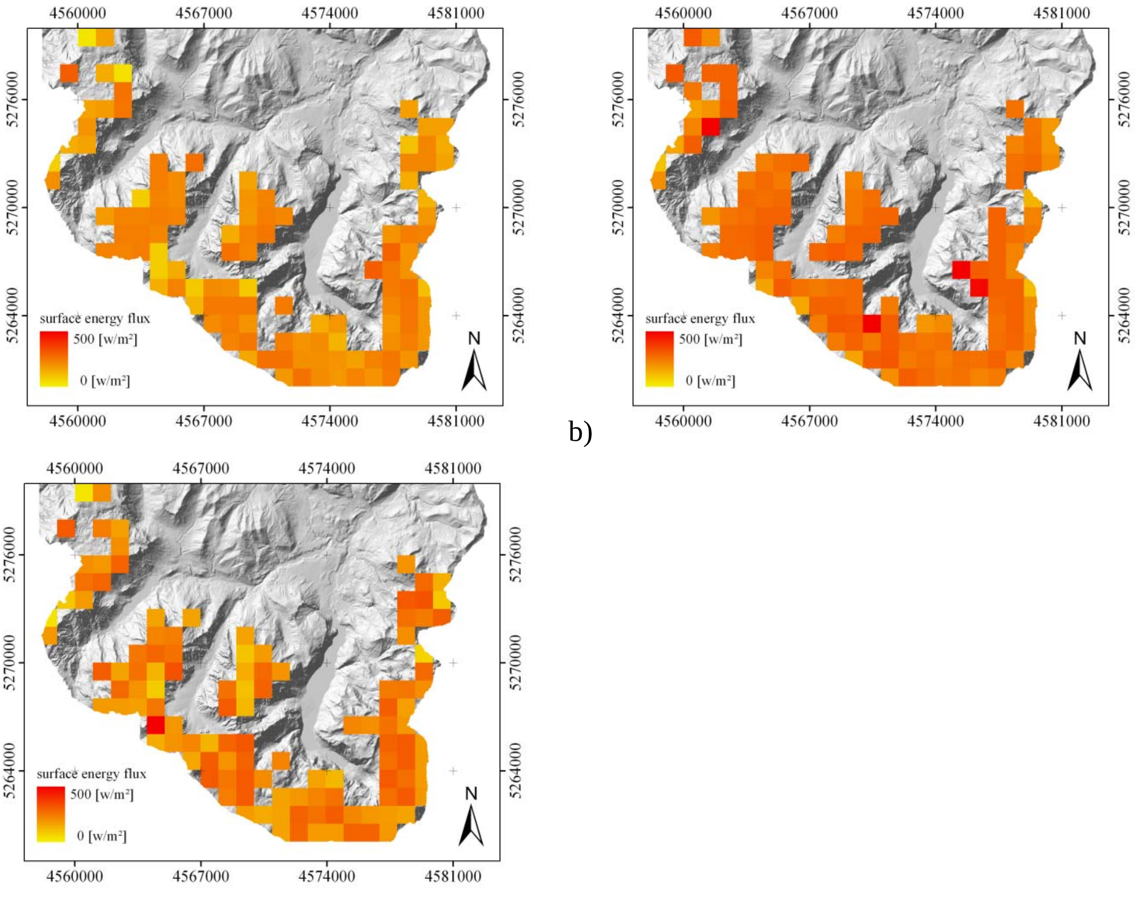

a)

b)

c)

Figure 68: Average available melt energy per km² grid cell: a) aggregated 30m results (equivalent to *MM5_30*), (220 W/m²) b) 1km² model runs without the subgrid routine (270 W/m²), c) corrected 1km² results using the subgrid routine (200 W/m²).

Commonly there are no area wide *micro* scale model runs with a complexity comparable to the presented one available for the parameterisation of *CV* values. So, an alternative scheme for the extrapolation of the presented *CV* values to other, similar regions was developed. For this purpose, the *CV* dataset was coupled with a set of topographic and meteorological information. The *CV* values were inserted into a database in combination with the respective values of mean aspect [°], elevation[m], slope[°], wind speed[m/sec] and wind direction [°] for the respective 1km² box. All values are based on averaged 30m data. The generated database enables the extrapolation of the data to areas with characteristics similar to the test site (fig. 69).

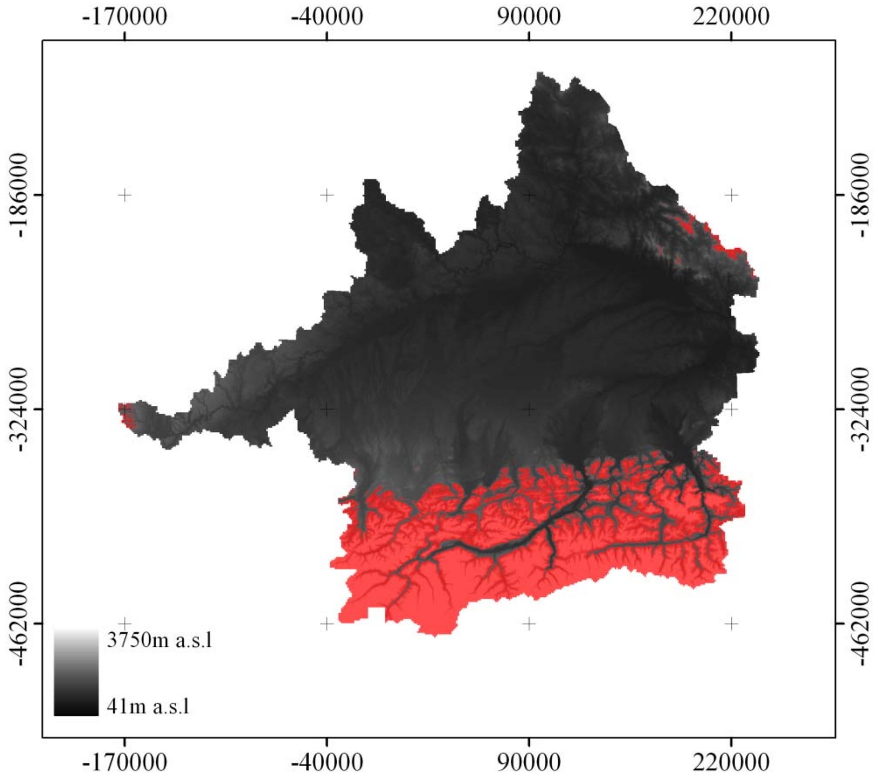

Figure 69: Upper Danube catchment. Red: Areas for which the parameterization results are potentially applicable.

The application and validation of the method proposed here is subject of future work. Nevertheless, first results presented in fig. 68 a) and b) are encouraging and clearly show the potential of the presented scheme.

6.2 Conclusion

Finally, it could be argued that only a few things have changed since Klemes (1988) has written his paper: *“The modelling of mountain hydrology: the ultimate challenge”*. As he has stated therein, the hydrological modelling in mountain regions has benefited from atmospheric models and remotely sensed data but problems like limited input and validation data and limited accessibility of the respective regions are still relevant. Hydrologic modelling of high mountain regions will be a challenge for the next generations of scientists. This, however, is no reason for a dash of sadness; because it guarantees that there will be a lot of challenging and interesting research in the next decades. The presented work has tried to answer just one of all the open questions. Its results presented in the previous *chapters*, provide some valuable answers with respect to the impact of snow transport processes on the snow cover in Alpine regions.

One of the goals of the presented thesis was to evaluate the efficiency of snow transport processes and to investigate the relative importance of these processes for the Alpine snow distribution. Model runs have shown that the effect of snow transport processes on the modelled *SWE* distribution results is extremely dependent on the selected model scale. Runs using a 200m grid cell size have indicated that the total *SWE* distribution in the test site heavily depends on snow transport processes. However, the 30m model runs revealed that snow transport processes can have a significant impact on the snow distribution in limited areas, but not on the overall *SWE* distribution of catchment. The same conclusion became evident with respect to sublimation. Modelled *SWE* losses due to sublimation of turbulent suspended snow can reach up to 920 mm *SWE* at the mountains crests but are less than 50mm in the valley regions and in the flatlands. The effect on the total *SWE* budget and therefore on the water balance is small in consequence.

It was also determined that the observed spatial heterogeneity of the snow cover can only partially be explained by the modelled processes. Hence, there have to be other mechanisms which are influencing the snow distribution in *Alpine* catchments. Strasser (2008) has shown that the simple inclusion of snow slides into his model environment leads to an improved reproduction of observed snow distribution as far as this distribution can be validated with optical data. Nevertheless, the quantification of the different snow transport processes (wind induced and gravitational) is impossible at the moment because there are no coupled models that simulate both processes simultaneously. Additionally, the effect of preferential snow distribution is completely unknown at the moment which complicates the resulting model calculations because of an unknown initial snow distribution.

The model validation at the *micro* and *meso* scale has shown that the model delivers acceptable data which is close to measurements at all sites (e.g. fig. 22). The used *Landsat ETM+* data have clearly shown the limitations of optical systems for the determination of a snow cover in forested regions but have also revealed that the results of *SnowModel* could be improved by an inclusion of *MM5* wind fields.

The subscale snow coverage routine which was presented in *Chapter 6* has produced encouraging initial results which will be validated in future work.

Finally, it can be concluded that:

- The estimation of the spatial distribution of SWE in alpine terrain using *SnowModel* was considerably improved by the use of the MM5 derived wind fields.
- The physically based *SnowModel/SnowTran-3D/MM5* couple delivers plausible results for distributed snow covers even in Alpine regions at the *micro* scale.
- The decreased accuracy of the results at the *meso* scale indicates that the simulation of snow transport processes should preferentially use small scales, especially if information about the snow distribution within a smaller area is needed. Despite their decreased accuracy, the *meso* scale results still show the principle functionality of the *SnowModel/MM5* bundle for larger areas.
- The presented thesis illustrates that present day regional atmospheric models should be used instead of interpolated meteorological data as input for land surface models when studying snow transport in hilly terrain.
- While the model scheme used here can simulate some of the observed snow cover heterogeneity within the study area, it becomes obvious that the real extent of the snow cover distribution cannot be reproduced fully by the model. Rather, the coupled model still underestimates the heterogeneity of the real snow cover.

It could be stated that the mountains do not give up their secrets easily (which is not only true for the Yeti) but the author hopes that he wrenched a little secret away from the mountains, which is now available in form of this thesis.

References

Adrian, G and Frühwald, D. 2002. Design der Modellkette GME/LM. *PROMET, 27.* 2002, pp. 106-110.

AEA, Technology. 2001. CFX 4.4 Solver Manual. *AEA Technology.* 2001.

Anderson, E A. 1976. A point energy and mass balance model of a snow cover. NOAA Tech. Rep. NWS-19

Armstrong, R L and Brodzik, M J. 2002. Hemispheric-scale comparison and evaluation of passive-microwave snow algorithms. *Annals of Glaciology, 34,* pp. 38-44

Bach, H. 1995. Die Bestimmung hydrologischer und landwirtschaftlicher Oberflächenparameter aus hyperspektralen Fernerkundungsdaten. *Münchener Geographische Abhandlungen,* Band B 21

Bagnold, R A. 1941. The Physics of Blown Sand and Desert Dunes. London, Chapman and Hall.

Balk, B and Elder, K. 2000. Combining binary decision tree and geostatistical methods to estimate snow distribution in a mountain watershed. *Water Resources Research, 36.* 2000, pp. 13-26.

Barnes, S L. 1964. A technique for maximizing details in numerical weather map analysis. *Journal of applied Meteorology, 3.* 1964, pp. 396-409.

Barnes, S L. 1973. Mesoscale objective analysis using weighted time series observations. NOAA Tech. Memo. ERL NSSL-62, National Severe Storms Laboratory, Norman.

Barros, A P and Lettenmaier, D P. 1994. Dynamic modeling of orographically induced precipitation. *Reviews of Geophysiks, 32,* pp. 265-284.

Barry, R G. 1992. Mountain weather and climate. Routledge, London

Bartelt, P and M. Lehning 2002. A physical SNOWPACK model for Avalanche Warning Services. Part I: numerical model, Cold Reg. Sci. Technol., 35, 123-145.

Bernhardt, G., Liston G E, Strasser U, M, Zängl and Mauser W. 2007. High resolution modelling of snow transport in complex terrain using simulated wind fields. *Berchtesgaden National Park Research Report (special issue Alpine*Snow*Workshop).* 2007.

Bernhardt, M, Liston G E, Strasser U. and Mauser W. 2008 a. Using wind fields from a high resolution atmospheric model for simulating snow dynamics in mountainous terrain. *Hydrological Processes.* 2008, accepted.

Bernhardt, M, Liston G E, Strasser U. and Mauser W. 2008 b. High resolution modelling of snow transport in complex terrain using simulated wind fields. *The Cryosphere.* 2008, submitted.

Blösch, G and Sivapalan, M. 1995. Scale issues in hydrological modeling. A review. *Hydrological Processes*. 9, 251-290.

Blöschl, G. 1999: Scaling issues in snow hydrology. *Hydrological Processes, 13,* pp. 2149-2175.

Bowling, L C, Pomeroy, J W and Lettenmaier, D P. 2004. Parameterization of Blowing-Snow Sublimation in a Macroscale Hydrology Model. *Journal of Hydrometeorology, 5.* 2004, pp. 745-762.

Bruland, O, Liston G E, Vonk, J, and Killingtveit, A, 2004. Modelling the snow distribution at two high arctic sites at Svalbard, Norway, and at an Alpine site in central Norway. *Nordic Hydrology, 35,* pp. 191-208.

Brun E, Martin E, Simon V, Gendre C, Coleou C. 1989. An energy and mass model of snow cover suitable for operational avalanche forecasting, *J. of Glaciol., 35,* pp. 333-342.

Brun E, David P, Sudul M, Brunot G. 1992. A numerical model to simulate snow-cover stratigraphy for operational avalanche forecasting. *Journal of Glaciology 38*: 13-22.

Buck, A L. 1981. New equations for computing vapor pressure and enhancement factor. *J. Appl. Meteor., 20,* 1527–1532.

Burridge, D M and Gadd A J. 1974. The meteorological office operational 10 level numerical weather prediction model. British Met. Office Tech. Notes Nos. 12 and 48 London R., Bracknell, Berkshire, RG12 2SZ, England

De Quervain, M and Meister, R. 1987. 50 years of snow profiles on the Weissfluhjoch and relations to the surrounding avalanche activity (1936/37-1985/86). *IAHS Publ. No. 162.* 1987, pp. 161-181.

Déry, S J and Yau, M K. 1999. A Bulk Blowing Snow Model. *Boundary-Layer Meteorology, 93.* 1999, 2, pp. 237-251.

Doesken, N J and Judson, A. 1996. *The Snow Booklet: A guide to the science, climatology, and measurement of snow in the United States.* Fort Collins : Colorado State University, 1996.

Doms, G and Schättler, U. 1999. *The nonhydrostatic Limited-Area model LM (Lokal-Modell) of DWD. Part I: Scientific Documentation.* Offenbach : Deutscher Wetterdienst, 1999.

Doms, G, Steppler, J and Adrian, G. 2002. Das Lokalmodell LM. *PROMET, 27.* 2002, pp. 123-128.

Donald, J R, Soulis E D, and Kouwen N. 1995. A land coverbased snow cover representation for distributed hydrologic models. *Water Resour. Res., 31,* pp. 995–1009.

Doorschot, J. 2002. Mass transport of drifting snow in high alpine environments. *http://e-collection.ethbib.ethz.ch/show?type=diss&nr=14515.* 2002.

Dozier, J. 1984. Snow reflectance from Landsat-4 thematic mapper. *I.E.E.E. Trans. Geosci. Remote Sens. 22,* pp.323-328.

Durand, Y, Guyomarc'h G, Mérindol L, and Corripio J G, 2005. Improvement of a numerical snow drift model and field validation. *Cold Regions Science and Technology 43,* pp. 93-103.

Durand, M. and Margulis S. 2005. Large-scale SWE Estimation: Optimal Use of Remote Sensing and Snow Modeling, *Southwest Hydrology, 4(2),* pp.20-21, 32.

Eidsvik, K J, et al. 2004. A Prediction System for Local Wind Variations in Mountainous Terrain. *Boundary-Layer Meteorology, 112.* 2004, pp. 557-586.

Ellis, A W and Leathers D J. 1999. Analysis of cold airmass temperature modification across the U.S. Great Plains as a consequence of snow depth and albedo. *J. Appl. Meteor., 38,* pp. 696–711.

Enders, G. 1979. Theoretische Topoklimatologie. *Forschungsbericht 1* des Nationalparks Berchtesgaden. Berchtesgaden.

Essery, R L, Li, L and Pomeroy, J W. 1999. A Distributed Model of Blowing Snow over Complex Terrain. *Hydrological Processes, 13.* 1999, pp. 2423-2438.

Essery, R L. 2001. Spatial statistics of windflow and blowing-snow fluxes over complex terrain. *Boundary-Layer Meteorology, 100.* 2001, pp. 131-147.

Essery, R L, et al. 2003. Sublimation of snow from boreal forests in a climate model. *Journal of Climate, 16.* 2003, pp. 1855-1864.

Essery, R L H, and Pomeroy J W. 2004. Vegetation and topographic control of wind-blown snow distributions in distributed and aggregated simulations for an Arctic tundra basin. *Journal of Hydrometeorology 5,* pp. 734-744.

Etchevers P, Martin E, Brown R, Fierz C, Lejeune Y, Bazile E, Boone A, Dai Y J, Essery R, Fernandez A, Gusev Y, Jordan R, Koren V, Kowalczyk E, Pyles R D, Schlosser A., Shmakin A B, Smirnova T G, Strasser U, Verseghy D, Yamazaki T, Yang Z L. 2002. SnowMIP, an intercomparison of snow models: first results. *Proceedings of the International Snow Science Workshop (ISSW 2002),* October 2002, Penticton, British Columbia, Canada.

Faria, D A, Pomeroy J W, and Essery R L H. 2000. Effect of covariance between ablation and snow water equivalent on depletion of snow-covered area in a forest. *Hydrol. Processes, 14,* pp. 2683–2695.

Frei, C and Schär, C. 1998. A precipitation climatology of the Alps from high-resolution raingauge observations. *Int. J. Climatol., 18,* pp. 873-900

Gal-Chen, T and Sommerville, R C. 1975. On the use of a coordinate transformation for the solution of the navier-stokes equations. *Journal of Computational Physics; 17.* 1975, pp. 209-228.

Gauer, P., 2001. Numerical modeling of blowing and drifting snow in Alpine terrain. *Journal of Glaciology 47,* pp. 97-110.

Gray, D.M, and others 1979. Snow accumulation and distribution. In *Proceedings of a Meeting on Modeling of Snow Cover Runoff.* Colbeck SC, Ray M (eds); 1978, Hanover, New

Hampshire. US Army Cold Regions Research and Engineering Laboratory: Hanover, New Hampshire: 3-33.

Greene, E M, Liston, G E and Pielke, R A. 1999. Simulation of above treeline snowdrift formation using a numerical snow-transport model. *Cold Regions Science and Technology, 30.* 1999, pp. 135-144.

Grell, G A, Dudhia, J and Stauffer, D R. 1995. *A description of the fifth generation Penn State/NCAR mesoscale model (MM5).* Boulder, Colorado, USA : s.n., 1995. Technical report, National Centre for Atmospheric Research.

Hall D K, Riggs G A, Salomonson V V. 1995. Development of methods for mapping global snow cover using moderate resolution imaging spectroradiometer data. *Remote Sens. Environ. 54,* pp. 127–140

Hall, D K, Foster, J L, Salomonson V V, Klein A G, and Chien J Y L. 2001. Development of a Technique to Assess Snow-Cover Mapping Errors from Space, *IEEE Transactions on Geoscience and Remote Sensing, 39(2),* pp. 432-438.

Hasholt, B, Liston, G E and Knudsen, N T. 2003. Snow-distribution modelling in the Ammassalik region, south east Greenland. *Nordic Hydrology, 34.* 2003, pp. 1-16.

Hiemstra, C A, Liston, G E and Reiners, W A. 2002. Snow redistribution by wind and interactions with vegetation at upper treeline in the Medicine Bow Mountains, Wyoming, USA. *Arctic Antarctic and Alpine Research, 34.* 2002, pp. 262-273.

Hiemstra, C A, Liston, G E and Reiners, W A. 2006. Observing, modelling, and validating snow redistribution by wind in a Wyoming upper treeline landscape. *Ecological Modelling.* 2006.

Hoinkes H. 1967. Glaciology in the international hydrological decade. IAHS Commision on Snow and Ice: *Reports and Discussions, 79,* pp. 7-16

Hood, E, Williams, M and Cline, D. 1999. Sublimation from a seasonal snowpack at a continental, mid-latitude alpine site. *Hydrological Processes, 13.* 1999, pp. 1781-1797.

Johansson, B and Chen, D. 2003. The influence of wind and topography on precipitation distribution in Sweden: Statistical analysis and modelling. *International Journal of Climatology, 23.* 2003, pp. 1523-1535.

Jordan, R. 1991. A one-dimensional temperature model for a snow cover: Technical documentation for SNTHERM.89. *U.S. Army Corps of Eng., Cold Reg. Res.and Eng. Lab.* Spec. Rep. 91-16, 1991.

Kirnbauer R and Blöschl G. 1994. How similar are snow cover patterns from year to year. Deutsche Gewässerkundliche Mitteilungen 1994

Koch, S E, Desjardins, M and Kocin, P J. 1983. An Interactive Barnes Objective Map Analysis Scheme for Use with Satellite and Conventional Data. *Journal of Climate and Applied Meteorology, 22.* 1983, pp. 1487-1503.

Knap, W H, Brock, B W, Oerlemans, J, Willis, I C. 1999. Comparison of Landsat-TM derived and ground-based albedo of Haut Glacier d'Arolla. *International Journal of Remote Sensing., 20,* pp.3293-3310.

Kneizys, F X, Shettle, E P, Abreu, L W, Chetwynd, J H, Fenn, R W, Gallery, W O, Selby, J E A, and Clough S. 1988. Atmospheric Transmittance/Radiance: Computer Code Lowtran 6, AFGL-TR-83-0187, Air Force Geophysics Laboratory, Hanscom AFB, Massachusetts

Kuhn, M. 1993. Zwei Gletscher im Karwendelgebirge. *Zeitschrift für Glaziologie und Gletscherkunde, 29/1*, pp. 85-92.

Kuhn, M. 1995. The mass balance of very small glaciers. *Zeitschrift für Glaziologie und Gletscherkunde, 31*, pp. 171-179.

Kuhn, M. 2003. Redistribution of snow and glacier mass balance from a hydrometeorological model. *Journal of Hydrology, 282.* 2003, pp. 95-103.

Kunkel, K E. 1989. Simple procedures for extrapolation of humidity variables in the mountainous western United States. *J. Climate, 2*, pp. 656–669.

Kyle, H L, Curran, R J, Barnes, W L, and Escoe, D. 1978. A cloud physics radiometer, *Third Conference on Atmospheric Radiation,* Davis, CA, pp. 107-109.

Kyle, H L, Ardanuy, P E, and Harley, E J. 1985. The status of the Nimbus-7 Earth Radiation Budget data set, Bull. Am. Meteorol. Soc., *66*, pp. 1378–1388.

Lehning, M, Doorschot, J, Raderschall, N, Bartelt, P. 2000. Combining snow drift and SNOWPACK models to estimate snow loading in avalanche slopes. *Snow Engineering.* 2000, pp. 113-122.

Lehning, M, Doorsschot, J, Fierz, C and. Radersschall, N. 2002. A 3D model for snow drift and snow cover development in steep alpine terrain. *Proceedings International Snow Science Workshop (ISSW).* 2002, pp. 579-586.

Lehning, M, Völksch, I, Gustafsson, D, Nguyen, T A, Stähli, M, Zappa, M. 2006. ALPINE3D: A detailed model of mountain surface processes and its application to snow hydrology, 20. *Hydrological Processes.* 2006, pp. 2111-2128.

Liston, G E. 1995. Local Advection of Momentum, Heat, and Moisture during the Melt of Patchy Snow Covers. *Journal of applied meteorology, 34.* 1995, pp. 1705-1715.

Liston, G E and Hall D K. 1995. An energy-balance model of lake-ice evolution. *Journal of Glaciology, 41*, pp. 373-382.

Liston, G E and Sturm, M. 1998. A snow-transport model for complex terrain. *Journal of Glaciology, 44.* 1998, pp. 498-516.

Liston, G E, Winther, J G, Bruland, O, Elevehøy, H, Sand, K. 1999. Below-surface ice melt on coastal Antarctic ice sheets. *Journal of Glaciology, 45,* pp.273-285

Liston, G E, Winther, J G, Bruland, O, Elevehøy, H, Sand, K, Karlöf, H. 2000. Snow and blue-ice distribution patterns on the coastal Antarctic Ice Sheet. *Antarctic Science, 12.* 2000, pp. 69-79

Liston, G E. 2004. Representing Subgrid Snow Cover Heterogeneities in Regional and Global Models. *Journal of Climate, 17.* 2004, pp. 1381-1397.

Liston, G E and Sturm, M. 2004. The role of winter sublimation in the Arctic moisture budget. *Nordic Hydrology, 35.* 2004, pp. 325-334.

Liston, G E and Elder, K. 2006. A meteorological distribution system for high resolution terrestial modelling (MicroMet). *Journal of Hydrometeorology, 7.* 2006, pp. 217-234 .

Liston, G E and Elder, K. 2006. A Distributed Snow-Evolution Modelling System (SnowModel). *Journal of Hydrometeorology, 7.* 2006, pp. 1259-1276 .

Liston, G E, Haehnel, R B; Sturm, M, Hiemstra, C A, Berezovskaya, S, Tabler, R D. 2007. Simulating Complex Snow Distributions in Windy Environments using SnowTran-3D. *Journal of Glaciology, 53*, pp. 241-256

Ludwig, R, et al. 2003. Web-based modelling of energy, water and matter fluxes to support decision making in mesoscale catchments-the integrative perspective of GLOWA-Danube. *Physics and Chemistry of the Earth.* 2003, pp. 621-634.

Marks D, Domingo J, Susong D, Link T, Garen D. 1999. A spatially distributed energy balance snowmelt model for application in mountain basins. *Hydrological Processes 13*. pp. 1935–1959.

Marsh, P. 1999. Snowcover formation and melt: recent advances and future prospects. *Hydrological Processes.* 1999, Vol. 13, pp. 2117-2134.

Mauser W and Bach H. 2008. PROMET – a Physical Hydrological Model to Study the Impact of Climate Change on the Water Flows of Medium Sized, Complex Watersheds. *Journal of Hydrology*. submitted

Plattner C, Braun L and Brenning A. (2006). The spatial variability of snow accumulation at Vernagtferner, Austrian Alps, in Winter 2003/2004, *Zeitschrift für Gletscherkunde und Glazialgeologie, 39*, pp. 43-57.

Pohl S and Marsh P. 2006. Small-scale modelling of spatially variable snowmelt in an arctic catchment. *Hydrological Processes,* 20, 1773-1792.

Pomeroy, J W. 1988. Wind Transport of Snow. PhD Thesis, Division of Hydrology, University of Saskatchewan, Saskatoon.

Pomeroy, J W and Gray, DM. 1990. Saltation of snow. *Water Resources Research, 26,* pp. 1583-1594.

Pomeroy, J W, Gray, D M and Landine, P G. 1993. The Prairie Blowing Snow Model - characteristics, validation, operation. *Journal of Hydrology, 144.* 1993, pp. 165-192.

Pomeroy, J W and Essery, R L. 1999. Turbulent fluxes during blowing snow: field tests of model sublimation predictions. *Hydrological Processes, 13.* 1999, pp. 2963-2975.

Pomeroy, J W, Gray, D M. 1995. Snowcover: Accumulation, Relocation, and Management. National Hydrology Research Institute, Saskatoon, Canada. *NHRI Science Report. 7*, pp.144

Pomeroy, J W, Marsh P, Gray D M. 1997. Application of a distributed blowing snow model to the arctic. *Hydrological Processes 11*: 1451-1464.

Pomeroy J W, Gray D M, Shook K R, Toth B, Essery R, Pietroniro A, Hedstrom NR. 1998. An evaluation of snow accumulation and ablation processes for land surface modelling. *Hydrological Processes* **12**: 2339–2367.

Prasad, R, Tarboton D G, Liston G E, Luce C H, and Seyfried M S. 2001. Testing a blowing snow model against distributed snow measurements at Upper Sheep Creek, Idaho, United States of America. *Water Resources Research, 37.* 2001, pp. 1341-1356.

Prasch, M, et al. 2007. Physically based modelling of snow cover dynamics in Alpine regions. *Proceedings of the International Congress 'Managing Alpine Future - strategies for sustainability in times of change'.* 2007.

Raderschall, N, Lehning, M und Doorshot, J. 2002. Boundary layer wind field over steep, snow covered, high alpine topography. *Proc. 10th Conference Mountain Meteorology.* 2002, S. 303-306.

Rees, G W. 2006. Remote Sensing of Snow and Ice. Taylor and Francis. Boca Raton

Rutter, N, and Essery R. 2006. Evaluation of forest snow processes models (SnowMIP2), *Geophysical Research Abstracts,* Vol. 8, 05921, 2006 SRef-ID: 1607-7962/gra/EGU06-A-05921

Ryan, B C. 1977. A mathematical model for diagnosis and prediction of surface winds in mountainous terrain. *Journal of Applied Meteorology, 16.* 1977, pp. 571-584.

Schmidt, R A. 1972. Sublimation of wind-transported snow - a model. *U.S. Forest Service, Rocky Mountain Forest and Range Experiment Station, Research Paper 90.* 1972.

Shafran, P C, Seaman, N L and Gayno, G A. 2000. Evaluation of numerical predictions of boundary layer structure during the Lake Michigan Ozone Study. *Journal of Applied Meteorology, 39.* 2000, pp. 412-426.

Sundsbø, P A, 1997. Numerical modelling and simulation of snow drift. Doctoral Dissertation, Narvik Institute of Technology, Department of Building Science, The Norwegian University of Science and Technology, 112 pp

Strasser, U, et al. 2007. Is snow sublimation important in the alpine water balance? *The Cryosphere Discuss., 1.* 2007, pp. 303-350.

Sturm, M, Holmgren, J and Liston, G E. 1995. A seasonal snow coverclassification system for local to global applications. *Journal of Climate.* 1995, 8, pp. 1261–1283.

Thornton, P E, Running, S W and White M A. 1997. Generating surfaces of daily meteorological variables over large regions of complex terrain. *J. Hydrol., 190,* pp. 214–251.

Tucker, C J. 1979. Red and photographic infiared linear combinations (or monitoring vegetation, *Remote Sens. Environ.,8,* pp.27-150.

Uematsu, T, Nakata T, Takeuchi K, Arisawa Y, and Kaneda Y, 1991. Three-dimensional numerical simulation of snowdrift. *Cold Regions Science and Technology 20*, 65-73.

UNESCO/IAHS/WMO. 1970. Seasonal snow cover. In: Technical Papers in Hydrology. Paris: UNESCO/IAHS/WMO

Walcek, C. J., 1994. Cloud cover and its relationship to relative humidity during a spring midlatitude cyclone. *Mon. Wea. Rev., 122,* pp. 1021–1035.

Walter, M T and McCool, D K. 2004. A simple snowdrift model for distributed hydrological modeling. *Journal of Hydrologic Engineering, 9.* 2004, pp. 280-287 .

Weber, M. 2005. *Mikrometeorologische Prozesse bei der Ablation eines Alpengletschers.* Institute for Meteorology and Geophysics. University of Innsbruck. : s.n., 2005.

Wergen, W. 2002. Datenassimilation - ein Überblick. *PROMET, 27.* 2002, pp. 142-149.

Wieser, A, Fiedler, F, and Corsemeier, U. 2001. The influence of the sensor design on wind measurements with sonic anemometer systems. *J. Atmos. Oceanic Technol., 18*, pp. 1585–1608.

Winkler, D. 2005. Der Blaueisgletscher in Not. Berchtesgadener Heimatkalender 2006, pp. 45-48.

Winstral, A and Marks, D. 2002. Simulating wind fields and snow redistribution using terrain-based parameters to model snow accumulation and melt over a semi-arid mountain catchment. *Hydrological Processes, 16.* 2002, pp. 3585-3603.

Winther, J G, and Hall, D K. 1999. Satellite derived snow cover related to hydropower production in Norway: present and future. *International Journal of Remote Sensing*, 20. pp. 2991-3008

Xiao, J, Bintanja R, Déry S J, Mann G and Taylor, P A.. 2000. An intercomparison among four models of blowing snow. *Boundary Layer Meteorology.* 2000, 97, pp. 109-135.

Xue, M, Droegemeier, K K and Wong, V. 2000. The Advanced Regional Prediction System The Advanced Regional Prediction System dynamics and verification. *Meteorology and Atmospheric Physics.* 2000, 75, pp. 161-193.

Xue, M, Droegemeier, K K, Wong, V, Shapiro A, Brewster K, Carr F, Weber D, Liu Y, and Wang, D H. 2001. The Advanced Regional Prediction System (ARPS) - A multiscale nonhydrostatic atmospheric simulation and prediction tool. Part II: Model physics and applications. *Meteorology and Atmospheric Physics.* 2001, 76, pp. 161-193.

Zängl, G. 2002. An Improved Method for Computing Horizontal Diffusion in a Sigma-Coordinate Model and Its Application to Simulations over Mountainous Topography. *Monthly Weather Review, 130.* 2002, pp. 1423-1432.

Zängl, G. 2003. Orographic Gravity Waves Close to the Nonhydrostatic Limit of Vertical Propagation. *Journal of the Atmospheric Sciences, 60.* 2003, pp. 2045-2063.

Appendix I

I) Additional Equations of the snow model (the total set of formulations can be found in Liston and Sturm (1998)

The following Equations are used for describing the sublimation process during transport:

Sublimation during transport is described as:

$$Q_v(x^*) = \psi_s \phi_s h_* + \int_{h_*}^{z_t} \psi_t(x^*, z)\phi_t(x^*, z)\, dz \qquad \text{(A-1)}$$

Q_v (kg m^{-2} s^{-1}) = sublimation rate of transported snow. Ψ_s / Ψ_t = sublimation loss rate coefficient for saltation and turbulent suspension. $Ø_s$ (kg m^{-3}) = saltation layer mass concentration. $Ø_t$ (kg m^{-3}) = vertical mass concentration within the turbulent suspension layer.

The sublimation loss rate is defined as:

$$\psi(x^*, z) = \frac{d\bar{m}(z)/dt}{\bar{m}(z)} \qquad \text{(A-2)}$$

t(s) = time, $\bar{m}(z)$ (kg) = mean particle mass at height z.

The average particle mass is simulated with:

$$\bar{m}(z) = \frac{4}{3}\pi\rho_i \overline{\bar{r}_r}(z)^3 \left(1 + \frac{3}{\alpha} + \frac{2}{\alpha^2}\right) \qquad \text{(A-3)}$$

ρ_i (kg m^{-3}) = density of ice, $\bar{r}$ mean radius of snow particles.

$$\bar{r}_r(z) = 4.6 * 10^{-5} z^{-0-258} \qquad \text{(A-4)}$$

z = height

Coefficient α is defined by:

$$\alpha = 4.08 + 12.6z \qquad \text{(A-5)}$$

Mass loss from an ice sphere is described by the combined influence of humidity gradients between particle and free atmosphere, as wells as intercepted solar radiation, particle size and ventilation influences:

$$\frac{d\bar{m}}{dt} = \frac{2\pi\bar{r}\sigma - \frac{S_p}{\lambda_t T_a Nu}\left[\frac{h_S M}{R T_a} - 1\right]}{\frac{h_S}{\lambda_t T_a Nu}\left[\frac{h_S M}{R T_a} - 1\right] + \frac{1}{D \rho_v Sh}} \qquad \text{(A-6)}$$

M (18.01 kg kmole^{-1}) = molecular weight of water, R (8313 J kmole^{-1} K^{-1}) = universal gas constant, T_a (K) = air temperature, λ_t (0.024J m^{-1} s^{-1} K^{-1}) = thermal conductivity of the atmosphere, h_s = latent heat of sublimation. D (m² s^{-1}) = diffusivity or water vapour in the atmosphere, ρ_v = (kg m^{-3}) = saturation density of water vapour. R_d (287 J deg^{-1} kg^{-1}) = gas constant for dry air, e_s = vapour pressure over ice. Nu = Nusselt Number, Sh = Sherwood Number.

The formulation for the radius of a snow particle $\bar{r}(z)(m)$, of mean particle mass $\bar{m}\ (z)$ is:

$$\bar{r}(z) = \left(\frac{3\bar{m}(z)}{4\pi\rho_i}\right)^{\frac{1}{3}} \qquad \text{(A-7)}$$

Nusselt and Sherwood numbers are related to the Reynolds number:

$$Nu(z) = Sh(z) = 1.79 + 0.606Re(z)^{0.5} \quad \text{(A-8)}$$

The particle Reynold's number (Re) is defined to be:

$$R_e(z) = \frac{2\bar{r}(z)V_V(z)}{v} \quad \text{(A-9)}$$

v = kinematic viscosity of the air, V_V = ventilation velocity.

The ventilation velocity consists of two components, the mean and the fluctuating velocity component (in the case of turbulent suspension V_t).

$$V_t(z) = \bar{w}(z) + 3x_r(z)cos\left(\frac{\pi}{4}\right) \quad \text{(A-10)}$$

Where the mean terminal fall velocity is given as:

$$\bar{\omega}(z) = 1.1 * 10^7\bar{r}(z)^{1.8} \quad \text{(A-11)}$$

And the fluctuating component:

$$x_r(z) = 0.005u(z)^{1.36} \quad \text{(A-12)}$$

For the case of saltation the formulation follows Pomeroy and Gray (1995):

$$V_s = 0.68u_* + 2.3u_{*t}$$

The solar radiation absorbed by the snow particle is described by:

$$S_p = \pi\bar{r}_r(z)^2\left(1 - \alpha_p\right)(1 + \alpha_s)S_i \quad \text{(A-13)}$$

α_p = smow particle albedo (assumed to be 0.5) and α_s = is the snow cover albedo (assumed to be 0.8).

S_i = the incoming solar radiation and follows Liston (1995):

$$S_i = S^*\Upsilon sin\omega \quad \text{(A-14)}$$

S^*= solar irradiance at the top of atmosphere (1370 W/m²), Υ = net sky transmissivity, sin ω = solar elevation angle.

II) Equations used for the subscale snow model used in chapter 6

The following section will present the subscale snow distribution model presented by Liston (2004). The model was used in *chapter 6* for describing the subscale snow heterogeneity of the snow cover.

If the snow free and the snow covered fractions are known, the per grid cell energy balance can be weighted linearly proportionally to the percentages of snow free and snow covered fractions (eq 38):

$$Q_{ga} = \Gamma Q_{sc} + (1 - \Gamma) Q_{sf} \qquad \text{(Eq. 38)}$$

Estimation of the grid averaged fluxes Q_{ga} = Q_{sc} = Snow covered flux, Q_{sf} = snow free flux, Γ = snow covered fraction.

The subscale snow distribution is described with a set of formulas based on the works of Donald *et al* (1995), Pomeroy *et al.* (1998), Faria *et al.* (2000) and Liston (1999 and 2004).

Liston (1999) found that the internal grid cell snow water equivalent distribution, the average melt rate and the snow covered fraction are interrelated. He has also demonstrated that any of the three parameters can be predicted if the other two are known. Equation 38 shows that every model cell includes a snow free and a snow covered fraction under melt conditions. The two fractions sum to 1 for any pixel:

$$\int_0^{D_m} f(D)dD + \int_{D_m}^{\infty} f(D)dD = 1 \qquad \text{(Eq. 39)}$$

Sum of the snow free and snow covered fraction of any grid cell. D_m = grid cell melt rate, f(D) = SWE depth probability function.

Thus the snow free fraction can be expressed by:

$$\Gamma(D_m) = 1 - \int_0^{D_m} f(D)dD \qquad \text{(Eq. 40)}$$

$\Gamma(D_m)$ snow covered fraction in dependence of the melt rate, f(D) SWE depth probability function.

According to Donald *et al.* (1995), Pomeroy *et al.* (1998) and Faria *et al.* (2000), snow water equivalent depth distributions can be approximated by a two parameter log-normal distribution:

$$f(D) = \frac{1}{D\xi\sqrt{2\pi}} exp\left\{-\frac{1}{2}\left[\frac{ln(D)-\lambda}{\xi}\right]^2\right\} \qquad \text{(Eq. 41)}$$

SWE distribution function f(D): D = SWE depth, λ and ζ are distribution parameters (Liston 2004).

The description of the first distribution parameter λ is based on Pomeroy *et al.* (1995):

$$\lambda = ln(\mu) - \frac{1}{2}\xi^2 \qquad \text{(Eq. 42)}$$

Distribution parameter λ: μ = mean SWE depth, ξ distribution parameter.

The second distribution parameter is mainly characterized by a coefficient of variation. Liston (2004) defined *CV* as equal to the ratio of the standard deviation to the mean of the *SWE* depth of a given area. *CV* modifies the general form of the log-normal distribution (fig. 65a):

$$\xi^2 = ln(1 + CV^2) \qquad \text{(Eq. 43)}$$

Distribution parameter ξ: CV = coefficient of variation (Donald *et al.* 1995)

The average *SWE* depth of a grid cell D_a under assumption of a certain melt depth D_m is given by Donald *et al.* (1995):

$$D_a(D_m) = \frac{1}{2}e^{(\lambda+\xi^2/2)}\mathrm{erfc}\left(\frac{z_{\mathrm{D_m}}-\xi}{\sqrt{2}}\right) - \mathrm{D_m}\Gamma(\mathrm{D_m}) \qquad \text{(Eq. 44)}$$

Average *SWE* depth of a grid cell D_a in dependence on the *SWE* melt depth D_m: λ and ξ = distribution parameters, z_{Dm} = eq. 39, ΓD_m = snow covered fraction in dependence on D_m

where z_{Dm} is defined by:

$$z_{D_m} = \frac{\ln(\mathrm{D})-\lambda}{\xi} \qquad \text{(Eq. 45)}$$

z_{Dm} is the result of a change in the integration variable from D to z. D = *SWE* depth, λ and ξ = distribution parameters.

Figures65a and 66 can be used to explain the operation of the presented routine. Figure 65a shows different log-normal functions which are representative for the sub-scale snow distribution of a grid element of e.g. a *SVAT* model. The area under the curves is 1 in any case. Figure 66 shows the shift of the curve in the direction of smaller *SWE* averages. The extent of the shift depends on the melt rates. If the curve intersects the y axis the area below of the curve will be reduced. The remaining proportion represents the snow covered fraction of the respective model grid.

III) Spatial characteristics of MM5 wind fields in dependency of the wind direction.

This part of the appendix should give an idea about the spatial heterogeneity of the predicted *MM5* wind fields. All of the presented wind fields were calculated under usage of identical input wind speeds (cp. fig 13) of 10 [m/sec] for the 10m *MM5* model level and 25[m/sec] for the 100hpa level. The resulting differences are due to wind-topography interactions. An analysis of the wind fields shows that the maximum wind speeds are reached when the input wind direction is around 180 degrees or around 270 degrees respectively. The increased wind speeds when using these input wind directions can be decaled by the fact that the highest wind speeds are reached if the wind direction is near to, or 90 degrees to the crest orientation which is north to south for the main massifs and east to west for the later branches. If this is the case modelled wind speeds can reach up to 25 [m/sec]. This is because of the reduced cross section the air masses have to pass through if they are forced to overflow the mountains massif. Otherwise the wind speed is moderate and only around 6 [m/sec] in maximum. It could be also seen that the maximum wind speeds are located in the direct environment of the crests. Here, a nonlinear increase of the modelled wind speed can be found. Windward and leeward effects are observable in all of the calculated *MM5* wind fields. The presented examples show how heterogeneous the calculated *MM5* wind fields can be under a constant input energy. The produced heterogeneity cannot be reproduced by an interpolation routine which was shown on the basis of the comparison to the available station measurements.

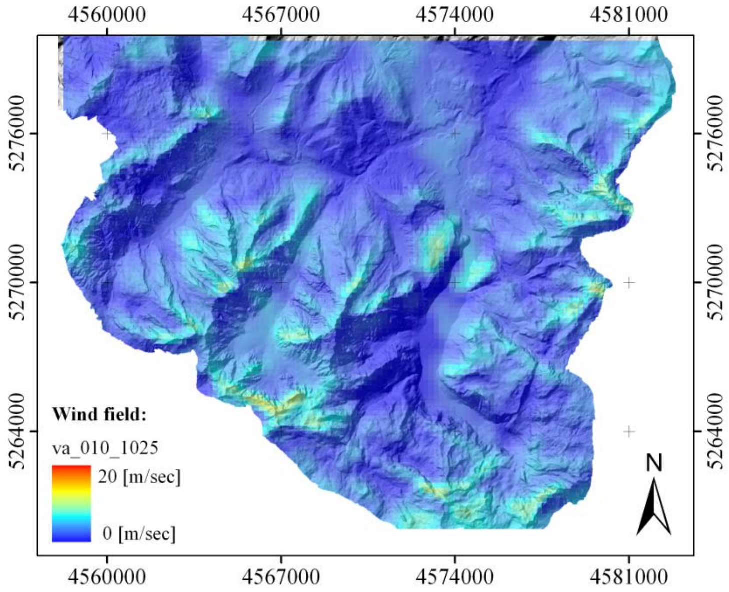
4560000
4567000
4574000
4581000
5276000
5270000
5264000
Wind field:
va_010_1025
20 [m/sec]
0 [m/sec]
N

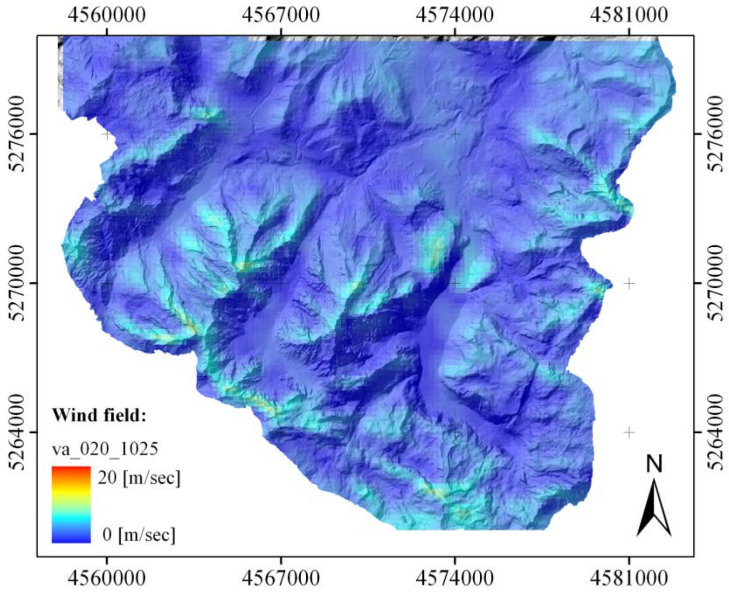
4560000
4567000
4574000
4581000
5276000
5270000
5264000
Wind field:
va_020_1025
20 [m/sec]
0 [m/sec]
N

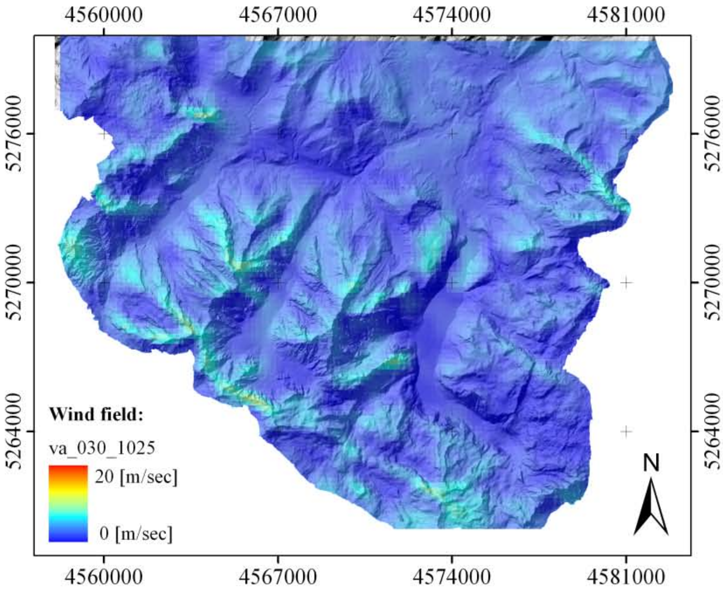
4560000
4567000
4574000
4581000
5276000
5270000
5264000
Wind field:
va_030_1025
20 [m/sec]
0 [m/sec]
N

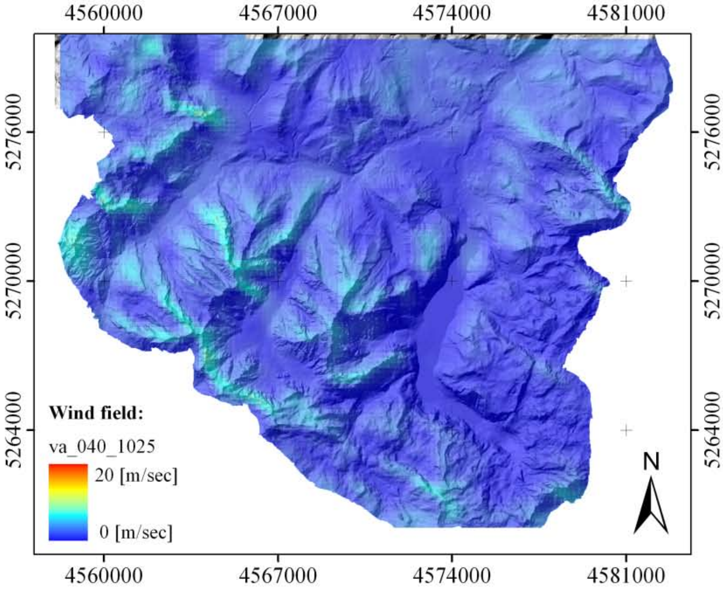
4560000
4567000
4574000
4581000
5276000
5270000
5264000
Wind field:
va_040_1025
20 [m/sec]
0 [m/sec]
N

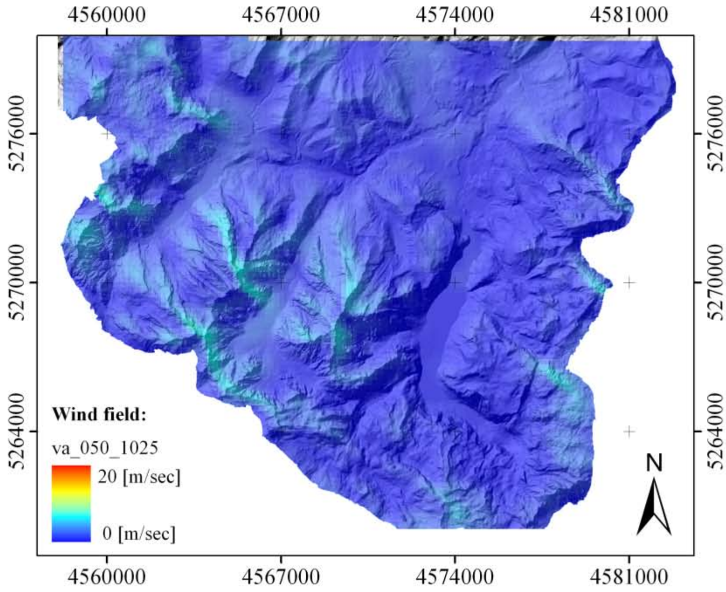
4560000
4567000
4574000
4581000
5276000
5270000
5264000
Wind field:
va_050_1025
20 [m/sec]
0 [m/sec]
N

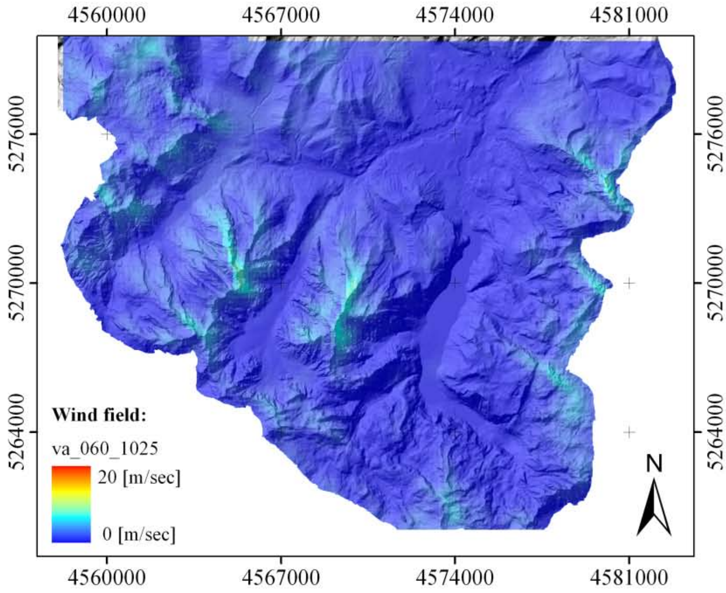
4560000
4567000
4574000
4581000
5276000
5270000
5264000
Wind field:
va_060_1025
20 [m/sec]
0 [m/sec]
N

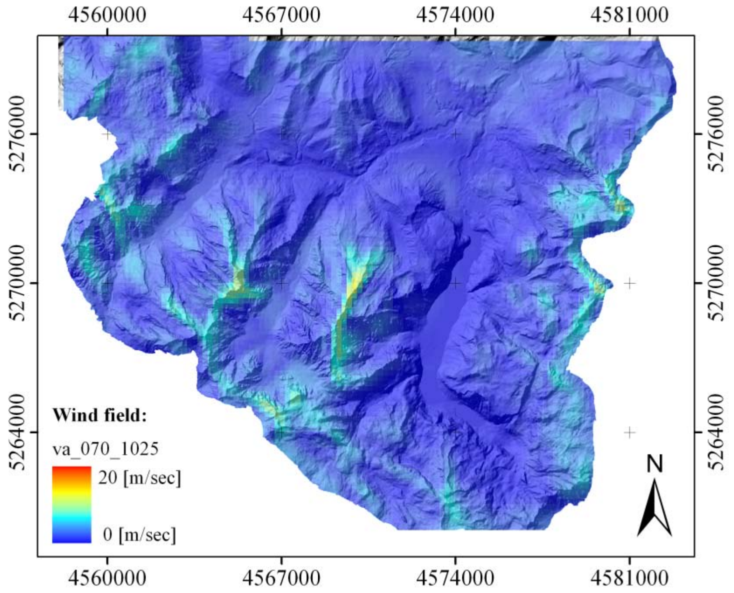
4560000
4567000
4574000
4581000
5276000
5270000
5264000
Wind field:
va_070_1025
20 [m/sec]
0 [m/sec]
N

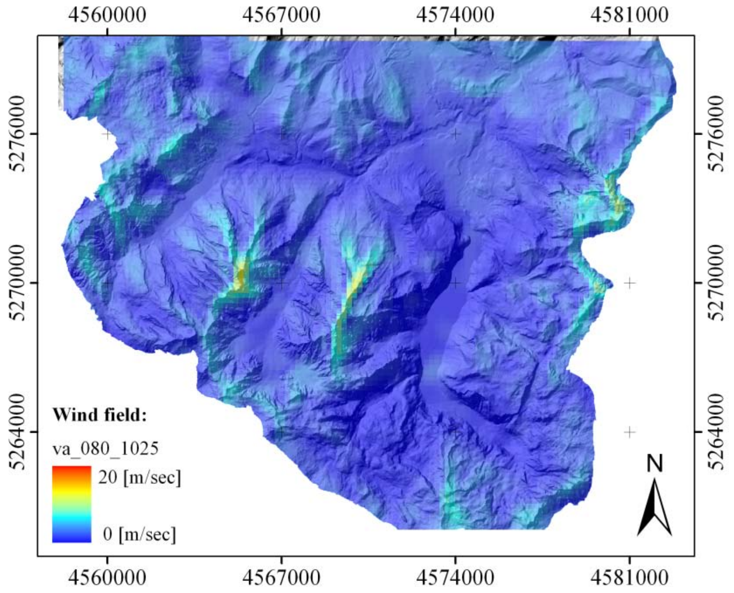
4560000
4567000
4574000
4581000
5276000
5270000
5264000
Wind field:
va_080_1025
20 [m/sec]
0 [m/sec]
N

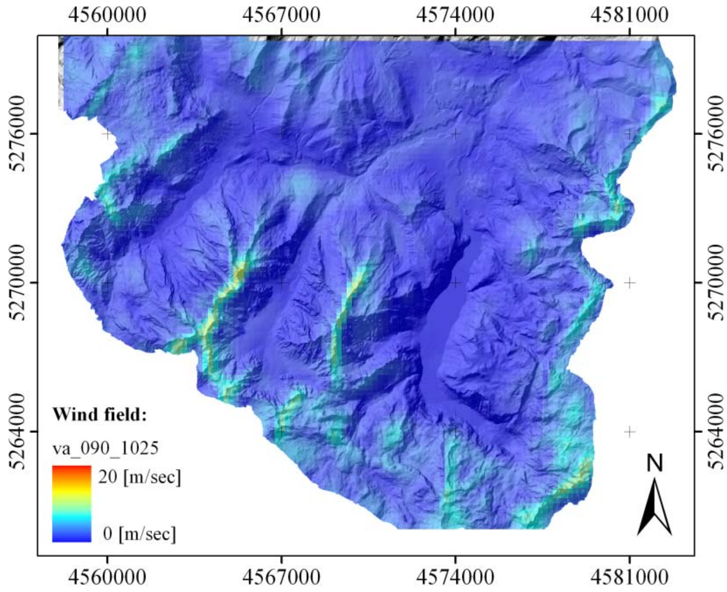
4560000
4567000
4574000
4581000
5276000
5270000
5264000
Wind field:
va_090_1025
20 [m/sec]
0 [m/sec]
N

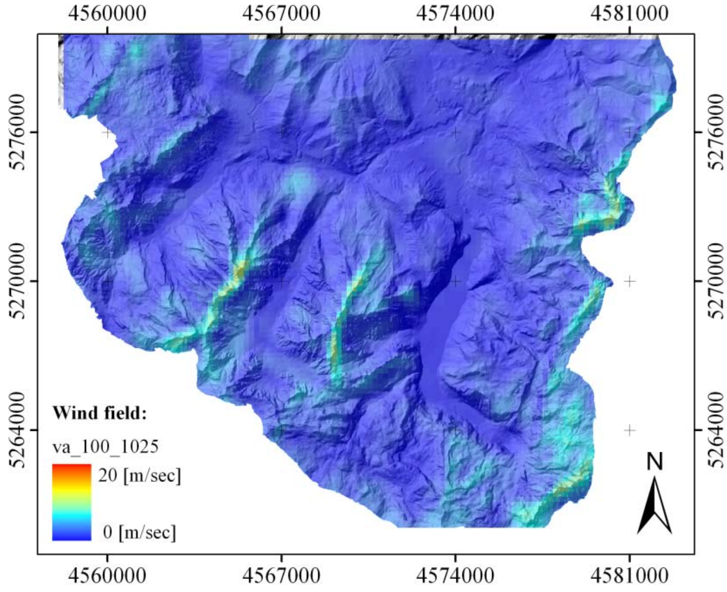
4560000
4567000
4574000
4581000
5276000
5270000
5264000
Wind field:
va_100_1025
20 [m/sec]
0 [m/sec]
N

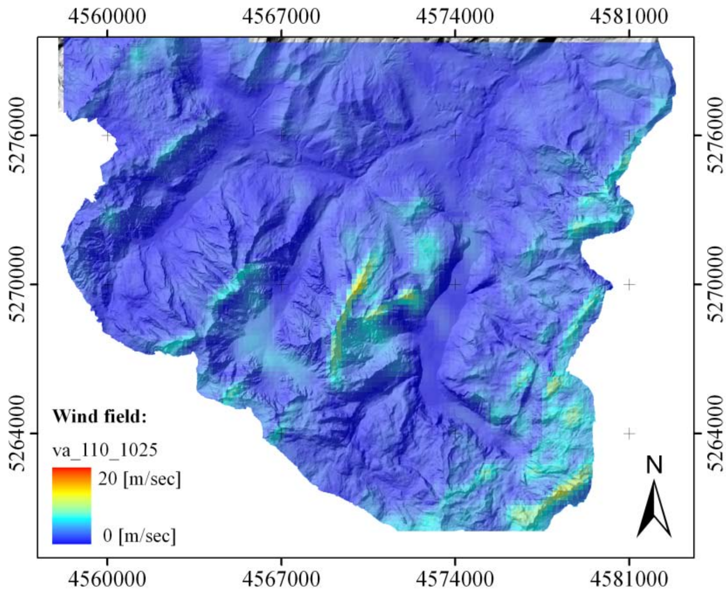
4560000
4567000
4574000
4581000
5276000
5270000
5264000
Wind field:
va_110_1025
20 [m/sec]
0 [m/sec]
N

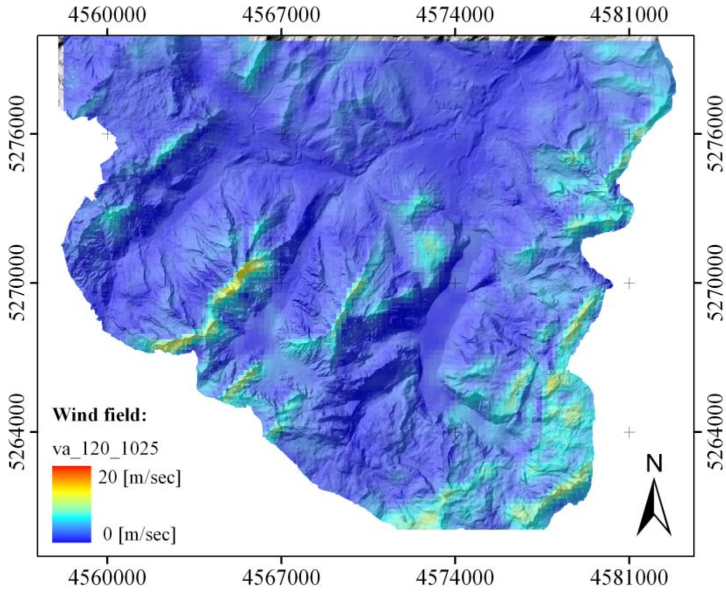
4560000
4567000
4574000
4581000
5276000
5270000
5264000
Wind field:
va_120_1025
20 [m/sec]
0 [m/sec]
N

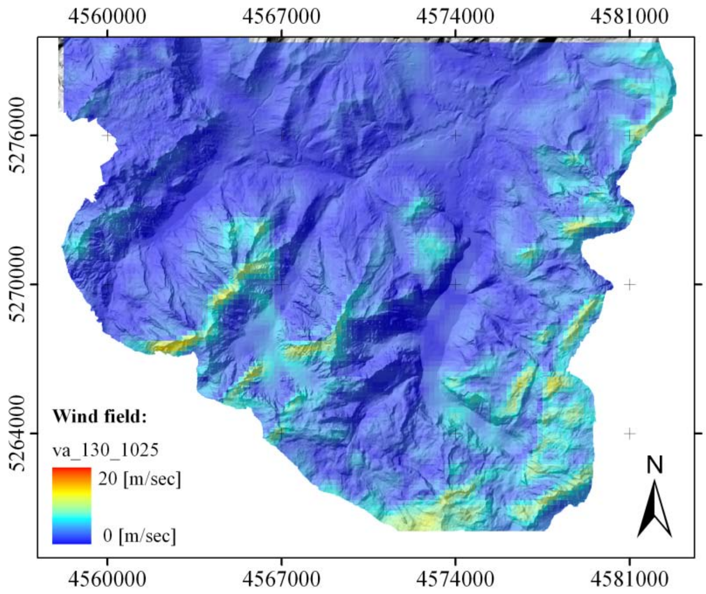
4560000
4567000
4574000
4581000
5276000
5270000
5264000
Wind field:
va_130_1025
20 [m/sec]
0 [m/sec]
N

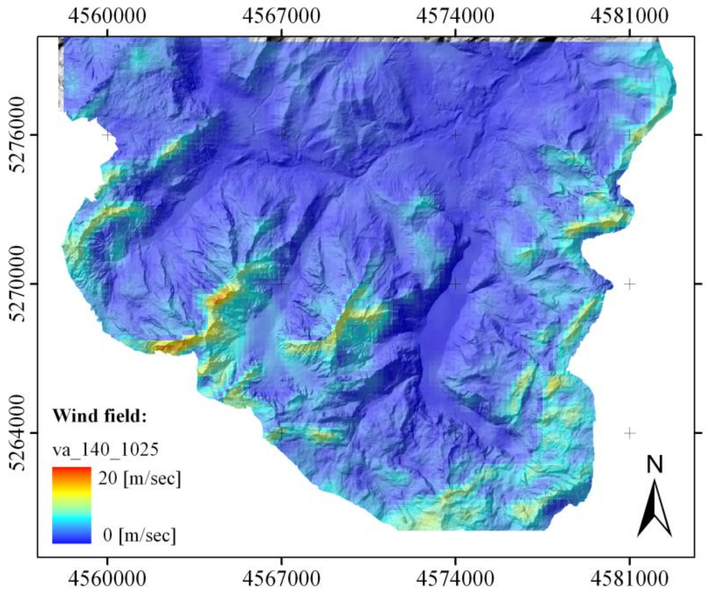
4560000
4567000
4574000
4581000
5276000
5270000
5264000
Wind field:
va_140_1025
20 [m/sec]
0 [m/sec]
N

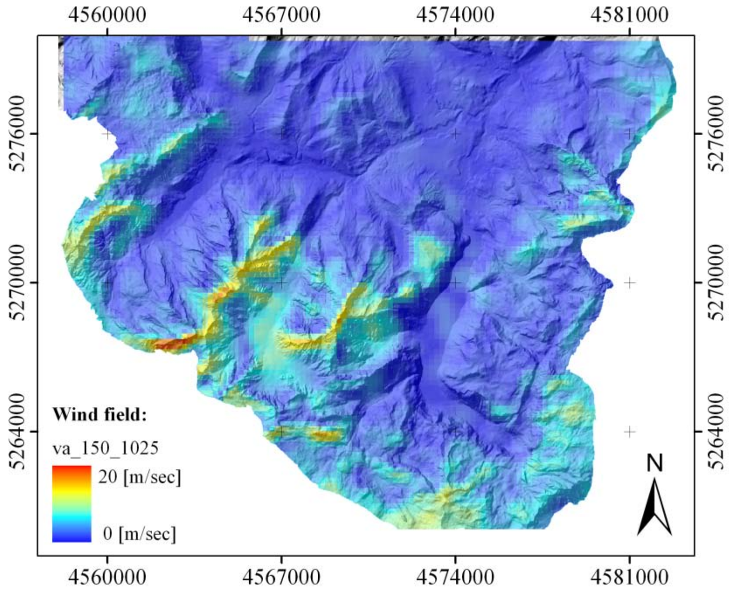
4560000
4567000
4574000
4581000
5276000
5270000
5264000
Wind field:
va_150_1025
20 [m/sec]
0 [m/sec]
N

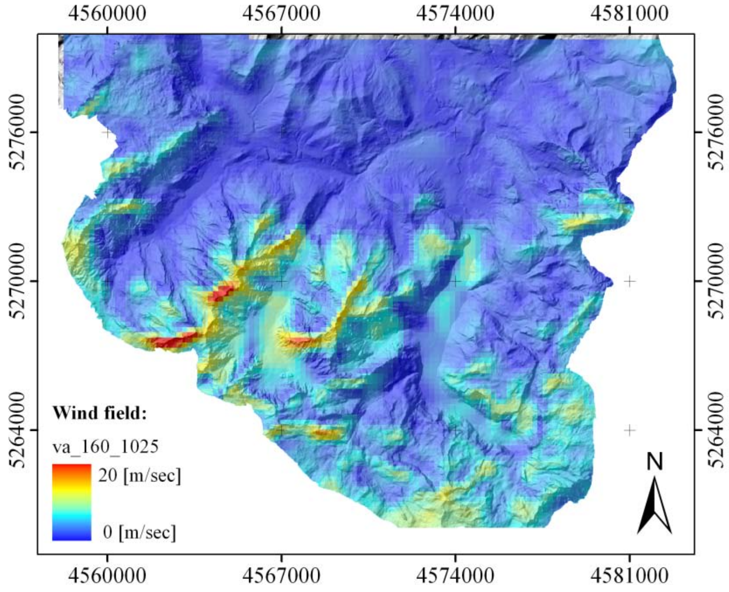
4560000
4567000
4574000
4581000
5276000
5270000
5264000
Wind field:
va_160_1025
20 [m/sec]
0 [m/sec]
N

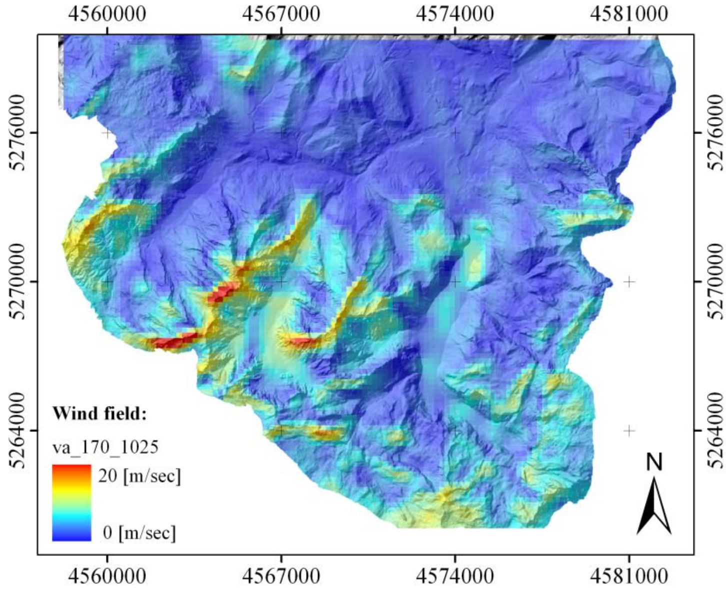
4560000
4567000
4574000
4581000
5276000
5270000
5264000
Wind field:
va_170_1025
20 [m/sec]
0 [m/sec]
N

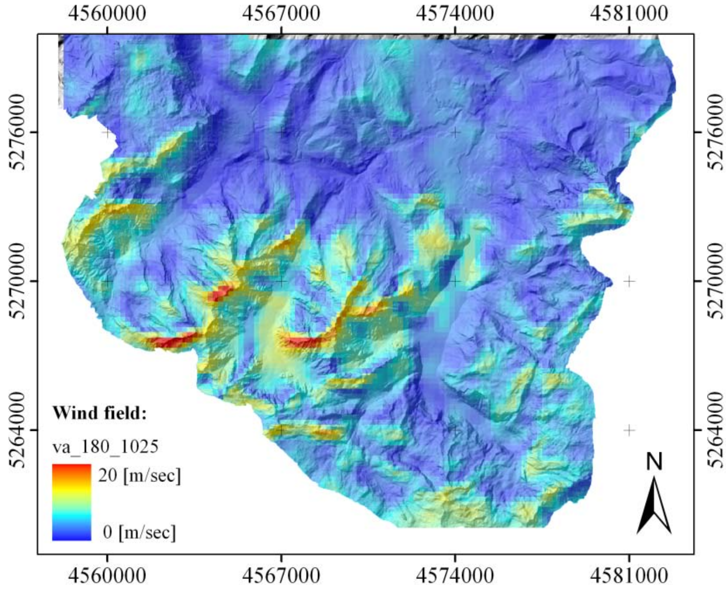
4560000
4567000
4574000
4581000
5276000
5270000
5264000
Wind field:
va_180_1025
20 [m/sec]
0 [m/sec]
N

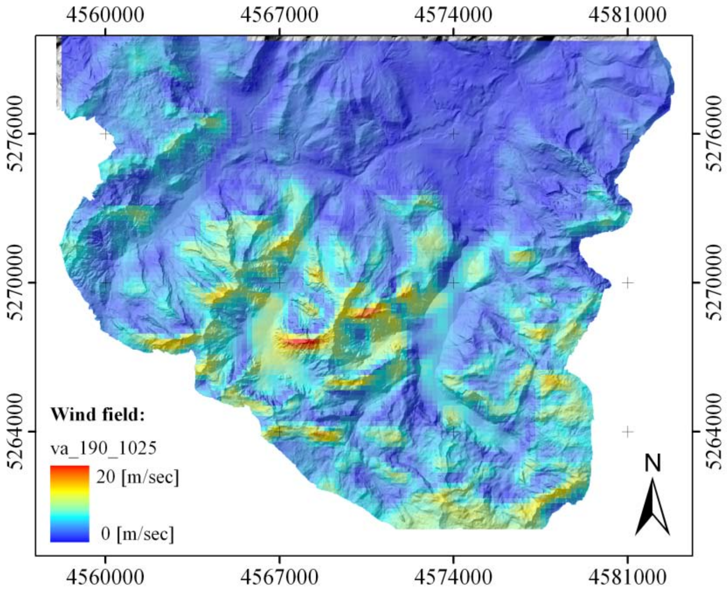
4560000
4567000
4574000
4581000
5276000
5270000
5264000
Wind field:
va_190_1025
20 [m/sec]
0 [m/sec]
N

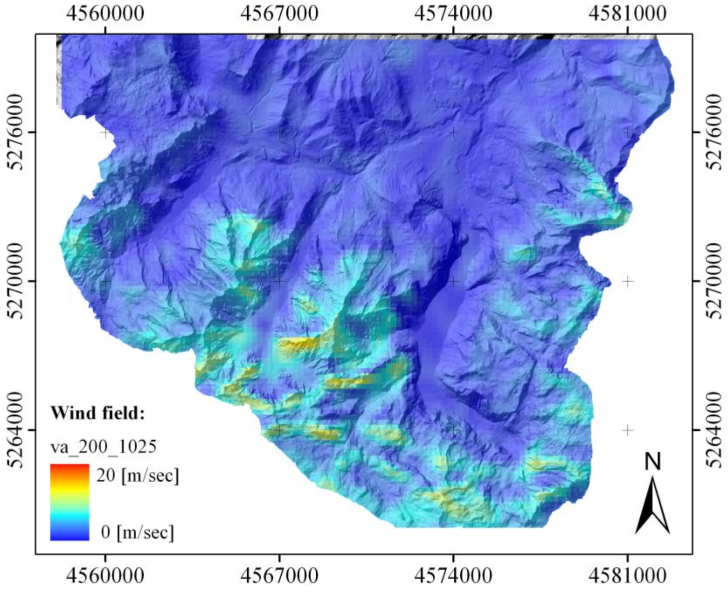
4560000
4567000
4574000
4581000
5276000
5270000
5264000
Wind field:
va_200_1025
20 [m/sec]
0 [m/sec]
N

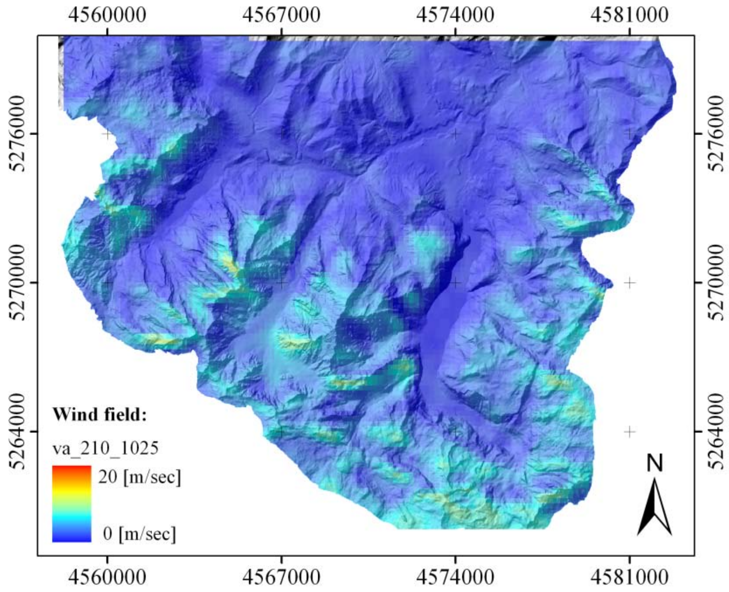
4560000
4567000
4574000
4581000
5276000
5270000
5264000
Wind field:
va_210_1025
20 [m/sec]
0 [m/sec]
N

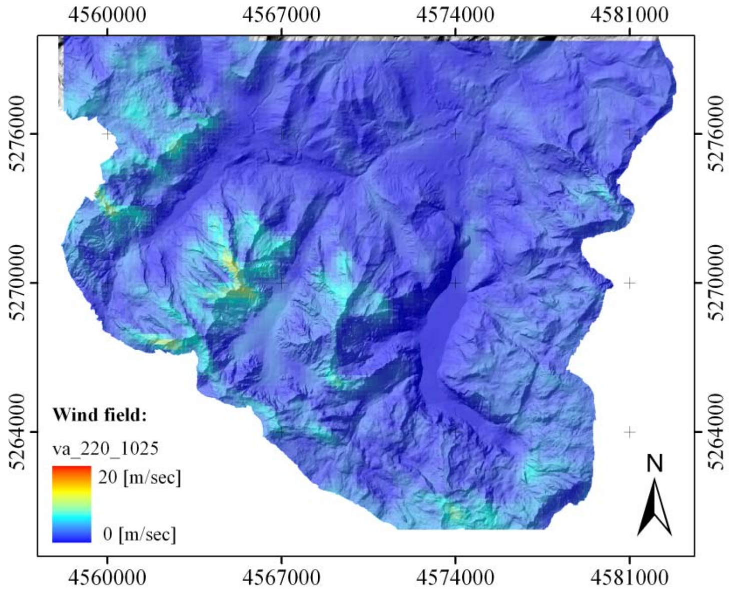
4560000
4567000
4574000
4581000
5276000
5270000
5264000
Wind field:
va_220_1025
20 [m/sec]
0 [m/sec]
N

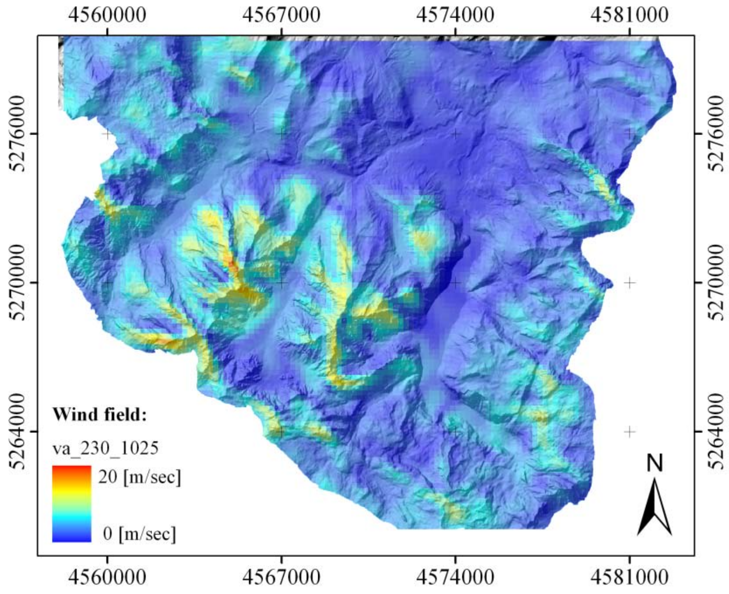
4560000
4567000
4574000
4581000
5276000
5270000
5264000
Wind field:
va_230_1025
20 [m/sec]
0 [m/sec]
N

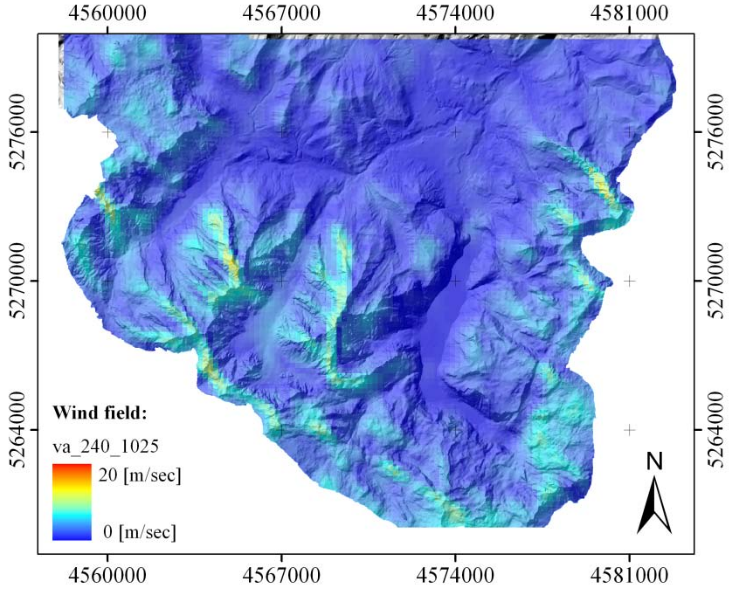
4560000
4567000
4574000
4581000
5276000
5270000
5264000
Wind field:
va_240_1025
20 [m/sec]
0 [m/sec]
N

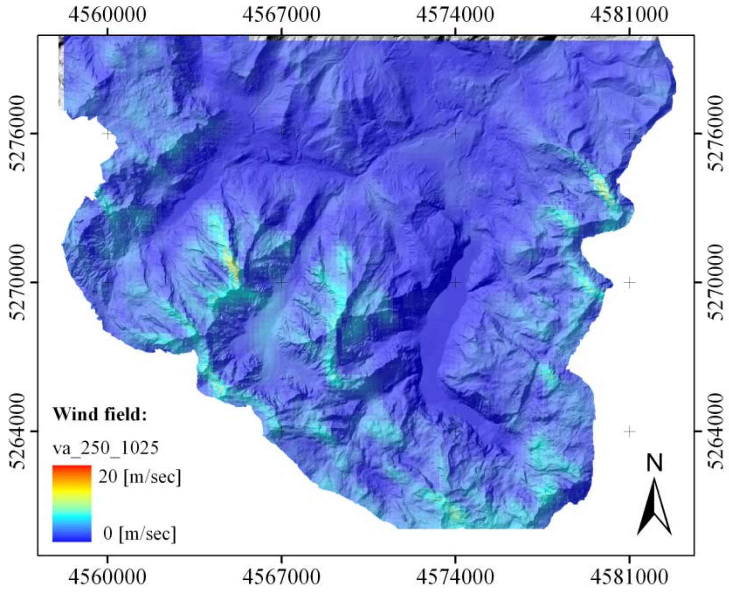
4560000
4567000
4574000
4581000
5276000
5270000
5264000
Wind field:
va_250_1025
20 [m/sec]
0 [m/sec]
N

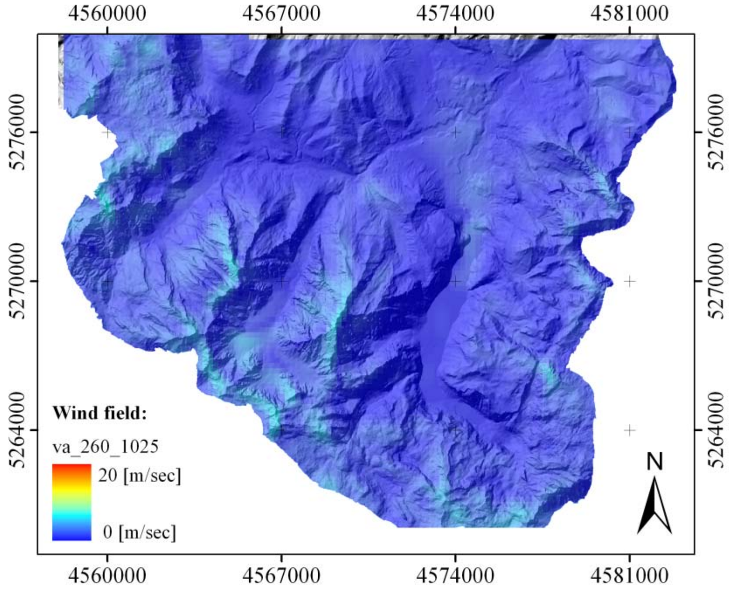
4560000
4567000
4574000
4581000
5276000
5270000
5264000
Wind field:
va_260_1025
20 [m/sec]
0 [m/sec]
N

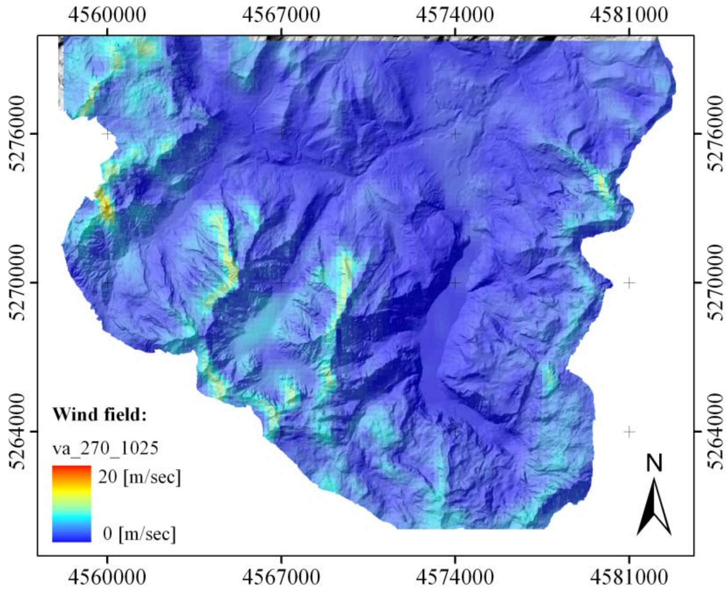
4560000
4567000
4574000
4581000
5276000
5270000
5264000
Wind field:
va_270_1025
20 [m/sec]
0 [m/sec]
N

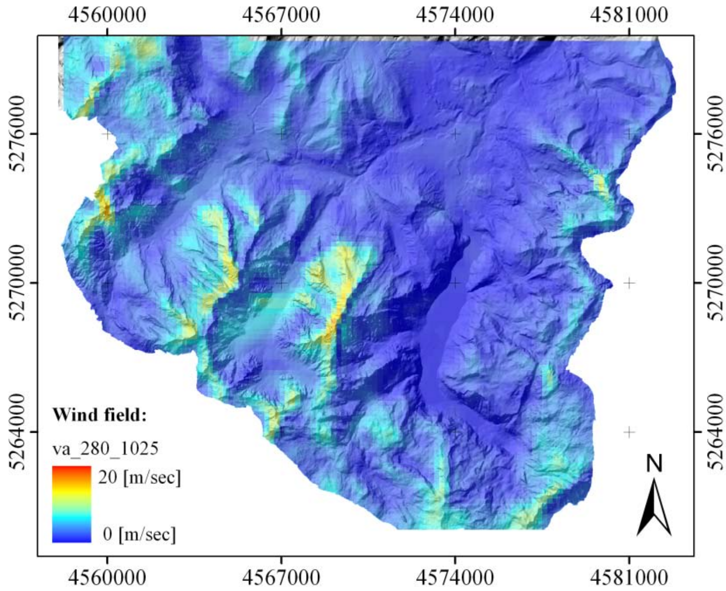
4560000
4567000
4574000
4581000
5276000
5270000
5264000
Wind field:
va_280_1025
20 [m/sec]
0 [m/sec]
N

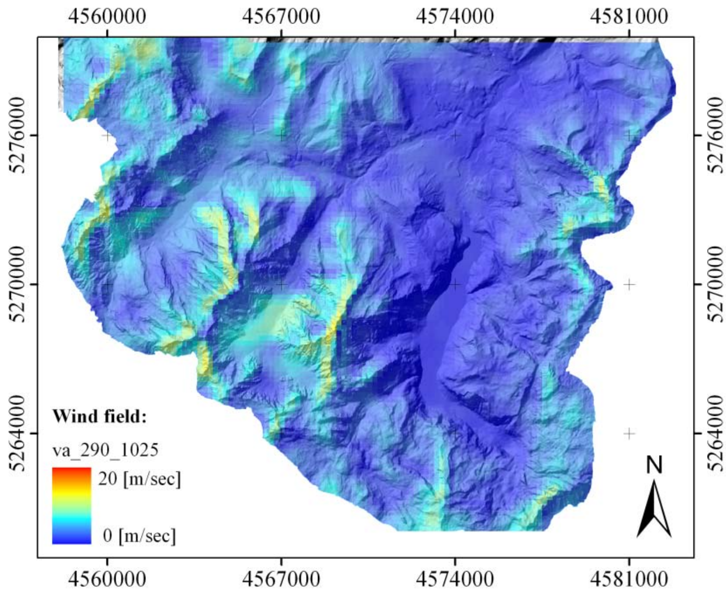
4560000
4567000
4574000
4581000
5276000
5270000
5264000
Wind field:
va_290_1025
20 [m/sec]
0 [m/sec]
N

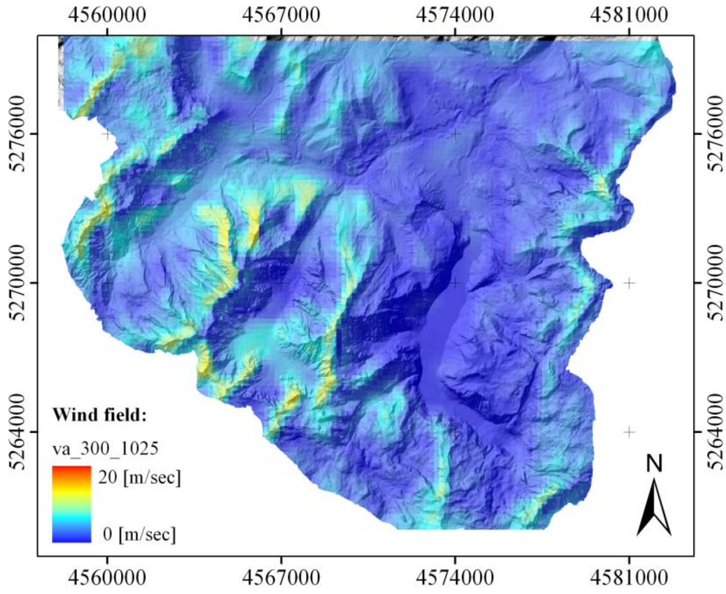
4560000
4567000
4574000
4581000
5276000
5270000
5264000
Wind field:
va_300_1025
20 [m/sec]
0 [m/sec]
N

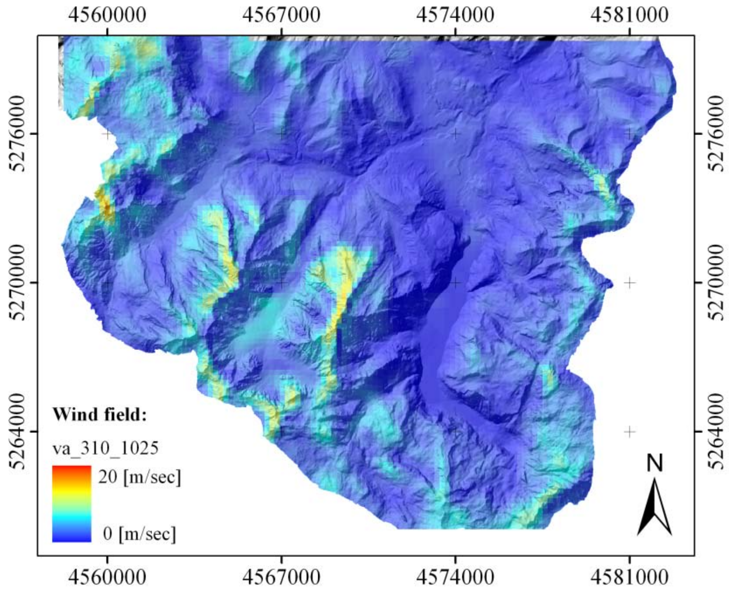
4560000
4567000
4574000
4581000
5276000
5270000
5264000
Wind field:
va_310_1025
20 [m/sec]
0 [m/sec]
N

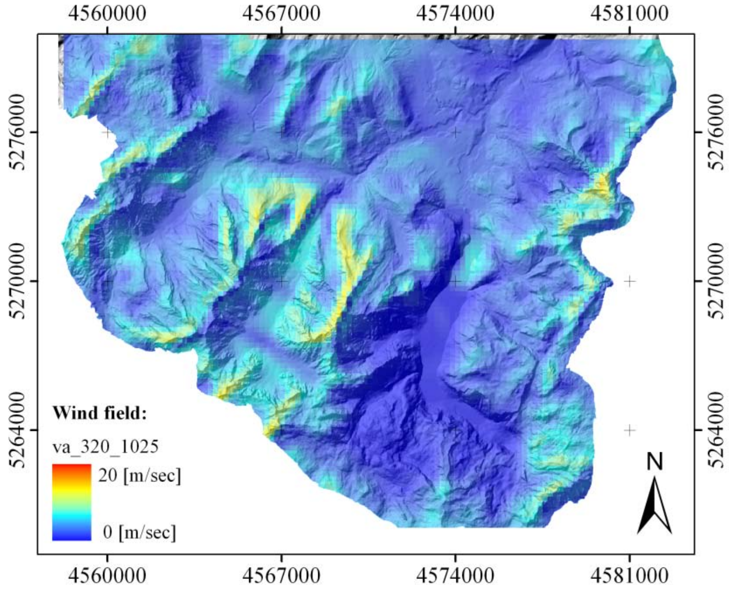
4560000
4567000
4574000
4581000
5276000
5270000
5264000
Wind field:
va_320_1025
20 [m/sec]
0 [m/sec]
N

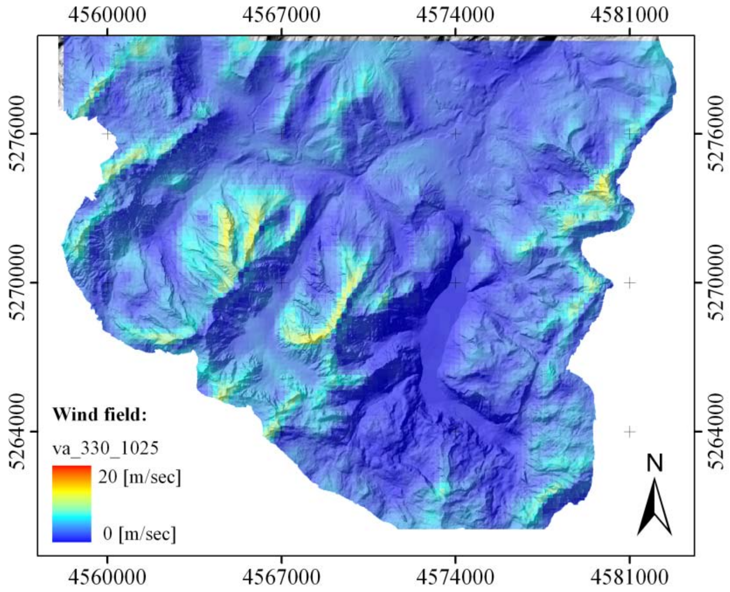
4560000
4567000
4574000
4581000
5276000
5270000
5264000
Wind field:
va_330_1025
20 [m/sec]
0 [m/sec]
N

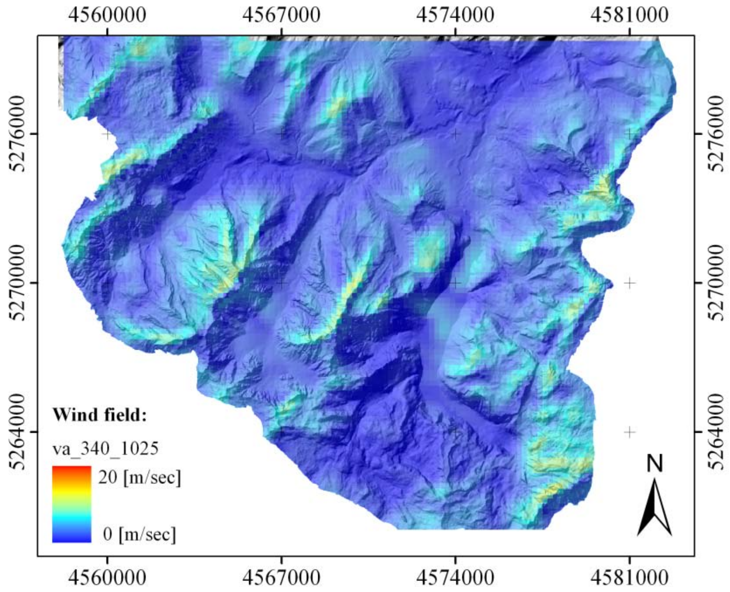
4560000
4567000
4574000
4581000
5276000
5270000
5264000
Wind field:
va_340_1025
20 [m/sec]
0 [m/sec]
N

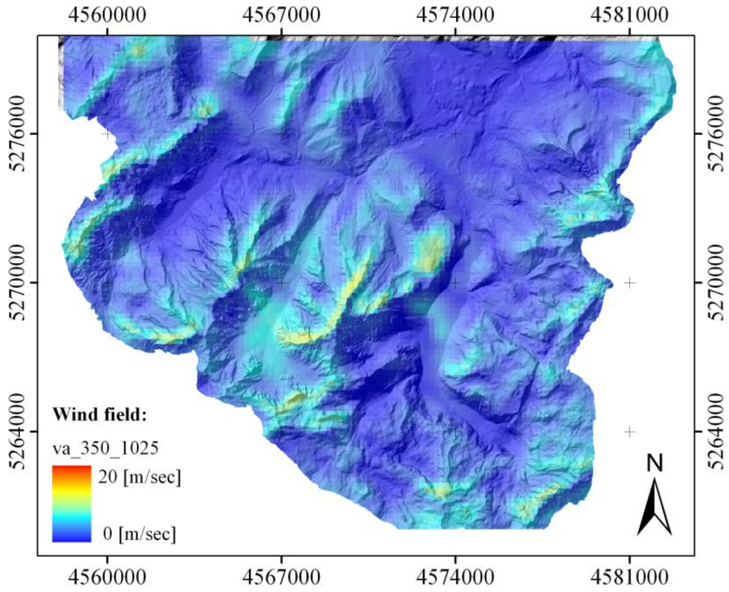
4560000
4567000
4574000
4581000
5276000
5270000
5264000
Wind field:
va_350_1025
20 [m/sec]
0 [m/sec]
N

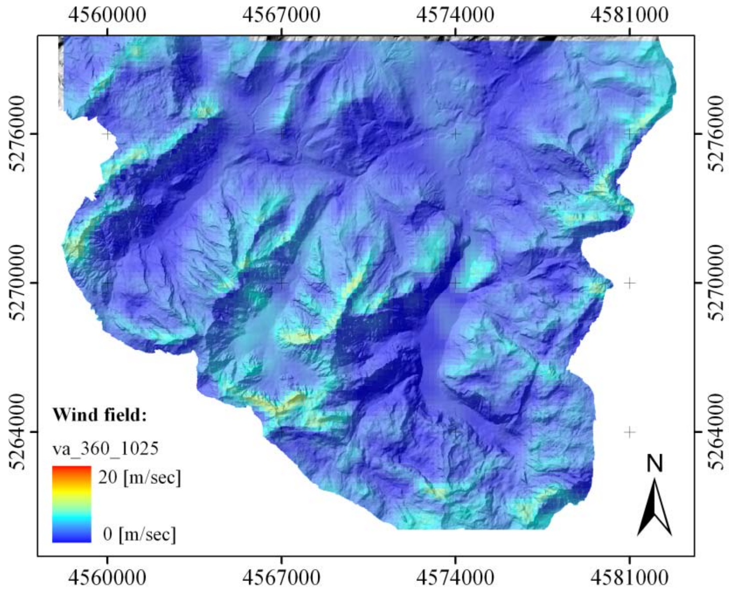
4560000
4567000
4574000
4581000
5276000
5270000
5264000
Wind field:
va_360_1025
20 [m/sec]
0 [m/sec]
N

IV) Some impressions of the test-site:

Kühroint

Field campaign

Personal CV

Contact Information:

Name: -- Bernhardt

First Name:-------------------------------------- Matthias

Address: --- Ickstattstr.9

80469 München

Telephone: -------------------------------------- 0049 179/5232822

Email: -- m.bernhardt@iggf.geo.uni-muenchen.de

Personal Information:

Date of Birth: ----------------------------------- 08.08.1977

Place of Birth: ---------------------------------- Rosenheim

Citizenship: -------------------------------------- German

Gender: -- Male

Marital Status: ---------------------------------- Unmarried

Academic CV:

1998-2004: -------------------------------------- Study in Geography, Remote Sensing and Zoology, University of Munich

2004: --- Diploma in Geography (Mark: 1.0).
Diploma thesis: Modelling nitrogen fluxes under wheat stand utilizing the physically based model WHNSIM (Mark: 1.3).

Since 2004:-------------------------------------- Scientific Staff member at the Department for Geography, Ludwig-Maximilians-University.

Scholar CV:

1986-1988: -------------------------------------- Primary school Au b. Bad Feilnbach
1988-1990: -------------------------------------- Primary school Schloßberg
1990-1997: -------------------------------------- Freie Waldorfschule Chiemgau
1997: --- “Abitur” certificate at the Ludwig-Thoma Gymnasium; Prien am Chiemsee.